Design of a Hydromechanical Transmission With Regeneration for a Passenger Vehicle

A THESIS
SUBMITTED TO THE FACULTY OF THE GRADUATE SCHOOL
OF THE UNIVERSITY OF MINNESOTA
BY

Stephen Joseph Sedler

IN PARTIAL FULFILLMENT OF THE REQUIREMENTS
FOR THE DEGREE OF
Master Of Science

Thomas R. Chase, Perry Y. Li

September, 2012

Acknowledgements

I would like to thank Dr. Thomas Chase and Dr. Perry Li for all of their guidance and support in completing this project. I would also like to thank my fellow Testbed 3 graduate students for all of their hard work on the project: Michael Olson, Jonathan Meyer, David Grandall, Justin Lapp, Teck Ping Sim, Robert Ertel, Felicitas Mensing, Kai Loon Cheong, Feng Wang, Shah Ramdan, Ross Makulec, Henry Kohring, and Zhekang Du. I would like to thank the CCEFP as well for the opportunity and financial support to obtain my degree. I want to thank the CCEFP staff and graduate students for their support and keeping me sane. And finally I would like to thank my committee members. This work was performed within the Engineering Research Center for Compact and Efficient Fluid Power (CCEFP), supported by the National Science Foundation under Grant No. EEC-0540834.

Dedication

To Mom

and Dad and T and Austyn
who are most definitely cruzin'
HTE

Abstract

The design of a four-mode, input-coupled, power-split hydromechanical transmission with energy storage is presented. The focus of this thesis is on the design process of the transmission utilizing Lagrange multiplier optimization and machine design principles to construct the prototype transmission for use on a Polaris Ranger chassis. The four-mode design presented facilitates vehicle operation in hydromechanical power-split mode, parallel mode, and two series modes. An optimal mode of operation map is determined and a maximum fuel economy of 78.5 mpg is calculated.

Contents

Acknowledgements **i**

Dedication **ii**

Abstract **iii**

List of Tables **vi**

List of Figures **vii**

1 Introduction **1**

1.1 Background 1

1.2 Previous Work 3

1.3 Overview 6

2 Final Transmission Design **7**

3 Design Optimization and Configuration **21**

3.1 Transmission Operating Principles 21

3.1.1 HMT mode 23

3.1.2 S-only mode 24

3.1.3 T-only mode 24

3.1.4 Parallel mode 25

3.2 Optimization Method and Simulation 25

3.2.1 Pump Models 27

3.2.2 Optimization Results 28

3.3 Transformation 28

4 Component Sizing Methods **33**
4.1 Gear Sizing 33
4.2 Shaft Sizing 37
4.3 Bearing Sizing 40
4.4 Overall Sizing 42

5 Conclusion and Discussion **43**
5.1 Review 43
5.2 Contributions 43
5.3 Future Work 44

References **46**

Appendix A. Transmission Optimization Code **49**

Appendix B. Pump/Motor Model Generation Code **61**

Appendix C. Representation of Original Transmission Configuration **66**
C.1 Torque and Speed Governing Equation Derivation 66

Appendix D. Redesign Configurations of HHPV Drivetrain **70**
D.1 Configuration 1 70
D.2 Configuration 2 73
D.3 Configuration 3 75
D.4 Configuration 4 78
D.5 Configuration 5 81
D.6 Configuration 6 84

Appendix E. Manufacturing Drawings **88**

List of Tables

3.1 Component connection to planetary gearset by configuration. 29
3.2 Transformed optimized ratios 30

List of Figures

1.1 Symbol definitions for schematics. 3
1.2 Configuration of the original power-split hydraulic hybrid vehicle. 4
2.1 Redesign HMT Configuration. 8
2.2 Polaris Ranger chassis, engine, transmission, and differential. 9
2.3 Standalone transmission 10
2.4 Transmission: Section 1 10
2.5 Transmission: *Section 1*. Exploded view. 11
2.6 Transmission: Section 2 13
2.7 Transmission: *Section 2*. Exploded view. 13
2.8 Transmission: Section 3 14
2.9 Transmission: *Section 3*. Exploded view. 15
2.10 Transmission: Section 4 17
2.11 Transmission: *Section 4*. Exploded view. 18
2.12 Transmission: *Torquer* Hydraulic Unit Section 18
2.13 Exploded view with *torquer* hydraulic unit and charge pump. 19
3.1 Initially Proposed HMT Configuration. 22
3.2 Redesigned HMT Configuration 30
3.3 Optimal operating modes at 1950 psi. 31
3.4 P/M S speed over the urban drive cycle. 32
3.5 P/M T speed over the urban drive cycle. 32
5.1 Transmission Comparison 45
C.1 Schematic representation of the originally built HMT configuration. . . 67
D.1 Redesign Configuration 1 71
D.2 Redesign Configuration 2 73

D.3 Redesign Configuration 3 76
D.4 Redesign Configuration 4 79
D.5 Redesign Configuration 5 82
D.6 Redesign Configuration 6 85

Chapter 1

Introduction

In this chapter, a background of the standard automobile drivetrain architectures is given. This is followed by an examination of previous work on relevant drivetrain configurations, and the architecture developed in this thesis is described.

1.1 Background

In the world of automotive drivetrains, an abundance of choices exist from which one must synthesize a design to meet the desired requirements. A choice of powerplant type is required; does one choose a standard IC engine type or something more exotic, a free-piston engine or hydrogen fuel cell perhaps? Then a choice of architecture is required; does one choose a standard transmission type or some sort of hybrid? These are just some of the issues that must be addressed when choosing the components making up the design.

The standard automotive transmission provides a direct relationship between the speed of the wheels and the speed of the engine shaft. The associated transmission and final drive ratios are chosen to meet the performance characteristics desired while balanced against the feasibility and cost in design. The discrete ratios that make-up the transmission do not allow for an optimal design in terms of system efficiency; the engine will roam across the spectrum of the torque versus speed efficiency map, depending on the drivecycle.

The parallel hybrid architecture[1] is similar to the standard transmission architecture with a small difference: the architecture maintains the pure mechanical path between the engine and the wheels but also augments power to the driveline with an auxiliary power source. The engine and wheels maintain their fixed ratios relationship, again causing the engine torque and speed to roam across its capability range.

The series hybrid architecture[1] removes the mechanical transmission link between the engine and the wheels and instead converts all of the mechanical energy from the engine to another type of energy for storage and use. The needed stored energy is then converted back to mechanical energy for use at the wheels. When storage is available in this architecture, full engine management can be realized, whereupon the instantaneous engine speed and torque operation is fully decoupled from the torque and speed requirements at the wheels.

The power-split architecture[1] is a combination of the series and parallel architectures. In the power-split architecture, the engine drives a shaft from which power is both split and recombined in a planetary gearset using auxiliary power and energy storage components. The engine is free to operate at any feasible torque and speed regardless of the needed wheel power by utilizing the auxiliary power and energy storage components. By adding regeneration, the kinetic energy of the moving vehicle can be transferred through the wheels and transmission, back into the energy storage components.

Any number of technologies can be used for the powerplant as well as the auxiliary components. This thesis focuses on hydraulic hybrid drivetrains, specifically the design of an input-coupled power-split transmission with regeneration architecture.

The transmission design process utilizes a Lagrange multiplier optimization strategy [2] [3] and four-mode transmission operation concept to determine optimal component ratios. The Lagrange optimization minimizes fuel consumption over the urban drive cycle. During this optimization process, the optimal gear ratios are determined along with optimal engine operating modes. The four modes of operation introduced in this design provide a blend of the conventional drivetrain with the series, parallel, and power-split architectures. The four-mode concept allows for a wider range of flexibility in vehicle operation, improving fuel economy. To realize a physical construct of the optimal design from the mathematical concepts and models, gear, shaft, and bearing machine

design concepts are utilized. The resultant manufactured design is presented herein.

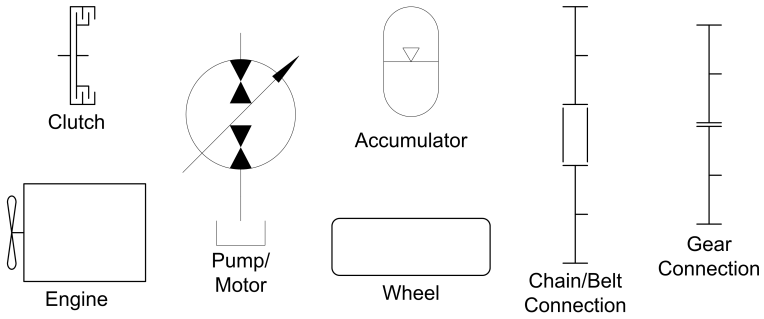

Figure 1.1: Symbol definitions for schematics.

The symbols used in the configuration schematics are defined in Fig. 1.1.

The power-split hydraulic hybrid vehicle project at the University of Minnesota provided the motivation for this work. The original configuration of the vehicle is shown in Fig. 1.2. In testing the original configuration, limitations of the design became apparent. One issue was that the chains used in the design created binding issues that would cause the vehicle to suddenly stop. Also, the flexibility in locating components, while nice in assembly, resulted in a design that could not withstand the loads transmitted and resulted in components moving. Additionally, the original differentials were not expected to sustain the transmission power levels. Furthermore, the axial piston pump/motors had low efficiencies and the overall design took up a large amount of space which included a gearbox that could only shift gears when stopped. Because of all of these issues, it was necessary to redesign the transmission.

1.2 Previous Work

Globally, automotive transmissions can be broken up into two groups: transmissions without energy storage and transmissions with energy storage.

In [4], an approach was developed to investigate the twelve possible configurations of connecting an engine, a hydrostatic unit, and an output shaft to a planetary gearset. The network analysis method used presented a method to minimize recirculation of the power within the transmission along with allowing synchronous clutch operation to switch between configurations. In contrast to the approach used in this work, the

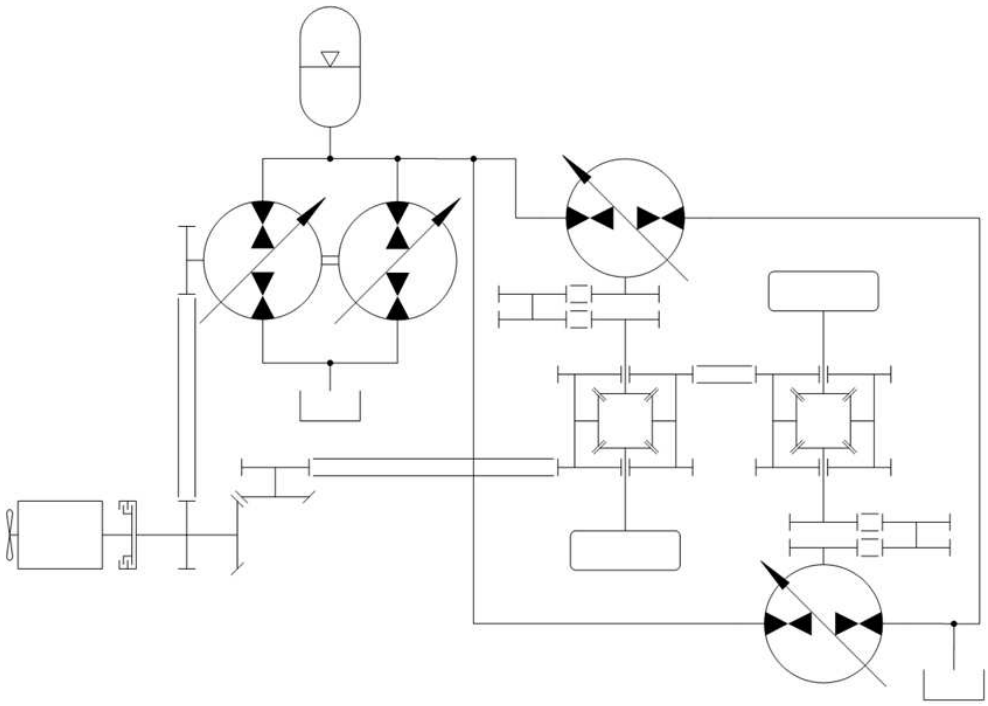

Figure 1.2: Configuration of the original power-split hydraulic hybrid vehicle.

work in this thesis addresses the efficiency optimization through a four-mode Lagrange multiplier optimization on a single configuration. In this manner, the recirculation is addressed by allowing for shifts in mode within a single configuration, rather than switching between different power-split configurations. Additionally, energy storage is available in the transmission discussed herein while no energy storage was investigated in [4]. The addition of energy storage with the four-mode architecture further reduces the likelihood of recirculation due to an increase in choices within modes due to full engine management.

In [5], design optimization procedures were developed for infinitely variable transmissions without energy storage. It was shown that input-coupled and output-coupled configurations could both perform well with variations dependent on the application under consideration. In [2], comparisons between the input-coupled and output-coupled transmissions with energy storage demonstrated that the efficiency varied only slightly.

In [6], the development of a parallel hybrid is presented. The transmission developed utilized four clutches, two planetary gearsets, and an electric motor to achieve a 16-mode parallel hybrid configuration. The transmission presented had the ability to function in a power-assist mode as well as a fully electric mode. The transmission also had the ability to store energy during braking events into batteries. The work presented herein simplifies the transmission design, reducing the number of clutches and planetary gearsets to one of each.

In [7], the optimization and development of a novel multi-mode electric hybrid with energy storage was discussed. In this transmission, a multiple gear transmission was combined with a continuously variable transmission gearset to produce a hybrid transmission with multiple driving gears and a power split mode gear. The multiple modes of this transmission were realized by a complex configuration of gears and clutches while the transmission presented herein achieves mode differentiation through hydraulic lockup of the different hydraulic units.

Other work within the Center for Compact and Efficient Fluid Power at the University of Minnesota has been performed on hydromechanical architectures. In [8], the development of a single mode hydromechanical transmission was presented along with a comparison to the series architecture. In [9], an analysis of various hybrid architectures was performed revealing the impact of the drive cycle and component efficiencies

on the efficiency of the design. In [10], a three level hierarchical control analysis was introduced that separated the real-time vehicle operation control from the drive cycle dependent operation. In [11], the low level control of a three level hyrdromechanical transmission control system was analyzed and designed. In [12], a control strategy for a hydromechanical transmission was developed along with a component sizing strategy with comparisons to series and parallel drivetrain architectures.

Other hybrid transmission development has been also been presented in the literature. Transmission development of the Toyota Prius hybrid system is described in [13]. Reference [14] presents work on a novel automotive two-mode infinitely variable transmission utilizing a continuously variable transmission, a planetary geartrain, and two ordinary transmissions. Reference [15] presents the design of a novel two-mode infinitely variable transmission utilizing one-way clutches for use in general mechanical industry and automobiles. Reference [16] presents the operating principles and analysis of a constant power continuously variable transmission traction drive belonging to the toroidal traction drive family. The work presented in [17] shows the design of a transmission utilizing two parallelly connected planetary gearsets and presents a method for synthesizing clutching sequences. Automatic transmission design using an automatic power flow generation algorithm is presented in [18]. Additionally, improvements in planetary gearset efficiency and transmission error is presented in [19]. Each of these works presents a different transmission design and approach to solving the general machine transmission question.

1.3 Overview

Chapter 2 gives an overview of the four-mode, power-split, hydromechanical transmission with regeneration final design developed within this thesis. Chapter 3 describes the design optimization strategy used to maximize fuel economy and the configuration decision method for architecture selection. Chapter 4 presents the sizing methods used in the transmission component design. Chapter 5 gives a review of the transmission design presented, a summary of the contributions of this work, and recommendations for future work.

Chapter 2

Final Transmission Design

This chapter contains an overview of the transmission design along with the operating principles of the hydromechanical transmission with regeneration.

The power-split architecture shown in Fig. 2.1 is a combination of the parallel and series architectures. As such, the power-split hydromechanical transmission allows for the benefits of each architecture to be realized. The efficient mechanical path is maintained between the engine and the wheels while also decoupling the direct connection between engine and wheels. This allows for the vehicle to operate with full engine management while maintaining an efficient mechanical connection. In addition, a downsized engine can be used. This is possible because the engine no longer needs to be the sole source of vehicle propulsion; using the power from the pump/motors (P/M) to supplement the engine power allows for the vehicle to meet intermittent peak power demands.

The vehicle operates in a 4-mode manner. The first mode is the hydromechanical transmission (HMT) power-split mode. In this mode the engine is engaged with the rest of the system while both the *torquer* hydraulic unit (P/M T) and *speeder* hydraulic unit (P/M S) are hydraulically engaged. The second mode is the P/M S-only mode. In this mode, only P/M S is used to drive the system; the engine is removed from the system via clutch disengagement and P/M T supplies a needed resistance torque at zero speed by having its shaft locked-up through hydraulic means. This mode is, in essence, a series transmission mode with only the drive side of a series transmission. The third mode of operation is the P/M T-only mode. In this mode, the engine is again removed from the system via the clutch disengagement. However, instead of locking-up P/M T

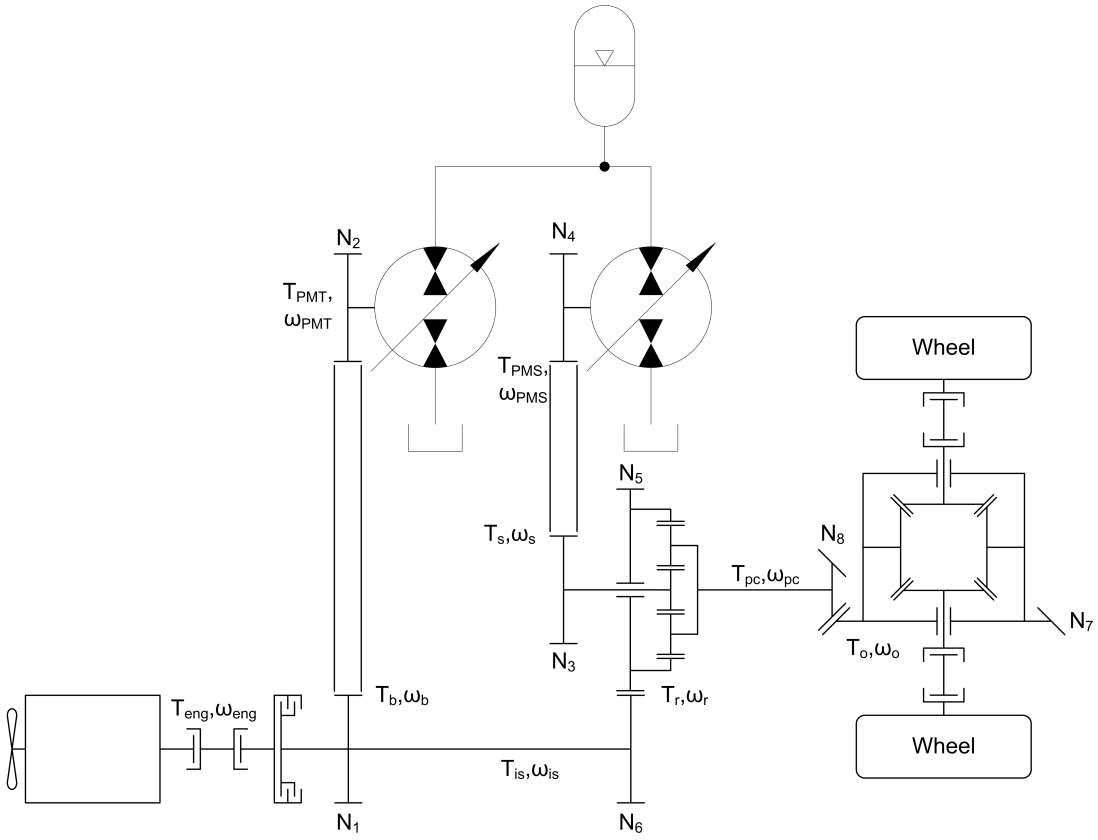

Figure 2.1: Redesign HMT Configuration. Schematic representation includes simplification from the actual architecture for graphical simplicity. The two belts shown do not exist in the actual architecture. In reality, gear N_2 drives gear N_5, gear N_6 does not actually exist, and gears N_3 and N_4 are separated by an idler gear.

and driving with P/M S only, like in the P/M S-only mode, P/M T now supplies the torque and speed necessary while P/M S supplies a resistance torque at zero speed by being hydraulically locked-up. The final mode of operation is the parallel mode. This mode is the same at the P/M T-only mode with the exception that the engine is added to the system via the engaged clutch.

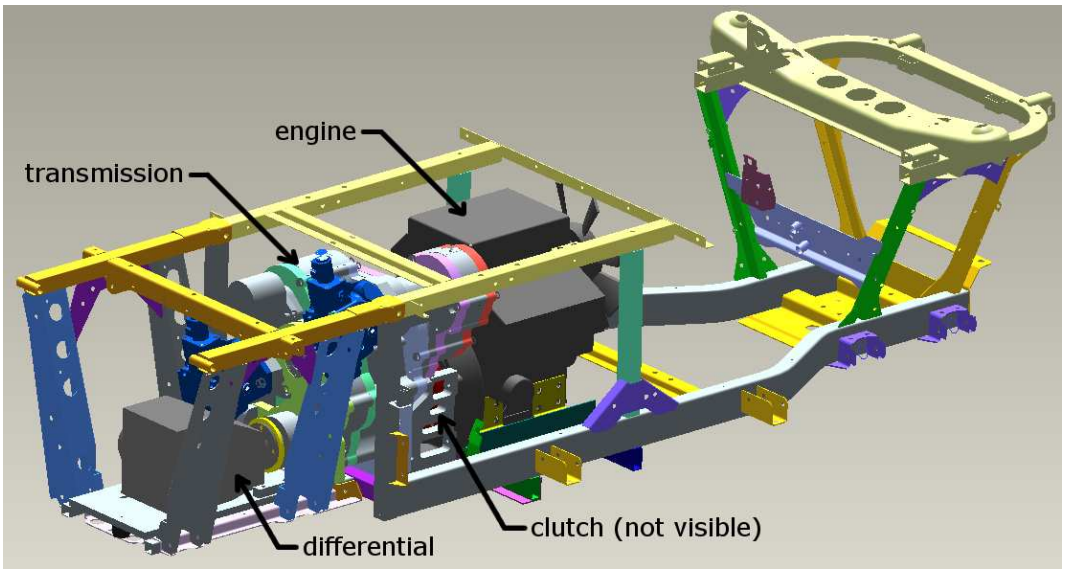

Figure 2.2: Polaris Ranger chassis, Perkins engine, transmission, and BMW differential.

The main drivetrain components are shown in Fig. 2.2. The chassis of the vehicle is that of a 2007 Polaris Ranger XP utility vehicle. The engine is a 21kW Perkins 403C-11, three cylinder diesel engine. The clutch is a Warner Electric CMS Clutch Part Number 5218-84. The transmission is a custom-made hydromechanical transmission that will be described in further detail, while the differential is a BMW E34 differential with a final drive ratio of 3.45.

The standalone transmission is shown in Fig. 2.3. The transmission consists of four internal sections comprised of mounting plates, casings, bearings, shafts, gears, spacers, keys, o-ring cord, and a planetary gearset. The remaining components external to the transmission are two Bosch Rexroth 28cc A6VE Variable Plug-In Motor bent-axis hydraulic units and one Eaton 22.5cc Series 26 gear pump hydraulic unit Model 26008-LZB, along with their respective mounting assemblies.

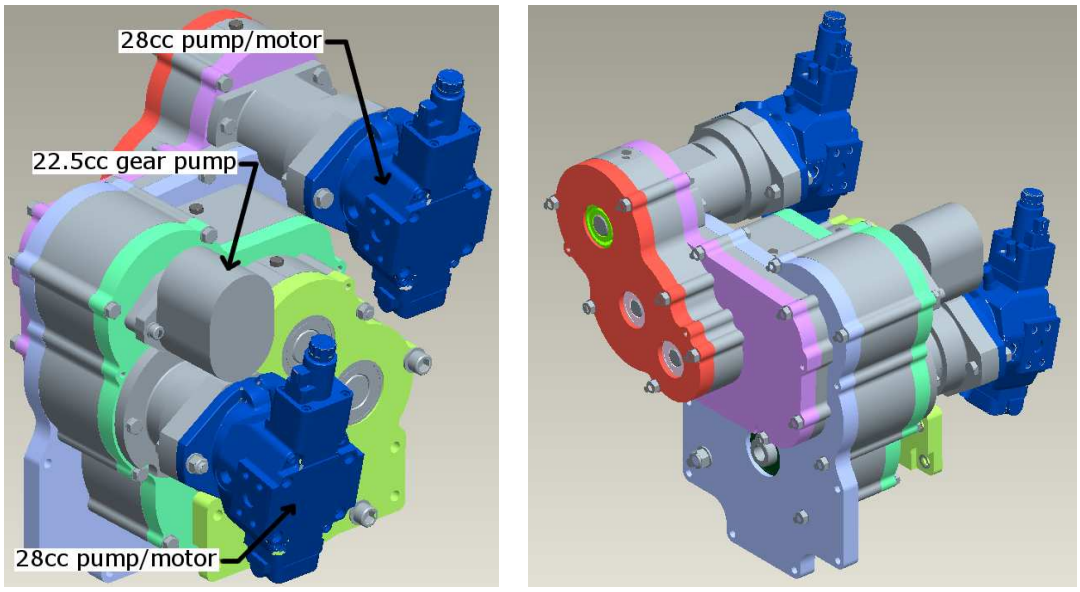

(a) (b)

Figure 2.3: Standalone transmission from (a) left-rear view and (b) left-front view.

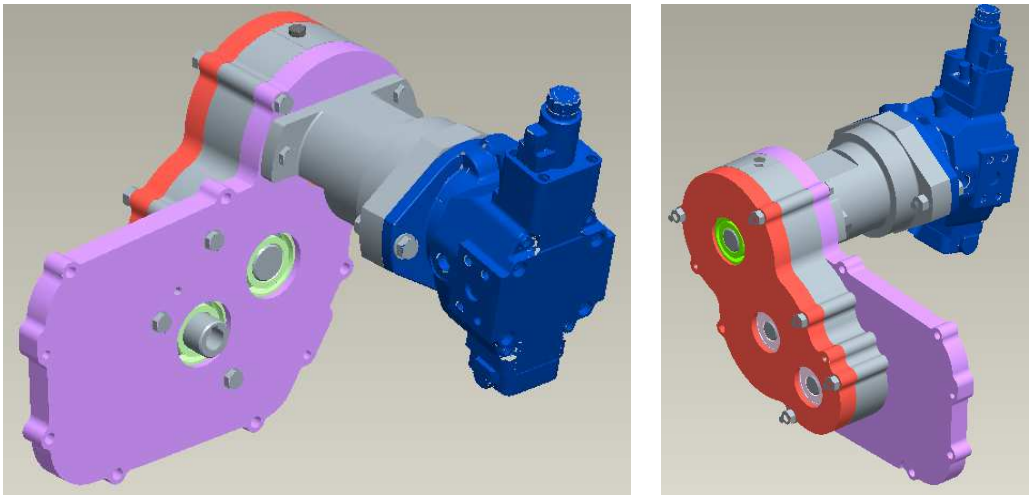

(a) (b)

Figure 2.4: *Section 1* of transmission with *speeder* hydraulic unit from (a) left-rear view and (b) left-front view.

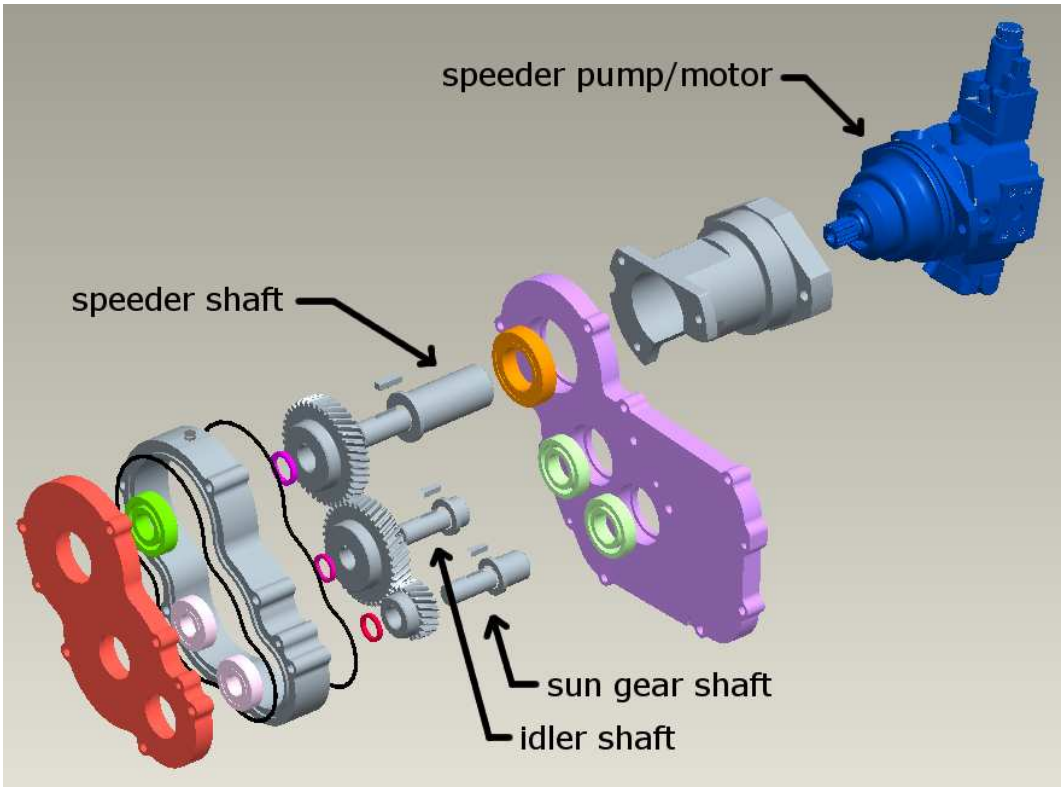

Figure 2.5: Transmission: *Section 1.* Exploded view.

Figures 2.4 and 2.5 show a standalone *Section 1* of the transmission and *Section 1* in an exploded view, respectively. Also included in the figures is the *speeder* hydraulic unit. *Section 1* of the transmission contains a series of three helical gears used to transmit power between the *speeder* hydraulic unit in *Section 1* and the planetary gearset in *Section 3*. The gearing in *Section 1* also is configured to alter torques and speeds from the hydraulic unit to the planetary gearset. The gears establish a 2:1 torque ratio from the hydraulic unit to the planetary gearset. Each gear is mounted on its own shaft and fixed in relation to the shaft circumferentially by a key, and axially by a spacer and shaft shoulder. The shafts are supported by a set of bearings on each side of the gears. The axial position of the shafts is determined by contact between the axial bearing face and shoulders on the shaft. The bearings are positioned in pockets machined into the section support plates. The gearing is enclosed by a shell casing that interfaces with the two section support plates. Between the interface of the shell casing and section support plates, an o-ring cord is compressed in a groove to seal the section from leaking its internal oil. The supporting plates and casing are held together with multiple bolts and precisely positioned using two dowel pins in each support plate. Threaded oil ports are included at the top and bottom of the casing to allow for filling and draining of the internal oil. The *speeder* hydraulic unit interfaces with one of the shafts through a spline connection. The hydraulic unit is positioned by mounting hardware that is supported from one of the support plates.

Section 2 of the transmission is shown in Figs. 2.6 and 2.7. *Section 2* functions as a go-between between *Section 1* and *Section 3*. The only shaft in *Section 2* is the shaft that interfaces on one end with the sun gear of the planetary gearset in *Section 3* and on the other end with the shaft supporting one of the gears in *Section 1*. The other main components of *Section 2* are the support plates that are shared with *Sections 1* and *3*, the shell casing, and the bearings mounted in the support plates. The shell casing interfaces with the two support plates in a similar manner as in *Section 1*. None of the bearings in the two support plates directly support any component within *Section 2*. Instead, the bearings support the various shafts and components in *Sections 1* and *3*. Because no gears are included in this section, oil is not needed in the case of this section. Between the interface of the shell casing and section support plates, an o-ring cord is compressed in a groove to seal the section from leaking oil that reaches the section due

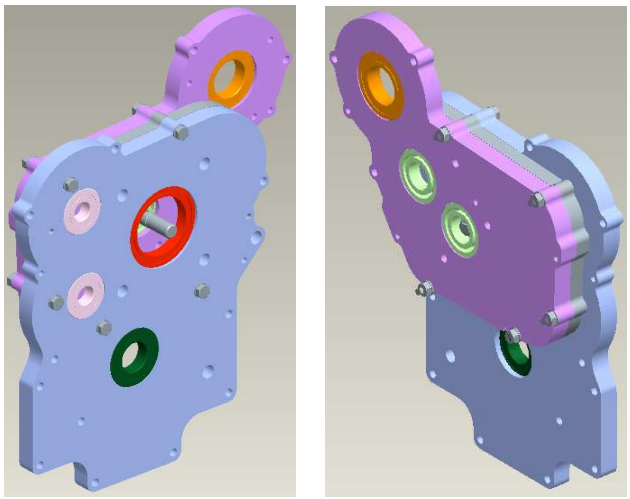

(a) (b)

Figure 2.6: *Section 2* of transmission from (a) left-rear view and (b) left-front view.

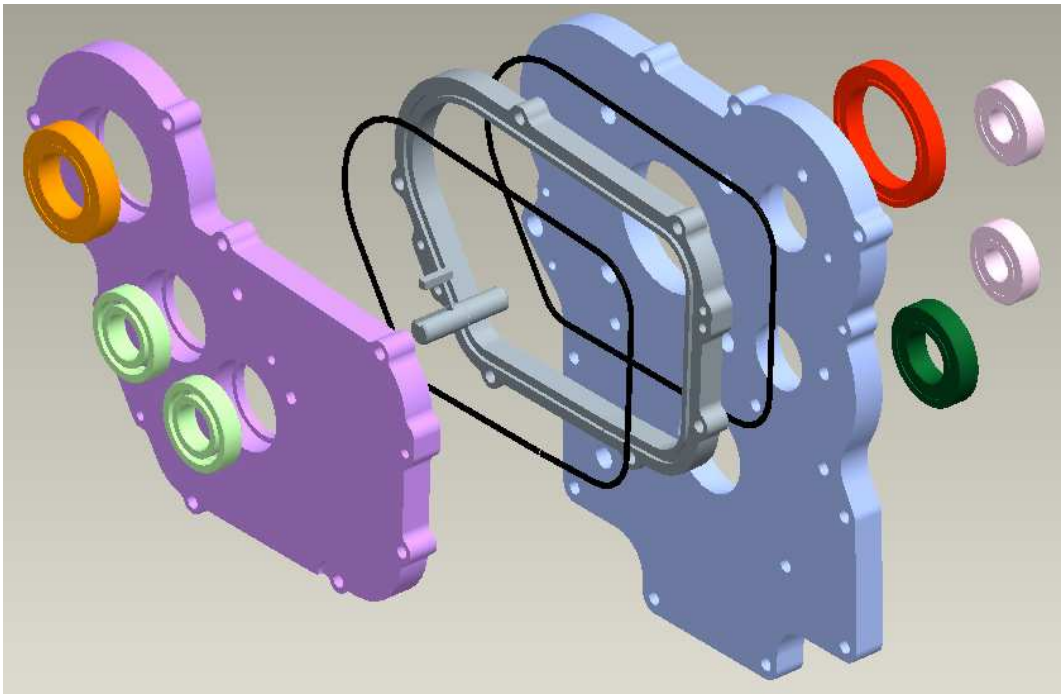

Figure 2.7: Transmission: *Section 2*. Exploded view.

to any internal leakage through the bearings.

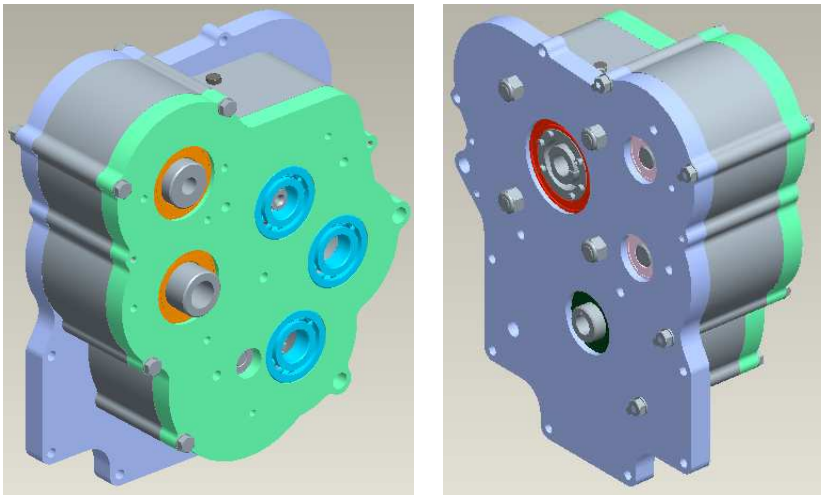

(a) (b)

Figure 2.8: *Section 3* of transmission from (a) left-rear view and (b) left-front view.

Section 3 of the transmission is shown in Figs. 2.8 and 2.9. *Section 3* is the section where the power from the engine and hydraulic components is combined. *Section 3* contains a series of gears and shafts that interface with the engine, interface with the *torquer* hydraulic unit, interface with the charge pump, and interface with the planetary gearset. The gear ratios of the gearing are determined as explained in subsequent chapters. The engine shaft is the main input to this section. It is externally connected to the clutch, mounted on the engine. The shaft is supported on both ends by bearings in the two *Section 3* support plates. The shaft is positioned axially with shaft shoulders that interface with the support bearings. The gear on the shaft meshes with a gear on the *torquer* shaft. The shaft transmits torque to the gear through a key. The gear is positioned axially by a shaft shoulder on one side and a spacer on the other side. The *torquer* shaft is supported on two bearings, one mounted in each support plate. The axial positioning is again maintained by shaft shoulders interfacing with the support plate bearings. Torque transmission between the shaft and gear is again carried through a shaft key. The axial position of the gear is maintained with a shaft shoulder on one side and spacers on the other side. The *torquer* shaft and gear transmit the combined torque from the engine and the *torquer* hydraulic unit to both the charge

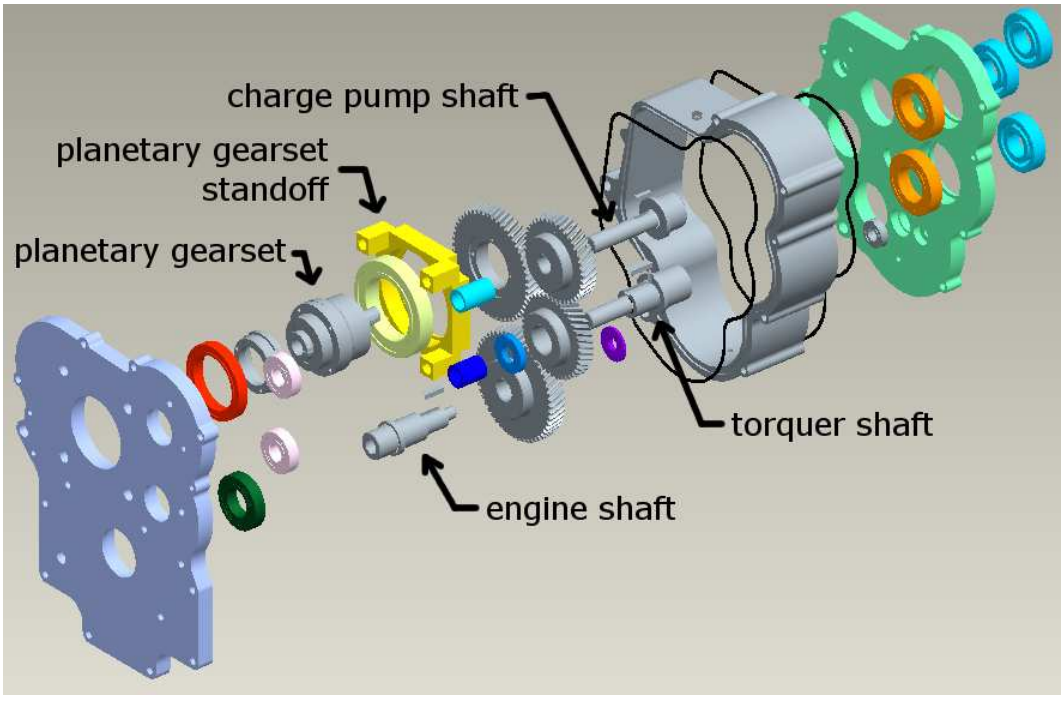

Figure 2.9: Transmission: *Section 3*. Exploded view.

pump shaft, and a gear bolted to the ring of the planetary gearset. The charge pump shaft is supported on each end by a bearing in each support plate. The axial position of the shaft is maintained through the use of shaft shoulders interfacing with the support plate bearings. The gear on the shaft transmits its power to the shaft through a key. The position of the gear is maintained by a shaft shoulder and a spacer.

Arguably the most important component of the transmission is the planetary gearset. Power from the hydraulic pump/motors and engine is combined within this component. The planetary gearset is its own standalone component that is fit within the transmission. The main components of the planetary gearset are the ring, sun, and planet gears. In the planetary gearset used in the transmission, the ring gear is affixed to the casing of the planetary gearset. This has the effect of coupling the rotation of the ring gear with anything that is attached to the casing. The sun gear is accessed through a shaft coupling on one end, while the planet carrier is accessed though an external shaft and key on the other end. On one end of the planetary gearset, a spacer component is bolted to the housing. The planetary gearset is supported by a bearing on both ends, one end on its housing and the other end on the spacer component. Permitting the rotation of the housing, through the mounting of the planetary gearset on bearings, allows for ring gear rotation, because the ring gear is rigidly attached to the housing. One bearing is mounted in one of the support plates. The other bearing is mounted in a standoff component. The standoff component is bolted to the support plate. This arrangement fixes the axial position of the planetary gearset, effectively clamping the planetary gearset into position.

The gear that meshes with the *torquer* shaft gear is attached with bolts to one end of the planetary gearset housing. This allows for the power from the engine and *torquer* hydraulic unit to connect with the ring gear of the planetary gearset. The *Section 2* shaft, that transmits power from *Section 1* and its *speeder* hydraulic unit, interfaces with the sun gear of the planetary gearset by way of a clamp within the planetary gearset assembly. This connection allows for the power from the *speeder* hydraulic unit to pass through the planetary gearset. The power from the sun and ring inputs is combined to provide a planet carrier output which is fed to *Section 4*. The shell casing of *Section 3* interfaces with the two support plates in a similar manner as in *Section 1*. An o-ring cord is compressed in a groove on each end of the casing to seal the section from leaking

oil.

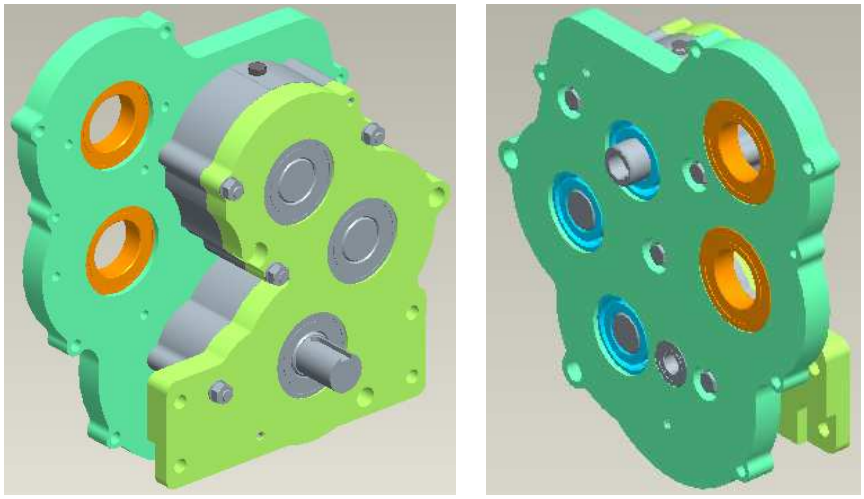

(a) (b)

Figure 2.10: *Section 4* of transmission from (a) left-rear view and (b) left-front view.

Section 4 of the transmission is shown in Figs. 2.10 and 2.11. *Section 4* of the transmission is used to position the output shaft of the transmission to be in-line with the rear differential. *Section 4* contains a series of gears transferring power between the planet carrier output of *Section 3* and the rear-end differential. The input to output gear ratio in *Section 4* is one to one because no further ratio change was needed to achieve the optimal design. The section contains three steel helical gears on shafts. The power is transmitted from the gears to the shafts by way of individual shaft keys. Each shaft and gear combination also has a spacer component on the shaft. The shafts are supported on each end by bearings mounted in the two support plates. Axial alignment of the shafts and gears are maintained by contact between a shaft shoulder and bearing face on one side, and contact between a spacer and bearing on the other side. The power is transmitted to and from the section on both sides by mating shafts with a key, the planet carrier shaft of the planetary gearset on one side and a coupler connecting to the rear-end differential on the other side. The internal components are encased in an aluminum shell casing that interfaces with the two support plates. At these two interfaces, an o-ring cord is compressed in a groove in the ends of the shell casing. This o-ring cord is used to contain the lubricating oil within the transmission case.

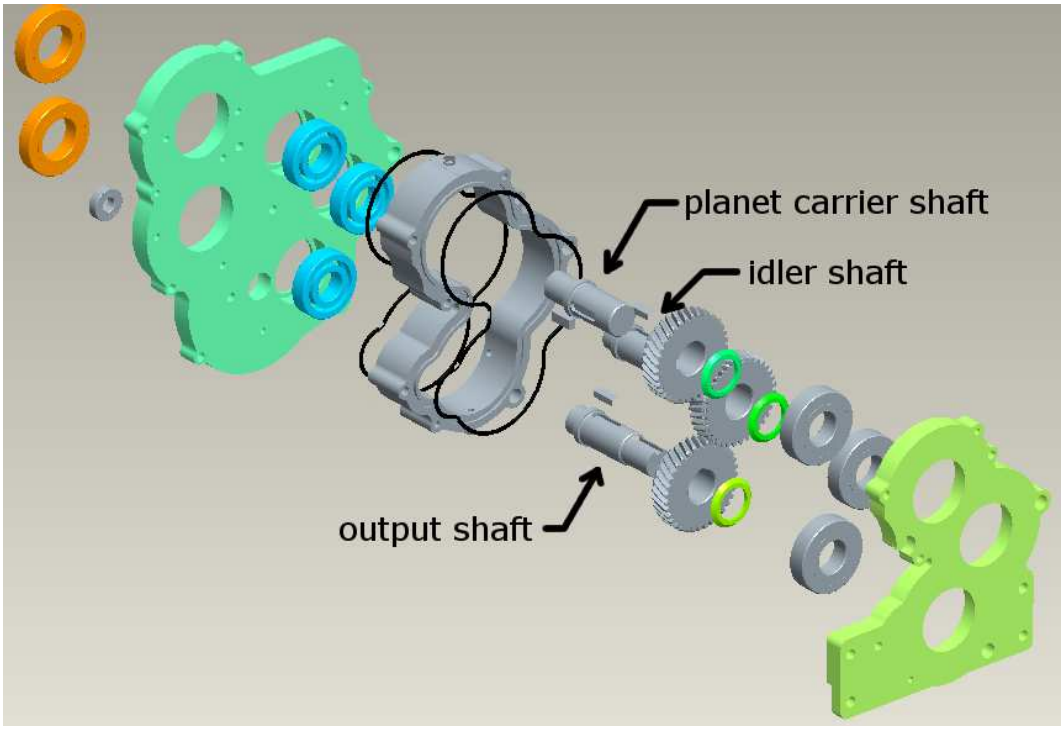

Figure 2.11: Transmission: *Section 4*. Exploded view.

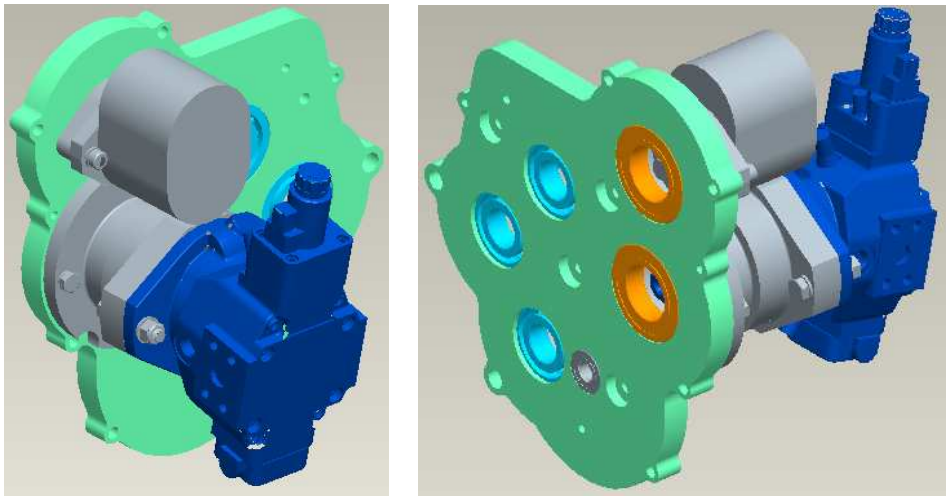

(a) (b)

Figure 2.12: "Torquer" Hydraulic Unit Section from (a) left-rear view and (b) left-front view.

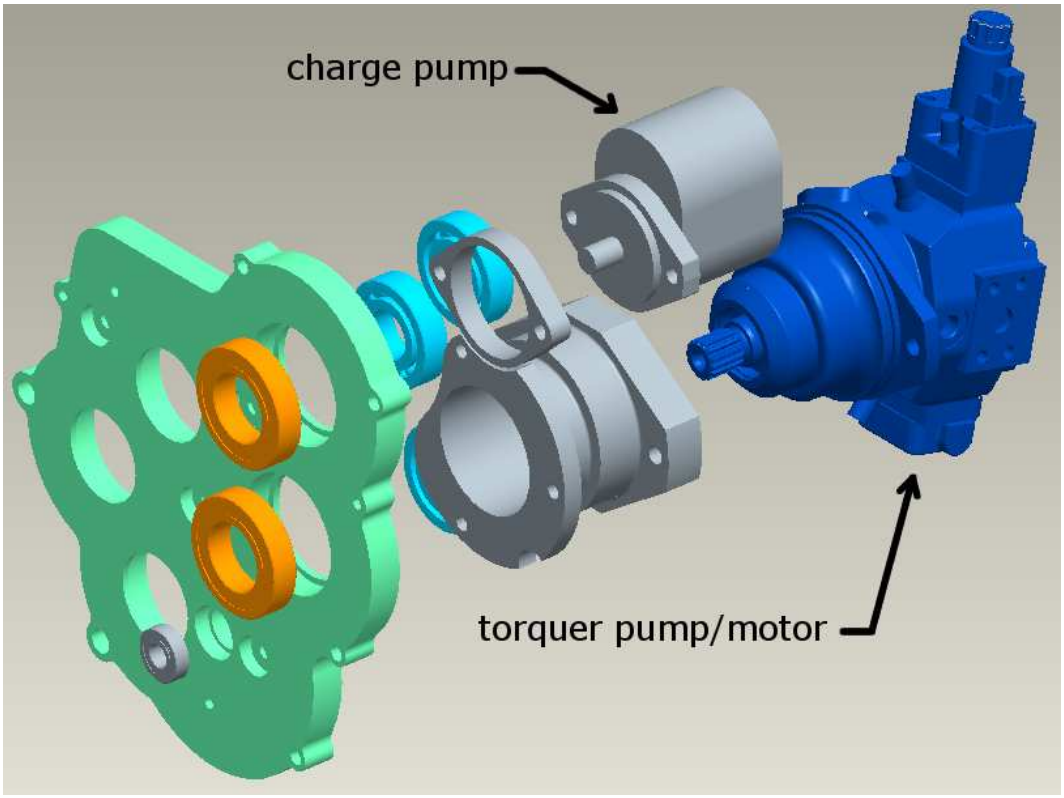

Figure 2.13: Exploded view with *torquer* hydraulic unit and charge pump.

Also externally attached to one of the support plates of *Section 3* is the *torquer* hydraulic unit assembly and the charge pump assembly. These components are shown in Figs. 2.12 and 2.13. Both hydraulic units are positioned with mounting brackets that attach to the support plate. An external spline is present on each shaft of the hydraulic units and mates with an internal spine on the corresponding shafts in *Section 3*.

Chapter 3

Design Optimization and Configuration

In this chapter, the transmission operation modes are described. In addition, the component optimization and architecture selection are presented.

3.1 Transmission Operating Principles

The hydromechanical transmission configuration that is used to visualize the operating modes as well as used for the optimization is shown in Fig. 3.1. This configuration is similar to the transmission architecture prior to the redesign. The output shaft of the engine is connected to a clutch. The torque and speed of this component is labeled as T_{eng} and ω_{eng}, respectively. The shaft continues on the output of the clutch with two elements on it. The first element is a toothed pulley; it is labeled as having N_1 teeth. The second element is a gear; it is labeled as having N_6 teeth. The torque that is transmitted to the shaft from the toothed pulley is labeled as T_b and its speed as ω_b. The toothed pulley interfaces with another toothed pulley on the shaft of P/M T by means of a belt. This toothed pulley has N_2 teeth and transmits a torque of T_{PMT} at a speed of ω_{PMT}. The gear element, the one with N_6 teeth, has a torque of T_a, speed of ω_a, and meshes with a gear with N_5 teeth. The gear with N_5 teeth shares a common shaft with the chain sprocket with N_7 teeth. While N_5 and N_6 are shown as bevel gears, this is for convenience in drawing the schematic compactly: they were

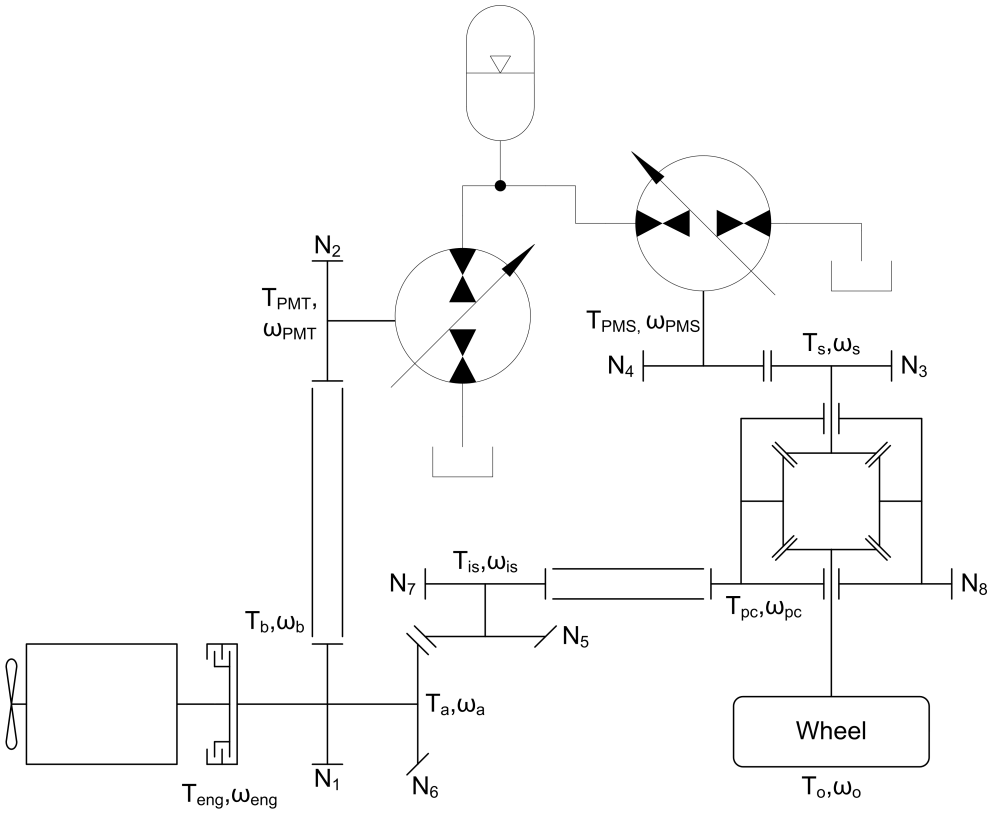

Figure 3.1: Initially Proposed HMT Configuration. Note the N_3/N_4 gear connection shown is analyzed as a belt/chain connection.

actually implemented as a gearbox. The common torque and speed of the gear and chain sprocket is T_{is} and ω_{is}, respectively. The N_7 toothed sprocket meshes, by way of a chain, with the N_8 toothed sprocket that carries a torque of T_{pc} at a speed of ω_{pc}. The N_8 toothed sprocket is connected to the carrier of a planetary gearset differential and rotates the housing about the output shaft to the wheel. The shaft of P/M S is connected to a gear with N_4 teeth. The torque transmitted through the N_4 toothed gear is T_{PMS} at a speed of ω_{PMS}. The gear meshes with another gear having N_3 teeth and transmitting a torque of T_s at speed ω_s. The N_3 toothed gear shares a shaft with the sun gear shaft of the planetary gearset differential. The second sun gear shaft of the planetary gearset differential is connected to the wheel and transmits a torque of T_o at a speed of ω_o.

The following subsections describe the engine and hydraulic units' operating modes. The derivation of these equations can be found in Appendix C.

3.1.1 HMT mode

The drive cycle torque and speed requirements determine the way in which the drivetrain components operate. P/M S always has a direct torque relationship with the wheel output torque as can be seen in equation 3.1.

$$T_{PMS} = -\frac{N_4}{N_3} T_o \tag{3.1}$$

Because there is this fixed relationship, the only remaining choice for P/M S operation is the speed at which it operates as shown in equation 3.2.

$$\omega_{PMS} = \frac{N_3}{N_4}\left(2\frac{N_6}{N_5}\frac{N_7}{N_8}\omega_{eng} - \omega_o\right) \tag{3.2}$$

For a given accumulator pressure, the torque required by equation 3.1 is achieved by setting the displacement of P/M S. Once the displacement is set, and the speed is determined from equation 3.2, a corresponding oil flow volume can be calculated from the pump models.

In HMT mode, the engine can operate at varying speeds and torques. At each operating condition, a volume of fuel used is calculated from the model of the engine. By dividing the distance traveled in the drive cycle by the volume of fuel consumed over the drive cycle, a fuel economy value can be determined. By allowing the engine

to operate at varying speeds and torques, two more variables are introduced into the operation of the system, ω_{eng} and T_{eng}.

The remaining operational characteristic to be determined is the torque supplied by or taken from the driveshaft by P/M T, shown in equation 3.3.

$$T_{PMT} = \frac{N_2}{N_1}\left(2\frac{N_6}{N_5}\frac{N_7}{N_8}T_o - T_{eng}\right) \tag{3.3}$$

The speed of P/M T is a fixed ratio of the speed of the engine, related by equation 3.4.

$$\omega_{PMT} = \frac{N_1}{N_2}\omega_{eng} \tag{3.4}$$

The torque that remains on the driveshaft and travels to the planetary gearset differential is a fixed ratio of the drive cycle torque required at the wheels, seen in equation 3.5.

$$T_a = 2\frac{N_6}{N_5}\frac{N_7}{N_8}T_o \tag{3.5}$$

Because of this, the power supplied to or taken from the driveshaft by P/M T is determined by the deficit or excess from the engine operation. As a result, P/M T operation, and corresponding oil flow volume, is dependent on the engine operation.

3.1.2 S-only mode

In S-only mode, all of the power to propel the vehicle is supplied by P/M S; the torque and speed of P/M S are a fixed ratio of that required at the wheels, as can be seen in equations 3.1 and 3.2 when $\omega_{eng} = 0$. P/M T operates in a hydraulically locked-up manner by using an on/off valve to prevent flow from passing through the hydraulic unit. The result is that the torque required from the engine shaft input into the planetary gearset is available. The clutch is disengaged, thereby isolating the engine from the rest of the system, so the engine is assumed to be off, consuming no fuel.

3.1.3 T-only mode

T-only mode is similar to that of S-only mode except for the P/M roles are swapped. In T-only mode, all of the power to propel the vehicle is supplied by P/M T. P/M S is hydraulically locked-up while the engine is still disengaged from the system and off. The torque relation between the drive cycle and P/M T can be seen in equation 3.3 with

$T_{eng} = 0$. The speed of P/M T is determined from equation 3.2 by setting $\omega_{PMS} = 0$ and $\omega_{eng} = \frac{N_2}{N_1}\omega_{PMT}$, resulting in

$$\omega_{PMT} = \frac{1}{2}\frac{N_1}{N_2}\frac{N_5}{N_6}\frac{N_8}{N_7}\omega_o \tag{3.6}$$

3.1.4 Parallel mode

Parallel mode is similar to T-only mode; the difference between the modes is that the clutch is engaged and the engine supplies power to the system in Parallel mode. Because the drive cycle torque and speed requirements dictate the torque and speed of the engine shaft, the engine and P/M T need to coordinate to supply the correct amount of torque at the necessary speed. Because the engine shaft speed is a fixed ratio of the drive cycle speed (equation 3.6 still holds), the only free variable becomes the engine torque (which in turn dictates the P/M T torque), as seen in equation 3.3.

3.2 Optimization Method and Simulation

The following section describes the optimization inputs used. Additionally, the procedure to define the hydraulic unit models used in the optimization is presented. Finally, the optimized ratios for the original configuration are presented.

To obtain a fuel economy that is not biased higher nor lower by using stored energy, it is necessary that the oil volume in the accumulator at the beginning of the drive cycle match the oil volume at the end of the drive cycle. This is due to the energy stored in the accumulator being directly related to the volume of oil in the accumulator. In each four-mode operating point, the corresponding accumulator energy and fuel usage are determined.

To reduce the number of variables in the simulation and speed the simulation time, some variables are fixed in the various modes. In all of the modes, the pressure is held at a constant. In the actual operation of the vehicle, the pressure would obviously vary, because the accumulator is not infinitely large. Maintaining a constant low accumulator pressure (near low, precharge levels) in the optimization would provide the assurance that the P/Ms are sized large enough to drive through the drive cycle.

In the HMT mode, the engine speed and torque are fixed at approximately the

most efficient point of the engine map, $T_{eng} = 70$ Nm and $\omega_{eng} = 2600$ rpm. By doing this, the resulting speeds and torques of both P/M T and P/M S are calculated from equations 3.1, 3.2, 3.3, and 3.4 for each drive cycle timestep. In Parallel mode, the engine is allowed to vary in speed (it must be allowed to because it is a fixed ratio of the wheel speed) and operates at a constant torque of $T_{eng} = 70$ Nm. This in turn determines the torque and speed at which P/M T must operate from equations 3.3 and 3.4. In S-only mode and T-only mode, no further variable choices exist to be removed. For each mode only two degrees of freedom exist, the wheel speed and wheel torque. As a result, the wheel torque and speed at individual timesteps of the drive cycle determine the operating conditions of the various components within the system.

For each timestep, the fuel consumed along with the amount of energy removed from or inserted into the accumulator is determined. Using Lagrange optimization, a maximum fuel economy can be found subject to the condition that the accumulator oil volume, and thus stored energy, at the beginning and end of the drive cycle be nearly identical. This optimization is done by calculating the energy losses in all modes, at all timesteps, and minimizing the fuel usage while constraining the net accumulator charge to be zero. The final optimized transmission gear ratios and scaled P/M sizes are then determined using the Nelder-Mead algorithm to maximize fuel economy[2].

The optimization process can be summarized as:

1. Initialize the gear ratios ($\frac{N_2}{N_1}$, $\frac{N_5}{N_6}\frac{N_8}{N_7}$, $\frac{N_3}{N_4}$) and pump/motor sizes.

2. Calculate the losses in each mode for every timestep in the drive cycle.

3. Check HMT mode driveability at every timestep with a positive wheel torque.

4. For every combination of modes, find the combination of modes that maximizes λ while minimizing the losses in:

$$\int_{drivecycle} \left(Loss_{mode}\left(\omega_o(t), T_o(t), P\right) + \lambda * PQ_{acc}\left(modes, t\right)\right) \mathrm{d}t \qquad (3.7)$$

   where $Loss_{mode}$ is the energy loss of a mode at a timestep: $T_{loss} * \omega + Q_{loss} * P$, Q_{acc} is the net flow to the accumulator, and λ is the Lagrange multiplier.

5. Evaluate the fuel economy for the mode combination.

6. Iterate the gear ratio and pump/motor sizes until a maximum fuel economy is achieved.

The MATLAB code used to simulate and optimize the drivetrain is available in Appendix A.

3.2.1 Pump Models

To account for efficiency losses present in the hydraulic pump/motors, a pump/motor model needed to be developed. The models were developed from the efficiency data provided for varying torques and speeds of the pump/motor units. Specifically, the Rexroth A6VE bent axis unit and Rexroth A10VG unit were investigated. The needed output from these models were the shaft torque, hydraulic flow, torque loss, flow loss, and overall efficiency, using the inputs of rotation speed, pressure, unit displacement, volumetric efficiency, and mechanical efficiency. Also desired in the pump model is the ability to reduce the losses by a factor, so that the effect of using higher efficiency pumps can be assessed. As a result, this is also an input to the calculation of the desired outputs.

For motoring conditions, the shaft torque, hydraulic flow, torque loss, flow loss, and overall efficiency, can be calculated, respectively, as

$$T = \left(1 - \left(1 - \eta_m\left(P, x, \omega\right)\right) f\right) xDP \tag{3.8}$$

$$Q = -\left(1 + \left(\frac{1}{\eta_v\left(P, x, \omega\right)} - 1\right) f\right) xD\omega \tag{3.9}$$

$$T_{loss} = \left(1 - \eta_m\left(P, x, \omega\right)\right) xDPf \tag{3.10}$$

$$Q_{loss} = \left(\frac{1}{\eta_v\left(P, x, \omega\right)} - 1\right) xD\omega f \tag{3.11}$$

$$\eta = \left(1 - \left(1 - \eta_v\left(P, x, \omega\right)\right) f\right)\left(1 - \left(1 - \eta_m\left(P, x, \omega\right)\right) f\right) \tag{3.12}$$

where $\eta_m\left(P, x, \omega\right)$ is the mechanical efficiency, $\eta_v\left(P, x, \omega\right)$ is the volumetric efficiency, D is the maximum pump/motor displacement, x is the fractional displacement command, P is the hydraulic pressure, ω is the shaft rotational speed, and f is the loss scale factor.

For pumping conditions, the shaft torque, hydraulic flow, torque loss, flow loss, and overall efficiency, can be calculated, respectively, as

$$T = \left(1 + \left(\frac{1}{\eta_m\left(P, x, \omega\right)} - 1\right) f\right) xDP \tag{3.13}$$

$$Q = -\left(1 - \left(1 - \eta_v\left(P, x, \omega\right)\right) f\right) xD\omega \tag{3.14}$$

$$T_{loss} = -\left(\frac{1}{\eta_m\left(P, x, \omega\right)} - 1\right) xDPf \tag{3.15}$$

$$Q_{loss} = -\left(1 - \eta_v\left(P, x, \omega\right)\right) xD\omega f \tag{3.16}$$

$$\eta = \left(1 - \left(1 - \eta_v\left(P, x, \omega\right)\right) f\right)\left(1 - \left(1 - \eta_m\left(P, x, \omega\right)\right) f\right) \tag{3.17}$$

where x, the fractional displacement command, is of opposite sign.

The mechanical efficiencies and volumetric efficiencies for the hydraulic units under investigation were supplied by the manufacturer in tables for discrete pressures, speeds, and displacements.

The MATLAB code used to generate the pump/motor models is available in Appendix B.

3.2.2 Optimization Results

After running the optimization over a combined UDDS and highway cycle with a fixed pressure of 1950 psi and utilizing the A6VE pump model, the optimized parameters obtained are $\frac{N_2}{N_1} = 0.99$, $\frac{N_5}{N_6}\frac{N_8}{N_7} = 8.06$, $\frac{N_3}{N_4} = 8.33$, *torquer* P/M size of 26.9 cc, and *speeder* P/M size of 28.1 cc. These ratios yield a fuel economy of 78.5 miles per gallon (mpg) for the urban cycle, and 56.2 mpg for the highway cycle. With these gear ratios, a design can be set for the configuration shown in Fig. 3.1.

3.3 Transformation

This section will discuss the process that occurs to take the optimized ratios and transform them to other configurations.

Configuration	Carrier	Sun	Ring
1	Differential	Engine	P/M S
2	Differential	P/M S	Engine
3	Engine	P/M S	Differential
4	Engine	Differential	P/M S
5	P/M S	Differential	Engine
6	P/M S	Engine	Differential

Table 3.1: Component connection to planetary gearset by configuration.

From the ratios obtained in the Lagrange optimization for the configuration shown in Fig. 3.1, a transformation can occur to obtain ratios for the configurations shown in Appendix D. These configurations maintain the input-coupled nature of the original configuration, but reconfigure the transmission to use a traditional planetary gearset configuration while also transitioning the final output drive to a stock automotive differential. The differences between Configurations 1-6 in Appendix D are summarized in table 3.1, showing which drivetrain component is connected to the parts of the planetary gearset.

Because only three gear ratios are present in the original configuration while five are present in the transformed configurations, two of the ratios can be design choices. This is possible because the speed and torque of the three driving components, the engine, *torquer* P/M, and *speeder* P/M, can all independently relate to the required wheel speed and torque. This allows maximum flexibility in the gear ratio optimization. The two ratios chosen as design choices were r_{plan}, the ratio of sun speed to planet carrier speed when the ring of the planetary gearset is held constant, and ratio $\frac{N_5}{N_6}$, the ratio of engine speed to planetary gearset ring speed. Choosing r_{plan} was done to permit the planetary gearset to be chosen as an off-the-shelf component, where fixed gear ratios are available. Using the transformation equations derived in Appendix D, the transformed ratios are calculated and are presented in table 3.2 for select choices. All of these ratios preserve the optimized fuel economy from the original configuration.

The results of the transformation are interesting. It is desirable for final drive ratio, R_{fd}, to be something similar to an off the shelf component in the 3 to 4 range, and the $\frac{N_3}{N_4}$ ratio, the gear ratio on P/M S, to be something in the 0.5 to 2 range to limit extreme ratios. Configuration 2 fits these requirements with an R_{fd} of 3.22 and an $\frac{N_3}{N_4}$

Configuration	R_{fd}	r_{plan}	$\frac{N_3}{N_4}$	$\frac{N_5}{N_6}$
1	0.81	5	-8.27	-
2	3.22	5	-0.52	1
3	5.04	5	0.41	1
4	20.14	5	1.65	-
5	-16.11	5	2.58	1
6	-1.01	5	10.34	1

Table 3.2: Transformed optimized ratios

ratio of -0.52. Configuration 2 is shown in Fig. 3.2 as a repeat of Fig. 2.1.

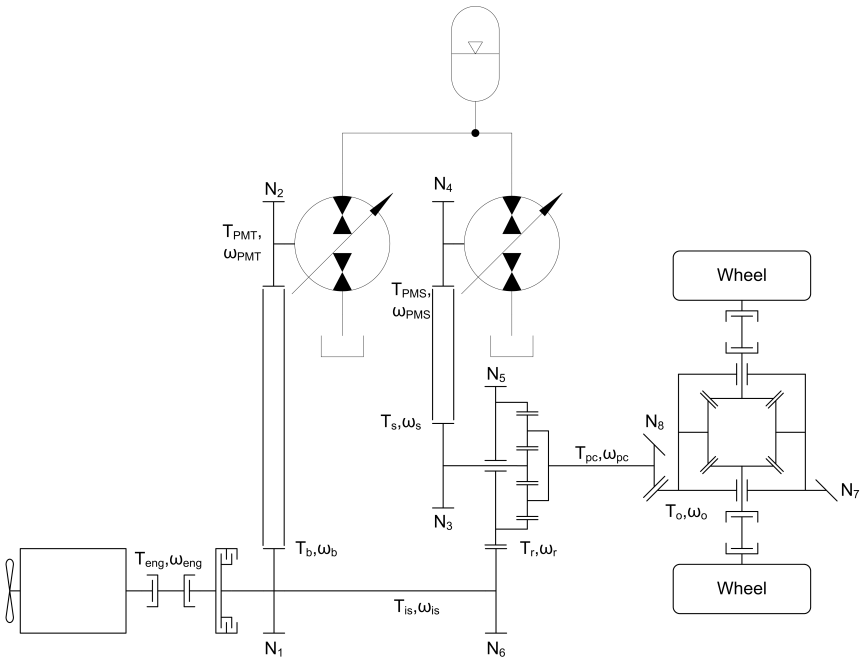

Figure 3.2: Redesigned HMT Configuration

Obtaining a final drive ratio of 3.22 from a stock automotive differential would be difficult, so a compromise needs to occur. For the automobile differential, a BMW E34 differential with a final drive ratio of 3.45 was chosen. For the remaining gear ratios, $\frac{N_3}{N_4}$ is taken to be -0.5 and $\frac{N_1}{N_2}$ is taken as 1.3 to satisfy zero to sixty mph time requirements of eight seconds.[1] For the torquer P/M and speeder P/M, a stock P/M size of 28.1cc

[1] This was calculated assuming acceleration at constant torque starting from zero speed with a fully

maximum displacement were used for each. Deviating from the optimal ratios in the build caused the simulated urban cycle fuel economy to drop from 78.5 mpg to 75.6 mpg and the highway cycle fuel economy to drop from 56.2 mpg to 53.6 mpg.

Optimum modes in which the vehicle will operate for the constructed transmission can be seen in Fig. 3.3. This plot also overlays the yellow UDDS drive cycle wheel torque versus wheel speed and the white highway drive cycle wheel torque versus wheel speed.

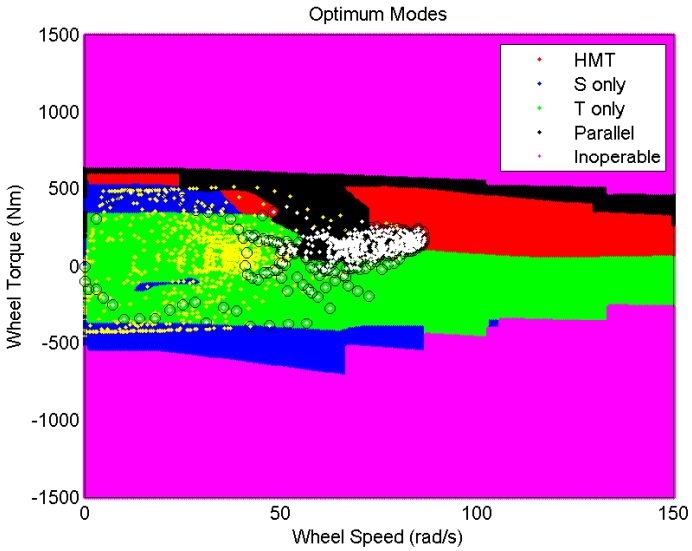

Figure 3.3: Optimal operating modes at 1950 psi.

The operating speeds of P/M S and P/M T during the optimized operation of the constructed transmission are visible in Figs. 3.4 and 3.5. The color variation of the points in the plots signify the different modes of operation. From these figures it becomes apparent that the operation of the transmission is important from a physical standpoint. Because it would be impossible to operate the transmission by switching modes every second, the fuel economy presented would be an upper bound on what could be achieved.

---

charged 345 bar (5000 psi) 38L accumulator with a 120 bar (1700 psi) precharge. The accumulator pressure was allowed to vary in this simulation.

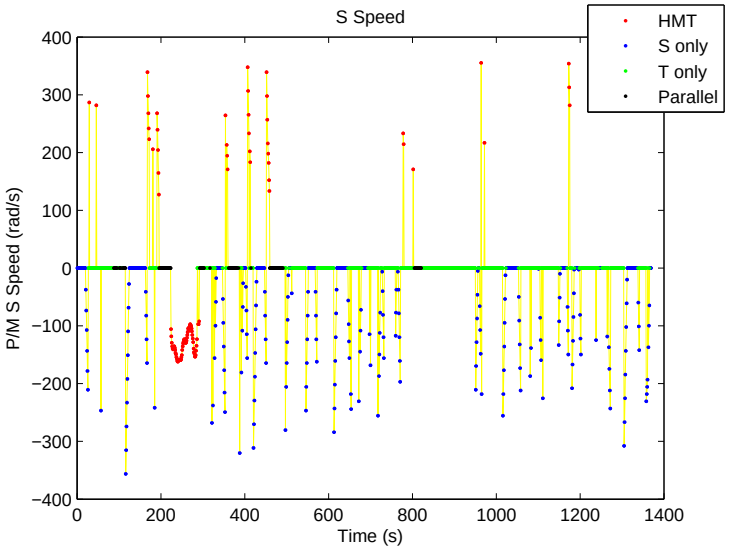

Figure 3.4: P/M S speed over the urban drive cycle.

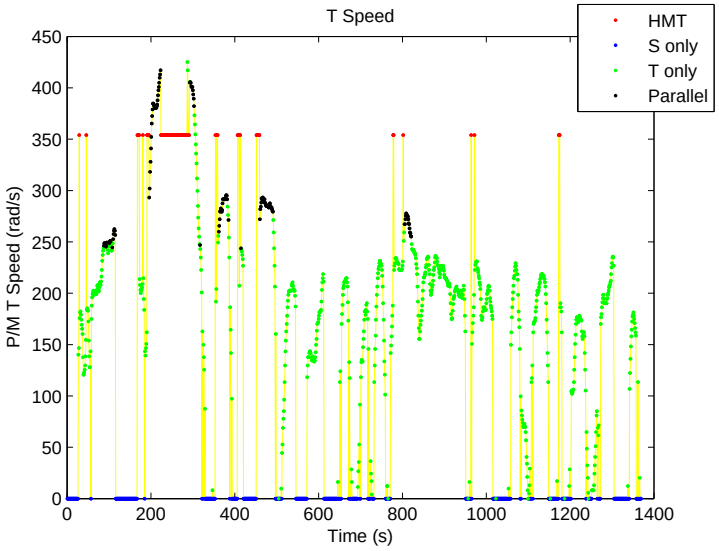

Figure 3.5: P/M T speed over the urban drive cycle.

Chapter 4

Component Sizing Methods

This chapter discusses the machine design analysis used to design the transmission described in the optimization procedure. Section 4.1 describes the approach used for determining the size of the gears within the transmission. Section 4.2 discusses the fatigue evaluation of the transmission shafts. Section 4.3 describes the bearing life evaluation while section 4.4 briefly mentions the miscellaneous considerations required. The example cases shown herein are those of the worst-stressed parts under worst case loading conditions.

4.1 Gear Sizing

With the gear ratios determined from the optimization, the specific size of the gears, that is the module, within the assembly needs to be determined. To determine the feasibility of different available gearing, the tooth bending strength from ANSI/AGMA 2101-D04: Fundamental Rating Factors and Calculation Methods for Involute Spur and Helical Gear Teeth[20] is used.

The sizing method relates the fundamental bending stress to the allowable bending stress as shown in eqn. (4.1):

$$\sigma_F \leq \frac{\sigma_{FP} Y_N}{S_F Y_\theta Y_Z} \tag{4.1}$$

where σ_F is the bending stress, σ_{FP} is the allowable bending stress, Y_N is the stress cycle factor for bending strength, S_F is the safety factor for bending strength, Y_θ is the

temperature factor, and Y_Z is the reliability factor.

To determine the bending stress, σ_F, eqn. (4.2) is used:

$$\sigma_F = F_t K_o K_v K_s \frac{1}{b m_t} \frac{K_H K_B}{Y_J} \tag{4.2}$$

where F_t is the transmitted tangential load, K_o is the overload factor, K_v is the dynamic factor, K_s is the size factor, b is the net face width, m_t is the transverse metric module, K_H is the load distribution factor, K_B is the rim thickness factor, and Y_J is the geometry factor.

To determine the various factors, tables and charts within the standard are used. Because of a desire to use off-the-shelf components, stock helical gears from catalogs were selected for use.

The following serves as an example gear set evaluation to determine feasibility for use in *Section 4* of the transmission, shown in Fig. 2.11. These gears have a transverse metric module of 3mm, a net face width of 25mm, and an operating pitch diameter of 105mm.

To determine the transmitted tangential load, F_t, eqn. (4.3) is used:

$$F_t = 2000 \frac{T}{d_{w1}} \tag{4.3}$$

where d_{w1} is the operating pitch diameter, T is the maximum transmitted torque, and the factor 2000 is used to convert from millimeters to meters and diameter to radius.

In the case of the example gear mesh, the torque is 326 Nm and the pitch diameter is 105 mm, so the transmitted tangential load is 6210 N.

As stated in the ANSI/AGMA standard, the overload factor, K_o, accounts for momentary force overloads above 200% of the nominal transmitted tangential load. The standard also states that "overload factors can only be established after considerable field experience is gained in a particular application." Given that this is a novel transmission design that does not have field experience, and the fact that the torque used for evaluation is the maximum torque expected in the transmission use cycle, an overload factor of unity is used.

The dynamic factor, K_v, can be calculated from empirically generated eqn. (4.4):

$$K_v = \left(\frac{C}{C + \sqrt{196.85 v_t}} \right)^B \tag{4.4}$$

where

$$C = 50 + 56\,(1.0 - B) \tag{4.5}$$

$$B = 0.25\,(A_v - 5.0)^{0.667} \tag{4.6}$$

and where A_v is related to the transmission accuracy grade number and v_t is the pitchline velocity of the gears.

For the example gear mesh, the A_v value was chosen as 8 because gears with ground teeth were used, but the mesh did not fall within the "Very Accurate Gearing" regime. The pitchline velocity was taken as 15.70 m/s, determined from the maximum wheel speed in the evaluation drivecycle. Solving eqn. (4.4) for the example, K_v is 1.33 from

$$K_v = \left(\frac{76.88}{76.88 + \sqrt{196.85 * 15.70}} \right)^{0.52} = 1.33 \tag{4.7}$$

The size factor, K_s, takes into account non-uniformity of the gear material properties. The selected gears are made of steel with induction hardened teeth. A size factor of unity is appropriate for this material.

The load distribution factor, K_H, takes into account the non-uniformity in loading across the tooth face. K_H, for relatively stiff gearing mounted between bearings, is determined by eqn. (4.8):

$$K_H = 1.0 + K_{Hmc}\,(K_{Hpf} K_{Hpm} + K_{Hma} K_{He}) \tag{4.8}$$

where K_{Hmc} is the lead correction factor, K_{Hpf} is the pinion proportion factor, K_{Hpm} is the pinion proportion modifier, K_{Hma} is the mesh alignment factor, and K_{He} is the mesh alignment correction factor.

For gearing with unmodified leads, the lead correction factor, K_{Hmc}, is unity. The

pinion proportion factor, K_{Hpf}, accounts for pinion deflection due to load and is determined by eqn. (4.9) when the net face width is less than or equal to 25mm.

$$K_{Hpf} = \frac{b}{10d_{w1}} - 0.025 \tag{4.9}$$

When the quantity $\frac{b}{10d_{w1}}$ is lower than 0.05, K_{Hpf} is taken as 0.025. For the example gearing, $\frac{b}{10d_{w1}} = \frac{25}{10*105} = 0.024 < 0.05$, so the pinion proportion factor is 0.025.

K_{Hpm} is determined from the axial position of the gear on its shaft. Because none of the gears in the transmission are mounted within the center 35% of the supported shaft length, the more conservative pinion proportion modifier of 1.1 is used.

The mesh alignment factor, K_{Hma}, accounts for axial misalignment of the gear shafts. K_{Hma} for open gearing, the worst case scenario, is given in eqn. (4.10).

$$K_{Hma} = 0.247 + 0.657(10)^{-3}b - 1.186(10)^{-7}b^2 \tag{4.10}$$

For the example, the mesh alignment factor is 0.26 from:

$$K_{Hma} = 0.247 + 0.657(10)^{-3}25 - 1.186(10)^{-7}25^2 \tag{4.11}$$

The mesh alignment correction factor, K_{He}, takes into account any post-assembly process to improve mesh alignment. For the case where no adjustment occurs, the mesh alignment correction factor is unity.

In summary, the load distribution factor for the example gearing, determined using eqn. (4.8) is:

$$K_H = 1.0 + 1\,(0.025 * 1.1 + 0.26 * 1) = 1.29 \tag{4.12}$$

The rim thickness factor, K_B, takes into account the strength of the gear rim as it relates to the overall gear strength. The backup ratio, m_B, is calculated as the ratio of the whole depth of the gear teeth to the rim thickness. For $m_B < 1.2$, K_B is calculated from eqn. (4.13).

$$K_B = 1.6 \ln\left(\frac{2.242}{m_B}\right) \tag{4.13}$$

For $m_B > 1.2$, the rim thickness factor is unity.

For the example where the rim thickness is 36.5 mm and the whole depth is 6.5 mm, $m_B = \frac{36.5}{6.5} = 5.62 > 1.2$. The result is that the rim thickness factor is unity.

The final factor to be determined in eqn. (4.2) is the geometry factor, Y_J. The geometry factor is determined by reading the values off a series of charts[21, pg. 741] taking into account the number of teeth in each gear, and the helix angle of the gears. For the example, the geometry factor is determined to be 0.54.

In conclusion, the bending stress can now be calculated using eqn. (4.2):

$$\sigma_F = 6210 * 1 * 1.33 * 1 \frac{1}{25 * 3} \frac{1.29 * 1}{0.54} = 263 \text{ MPa} \tag{4.14}$$

The σ_F value then needs to be compared to the allowable bending stress number and factors shown in the right-hand-side of eqn. (4.1).

The example gear is fabricated from a grade 1 steel with an induction hardened surface. From the ANSI/AGMA standard, the allowable bending stress, σ_{FP}, for this material is 310 MPa. The stress cycle factor, Y_N, is unity for 10^7 cycles at full power. The safety factor for bending, S_F, is chosen as 1.15 due to the use of assumed maximum load for 100% of the time. The temperature factor, Y_θ, is unity for temperatures less than $120°C$. The reliability factor, Y_Z, is unity for 99% reliability.

Solving eqn. (4.1) with the allowable bending stress and factors results in

$$263 \text{ MPa} \leq \frac{310 * 1}{1.15 * 1 * 1} = 270 \text{ MPa} \tag{4.15}$$

This result shows that the gearing is expected to hold up to the expected loads, even under continuous full power conditions.

4.2 Shaft Sizing

The driving loads calculated to pass through the transmission gears is the basis for determining the shaft sizes. To solve for the fatigue factor of safety due to the stresses within the shafts, the loads and shaft dimensions must be known. The following will serve as an example of determining the fatigue factor of safety for the shaft in *Section 2* of the transmission, shown in Fig. 2.7.

The shaft in this example is loaded purely in a torsional manner. This purely torsional loading is a unique case within the transmission, but due to the small diameter

of the shaft and the large keyway present, this shaft presents the highest stress condition in the transmission. The maximum torque transmitted through the shaft is 65Nm. This torque has the potential to fully alternate as a worst case scenario. The nominal shear stress in the shaft is determined by eqn. (4.16) for a solid circular shaft[21, pg. 137]:

$$\tau_{xy} = \frac{16T}{\pi d^3} \tag{4.16}$$

where T is the fully alternating torque and d is the shaft diameter. For the example, τ_{xy} is calculated as 41.38 MPa.

For the pure shear case in this example, the shear stress is converted to an equivalent alternating von Mises normal stress, σ'_a, using the distortion energy theory[21, pg. 262]:

$$\sigma'_a = \sqrt{3}\tau_{xy} = 71.7 \text{ MPa} \tag{4.17}$$

The endurance limit for infinite fatigue life of a steel is estimated as[21, pg. 328]:

$$S_e = k_a k_b k_c k_d k_e k_f \left(0.504 S_{ut}\right) \tag{4.18}$$

where S_{ut} is the ultimate tensile strength of the shaft material, k_a is the surface condition modification factor, k_b is the size modification factor, k_c is the load modification factor, k_d is the temperature modification factor, k_e is the reliability factor, and k_f is the miscellaneous-effects factor.

The surface modification factor is calculated using eqn. (4.19), where a and b are constants dependent on the surface finishing method, and S_{ut} is the ultimate tensile strength in MPa.

$$k_a = a S_{ut}^b \tag{4.19}$$

For the example shaft, the shaft has a machined surface for which $a = 4.51$ and $b = -0.265$. The surface condition modification factor is calculated as 0.922 shown from

$$k_a = 4.51 * 400^{-0.265} = 0.922 \tag{4.20}$$

The size modification factor is calculated from eqn. (4.21).

$$k_b = \left(\frac{d}{0.00762}\right)^{-0.107} \tag{4.21}$$

For the example shaft, at the point of interest where the keyway stress concentration is present, the diameter is 0.020m, so the size modification factor is 0.902.

The load modification factor takes into account the type of loading and its effect on the endurance limit and how it relates to the ultimate tensile strength. If all stresses are converted to the von Mises equivalent stresses, then the load modification factor, k_c, is unity.

The temperature modification factor accounts for the change in tensile strength as it relates to a variation in temperature from room temperature conditions. The factor comes from a curve fit to strength data for steel at varying temperatures. The data shows an increase in strength at slightly varying temperatures up to 150°C, but then falls off. For the temperatures expected in the example transmission shaft, the temperature modification factor, k_d, is taken as 1.010.

The reliability factor takes into account the statistical variation of measured endurance strengths. For the example case and a 99% reliability, the reliability factor, k_e is 0.814.

The miscellaneous-effects factor is used to take into account any other factors that may alter the endurance limit. For the example shaft, the miscellaneous-effects factor, k_f, is taken as unity.

In summary, the endurance limit for the example shaft is:

$$S_e = 0.922 * 0.902 * 1 * 1.010 * 0.814 * 1 * 0.504 * 400 = 137.8 \text{ MPa} \tag{4.22}$$

The keyway in the shaft introduces a stress concentration. The fatigue stress concentration factor, K_f, is read from a table[22, pg. 700] and is dependent on the type of keyway, loading situation, and Brinell Hardness Number of the material.

For the example shaft, the keyway is endmilled, loaded in torsion, and has a Brinell Hardness Number of 116, resulting in a fatigue stress concentration factor, K_f, of 1.3.

The fatigue factor of safety, n, is calculated using eqn. (4.23).

$$n = \frac{S_e}{K_f \sigma'_a} \tag{4.23}$$

For the example shaft, the fatigue factor of safety is calculated as 1.48 shown from

$$n = \frac{137.8}{1.3 * 71.67} = 1.48 \tag{4.24}$$

With a factor of safety above unity, while using the worst case conditions of fully reversible torque at maximum load, the shaft is expected to have infinite life.

4.3 Bearing Sizing

To determine the bearing sizes needed, an L_{10} life of at least approximately 4000 hours under full load was desired. At the intermittent loads seen within the transmission, the bearing life is expected to be significantly longer due to the calculations using 100% max load condiditons. The initial size of bearing selected was one which minimized the steps within the shaft, followed by the requirement that the bearing fit within the space available.

Using the tangential load determined from the gear sizing process, the radial and axial load can be determined as shown in eqns. (4.25) and (4.26), respectively:

$$F_r = F_t \tan(\phi_t) \tag{4.25}$$

$$F_a = F_t tan(\psi) \tag{4.26}$$

where F_r is the radial force, ϕ_t is the transverse pressure angle of the helical gear, F_a is the axial force, and ψ is the helix angle of the helical gear.

Because the shafts are supported by two bearings, the load will be divided between the two bearings. Due to the nature of the helical gear alternating direction based on transmission operation, and thus alternating axial load direction, the load on the bearing is simplified to be equivalent to all of the load from the gear when driven in either direction at maximum torque. This approach places the full load on each individual bearing and has the effect of underestimating the life of the bearing, resulting in a

conservative design. To first determine the L_{10} life, the dynamic equivalent radial load, P_r, is determined by the greater of

$$P_r = F_r \tag{4.27}$$

and

$$P_r = 0.56F_r + Y_1F_a \tag{4.28}$$

where Y_1 is the axial load factor found in the vendor catalog[23, pg. A30]. With the P_r value determined, the L_{10} life can be calculated by

$$L_{10} = \left(\frac{C_e}{P_r}\right)^3 \left(\frac{10^6}{60n}\right) \tag{4.29}$$

where C_e is the extended dynamic load rating of the bearing and n is the bearing rotation speed in revolutions per minute.

As an example, consider one of the bearings supporting the shaft connected to the engine input. The candidate bearing being evaluated is a Timken ball bearing, part number 202K. This bearing has an extended dynamic load rating of 8650 N and maximally operates at a speed of 3000 rpm. The maximum tangential load on the gear which it supports is 900 N. The transverse pressure angle of the helical gear is 20°. Using eqn. (4.25), the radial force can be computed as

$$F_r = 900tan(20^\circ) = 328 \text{ N} \tag{4.30}$$

The helix angle of the gear is 21.5°. Using eqn. (4.26), the axial force can be computed as

$$F_a = 900tan(21.5^\circ) = 355 \text{ N} \tag{4.31}$$

Using the axial loading information, the axial load factor, Y_1 , is determined to be 1.48. The dynamic equivalent radial load, P_r, is then found as the greater of eqns. (4.27) and (4.28).

$$P_r = 328 \text{ N} \tag{4.32}$$

and

$$P_r = 0.56 * 328 + 1.48 * 355 = 708 \text{ N} \tag{4.33}$$

The dynamic equivalent radial load is taken as 708 N. The L_{10} life is calculated by using eqn. (4.29) as

$$L_{10} = \left(\frac{8650}{708}\right)^3 \left(\frac{10^6}{60 * 3000}\right) = 10126 \text{ hr} \tag{4.34}$$

With a calculated L_{10} life of 10126 hr, the bearing is expected to meet the demands of the transmission loads.

4.4 Overall Sizing

Consideration of component location within the overall assembly was also required. Limited space was present between the engine and the differential, constraining the axial length of the transmission. Additionally, vehicle frame members constrained the location of the hydraulic units. The sole purpose of the idler gears in *Sections 1* and *4* of the transmission, shown in Figs. 2.5 and 2.11, respectively, was to avoid interference between the *speeder* hydraulic unit and casing, and to align the output shaft of the transmission with the differential. Gear positioning also took place to align the transmission input with the engine shaft along with avoiding chassis frame members. Furthermore, o-ring glands and bearing bores were specified to manufacturer standards.

Chapter 5

Conclusion and Discussion

5.1 Review

An overview of the design of a four-mode, input-coupled, power-split hydromechanical transmission with energy storage has been presented. In chapter 2, a four-mode operating principle is presented to permit functioning as a power-split, parallel, and multiple series hybrid. The four-mode transmission architecture was optimized in chapter 3 using the Lagrange multiplier method with regards to fuel economy and the resulting design was defined. Additionally, examples of machine design calculations used to size components within the transmission were provided in chapter 4.

5.2 Contributions

The work presented utilized a different optimization strategy than previous works. Additionally, the four-mode architecture with energy storage increased the flexibility of operation from that seen in other works, thereby increasing attainable fuel economy over a single-mode architecture. Finally, the work presented went beyond just the theory of the design and specified the components from which the transmission was constructed.

The original transmission configuration compared with the new transmission is shown in Fig. 5.1. The transmission has a more compact design that also addresses the chain and belt weaknesses in the original transmission. Furthermore, the reduced

transmission footprint is achieved through the use of bent-axis hydraulic units properly sized for the vehicle requirements.

5.3 Future Work

Future work on the transmission design continues within the Center for Compact and Efficient Fluid Power (CCEFP) Engineering Research Center at the University of Minnesota. Further experimental efficiency mapping of the transmission, along with automotive control design and testing, is ongoing. The addition of gear efficiency to the simulation will also improve the model for experimental validation. On the hardware side, the addition of seals on external bearings is suggested to reduce oil leakage. Also, the modular design of the hydraulic units on the transmission will allow for further improvements in efficiency as hydraulic components improve. While the efficiency of bent axis pump/motors is good, evolving piston-by-piston control pump/motors would be even better. Additionally, improved accumulator, valving, and hose technologies are also feasible improvements to increase efficiency. This work will demonstrate and highlight the discoveries emerging within the CCEFP.

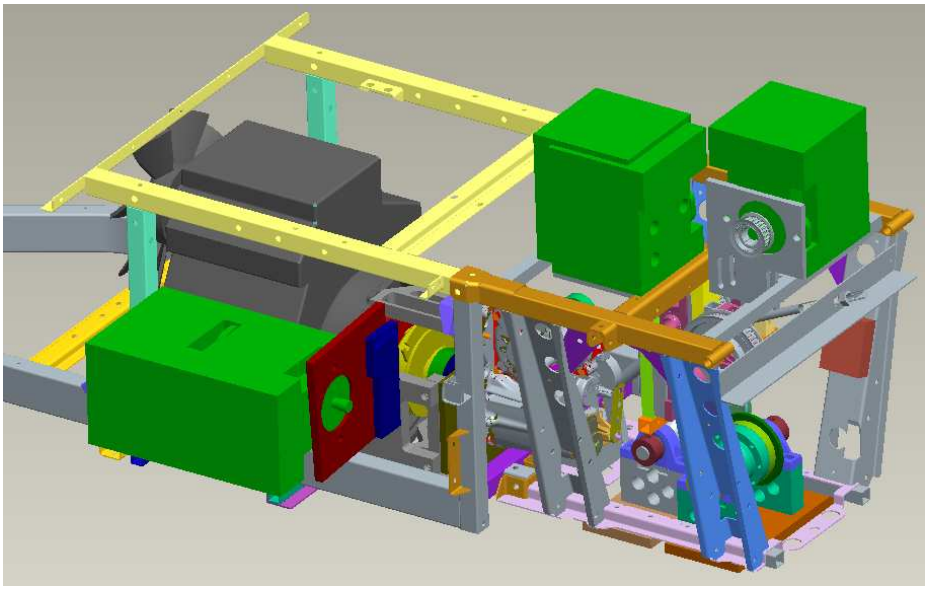

(a)

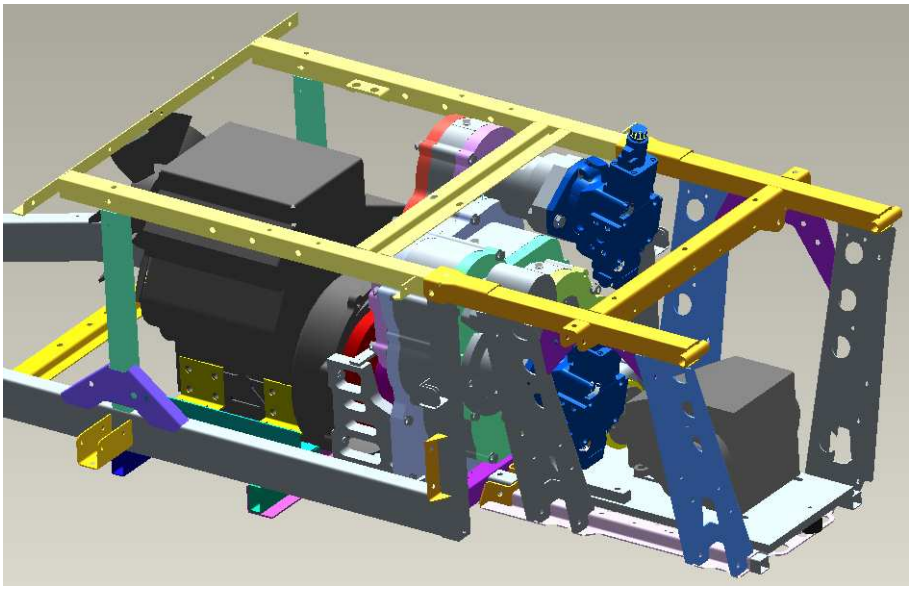

(b)

Figure 5.1: Comparison of the transmission in the (a) original configuration and (b) new configuration.

References

[1] J.D. Wishart. *Modelling, Simulation, Testing, and Optimization of Advanced Hybrid Vehicle Powertrains*. PhD thesis, University of Victoria, 2008.

[2] K.L. Cheong, P.Y. Li, S. Sedler, and T.R. Chase. Comparison between input coupled and output coupled power-split configurations in hybrid vehicles. In *IFPE Conference Proceedings*, pages 243–52, 2011.

[3] K.L. Cheong, P.Y. Li, and T.R. Chase. Optimal design of power-split transmissions for hydraulic hybrid passenger vehicles. In *2011 American Control Conference*, 2011.

[4] D. Sung, S. Hwang, and H. Kim. Design of hydromechanical transmission using network analysis. *Proceedings of the Institution of Mechanical Engineers, Part D (Journal of Automobile Engineering)*, 219:53–63, 2005.

[5] S. S. Volpe, G. Carbone, M. Napolitano, and E. Sedoni. Design optimization of input and output coupled power split infinitely variable transmissions. *Journal of Mechanical Design*, 131:111002, 2009.

[6] L. W. Tsai and G. Schultz. A motor-integrated parallel hybrid transmission. *Transactions of the ASME. Journal of Mechanical Design*, 126:889–94, 2004.

[7] Y. Zhang, H. Lin, B. Zhang, and C. Mi. Performance modeling and optimization of a novel multi-mode hybrid powertrain. *Transactions of the ASME. Journal of Mechanical Design*, 128:79–89, 2006.

[8] J. Van de Ven, M. Olson, and P.Y. Li. Development of a hydro-mechanical hydraulic hybrid drive train with independent wheel torque control for an urban passenger vehicle. In *IFPE Conference Proceedings*, 2008.

[9] M.W. Olson. A comparison of hydraulic hybrid vehicle architectures. Master's thesis, University of Minnesota, September 2009.

[10] P.Y. Li and F. Mensing. Optimization and control of hydro-mechanical transmission based hydraulic hybrid passenger vehicle. In *Proceedings of the 7th International fluid Power Conference (IFK)*, 2010.

[11] T.P. Sim and P.Y. Li. Analysis and control design of a hydro-mechanical hydraulic hybrid passenger vehicle. In *Proceedings of the ASME 2009 Dynamic Systems and Control Conference*, 2009.

[12] F.B. Mensing. A hierarchical control strategy for hybrid vehicles. Master's thesis, University of Minnesota, July 2010.

[13] K. Muta, M. Yamazaki, , and J. Tokieda. Development of new-generation hybrid system ths ii - drastic improvement of power performance and fuel economy. In *SAE Technical Paper 2004-01-0064*, March 2004.

[14] F. Bottiglione and G. Mantriota. Mg-ivt: an infinitely variable transmission with optimal power flows. *Journal of Mechanical Design*, 130:112603, 2008.

[15] F.G. Benitez, J.M. Madrigal, and J.M. del Castillo. Infinitely variable transmission of racheting drive type based on one-way clutches. *Journal of Mechanical Design*, 126:673–82, 2004.

[16] O.S. Cretu and R.P. Glovnea. Constant power continuously variable transmission (cp-cvt): Operating principle and analysis. *Journal of Mechanical Design*, 127:114–9, 2005.

[17] C.H. Hsu and R.H. Huang. Design of parallel-connected epicyclic-type automatic transmissions with two fundamental geared entities. *Journal of Automobile Engineering*, 222:371–81, 2008.

[18] J. Seo and S.J. Yi. Design of an automatic transmission system having an arbitrary power flow using the automatic power flow generation algorithm. *Journal of Automobile Engineering*, 219:1085–97, 2005.

[19] F.L. Litvin, D. Vecchiato, A. Demenego, E. Karedes, B. Hansen, and R. Handschuh. Design of one stage planetary gear train with improved conditions of load distribution and reduced transmission errors. *Journal of Mechanical Design*, 124:745–52, 2002.

[20] American Gear Manufacturers Association. *ANSI/AGMA 2104-D04: Fundamental Rating Factors and Calculation Methods for Involute Spur and Helical Gear Teeth.* ANSI/AGMA Standard Series. American Gear Manufacturers Association, 2004.

[21] J.E. Shigley, C.R. Mischke, and R.G. Budynas. *Mechanical Engineering Design.* McGraw Hill, 7th edition, 2004.

[22] R.C. Juvinall and K.M. Marshek. *Fundamentals of Machine Component Design.* John Wiley and Sons, Inc., 4th edition, 2006.

[23] The Timken Company. *Timken Products Catalog*, 2008.

Appendix A

Transmission Optimization Code

```
function [neg_mpg,modelist,TOTAL,ACC,v,J,ll,WSlist,xs,WTlist,xt,...
    Tengine,Wengine,lam]=onesize_ngear_perkins_newpump(params,...
    goplot,weight);
global total_loss P_acc urban hway urban_hway

rpm=2*pi/60;            %rad/s
psi=6894.75729;           %Pa
miles=1609.344;         %meters

cyc=urban_hway;
N=length(cyc.time);
Nurban=length(urban.time);

modes=['HMT1  ';'E1only';'Bonly ';'Parall']'; % HMT 1 gear, 1 E-ratio

P_acc=[]; total_loss=[]; WSlist=[]; xs=[]; WTlist=[]; xt=[]; ...
    Tengine=[]; Wengine=[];
for mode=modes;
    [t_loss_mode,p_acc_mode,WSlist_mode,xs_mode,WTlist_mode,...
        xt_mode,Teng_mode,Weng_mode]=modeloss(mode',cyc,params,goplot);
    total_loss=[total_loss,t_loss_mode];
```

```
    P_acc=[P_acc,p_acc_mode(:)];
    WSlist=[WSlist,WSlist_mode(:)];
    xs=[xs,xs_mode(:)];
    WTlist=[WTlist,WTlist_mode(:)];
    xt=[xt,xt_mode(:)];
    Tengine=[Tengine,Teng_mode(:)];
    Wengine=[Wengine,Weng_mode(:)];
end;

% Make sure that it runs in HMT mode
% Modify this for different architectures (specify the HMT modes in
% first line, and other modes in 2nd).
ind=find(cyc.torque > 0 & isinf(min(total_loss(:,[1,1])')))';
total_loss(ind,[2,3,4])=inf;

TOTAL=total_loss;
ACC=P_acc;

if isfield(cyc,'name'),
    if cyc.name=='urban_hway';
    total_loss(1:Nurban,:)=weight*total_loss(1:Nurban,:);
    P_acc(1:Nurban,:)=weight*P_acc(1:Nurban,:);
    end;
end;

% Optimization
[ll,modelist,Power,lam,J]=cycle_opt(-2.7);
totalloss=sum(ll);
sumpower=sum(Power);
lam;

heatcap=38.6e6; %J/liter
```

```
miles=1609; %m
gallons=3.81; %liters
if isfield(cyc,'name'),
    if cyc.name=='urban_hway';
    work=sum(cyc.power(1:Nurban)*weight)+sum(cyc.power(Nurban+1:N));
    distance=cyc.distance(Nurban)*weight+(cyc.distance(N)...
        -cyc.distance(Nurban));
    end;
else
    distance=cyc.distance(N);
    work=sum(cyc.power);
end;
fuel=(totalloss+work)/(heatcap);
mpg=distance/fuel*gallons/miles
params
neg_mpg=-mpg;
lam;
v=[distance,fuel,totalloss,work];
%%%%%%%%%%%%%%%%%%%%%%%%%%%%%%%%%%%%
% Cycle optimization

function [ll,modelist,Power,lam,J]=cycle_opt(init_lam)
global total_loss P_acc
lam=fminsearch(@(lam) onestep_sizing_in(lam),init_lam);
J=total_loss'+lam*P_acc';

[ll,modelist]=min(J);
Power=choose(P_acc,modelist);

function chosen=choose(set,list)
[tdim,ldim]=size(set);
if (length(list(:))~=tdim || max(list) > ldim || min(list) < 1)
```

```
    disp('Error');
    return;
end;
chosen=set';
chosen=chosen([0:tdim-1]'*ldim+list(:));

function [t_loss_mode,p_acc_mode,WSlist_mode,xs_mode,...
    WTlist_mode,xt_mode,Teng_mode,Weng_mode]...
    =modeloss(mode,cyc,params,goplot)
global TT_S PP_S WW_S PPP_S XXX_S WWW_S XX2_S WW2_S Pclist_S w_S;
global TT_T PP_T WW_T PPP_T XXX_T WWW_T XX2_T WW2_T Pclist_T w_T;
global x;
global Tloss_S Qloss_S T_S Eloss_S Eff_S XX_S Q_S T1_S P_S;
global Tloss_T Qloss_T T_T Eloss_T Eff_T XX_T Q_T T1_T P_T;

% Modify parameter assignments according to the architecture being
% studied
R_B=params(1);
gears=params(2);

H_Reduct1=params(3);
H_Reduct2=params(3);
%%%%
Tfactor=1;%params(4);
Sfactor=1;%params(5);
%%%%

factor=1.0;
R_Reduct = 2.66;

rpm=2*pi/60;            %rad/s
psi=6894.75729;           %Pa
```

```
miles=1609.344;         %meters

if (all(mode=='HMT1  ') || all(mode=='E1only') )
    theH_Reduct=H_Reduct1;
else
    theH_Reduct=H_Reduct2;
end;

if (all(mode=='HMT1b ') || all(mode=='HMT2b ') ||...
        all(mode=='Bonlyb') || all(mode=='Para-b'))
    the_gear=gears(2);
else
    the_gear=gears(1);
end;

rat=R_Reduct*the_gear;
wc_cycle=cyc.w/2*rat/rpm; tc_cycle=2*cyc.torque/rat;

switch mode
    case {'HMT1  ','HMT2  ','HMT1b ','HMT2b '}
        Teng=70;
        Teng_mode(1:length(cyc.w),1)=Teng;
        Weng=2600*rpm;
        Weng_mode(1:length(cyc.w),1)=Weng;
        eff_e = 0.2929;
        eng_loss=(Teng.*Weng)*(1-eff_e)./(eff_e);%+eps);
        WElist=2/rat*theH_Reduct*(Weng-wc_cycle*rpm);
        WSlist_mode=WElist;
        TE=-cyc.torque/theH_Reduct; % Required E pump torque
        xe=interpn(T1_S,P_S,w_S,XX_S,TE/Sfactor,P_S(Pclist_S)...
            *ones(size(WElist)),WElist);
        xs_mode=xe;
```

```
% Apply brakes on E when exceeding pumping displacement
indbrake=find(xe.*sign(WElist)<-1);
xe(indbrake)=-sign(WElist(indbrake));

ind=find(abs(xe)<=1);

loss_E=inf(size(xe)); Q_E=nan(size(xe));
loss_E1=interpn(XX2_S,WW2_S,squeeze...
    (Eloss_S(Pclist_S,:,:)),xe(ind),WElist(ind))*Sfactor;
Q_E1=interpn(XX2_S,WW2_S,squeeze(Q_S(Pclist_S,:,:)),...
    xe(ind),WElist(ind))*Sfactor;
loss_E(ind)=loss_E1;
Q_E(ind)=Q_E1;
brakepumptorque=interp1(w_S,squeeze(T_S(Pclist_S,1,:)),...
    WElist(indbrake))*Sfactor;
loss_E(indbrake)=loss_E(indbrake)-(TE(indbrake)-...
    brakepumptorque).*WElist(indbrake);

TB=(tc_cycle-Teng)*R_B;
WB=Weng/R_B;
WTlist_mode(1:length(cyc.w),1)=WB;
xb=interpn(T1_T,P_T,w_T,XX_T,TB/Tfactor,P_T(Pclist_T),WB);
xt_mode=xb;
loss_B=inf(size(xb));
ind=find(abs(xb)<=1);
loss_B1=interpn(XX2_T,WW2_T,squeeze(Eloss_T(Pclist_T,...
    :,:)),xb(ind),WB)*Tfactor;
loss_B(ind)=loss_B1;
Q_B1=interpn(XX2_T,WW2_T,squeeze(Q_T(Pclist_T,:,:)),...
    xb(ind),WB)*Tfactor;
Q_B=nan(size(xb));
```

```
    Q_B(ind)=Q_B1;

    if goplot,
        if mode=='HMT1  ', figure(1); else figure(3); end;
        plot(wc_cycle,tc_cycle,'.',Weng/rpm,Teng,'rx');
        title([mode,': (Wmech, Tmech) ']);
        if mode=='HMT1  ', figure(2); else figure(4); end;
        subplot(211)
        plot3(abs(WElist),sign(WElist).*xe,loss_E,'.');
        grid on;
        title([mode,': Pump/Motor E energy loss']);
        xlabel('Speed - rad/s'); ylabel('Displacement');
        zlabel('Loss - W');
        subplot(212);
        plot(xb,loss_B,'.'); grid on;
        title([mode, ': Pump/Motor B energy loss']);
        xlabel('Displacement'); ylabel('Loss - W');
    end;

    t_loss_mode=eng_loss+(loss_B+loss_E);
    p_acc_mode = Q_B*P_T(Pclist_T)+Q_E*P_S(Pclist_S);

case {'E1only', 'E2only'}
    % Engine off (E only) mode
    WElist=-2/rat*theH_Reduct*wc_cycle*rpm;
    WSlist_mode=WElist;
    TE=-cyc.torque/theH_Reduct; % Required E pump torque
    xe=interpn(T1_S,P_S,w_S,XX_S,TE/Sfactor,P_S(Pclist_S)...
        *ones(size(WElist)),WElist);
    xs_mode=xe;

    % Apply brakes on E when exceeding pumping displacement
```

```
indbrake=find(xe.*sign(WElist)<-1);
xe(indbrake)=-sign(WElist(indbrake));

ind=find(abs(xe)<=1);
loss_E1=interpn(XX2_S,WW2_S,squeeze(Eloss_S(Pclist_S,...
    :,:)),xe(ind),WElist(ind))*Sfactor;
Q_E1=interpn(XX2_S,WW2_S,squeeze(Q_S(Pclist_S,:,:)),...
    xe(ind),WElist(ind))*Sfactor;
Q_E=nan(size(xe));
Q_E(ind)=Q_E1;
loss_E=inf(size(xe));
loss_E(ind)=loss_E1;
brakepumptorque=interp1(w_S,squeeze(T_S(Pclist_S,...
    1,:)),WElist(indbrake))*Sfactor;
loss_E(indbrake)=loss_E(indbrake)-(TE(indbrake)-...
    brakepumptorque).*WElist(indbrake);

if goplot,
    if mode=='E1only', figure(5); else figure(6); end;
    plot3(abs(WElist),sign(WElist).*xe,loss_E,'.');
    grid on;
    title([mode,': Pump/Motor E energy loss']);
    xlabel('Speed - rad/s'); ylabel('Displacement');
    zlabel('Loss - W');
end;

t_loss_mode=loss_E;
p_acc_mode=(Q_E)*P_S(Pclist_S);
WTlist_mode(1:length(cyc.w),1)=NaN;
xt_mode(1:length(cyc.w),1)=NaN;
Teng_mode(1:length(cyc.w),1)=NaN;
Weng_mode(1:length(cyc.w),1)=NaN;
```

```
case {'Bonly ','Bonlyb'}
    % Engine off (B only) mode
    WB=wc_cycle*rpm/R_B;
    WTlist_mode=WB;
    TB=(tc_cycle)*R_B;

    xb=interpn(T1_T,P_T,w_T,XX_T,TB/Tfactor,P_T(Pclist_T)...
        *ones(size(WB)),WB);
    xt_mode=xb;
    loss_B=inf(size(xb));
    ind=find(abs(xb)<=1);
    loss_B1=interpn(XX2_T,WW2_T,squeeze(Eloss_T(Pclist_T,...
        :,:)),xb(ind),WB(ind))*Tfactor;
    loss_B(ind)=loss_B1;
    Q_B1=interpn(XX2_T,WW2_T,squeeze(Q_T(Pclist_T,:,:)),...
        xb(ind),WB(ind))*Tfactor;
    Q_B=nan(size(xb));
    Q_B(ind)=Q_B1;

    t_loss_mode=loss_B;
    p_acc_mode=(Q_B)*P_T(Pclist_T);
    WSlist_mode(1:length(cyc.w),1)=NaN;
    xs_mode(1:length(cyc.w),1)=NaN;
    Teng_mode(1:length(cyc.w),1)=NaN;
    Weng_mode(1:length(cyc.w),1)=NaN;

    if goplot,
        figure(7);
        plot3(abs(WB),sign(WB).*xb,loss_B,'.'); grid on;
        title([mode,': Pump/Motor B energy loss']);
        xlabel('Speed - rad/s'); ylabel('Displacement');
```

```
        zlabel('Loss - W');
    end;

case {'Parall','Para-b'}
    % Engine on - parallel mode

    Weng=wc_cycle*rpm;
    Weng_mode=Weng;
    Teng=70;
    Teng_mode(1:length(cyc.w),1)=Teng;
    TB=(tc_cycle-Teng)*R_B;

    [eng_loss,eff_e]=engine_small(Teng*ones(size(Weng)),...
        Weng,'n',1);
    WB=Weng/R_B;
    WTlist_mode(1:length(cyc.w),1)=WB;
    xb=interpn(T1_T,P_T,w_T,XX_T,TB/Tfactor,P_T(Pclist_T)...
        *ones(size(WB)),WB);
    xt_mode=xb;
    loss_B=inf(size(xb));
    ind=find(abs(xb)<=1);
    loss_B1=interpn(XX2_T,WW2_T,squeeze(Eloss_T(Pclist_T,...
        :,:)),xb(ind),WB(ind))*Tfactor;
    loss_B(ind)=loss_B1;
    Q_B1=interpn(XX2_T,WW2_T,squeeze(Q_T(Pclist_T,:,:)),...
        xb(ind),WB(ind))*Tfactor;
    Q_B=nan(size(xb));
    Q_B(ind)=Q_B1;

    t_loss_mode=eng_loss+loss_B;
    p_acc_mode = Q_B*P_T(Pclist_T);
    WSlist_mode(1:length(cyc.w),1)=NaN;
```

```
        xs_mode(1:length(cyc.w),1)=NaN;

        if goplot,
            figure(8);
            plot3(abs(WB),sign(WB).*xb,loss_B,'.');
            grid on;
            title('Engine on - parallel: P/M B energy loss');
            xlabel('Speed - rad/s'); ylabel('Displacement');
            zlabel('Loss - W');
        end;
    otherwise,
        disp([mode, 'Error in modes']);
end

function [total]=onestep_sizing_in(lam)
global total_loss P_acc
[tdim,ldim]=size(total_loss);
J=total_loss'+lam*P_acc';
[ll,list]=min(J);
list1=[0:tdim-1]'*ldim+list';
Pchosen=P_acc';
Pchosen=Pchosen(list1);
total=-sum(ll);

function []=plotcycle_in(list,params,modes);

Bfactor=params(1);
R_B=params(2);
gears=params(3:4);
H_Reduct1=params(5);
H_Reduct2=params(6);
Efactor=params(7);
```

```
R_Reduct = 2.66;

rat1=R_Reduct*gears(1);
wc_cycle=cyc.w/2*rat1/rpm; tc_cycle=2*cyc.torque/rat1;

rat2=R_Reduct*gears(2);
wc_cycle=cyc.w/2*rat2/rpm; tc_cycle=2*cyc.torque/rat2;

colorlist=['g.';'go';'r*';'ro';'b.';'b*'];

figure(11); hold on;
for i=1:6,
    ind=find(list(1:1369)==i); [i,length(ind)],
    if ~isempty(ind), plot(wc_cycle(ind),tc_cycle(ind),...
            colorlist(i,:)); end;
end; hold off;

figure(12); hold on;
for i=1:6,
    ind=find(list==i & [1:N]>1369); [i,length(ind)],
    if ~isempty(ind), plot(wc_cycle(ind),tc_cycle(ind),...
            colorlist(i,:)); end;
end; hold off;
```

Appendix B

Pump/Motor Model Generation Code

```
function [T,Q,Tloss,Qloss,Eloss,Eff]=generate(factor,Dm)

%%%%% Select P/M characteristics %%%%%
factor=1;
Dm=1.8e-5;  %m^3/rev  [1.8e-5, 2.8e-5, 4.6e-5]  Change these lines
%together
maxspeed=5000;  %rpm   [5000, 4250, 3800]  Change these lines
%together
%%%%%%%%%%%%%%%%%%%%%%%%%%%%%%%%%%%%%%%%%%

A10VGraw = load('A10VG_matlabinput.txt'); %Load the raw eff data

bar=1e5; %Pa

Prange=(50:5:350)*bar; %Range of interested pressures (Pa)
wrange=(0:50:maxspeed)*2*pi/60; %Range of interested speeds (rad/s)
xrange=(-1:0.05:1); %Range of interested fractional displacements
%(Fraction)
```

```
%%%%% Load the raw eff data in 3D matrices %%%%%
[PP,xx,ww]=ndgrid(A10VGraw(2:8,2),A10VGraw(1,3:6),[A10VGraw(2,1)...
,A10VGraw(9,1),A10VGraw(16,1),A10VGraw(23,1),A10VGraw(30,1)...
,A10VGraw(37,1),A10VGraw(44,1),A10VGraw(51,1),A10VGraw(58,1)...
,A10VGraw(65,1)]);
eff_V=zeros(7,4,10);
eff_V(:,:,1)=A10VGraw(2:8,3:6);
eff_V(:,:,2)=A10VGraw(9:15,3:6);
eff_V(:,:,3)=A10VGraw(16:22,3:6);
eff_V(:,:,4)=A10VGraw(23:29,3:6);
eff_V(:,:,5)=A10VGraw(30:36,3:6);
eff_V(:,:,6)=A10VGraw(37:43,3:6);
eff_V(:,:,7)=A10VGraw(44:50,3:6);
eff_V(:,:,8)=A10VGraw(51:57,3:6);
eff_V(:,:,9)=A10VGraw(58:64,3:6);
eff_V(:,:,10)=A10VGraw(65:71,3:6);

%[PP,xx,ww]=ndgrid(A10VGraw(2:8,2),A10VGraw(1,7:10),...
[A10VGraw(2,1),A10VGraw(9,1),A10VGraw(16,1),A10VGraw(23,1),...
A10VGraw(30,1),A10VGraw(37,1),A10VGraw(44,1),A10VGraw(51,1),...
A10VGraw(58,1),A10VGraw(65,1)]);
eff_M=zeros(7,4,10);
eff_M(:,:,1)=A10VGraw(2:8,7:10);
eff_M(:,:,2)=A10VGraw(9:15,7:10);
eff_M(:,:,3)=A10VGraw(16:22,7:10);
eff_M(:,:,4)=A10VGraw(23:29,7:10);
eff_M(:,:,5)=A10VGraw(30:36,7:10);
eff_M(:,:,6)=A10VGraw(37:43,7:10);
eff_M(:,:,7)=A10VGraw(44:50,7:10);
eff_M(:,:,8)=A10VGraw(51:57,7:10);
eff_M(:,:,9)=A10VGraw(58:64,7:10);
```

```
eff_M(:,:,10)=A10VGraw(65:71,7:10);

%%%%% Preallocate matrices %%%%%
T=zeros(length(Prange),length(xrange),length(wrange));
Q=zeros(length(Prange),length(xrange),length(wrange));
Tloss=zeros(length(Prange),length(xrange),length(wrange));
Qloss=zeros(length(Prange),length(xrange),length(wrange));
Eloss=zeros(length(Prange),length(xrange),length(wrange));
Eff=zeros(length(Prange),length(xrange),length(wrange));
%%%%%%%%%%%%%%%%%%%%%%%%%%%%%%%

l=0;
for P=Prange, %Pa
    l=l+1;
    k=0;
    for x=xrange; %Fraction
    k=k+1;
    w=wrange; %rad/s

    [T(l,k,:),Q(l,k,:),Tloss(l,k,:),Qloss(l,k,:),Eloss(l,k,:),...
    Eff(l,k,:)]=pump(x,P,w,factor,Dm,PP,xx,ww,eff_V,eff_M,...
    maxspeed,bar);
    end;
end;
disp('Done pump!  Working on inverse pump');

w=wrange; % rad/s
x=xrange;
P=Prange;
[XX,T1]=invpump(T,P,w,x);

pumpinfo=['Tloss(P,x,w) ','Qloss(P,x,w) ','T(P,x,w) ',...
```

```
'Eloss(P,x,w)','Eff(P,x,w) ', 'XX(T1,P,w) '];
save pump18ccnolock_A10VG_factor100.mat T Q Tloss Qloss Eloss...
 Eff x w P pumpinfo XX T1;

function[Th1,Qh1,Tloss1,Qloss1,Eloss,eff]=pump(pmcmdl,P,w,factor...
,Dm,PP,xx,ww,eff_V,eff_M,maxspeed,bar)

Dm=Dm/2/pi;     %m^3/rad
w=w/maxspeed*60/2/pi;   %fraction of maxspeed
P=P/bar;        %bar

if (pmcmdl>=0) %motoring-yes(positive torque to drivetrain)
    Th1=(1-(1-(interpn(PP,xx,ww,eff_M,P,pmcmdl,w,'spline')/...
    1000))*factor)*pmcmdl*Dm*(P*bar);
    %Th1=(1-(1-effM)*factor)*x*D*P
    Qh1=-pmcmdl*Dm*(w*maxspeed*2*pi/60).*(1+(squeeze(1000/...
    interpn(PP,xx,ww,eff_V,P,pmcmdl,w,'spline'))'-1)*factor);
    %Qh1=-x*D*w*(1+((1/eff_V)-1)*factor)
    Tloss1=(1-(interpn(PP,xx,ww,eff_M,P,pmcmdl,w,'spline'))/...
    1000)*pmcmdl*Dm*(P*bar)*factor;
    %Tloss=(1-effM)*x*D*P*factor
    Qloss1=(squeeze(1000/interpn(PP,xx,ww,eff_V,P,pmcmdl,w,...
    'spline'))-1)'*pmcmdl*Dm.*(w*maxspeed*2*pi/60)*factor;
    %Qloss=((1/effV)-1)*x*D*w*factor
    Eloss=abs(P*bar*Qh1+squeeze(Th1)'.*w*maxspeed*2*pi/60);
    eff=(1-(1-(interpn(PP,xx,ww,eff_M,P,pmcmdl,w,'spline')))*...
    factor).*(1-(1-(interpn(PP,xx,ww,eff_V,P,pmcmdl,w,'spline')...
    ))*factor)/10^6;
    %eff=(1-(1-eff_V)*factor)*(1-(1-eff_M)*factor)

else  %pumping
    pmcmdl=-pmcmdl;
```

```
    Th1=-pmcmdl*Dm*(P*bar)*(1+((1000/interpn(PP,xx,ww,eff_M,P...
    ,pmcmdl,w,'spline'))-1)*factor);
    %Th1=x*D*P*(1+((1/eff_M)-1)*factor)
    Qh1=-(1-(1-squeeze(interpn(PP,xx,ww,eff_V,P,pmcmdl,w,...
    'spline')/1000))*factor)'*-pmcmdl*Dm.*(w*maxspeed*2*pi/60);
    %Qh1=-(1-(1-eff_V)*factor)*x*D*w
    Tloss1=-((1000/interpn(PP,xx,ww,eff_M,P,pmcmdl,w,'spline')...
    )-1)*-pmcmdl*Dm*(P*bar)*factor;
    %Tloss=-((1/eff_M)-1)*x*D*P*factor
    Qloss1=-(1-squeeze(interpn(PP,xx,ww,eff_V,P,pmcmdl,w,...
    'spline')/1000))'*-pmcmdl*Dm.*(w*maxspeed*2*pi/60)*factor;
    %Qloss=-(1-eff_V)*x*D*w*factor
    Eloss=abs(P*bar*Qh1+squeeze(Th1)'.*w*maxspeed*2*pi/60);
    eff=(1-(1-(interpn(PP,xx,ww,eff_M,P,pmcmdl,w,'spline')))...
    *factor).*(1-(1-(interpn(PP,xx,ww,eff_V,P,pmcmdl,w,'spline')...
    ))*factor)/10^6;
    %eff=(1-(1-eff_V)*factor)*(1-(1-eff_M)*factor)
end

function [XX,T1]=invpump(T,P,w,x)
% X(P,w,T) such that TI=T(X(P,w,TI),P,w);
% TI are the torques that the inverse function is interpolated at.
T1=linspace(min(T(:)),max(T(:)),50);
l=0;
for pp=P
    l=l+1;
    k=0;
    for ww=w
        k=k+1;
        XX(:,l,k)=interp1(squeeze(T(l,:,k)),x,T1,'linear','extrap');
    end;
end;
```

Appendix C

Representation of Original Transmission Configuration

C.1 Torque and Speed Governing Equation Derivation

The '$\rightarrow$' symbol represents the result of a combination of multiple equations.

$$T_s = -T_o \tag{C.1}$$

$$T_{PMS} = \frac{N_4}{N_3} T_s \tag{C.2}$$

$$\rightarrow T_{PMS} = -\frac{N_4}{N_3} T_o \tag{C.3}$$

$$\omega_{PMS} = \frac{N_3}{N_4} \omega_s \tag{C.4}$$

$$2\omega_{pc} = \omega_o + \omega_s \tag{C.5}$$

$$2\omega_{pc} = \omega_o + \frac{N_4}{N_3} \omega_{PMS} \tag{C.6}$$

$$\rightarrow \omega_{PMS} = \frac{N_3}{N_4} \left(2\omega_{pc} - \omega_o\right) \tag{C.7}$$

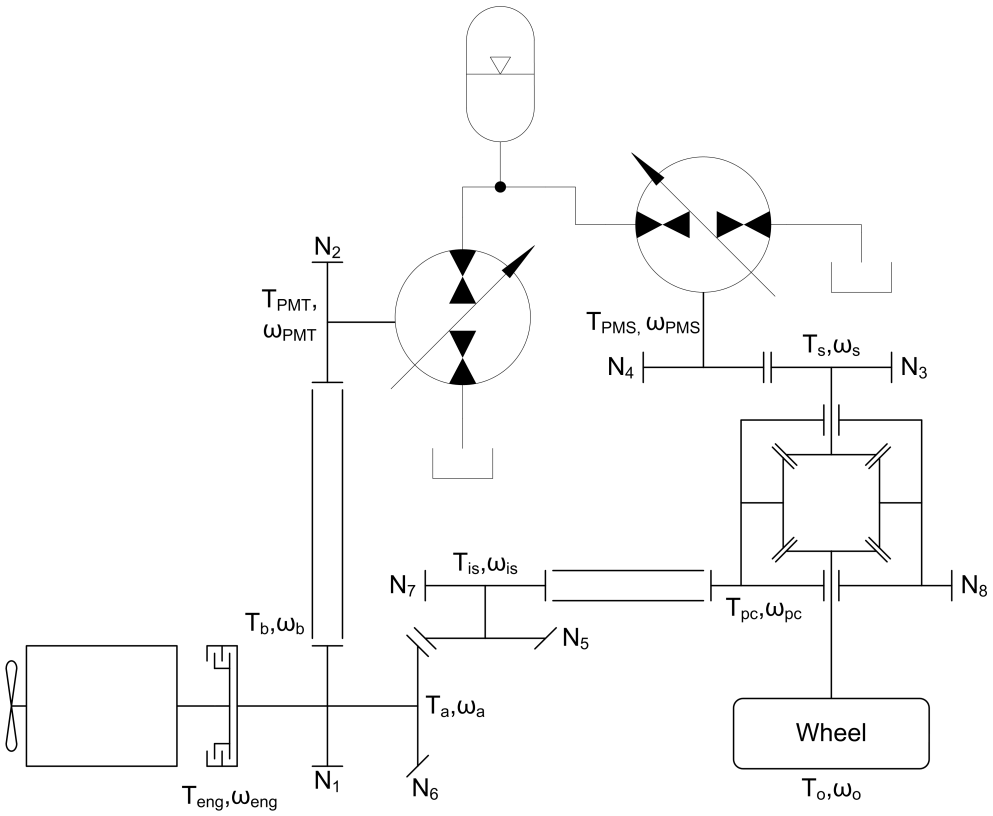

Figure C.1: Schematic representation of the originally built HMT configuration. Comparison with Fig. 1.2 reveals that simplifications have been made from the actual architecture.

$$\omega_{eng} = \frac{N_5}{N_6}\frac{N_8}{N_7}\omega_{pc} \tag{C.8}$$

$$\rightarrow \omega_{PMS} = \frac{N_3}{N_4}\left(2\frac{N_6}{N_5}\frac{N_7}{N_8}\omega_{eng} - \omega_o\right) \tag{C.9}$$

$$T_{pc} = 2T_o \tag{C.10}$$

$$T_{is} = \frac{N_7}{N_8}T_{pc} \tag{C.11}$$

$$T_a = \frac{N_6}{N_5}T_{is} \tag{C.12}$$

$$\rightarrow T_a = 2\frac{N_6}{N_5}\frac{N_7}{N_8}T_o \tag{C.13}$$

$$T_b = \frac{N_1}{N_2}T_{PMT} \tag{C.14}$$

$$T_a = T_{eng} + T_b \rightarrow T_b = T_a - T_{eng} \tag{C.15}$$

$$\rightarrow T_{PMT} = \frac{N_2}{N_1}\left(T_a - T_{eng}\right) \tag{C.16}$$

$$\rightarrow T_{PMT} = \frac{N_2}{N_1}\left(2\frac{N_6}{N_5}\frac{N_7}{N_8}T_o - T_{eng}\right) \tag{C.17}$$

$$\omega_{is} = \frac{N_8}{N_7}\omega_{pc} \tag{C.18}$$

$$\omega_a = \frac{N_5}{N_6}\omega_{is} \tag{C.19}$$

$$\omega_{eng} = \omega_a \tag{C.20}$$

$$\rightarrow \omega_{eng} = \frac{N_5}{N_6}\frac{N_8}{N_7}\omega_{pc} \tag{C.21}$$

$$\omega_b = \frac{N_2}{N_1}\omega_{PMT} \tag{C.22}$$

$$\omega_b = \omega_a \tag{C.23}$$

$$\rightarrow \omega_{PMT} = \frac{N_1}{N_2}\omega_{eng} \tag{C.24}$$

Appendix D

Redesign Configurations of HHPV Drivetrain

D.1 Configuration 1

$$T_s = T_b + T_{eng} \tag{D.1}$$

$$\omega_{eng} = \omega_b = \omega_s \tag{D.2}$$

$$T_{PMT} = \frac{N_2}{N_1} T_b \tag{D.3}$$

$$\omega_{PMT} = \frac{N_1}{N_2} \omega_b \tag{D.4}$$

$$T_{PMS} = \frac{N_4}{N_3} T_r \tag{D.5}$$

$$\omega_{PMS} = \frac{N_3}{N_4} \omega_r \tag{D.6}$$

$$T_{pc} = \frac{T_o}{R_{fd}} \tag{D.7}$$

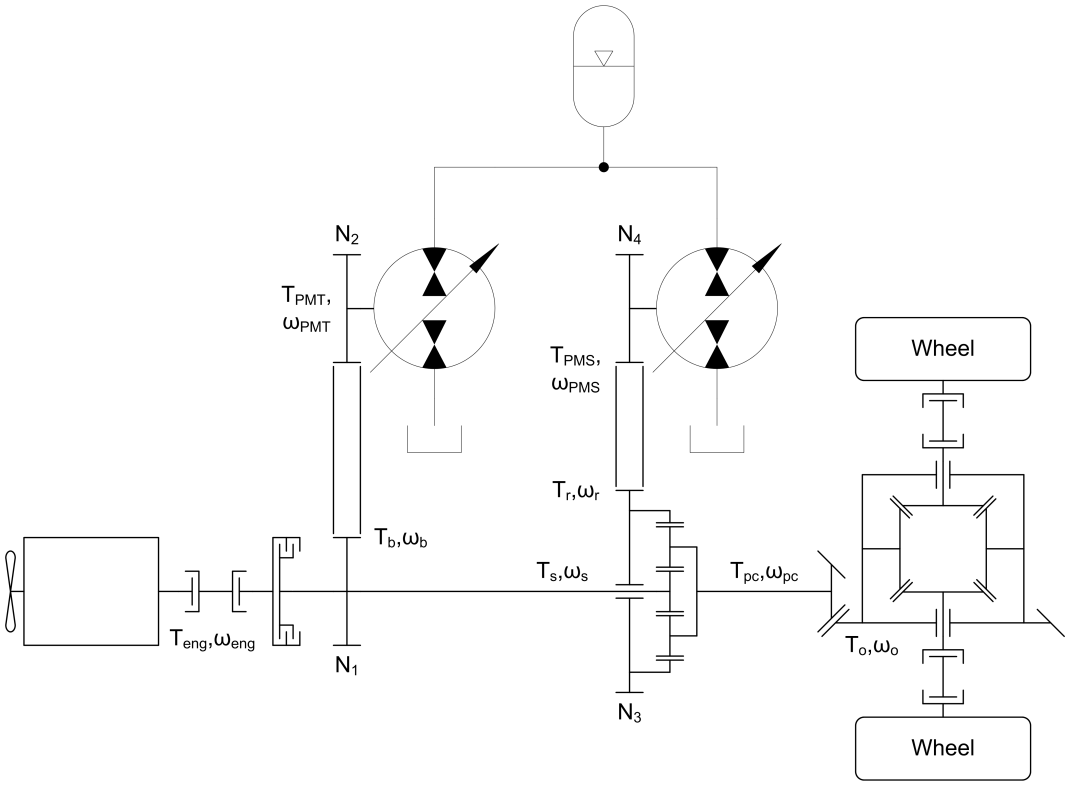

Figure D.1: Redesign Configuration 1

$$\omega_{pc} = R_{fd} * \omega_o \tag{D.8}$$

$$T_r = \frac{r_{plan} - 1}{r_{plan}} T_{pc} = \frac{1}{R_{fd}} \frac{r_{plan} - 1}{r_{plan}} T_o \tag{D.9}$$

$$T_s = \frac{1}{r_{plan}} T_{pc} = \frac{1}{R_{fd} * r_{plan}} T_o \tag{D.10}$$

$$\omega_{pc} = \frac{1}{r_{plan}} \omega_s + \frac{r_{plan} - 1}{r_{plan}} \omega_r \tag{D.11}$$

$$\omega_o * R_{fd} = \frac{1}{r_{plan}} \omega_{eng} + \frac{r_{plan} - 1}{r_{plan}} \frac{N_4}{N_3} \omega_{PMS} \tag{D.12}$$

$$\Rightarrow \omega_{PMS} = \frac{N_3}{N_4} \frac{r_{plan}}{r_{plan} - 1} \left[\omega_o * R_{fd} - \frac{1}{r_{plan}} \omega_{eng} \right] \tag{D.13}$$

If $\omega_{PMS} = 0$, then

$$\omega_c = R_{fd} * r_{plan} * \omega_o \Rightarrow \omega_o = \frac{1}{R_{fd} * r_{plan}} \omega_c \tag{D.14}$$

$$\Rightarrow \omega_{PMS,list} = \frac{N_3}{N_4} \frac{r_{plan}}{r_{plan} - 1} \left[\frac{1}{R_{fd} * r_{plan}} \omega_c * R_{fd} - \frac{1}{r_{plan}} \omega_{eng,list} \right] \tag{D.15}$$

$$\Rightarrow \omega_{PMS,list} = \frac{N_3}{N_4} \frac{1}{r_{plan} - 1} \left[\omega_c - \omega_{eng,list} \right] \tag{D.16}$$

$\omega_{PMS,list} = \frac{H_{reduct,new}}{r_{plan}-1} \left[\omega_c - \omega_{eng,list} \right]$ where $H_{reduct,new} = \frac{N_3}{N_4}$

Note: $\omega_{eng,list}$ is the list of possible engine speeds, while ω_c is the engine speed based on ω_o and $\omega_{PMS} = 0$.

$$T_{PMS} = \frac{N_4}{N_3} \frac{r_{plan} - 1}{r_{plan}} \frac{1}{R_{fd}} T_o \tag{D.17}$$

The equations needed for ratio transformation are the ω_c equation and the $\omega_{PMS,list}$ equation.

$$\omega_c = \frac{rat}{2} \omega_o \tag{D.18}$$

$$\omega_{PMS,list} = \frac{2 * H_{reduct,old}}{rat} \left[\omega_{eng,list} - \omega_c\right] \tag{D.19}$$

Setting the new and old equations equal to each other yields:

$$R_{fd} * r_{plan} = \frac{rat}{2} \tag{D.20}$$

$$H_{reduct,new} = \frac{-2 * H_{reduct,old}}{rat} \left(r_{plan} - 1\right) \tag{D.21}$$

D.2 Configuration 2

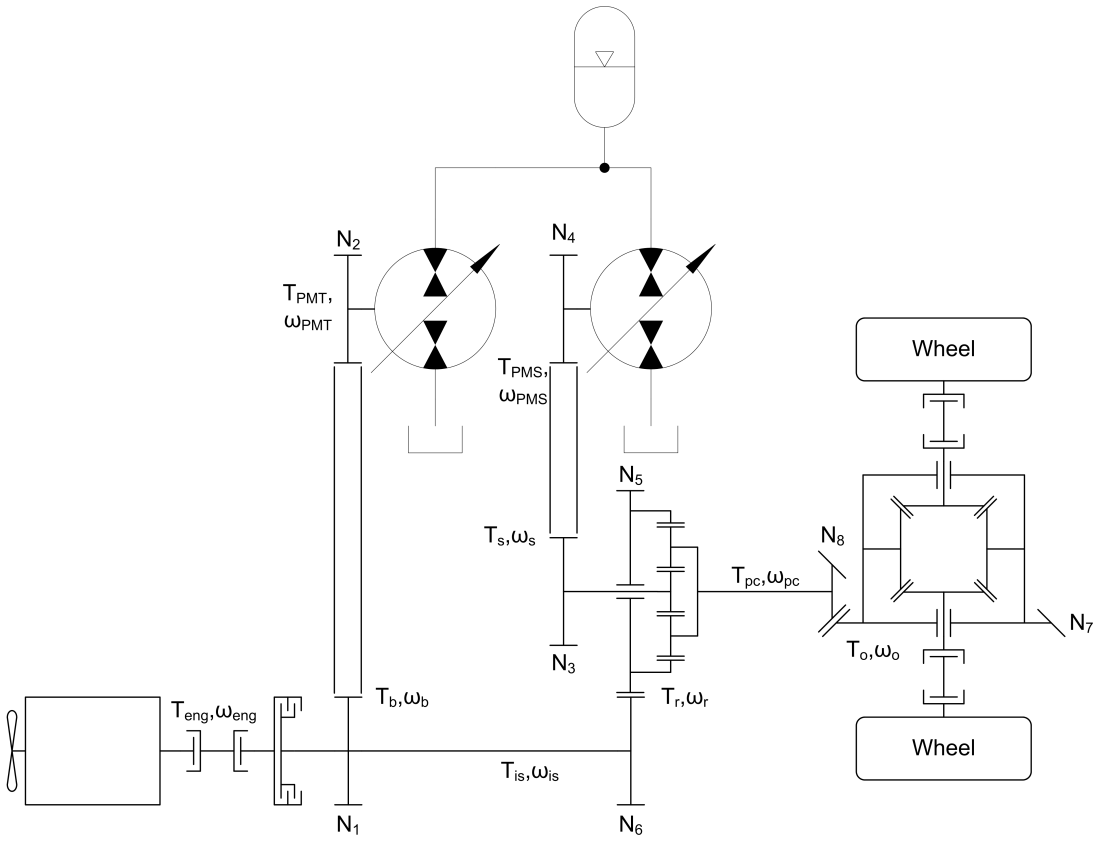

Figure D.2: Redesign Configuration 2

$$T_{is} = T_b + T_{eng} \tag{D.22}$$

$$\omega_{eng} = \omega_b = \omega_{is} \tag{D.23}$$

$$T_{PMT} = \frac{N_2}{N_1} T_b \tag{D.24}$$

$$\omega_{PMT} = \frac{N_1}{N_2} \omega_b \tag{D.25}$$

$$T_{PMS} = \frac{N_4}{N_3} T_s \tag{D.26}$$

$$\omega_{PMS} = \frac{N_3}{N_4} \omega_s \tag{D.27}$$

$$T_{is} = \frac{N_6}{N_5} T_r \tag{D.28}$$

$$\omega_{is} = \frac{N_5}{N_6} \omega_r \tag{D.29}$$

$$T_{pc} = \frac{T_o}{R_{fd}} \tag{D.30}$$

$$\omega_{pc} = R_{fd} * \omega_o \tag{D.31}$$

$$T_r = \frac{r_{plan} - 1}{r_{plan}} T_{pc} = \frac{1}{R_{fd}} \frac{r_{plan} - 1}{r_{plan}} T_o \tag{D.32}$$

$$T_s = \frac{1}{r_{plan}} T_{pc} = \frac{1}{R_{fd} * r_{plan}} T_o \tag{D.33}$$

$$\omega_{pc} = \frac{1}{r_{plan}} \omega_s + \frac{r_{plan} - 1}{r_{plan}} \omega_r \tag{D.34}$$

$$\omega_o * R_{fd} = \frac{1}{r_{plan}} \frac{N_4}{N_3} \omega_{PMS} + \frac{r_{plan} - 1}{r_{plan}} \frac{N_6}{N_5} \omega_{eng} \tag{D.35}$$

$$\Rightarrow \omega_{PMS} = \frac{N_3}{N_4} r_{plan} \left[\omega_o * R_{fd} - \frac{r_{plan} - 1}{r_{plan}} \frac{N_6}{N_5} \omega_{eng} \right] \tag{D.36}$$

If $\omega_{PMS} = 0$, then

$$\omega_c = R_{fd}\frac{r_{plan}}{r_{plan}-1}\frac{N_5}{N_6} * \omega_o \Rightarrow \omega_o = \frac{r_{plan}-1}{r_{plan}}\frac{1}{R_{fd}}\frac{N_6}{N_5}\omega_c \tag{D.37}$$

$$\Rightarrow \omega_{PMS,list} = \frac{N_3}{N_4}r_{plan}\left[\frac{r_{plan}-1}{r_{plan}}\frac{1}{R_{fd}}\frac{N_6}{N_5}\omega_c * R_{fd} - \frac{r_{plan}-1}{r_{plan}}\frac{N_6}{N_5}\omega_{eng,list}\right] \tag{D.38}$$

$$\Rightarrow \omega_{PMS,list} = \frac{N_3}{N_4}\frac{N_6}{N_5}\left(r_{plan}-1\right)\left[\omega_c - \omega_{eng,list}\right] \tag{D.39}$$

$\omega_{PMS,list} = H_{reduct,new}\frac{N_6}{N_5}\left(r_{plan}-1\right)\left[\omega_c - \omega_{eng,list}\right]$ where $H_{reduct,new} = \frac{N_3}{N_4}$

Note: $\omega_{eng,list}$ is the list of possible engine speeds, while ω_c is the engine speed based on ω_o and $\omega_{PMS} = 0$.

$$T_{PMS} = \frac{N_4}{N_3}\frac{1}{R_{fd} * r_{plan}}T_o \tag{D.40}$$

The equations needed for ratio transformation are the ω_c equation and the $\omega_{PMS,list}$ equation.

$$\omega_c = \frac{rat}{2}\omega_o \tag{D.41}$$

$$\omega_{PMS,list} = \frac{2 * H_{reduct,old}}{rat}\left[\omega_{eng,list} - \omega_c\right] \tag{D.42}$$

Setting the new and old equations equal to each other yields:

$$R_{fd} * \frac{r_{plan}}{r_{plan}-1}\frac{N_5}{N_6} = \frac{rat}{2} \tag{D.43}$$

$$H_{reduct,new} = \frac{-2 * H_{reduct,old}}{rat * \left(r_{plan}-1\right)}\frac{N_5}{N_6} \tag{D.44}$$

D.3 Configuration 3

$$T_{pc} = T_b + T_{eng} \tag{D.45}$$

$$\omega_{eng} = \omega_b = \omega_{pc} \tag{D.46}$$

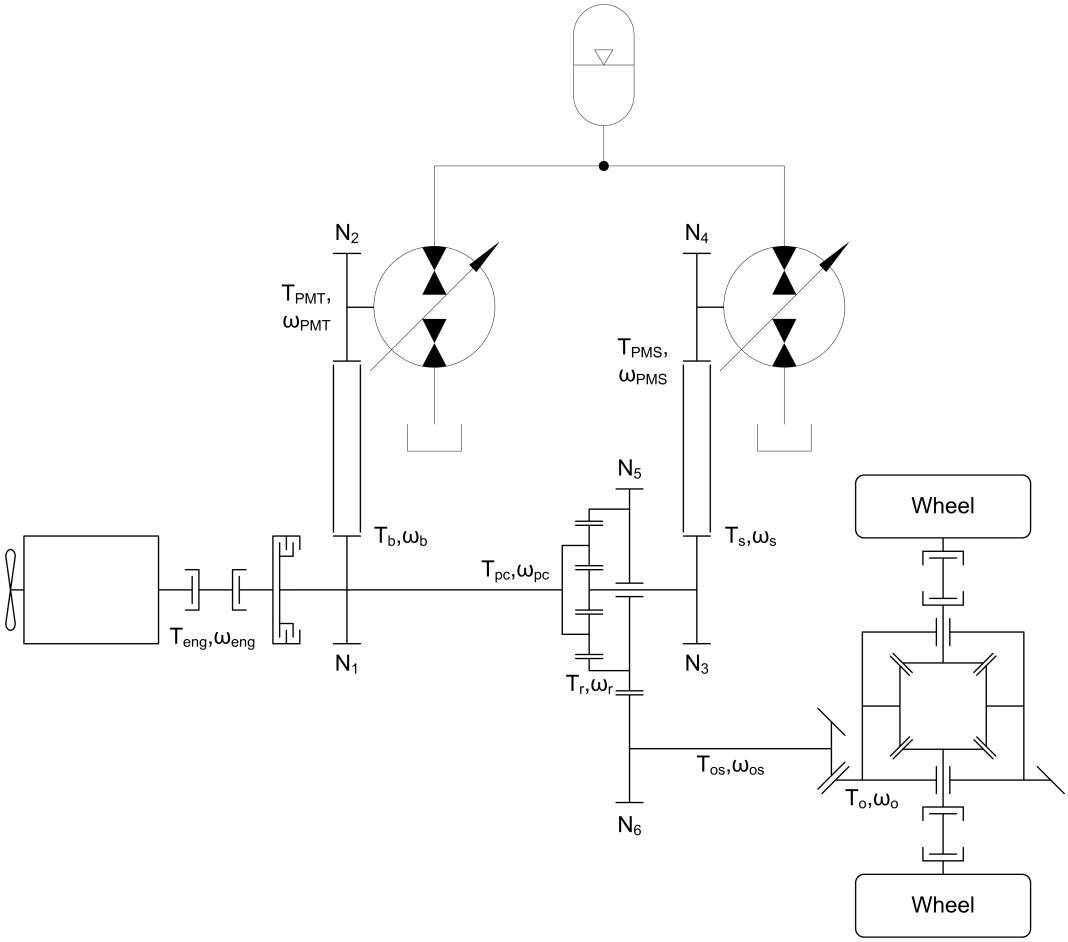

Figure D.3: Redesign Configuration 3

$$T_{PMT} = \frac{N_2}{N_1} T_b \tag{D.47}$$

$$\omega_{PMT} = \frac{N_1}{N_2} \omega_b \tag{D.48}$$

$$T_{PMS} = \frac{N_4}{N_3} T_s \tag{D.49}$$

$$\omega_{PMS} = \frac{N_3}{N_4} \omega_s \tag{D.50}$$

$$T_{os} = \frac{N_6}{N_5} T_r \tag{D.51}$$

$$\omega_{os} = \frac{N_5}{N_6} \omega_r \tag{D.52}$$

$$T_{os} = \frac{T_o}{R_{fd}} \tag{D.53}$$

$$\omega_{os} = R_{fd} * \omega_o \tag{D.54}$$

$$T_{pc} = \frac{r_{plan}}{r_{plan} - 1} T_r = \frac{1}{R_{fd}} \frac{r_{plan}}{r_{plan} - 1} \frac{N_5}{N_6} T_o \tag{D.55}$$

$$T_s = -\frac{1}{r_{plan} - 1} T_r = -\frac{1}{r_{plan} - 1} \frac{N_5}{N_6} \frac{1}{R_{fd}} T_o \tag{D.56}$$

$$\omega_{pc} = \frac{1}{r_{plan}} \omega_s + \frac{r_{plan} - 1}{r_{plan}} \omega_r \tag{D.57}$$

$$\omega_{eng} = \frac{1}{r_{plan}} \frac{N_4}{N_3} \omega_{PMS} + R_{fd} \frac{r_{plan} - 1}{r_{plan}} \frac{N_6}{N_5} \omega_o \tag{D.58}$$

$$\Rightarrow \omega_{PMS} = \frac{N_3}{N_4} r_{plan} \left[\omega_{eng} - R_{fd} \frac{r_{plan} - 1}{r_{plan}} \frac{N_6}{N_5} \omega_o \right] \tag{D.59}$$

If $\omega_{PMS} = 0$, then

$$\omega_c = R_{fd}\frac{r_{plan}-1}{r_{plan}}\frac{N_6}{N_5} * \omega_o \Rightarrow \omega_o = \frac{r_{plan}}{r_{plan}-1}\frac{1}{R_{fd}}\frac{N_5}{N_6}\omega_c \tag{D.60}$$

$$\Rightarrow \omega_{PMS,list} = \frac{N_3}{N_4}r_{plan}\left[\omega_{eng,list} - R_{fd}\frac{r_{plan}-1}{r_{plan}}\frac{N_6}{N_5}\frac{r_{plan}}{r_{plan}-1}\frac{1}{R_{fd}}\frac{N_5}{N_6}\omega_c\right] \tag{D.61}$$

$$\Rightarrow \omega_{PMS,list} = \frac{N_3}{N_4}r_{plan}\left[\omega_{eng,list} - \omega_c\right] \tag{D.62}$$

$\omega_{PMS,list} = H_{reduct,new} * r_{plan}\left[\omega_{eng,list} - \omega_c\right]$ where $H_{reduct,new} = \frac{N_3}{N_4}$

Note: $\omega_{eng,list}$ is the list of possible engine speeds, while ω_c is the engine speed based on ω_o and $\omega_{PMS} = 0$.

$$T_{PMS} = -\frac{N_4}{N_3}\frac{1}{r_{plan}-1}\frac{N_5}{N_6}\frac{1}{R_{fd}}T_o \tag{D.63}$$

The equations needed for ratio transformation are the ω_c equation and the $\omega_{PMS,list}$ equation.

$$\omega_c = \frac{rat}{2}\omega_o \tag{D.64}$$

$$\omega_{PMS,list} = \frac{2 * H_{reduct,old}}{rat}\left[\omega_{eng,list} - \omega_c\right] \tag{D.65}$$

Setting the new and old equations equal to each other yields:

$$R_{fd} * \frac{r_{plan}-1}{r_{plan}}\frac{N_6}{N_5} = \frac{rat}{2} \tag{D.66}$$

$$H_{reduct,new} = \frac{2 * H_{reduct,old}}{rat * r_{plan}} \tag{D.67}$$

D.4 Configuration 4

$$T_{pc} = T_b + T_{eng} \tag{D.68}$$

$$\omega_{eng} = \omega_b = \omega_{pc} \tag{D.69}$$

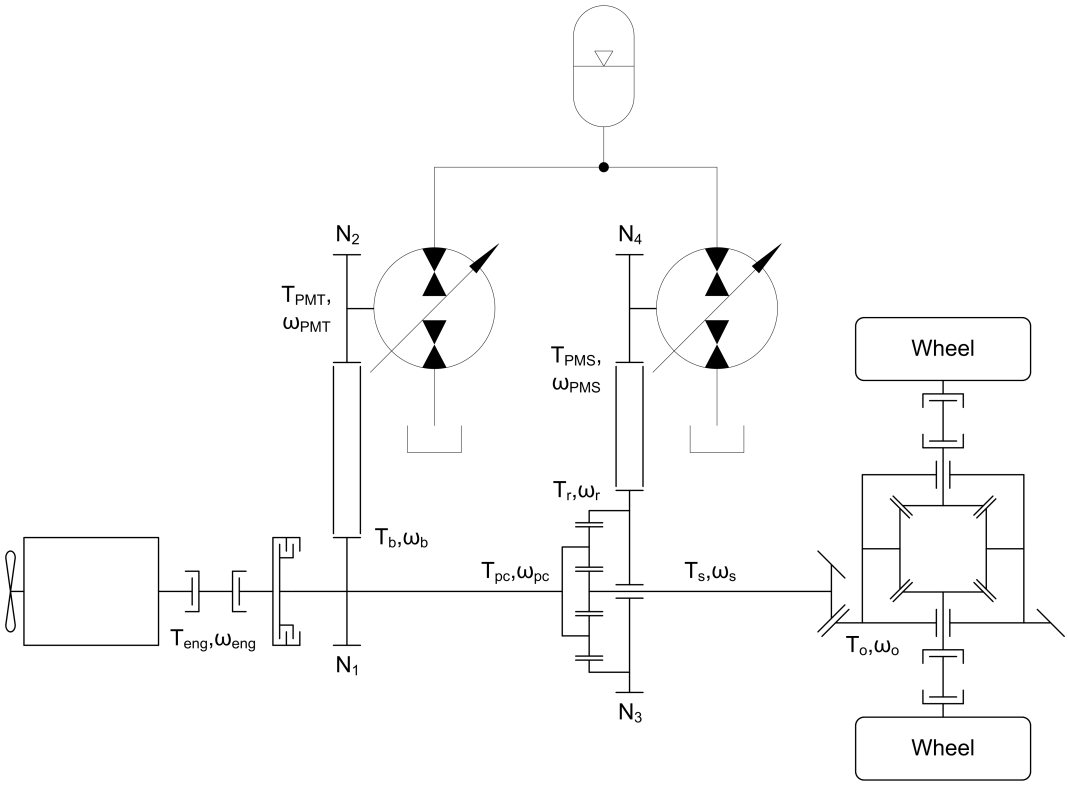

Figure D.4: Redesign Configuration 4

$$T_{PMT} = \frac{N_2}{N_1} T_b \tag{D.70}$$

$$\omega_{PMT} = \frac{N_1}{N_2} \omega_b \tag{D.71}$$

$$T_{PMS} = \frac{N_4}{N_3} T_r \tag{D.72}$$

$$\omega_{PMS} = \frac{N_3}{N_4} \omega_r \tag{D.73}$$

$$T_s = \frac{T_o}{R_{fd}} \tag{D.74}$$

$$\omega_s = R_{fd} * \omega_o \tag{D.75}$$

$$T_r = -\left(r_{plan} - 1\right) T_s = -\frac{r_{plan} - 1}{R_{fd}} T_o \tag{D.76}$$

$$T_{pc} = r_{plan} * T_s = \frac{r_{plan}}{R_{fd}} T_o \tag{D.77}$$

$$\omega_{pc} = \frac{1}{r_{plan}} \omega_s + \frac{r_{plan} - 1}{r_{plan}} \omega_r \tag{D.78}$$

$$\omega_{eng} = \frac{R_{fd}}{r_{plan}} \omega_o + \frac{r_{plan} - 1}{r_{plan}} \frac{N_4}{N_3} \omega_{PMS} \tag{D.79}$$

$$\Rightarrow \omega_{PMS} = \frac{N_3}{N_4} \frac{r_{plan}}{r_{plan} - 1} \left[\omega_{eng} - \frac{R_{fd}}{r_{plan}} \omega_o \right] \tag{D.80}$$

If $\omega_{PMS} = 0$, then

$$\omega_c = \frac{R_{fd}}{r_{plan}} \omega_o \Rightarrow \omega_o = \frac{r_{plan}}{R_{fd}} \omega_c \tag{D.81}$$

$$\Rightarrow \omega_{PMS,list} = \frac{N_3}{N_4} \frac{r_{plan}}{r_{plan} - 1} \left[\omega_{eng,list} - \frac{R_{fd}}{r_{plan}} \frac{r_{plan}}{R_{fd}} \omega_c \right] \tag{D.82}$$

$$\Rightarrow \omega_{PMS,list} = \frac{N_3}{N_4} \frac{r_{plan}}{r_{plan} - 1} \left[\omega_{eng,list} - \omega_c \right] \tag{D.83}$$

$\omega_{PMS,list} = H_{reduct,new}\frac{r_{plan}}{r_{plan}-1}\left[\omega_{eng,list} - \omega_c\right]$ where $H_{reduct,new} = \frac{N_3}{N_4}$

Note: $\omega_{eng,list}$ is the list of possible engine speeds, while ω_c is the engine speed based on ω_o and $\omega_{PMS} = 0$.

$$T_{PMS} = -\frac{N_4}{N_3}\frac{r_{plan}-1}{R_{fd}}T_o \tag{D.84}$$

The equations needed for ratio transformation are the ω_c equation and the $\omega_{PMS,list}$ equation.

$$\omega_c = \frac{rat}{2}\omega_o \tag{D.85}$$

$$\omega_{PMS,list} = \frac{2 * H_{reduct,old}}{rat}\left[\omega_{eng,list} - \omega_c\right] \tag{D.86}$$

Setting the new and old equations equal to each other yields:

$$\frac{R_{fd}}{r_{plan}} = \frac{rat}{2} \tag{D.87}$$

$$H_{reduct,new} = \frac{2 * H_{reduct,old}}{rat}\frac{r_{plan}-1}{r_{plan}} \tag{D.88}$$

D.5 Configuration 5

$$T_{is} = T_b + T_{eng} \tag{D.89}$$

$$\omega_{eng} = \omega_b = \omega_{is} \tag{D.90}$$

$$T_{PMT} = \frac{N_2}{N_1}T_b \tag{D.91}$$

$$\omega_{PMT} = \frac{N_1}{N_2}\omega_b \tag{D.92}$$

$$T_{PMS} = \frac{N_4}{N_3}T_{pc} \tag{D.93}$$

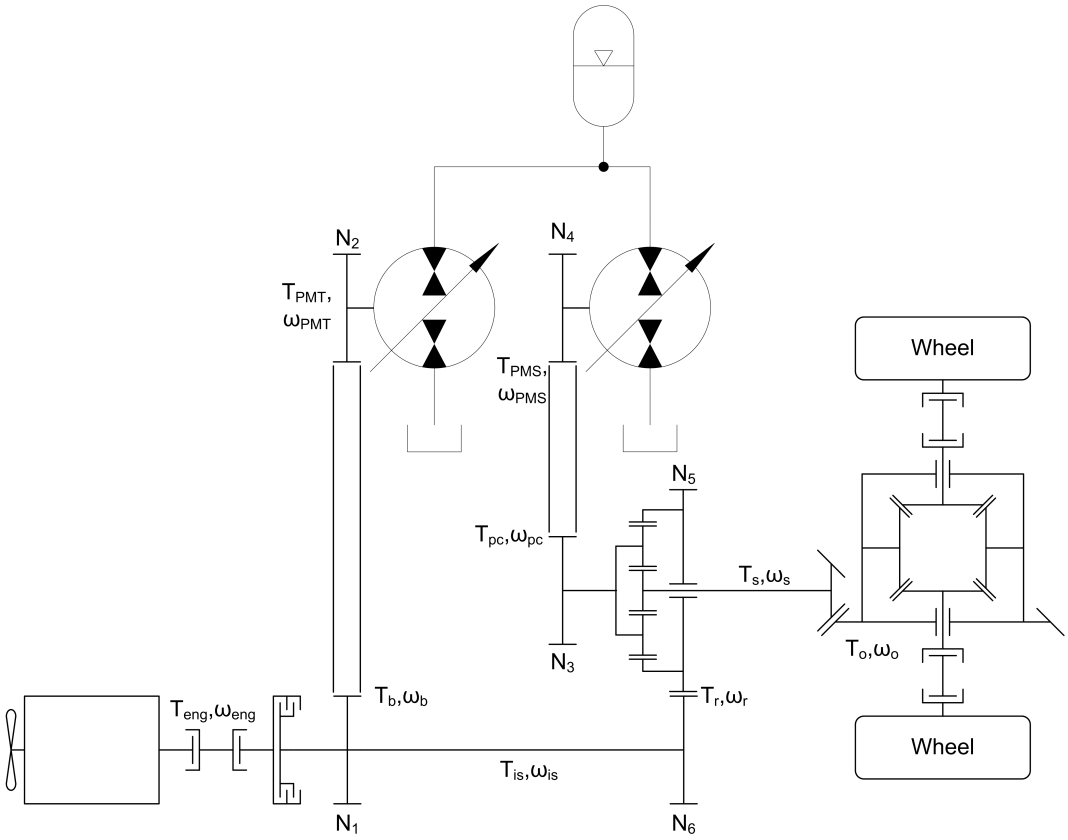

Figure D.5: Redesign Configuration 5

$$\omega_{PMS} = \frac{N_3}{N_4}\omega_{pc} \tag{D.94}$$

$$T_{is} = \frac{N_6}{N_5}T_r \tag{D.95}$$

$$\omega_{is} = \frac{N_5}{N_6}\omega_r \tag{D.96}$$

$$T_s = \frac{T_o}{R_{fd}} \tag{D.97}$$

$$\omega_s = R_{fd} * \omega_o \tag{D.98}$$

$$T_r = -\left(r_{plan} - 1\right) T_s = -\frac{r_{plan} - 1}{R_{fd}} T_o \tag{D.99}$$

$$T_{pc} = r_{plan} * T_s = \frac{r_{plan}}{R_{fd}} T_o \tag{D.100}$$

$$\omega_{pc} = \frac{1}{r_{plan}}\omega_s + \frac{r_{plan} - 1}{r_{plan}}\omega_r \tag{D.101}$$

$$\frac{N_4}{N_3}\omega_{PMS} = \frac{1}{r_{plan}}\omega_o * R_{fd} + \frac{r_{plan} - 1}{r_{plan}}\frac{N_6}{N_5}\omega_{eng} \tag{D.102}$$

$$\Rightarrow \omega_{PMS} = \frac{N_3}{N_4}\frac{1}{r_{plan}}\left[\omega_o * R_{fd} + \left(r_{plan} - 1\right)\frac{N_6}{N_5}\omega_{eng}\right] \tag{D.103}$$

If $\omega_{PMS} = 0$, then

$$\omega_c = -\frac{R_{fd}}{r_{plan} - 1}\frac{N_5}{N_6} * \omega_o \Rightarrow \omega_o = -\frac{r_{plan} - 1}{R_{fd}}\frac{N_6}{N_5}\omega_c \tag{D.104}$$

$$\Rightarrow \omega_{PMS,list} = \frac{N_3}{N_4}\frac{1}{r_{plan}}\left[-\frac{r_{plan} - 1}{R_{fd}}\frac{N_6}{N_5}\omega_c * R_{fd} + \left(r_{plan} - 1\right)\frac{N_6}{N_5}\omega_{eng,list}\right] \tag{D.105}$$

$$\Rightarrow \omega_{PMS,list} = \frac{N_3}{N_4}\frac{N_6}{N_5}\frac{r_{plan} - 1}{r_{plan}}\left[\omega_{eng,list} - \omega_c\right] \tag{D.106}$$

$\omega_{PMS,list} = H_{reduct,new}\frac{N_6}{N_5}\frac{r_{plan}-1}{r_{plan}}\left[\omega_{eng,list} - \omega_c\right]$ where $H_{reduct,new} = \frac{N_3}{N_4}$

Note: $\omega_{eng,list}$ is the list of possible engine speeds, while ω_c is the engine speed based on ω_o and $\omega_{PMS} = 0$.

$$T_{PMS} = \frac{N_4}{N_3}\frac{r_{plan}}{R_{fd}}T_o \tag{D.107}$$

The equations needed for ratio transformation are the ω_c equation and the $\omega_{PMS,list}$ equation.

$$\omega_c = \frac{rat}{2}\omega_o \tag{D.108}$$

$$\omega_{PMS,list} = \frac{2 * H_{reduct,old}}{rat}\left[\omega_{eng,list} - \omega_c\right] \tag{D.109}$$

Setting the new and old equations equal to each other yields:

$$-\frac{R_{fd}}{r_{plan}-1}\frac{N_5}{N_6} = \frac{rat}{2} \tag{D.110}$$

$$H_{reduct,new} = \frac{N_5}{N_6}\frac{r_{plan}}{r_{plan}-1}\frac{2 * H_{reduct,old}}{rat} \tag{D.111}$$

D.6 Configuration 6

$$T_s = T_b + T_{eng} \tag{D.112}$$

$$\omega_{eng} = \omega_b = \omega_s \tag{D.113}$$

$$T_{PMT} = \frac{N_2}{N_1}T_b \tag{D.114}$$

$$\omega_{PMT} = \frac{N_1}{N_2}\omega_b \tag{D.115}$$

$$T_{PMS} = \frac{N_4}{N_3}T_{pc} \tag{D.116}$$

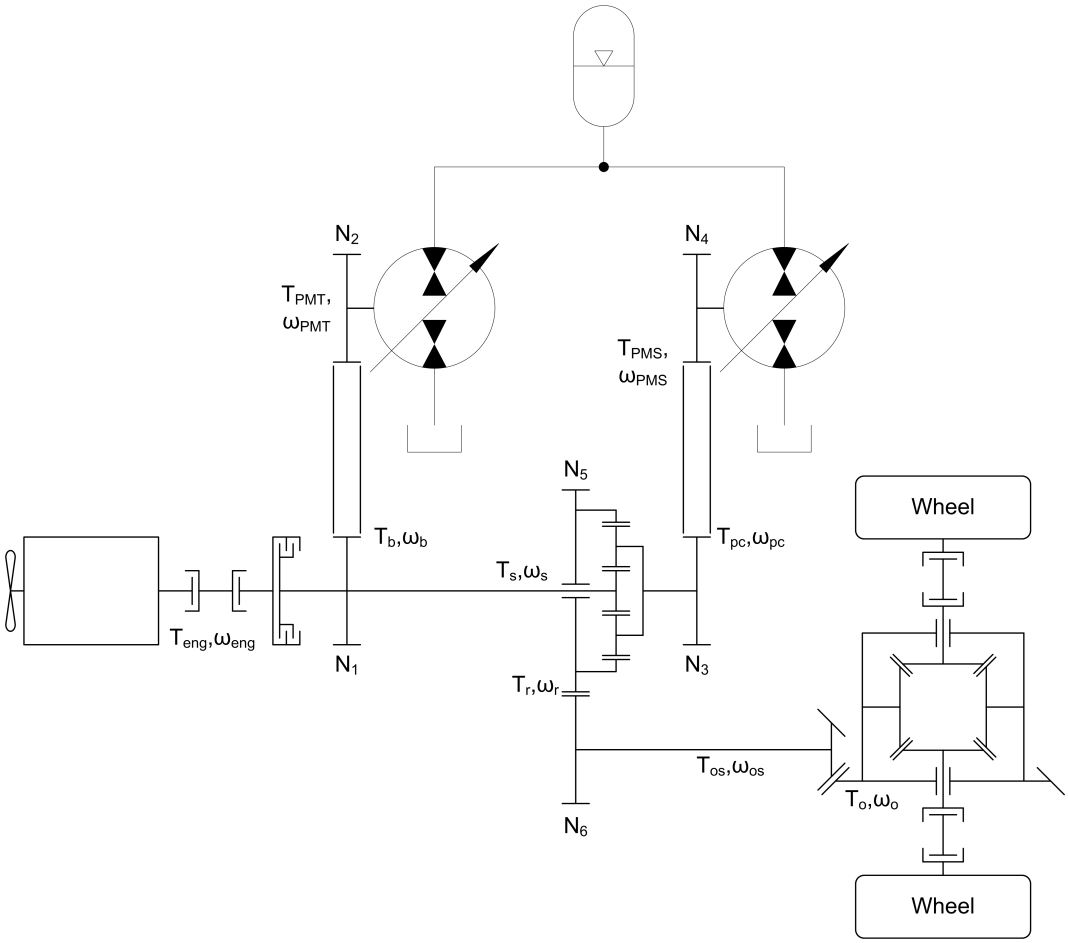

Figure D.6: Redesign Configuration 6

$$\omega_{PMS} = \frac{N_3}{N_4}\omega_{pc} \tag{D.117}$$

$$T_{os} = \frac{N_6}{N_5}T_r \tag{D.118}$$

$$\omega_{os} = \frac{N_5}{N_6}\omega_r \tag{D.119}$$

$$T_{os} = \frac{T_o}{R_{fd}} \tag{D.120}$$

$$\omega_{os} = R_{fd} * \omega_o \tag{D.121}$$

$$T_{pc} = \frac{r_{plan}}{r_{plan}-1} T_r = \frac{1}{R_{fd}} \frac{r_{plan}}{r_{plan}-1} \frac{N_5}{N_6} T_o \tag{D.122}$$

$$T_s = -\frac{1}{r_{plan}-1} T_r = -\frac{1}{r_{plan}-1} \frac{N_5}{N_6} \frac{1}{R_{fd}} T_o \tag{D.123}$$

$$\omega_{pc} = \frac{1}{r_{plan}} \omega_s + \frac{r_{plan}-1}{r_{plan}} \omega_r \tag{D.124}$$

$$\frac{N_4}{N_3} \omega_{PMS} = \frac{1}{r_{plan}} \omega_{eng} + R_{fd} \frac{r_{plan}-1}{r_{plan}} \frac{N_6}{N_5} \omega_o \tag{D.125}$$

$$\Rightarrow \omega_{PMS} = \frac{N_3}{N_4} \frac{1}{r_{plan}} \left[\omega_{eng} + R_{fd} \left(r_{plan} - 1 \right) \frac{N_6}{N_5} \omega_o \right] \tag{D.126}$$

If $\omega_{PMS} = 0$, then

$$\omega_c = -R_{fd} \left(r_{plan} - 1 \right) \frac{N_6}{N_5} * \omega_o \Rightarrow \omega_o = -\frac{1}{r_{plan}-1} \frac{1}{R_{fd}} \frac{N_5}{N_6} \omega_c \tag{D.127}$$

$$\Rightarrow \omega_{PMS,list} = \frac{N_3}{N_4} \frac{1}{r_{plan}} \left[\omega_{eng,list} - R_{fd} \left(r_{plan} - 1 \right) \frac{N_6}{N_5} \frac{1}{r_{plan}-1} \frac{1}{R_{fd}} \frac{N_5}{N_6} \omega_c \right] \tag{D.128}$$

$$\Rightarrow \omega_{PMS,list} = \frac{N_3}{N_4} \frac{1}{r_{plan}} \left[\omega_{eng,list} - \omega_c \right] \tag{D.129}$$

$\omega_{PMS,list} = H_{reduct,new} \frac{1}{r_{plan}} \left[\omega_{eng,list} - \omega_c \right]$ where $H_{reduct,new} = \frac{N_3}{N_4}$

Note: $\omega_{eng,list}$ is the list of possible engine speeds, while ω_c is the engine speed based on ω_o and $\omega_{PMS} = 0$.

$$T_{PMS} = \frac{N_4}{N_3} \frac{r_{plan}}{r_{plan}-1} \frac{N_5}{N_6} \frac{1}{R_{fd}} T_o \tag{D.130}$$

The equations needed for ratio transformation are the ω_c equation and the $\omega_{PMS,list}$ equation.

$$\omega_c = \frac{rat}{2} \omega_o \tag{D.131}$$

$$\omega_{PMS,list} = \frac{2 * H_{reduct,old}}{rat} \left[\omega_{eng,list} - \omega_c\right] \tag{D.132}$$

Setting the new and old equations equal to each other yields:

$$-R_{fd} * (r_{plan} - 1) \frac{N_6}{N_5} = \frac{rat}{2} \tag{D.133}$$

$$H_{reduct,new} = \frac{2 * H_{reduct,old}}{rat} r_{plan} \tag{D.134}$$

Appendix E

Manufacturing Drawings

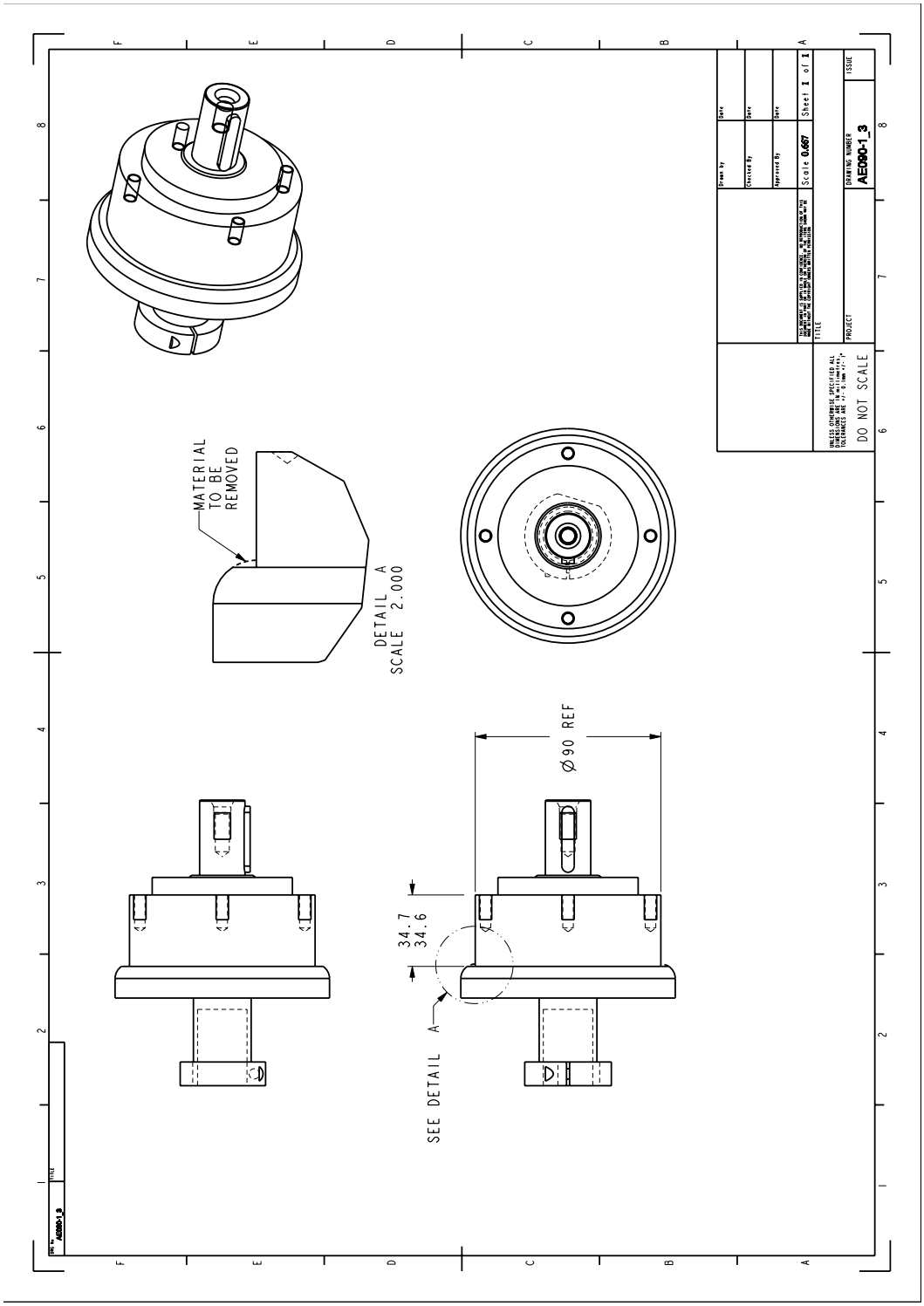
MATERIAL
TO BE
REMOVED
DETAIL A
SCALE 2.000
Ø90 REF
34.7
34.6
SEE DETAIL A
DO NOT SCALE
Scale 0.667
Sheet 1 of 1
AE090-1_3

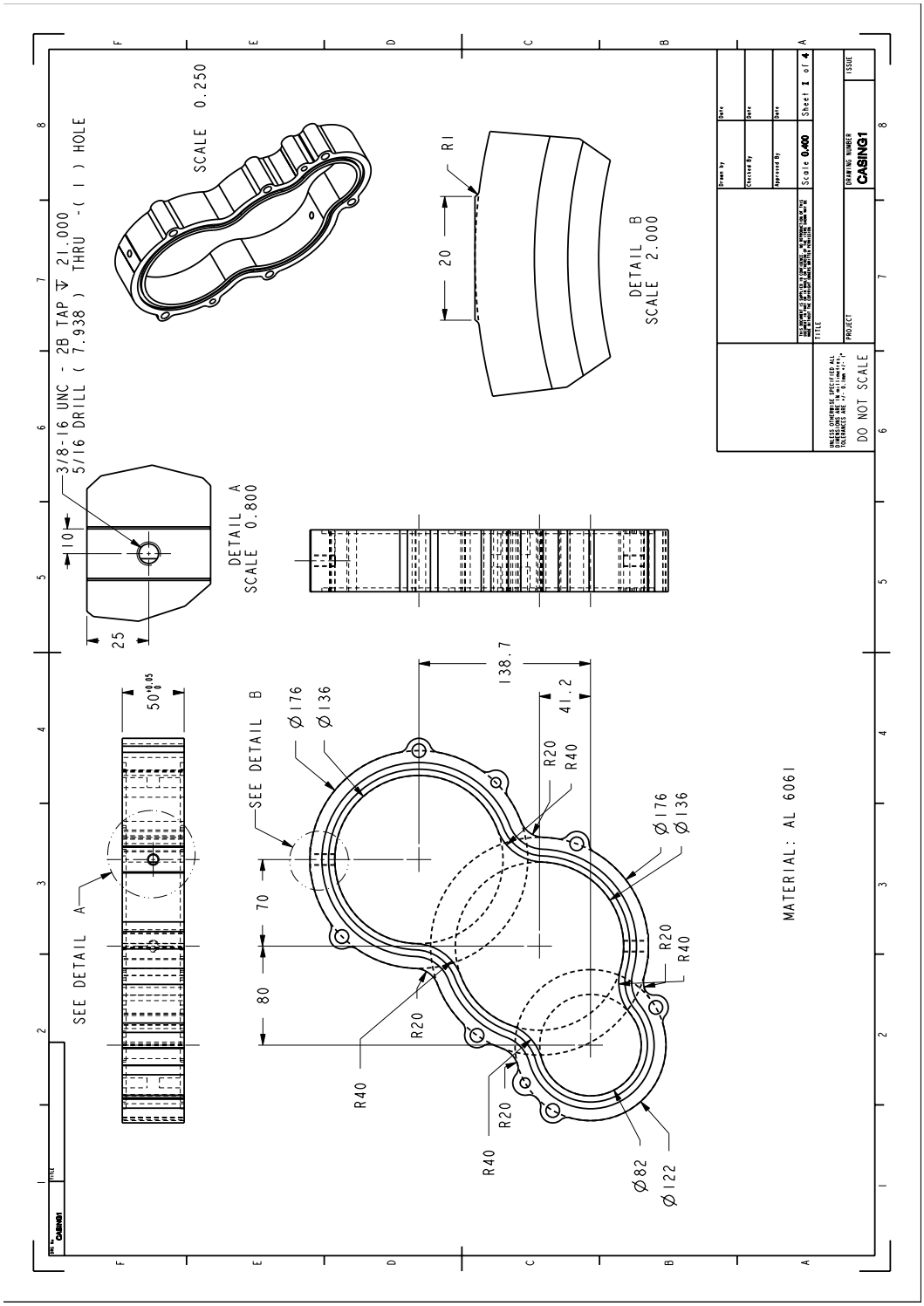
3/8-16 UNC - 2B TAP ↧ 21.000
5/16 DRILL (7.938) THRU -(1 1) HOLE
SCALE 0.250
R1
20
DETAIL B
SCALE 2.000
10
25
DETAIL A
SCALE 0.800
SEE DETAIL A
SEE DETAIL B
138.7
41.2
Ø176
Ø136
R20
R40
70
80
Ø82
Ø122
MATERIAL: AL 6061
DO NOT SCALE
Scale 0.400
Sheet 1 of 4
CASING1

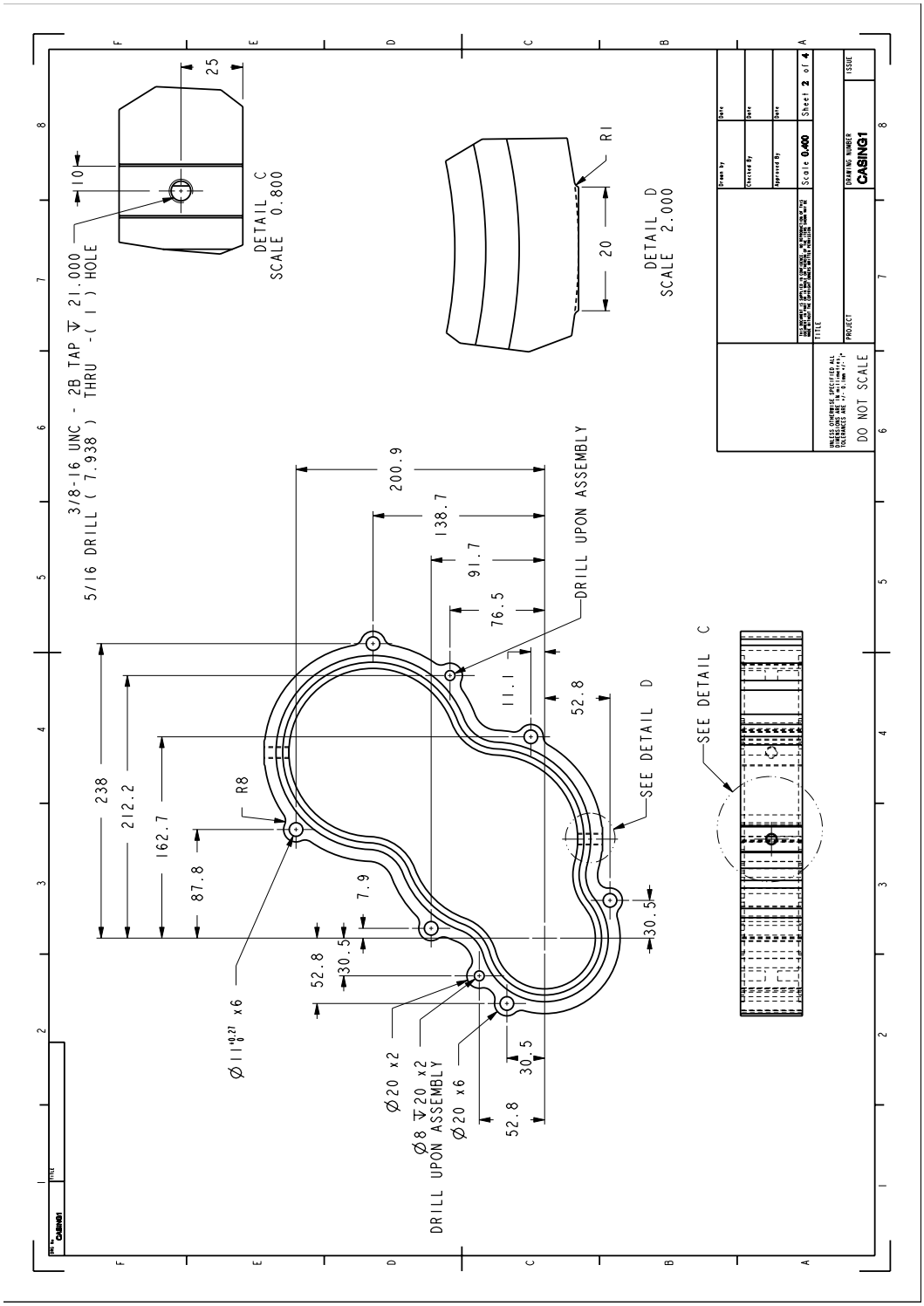
3/8-16 UNC - 2B TAP ↧ 21.000
5/16 DRILL (7.938) THRU -(1)- HOLE
10
25
DETAIL C
SCALE 0.800
R1
20
DETAIL D
SCALE 2.000
DRILL UPON ASSEMBLY
200.9
138.7
91.7
76.5
11.1
52.8
SEE DETAIL D
SEE DETAIL C
238
212.2
162.7
87.8
R8
7.9
30.5
52.8
30.5
Ø11 +0.27 -0 x6
Ø20 x2
Ø8 ↧ 20 x2
DRILL UPON ASSEMBLY
Ø20 x6
52.8
30.5
Scale 0.400
Sheet 2 of 4
DRAWING NUMBER
CASING1
ISSUE
PROJECT
DO NOT SCALE

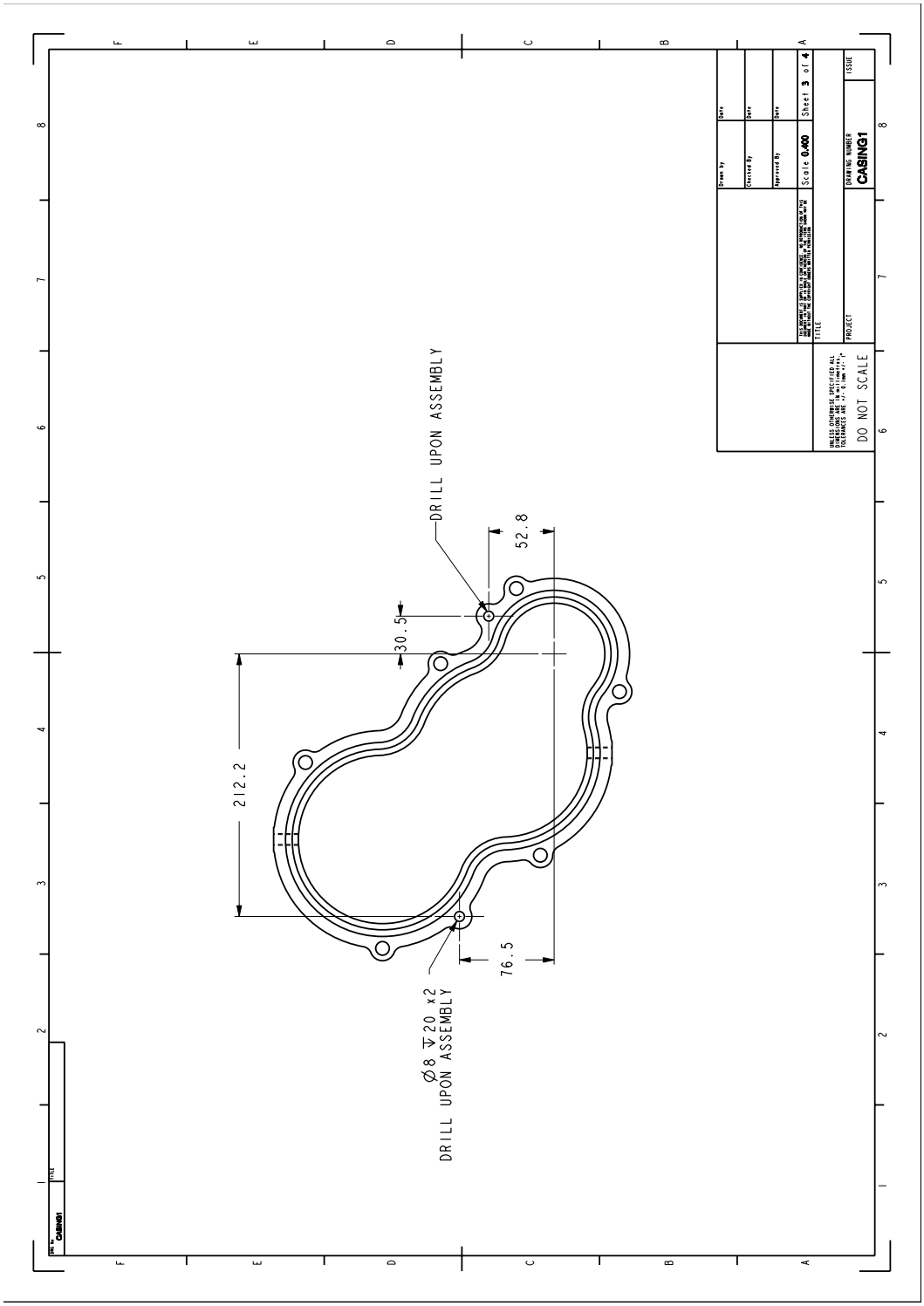
DRILL UPON ASSEMBLY
52.8
30.5
212.2
76.5
Ø8 ↧20 x2
DRILL UPON ASSEMBLY
Scale 0.400
Sheet 3 of 4
DRAWING NUMBER
CASING1
ISSUE
PROJECT
DO NOT SCALE

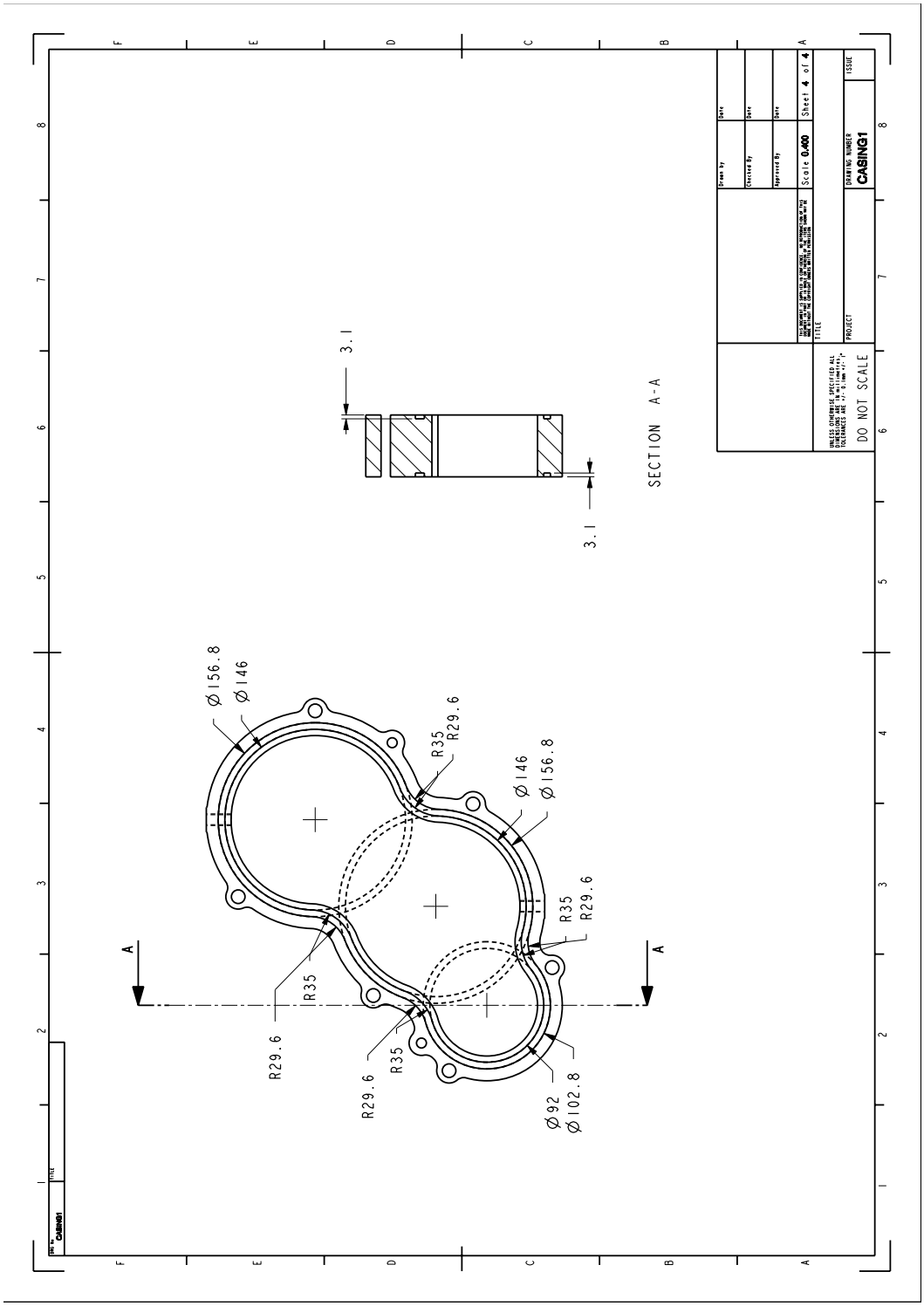
SECTION A-A
3.1
3.1
Ø156.8
Ø146
R35
R29.6
Ø146
Ø156.8
R35
R29.6
R35
R29.6
R29.6
R35
Ø92
Ø102.8
A
A
DO NOT SCALE
Scale 0.400
Sheet 4 of 4
CASING1

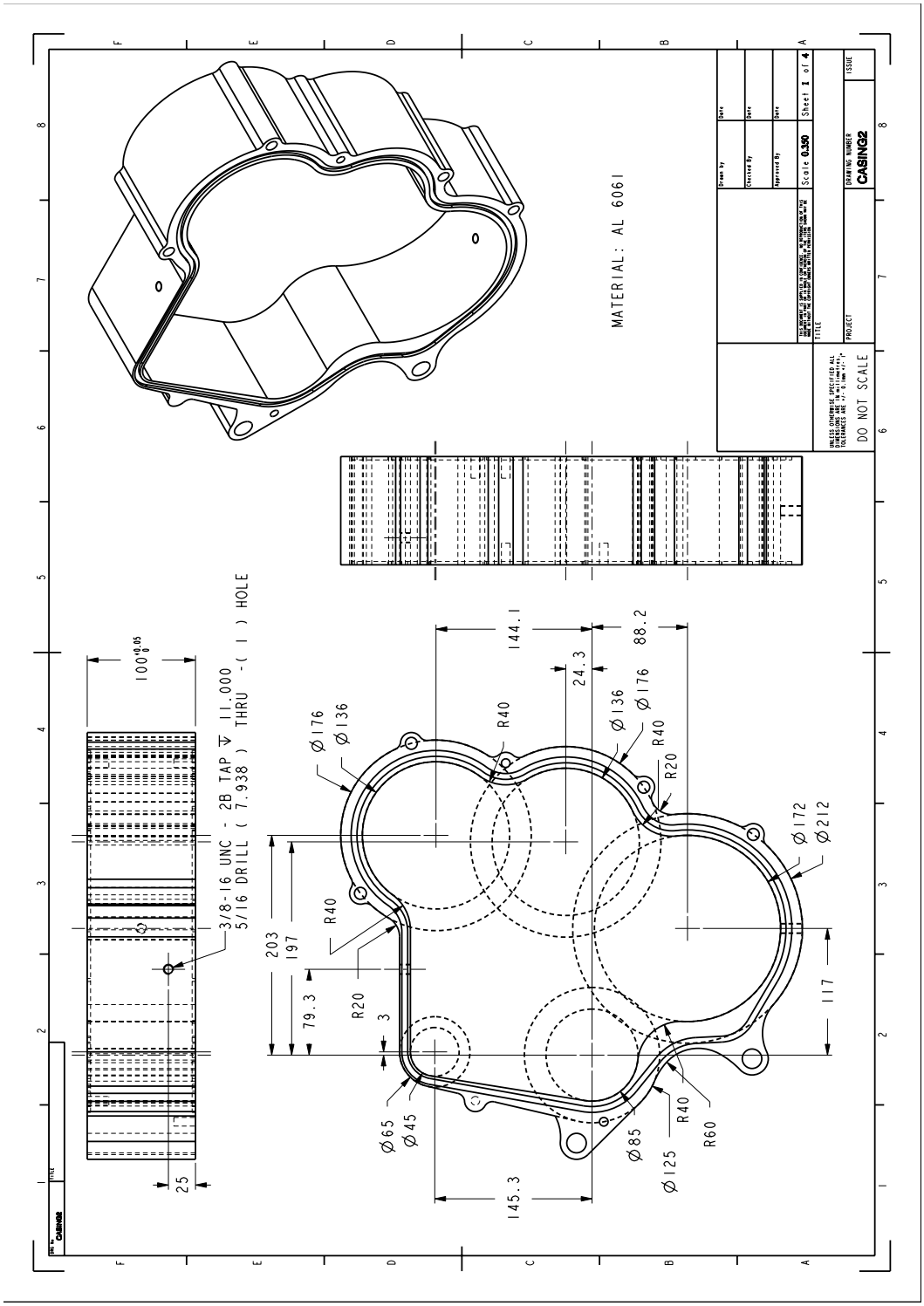
MATERIAL: AL 6061
DO NOT SCALE
CASING2
Scale 0.350
Sheet 1 of 4
3/8-16 UNC - 2B TAP ↧ 11.000
5/16 DRILL (7.938) THRU -(1)- HOLE
144.1
88.2
24.3
203
197
79.3
R40
R20
R60
Ø176
Ø136
Ø172
Ø212
Ø65
Ø45
Ø85
Ø125
117
145.3
25

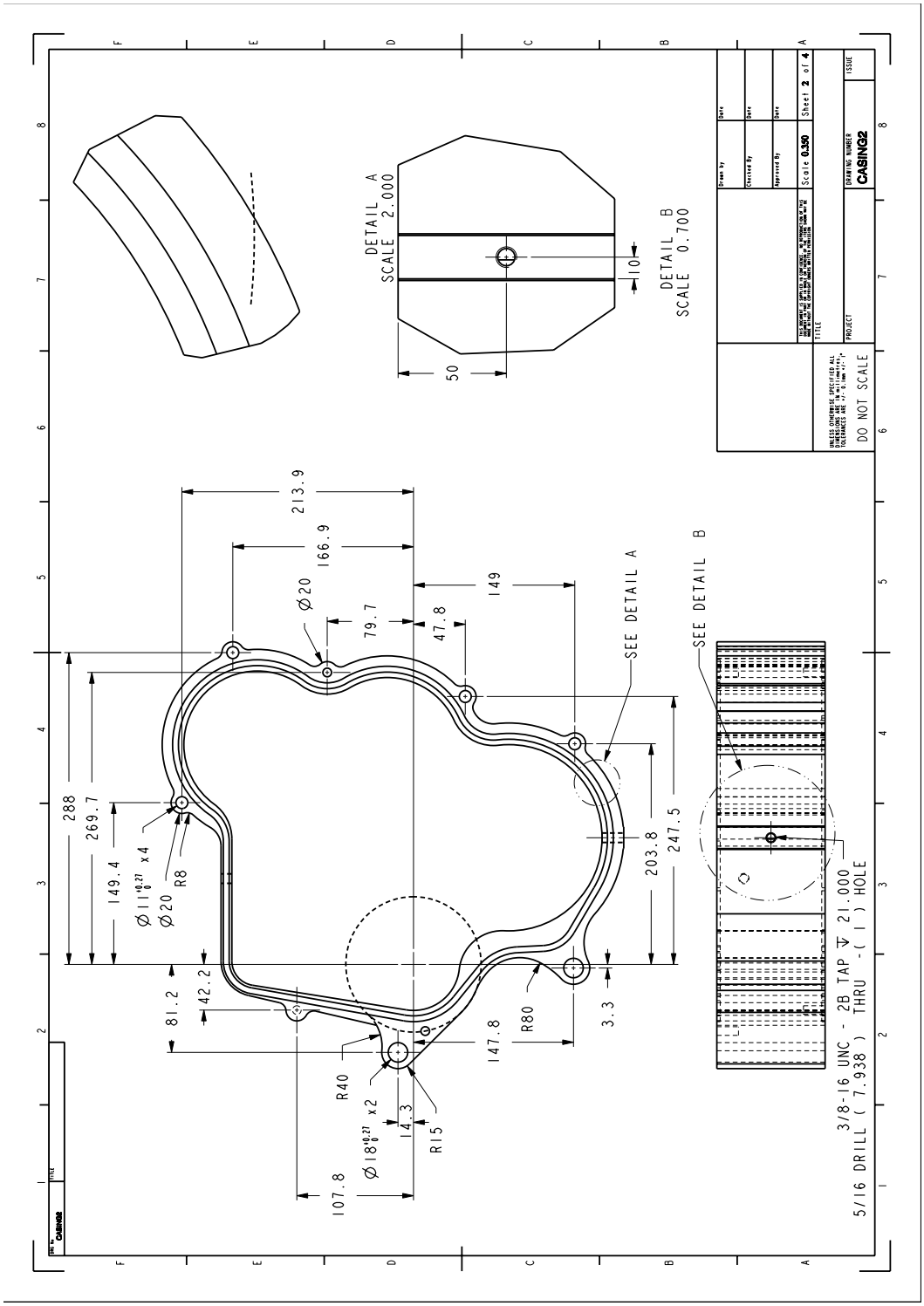
DETAIL A
SCALE 2.000
DETAIL B
SCALE 0.700
SEE DETAIL A
SEE DETAIL B
213.9
166.9
149
79.7
47.8
288
269.7
149.4
81.2
42.2
203.8
247.5
147.8
R80
3.3
107.8
R40
R15
14.3
50
10
R8
Ø20
Ø20
x4
x2
3/8-16 UNC - 2B TAP ∓ 21.000
5/16 DRILL (7.938) THRU -(11) HOLE
DO NOT SCALE
PROJECT
DRAWING NUMBER
CASING2
ISSUE
Scale 0.350
Sheet 2 of 4
Drawn by
Checked By
Approved By
Date
TITLE

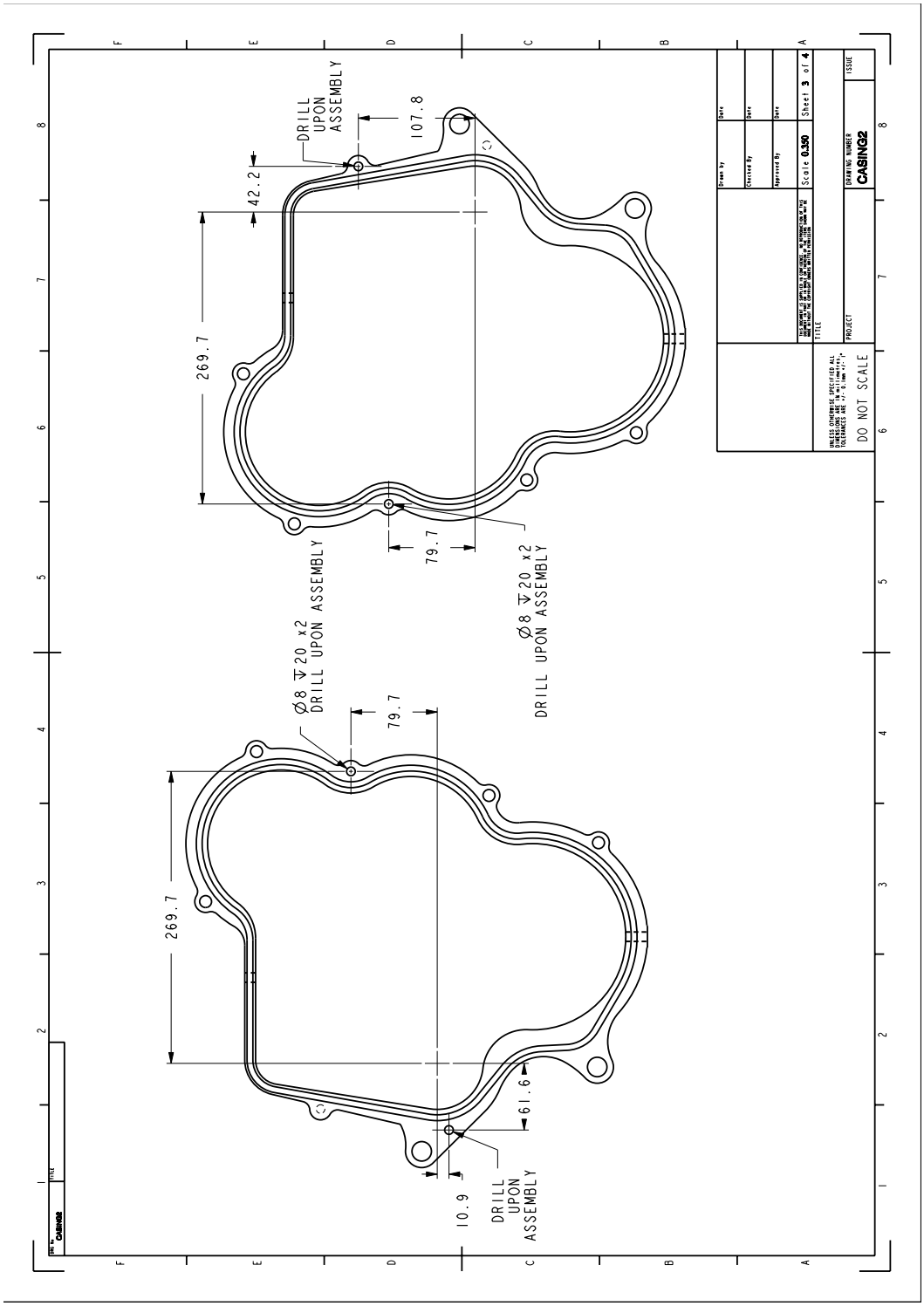
DRILL UPON ASSEMBLY
107.8
42.2
269.7
79.7
Ø8 ∓20 x2 DRILL UPON ASSEMBLY
Ø8 ∓20 x2 DRILL UPON ASSEMBLY
79.7
269.7
61.6
10.9
DRILL UPON ASSEMBLY
DO NOT SCALE
CASING2
Scale 0.350
Sheet 3 of 4

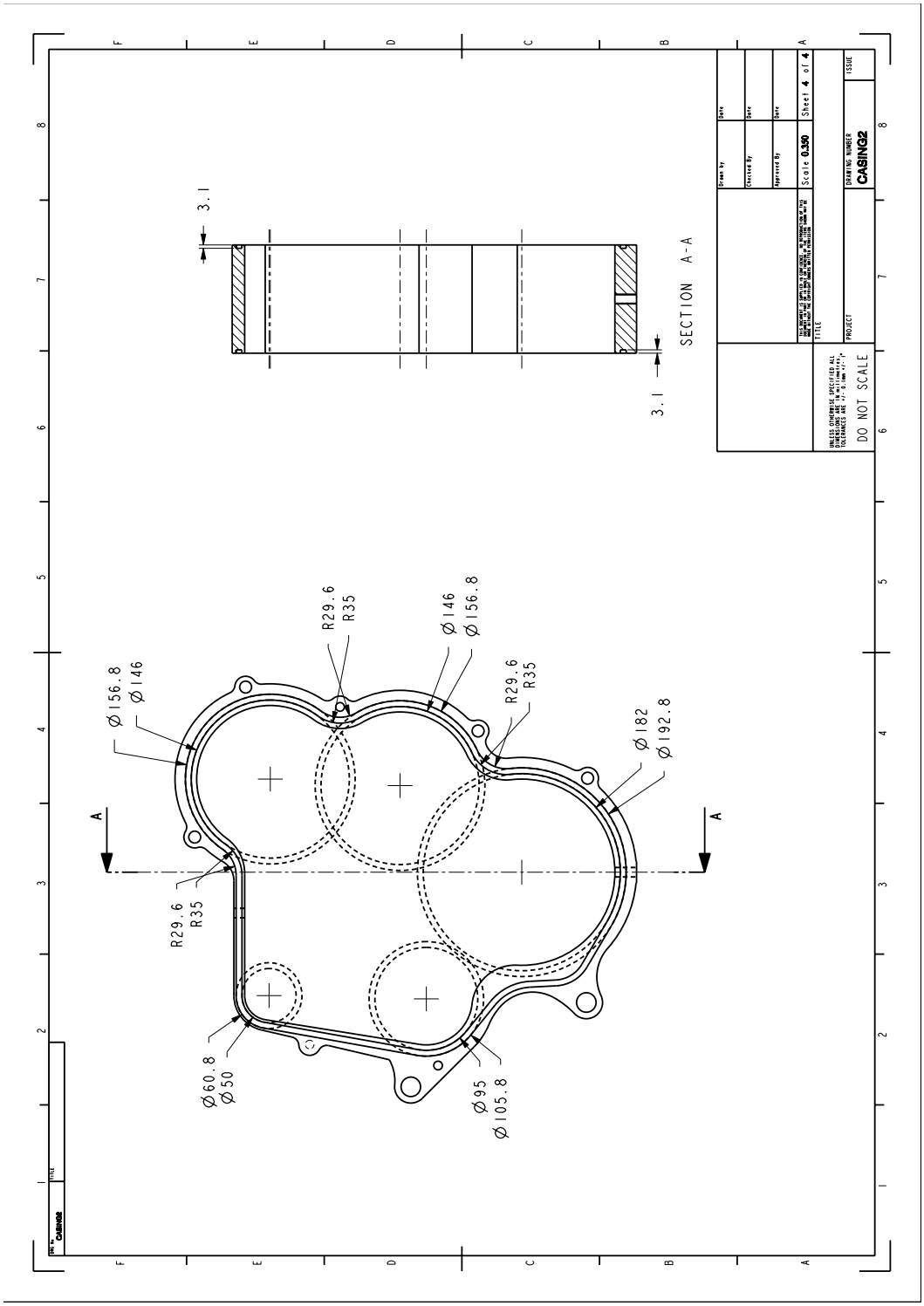
3.1
3.1
SECTION A-A
Ø156.8
Ø146
R29.6
R35
Ø146
Ø156.8
R29.6
R35
Ø182
Ø192.8
A
A
R29.6
R35
Ø60.8
Ø50
Ø95
Ø105.8
DO NOT SCALE
CASING2
Scale 0.330
Sheet 4 of 4

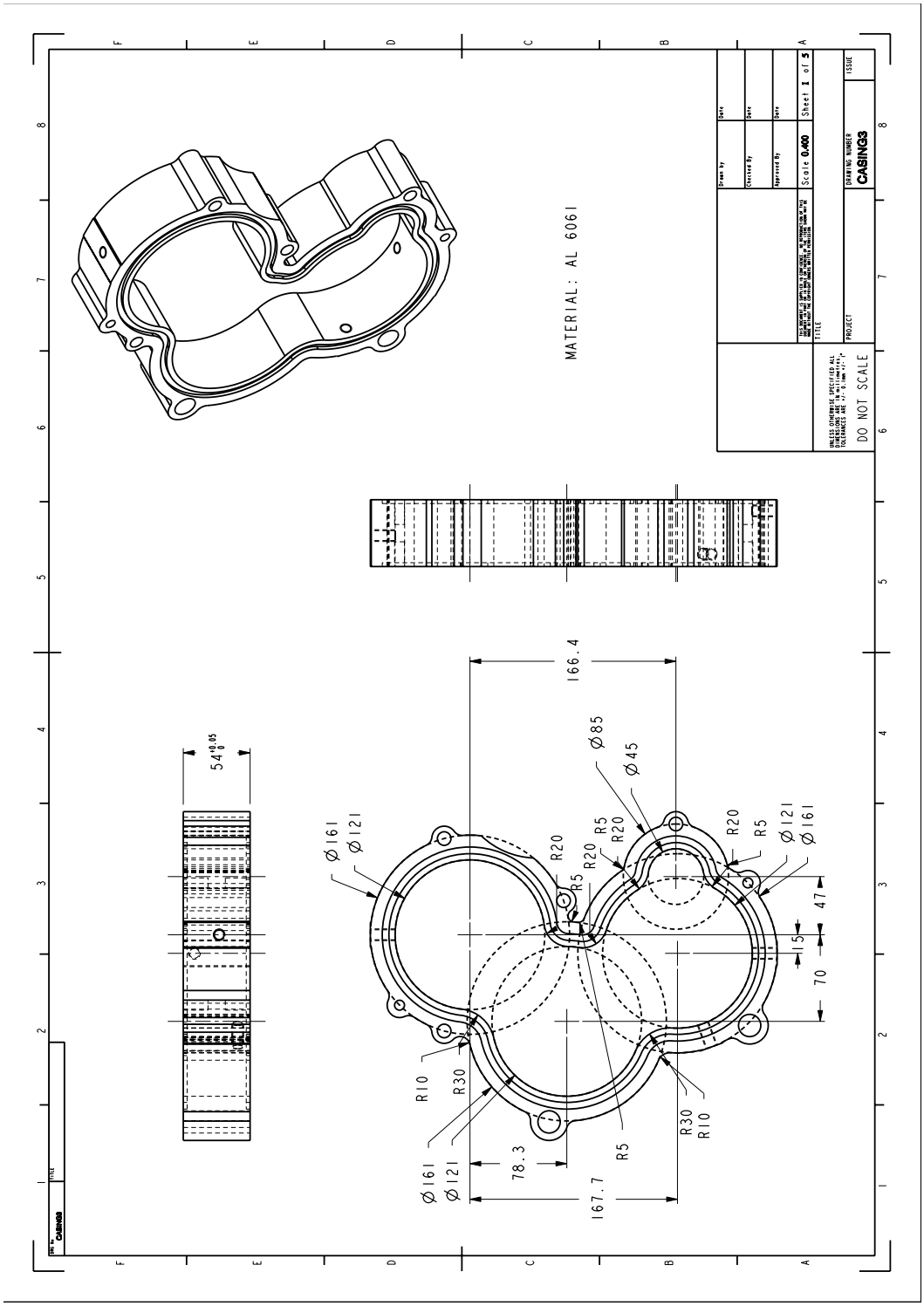
MATERIAL: AL 6061
DO NOT SCALE
CASINGS
Scale 0.400
Sheet 1 of 5
166.4
167.7
78.3
54 +0.05 -0.0
Ø85
Ø45
Ø161
Ø121
R20
R5
R10
R30
47
15
70

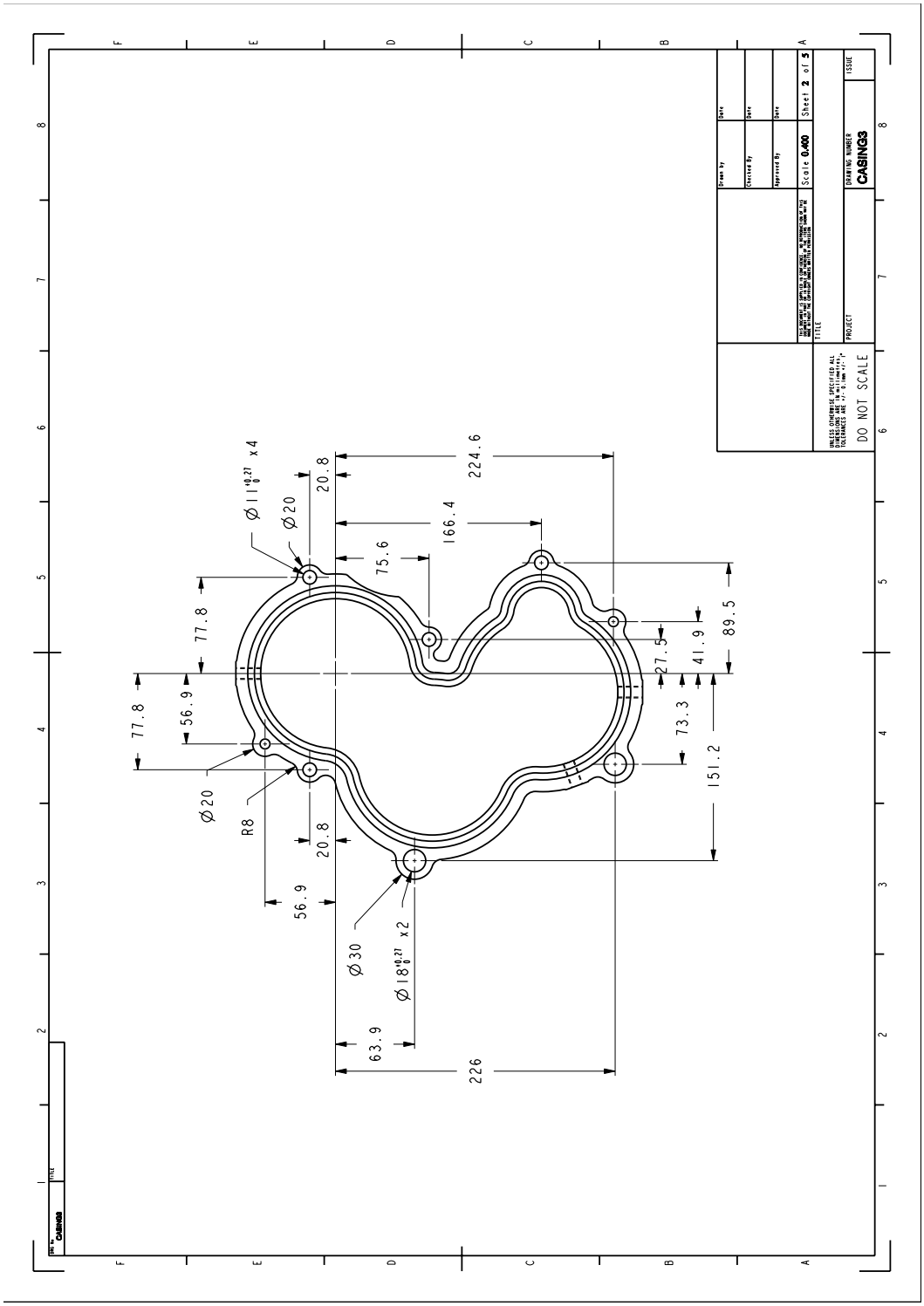
Ø111 +0.27 0 x4
Ø20
20.8
224.6
166.4
75.6
77.8
89.5
41.9
27.5
77.8
56.9
73.3
151.2
Ø20
R8
20.8
56.9
Ø30
Ø18 +0.27 0 x2
63.9
226
Scale 0.400
Sheet 2 of 5
DRAWING NUMBER
CASINGS
ISSUE
PROJECT
DO NOT SCALE

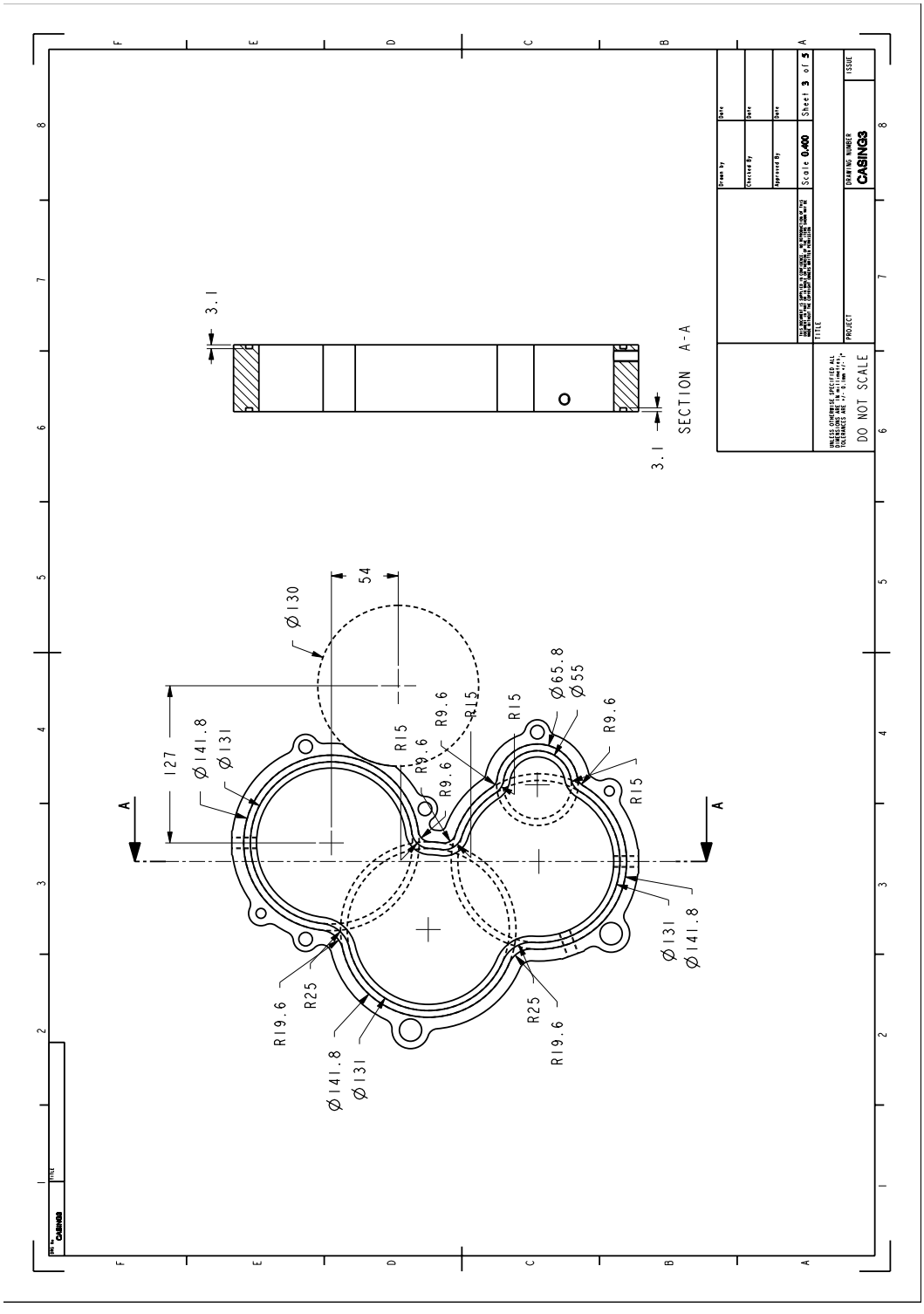
3.1
SECTION A-A
3.1
Ø130
54
127
Ø141.8
Ø131
R15
R9.6
R9.6
R9.6
R15
R15
Ø65.8
Ø55
R9.6
R15
A
A
R19.6
R25
Ø141.8
Ø131
R25
R19.6
Ø131
Ø141.8
Scale 0.400
Sheet 3 of 5
DRAWING NUMBER
CASINGS
ISSUE
PROJECT
DO NOT SCALE

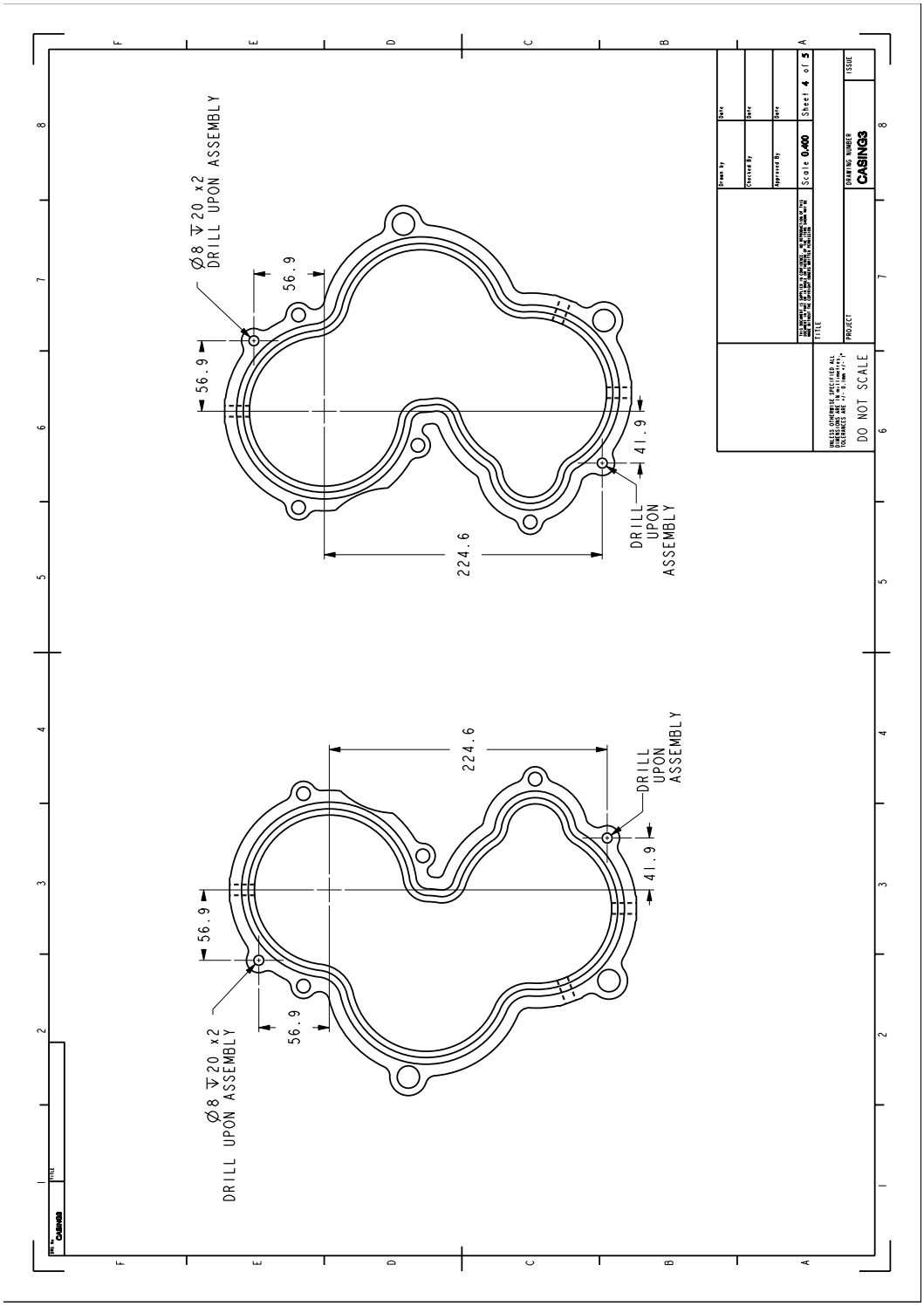
Ø8 ⊽20 x2
DRILL UPON ASSEMBLY
56.9
56.9
224.6
41.9
DRILL
UPON
ASSEMBLY
Ø8 ⊽20 x2
DRILL UPON ASSEMBLY
56.9
56.9
224.6
41.9
DRILL
UPON
ASSEMBLY
Drawn by
Date
Checked By
Date
Approved By
Date
Scale 0.400
Sheet 4 of 5
PROJECT
DRAWING NUMBER
CASINGS
ISSUE
DO NOT SCALE

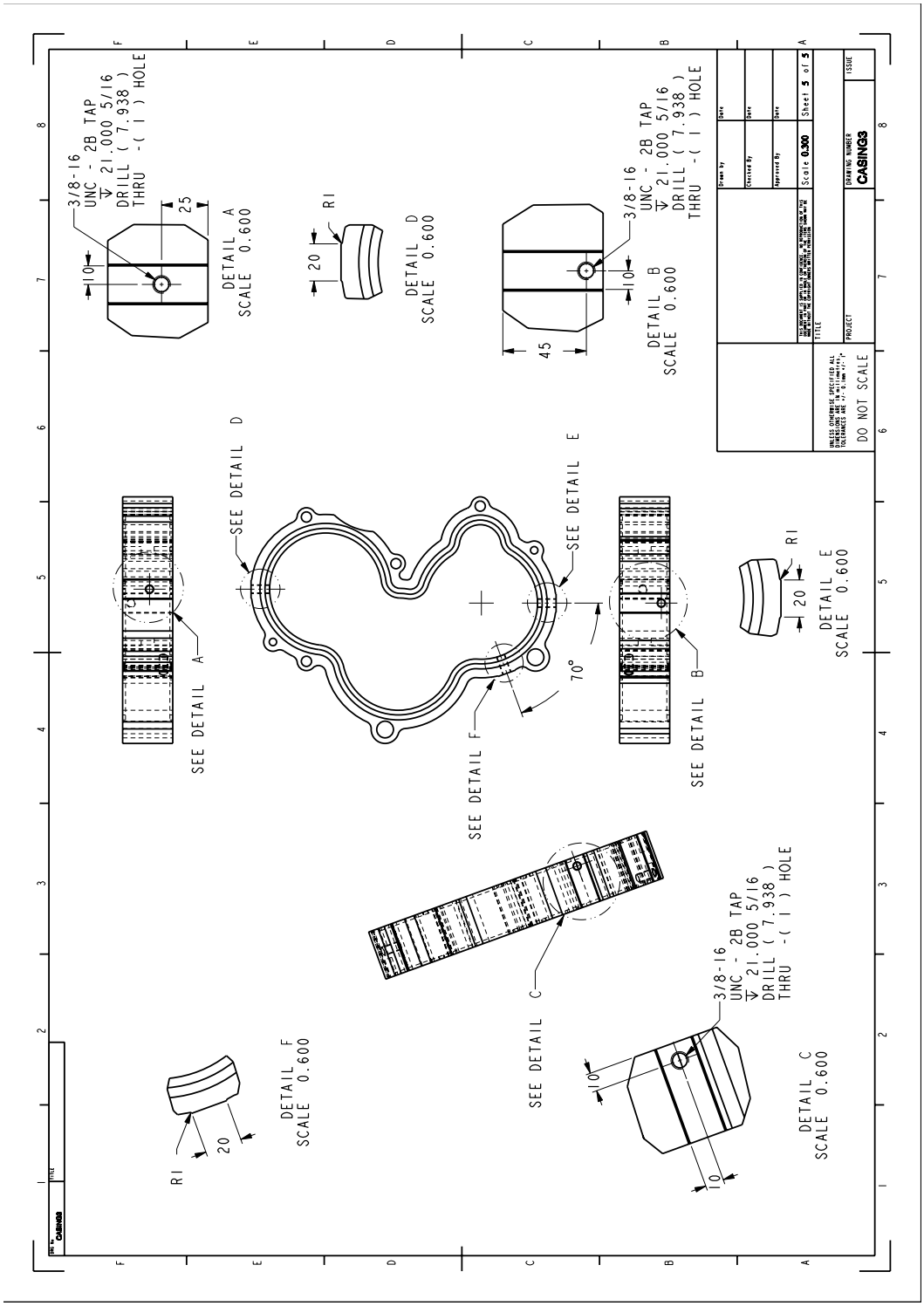
3/8-16
UNC - 2B TAP
↧ 21.000 5/16
DRILL (7.938)
THRU -(1)- HOLE
25
10
DETAIL A
SCALE 0.600
R1
20
DETAIL D
SCALE 0.600
45
DETAIL B
SCALE 0.600
SEE DETAIL A
SEE DETAIL D
SEE DETAIL E
SEE DETAIL B
SEE DETAIL F
70°
SEE DETAIL C
DETAIL E
SCALE 0.600
DETAIL F
SCALE 0.600
DETAIL C
SCALE 0.600
Scale 0.300
Sheet 5 of 5
DRAWING NUMBER
CASINGS
DO NOT SCALE

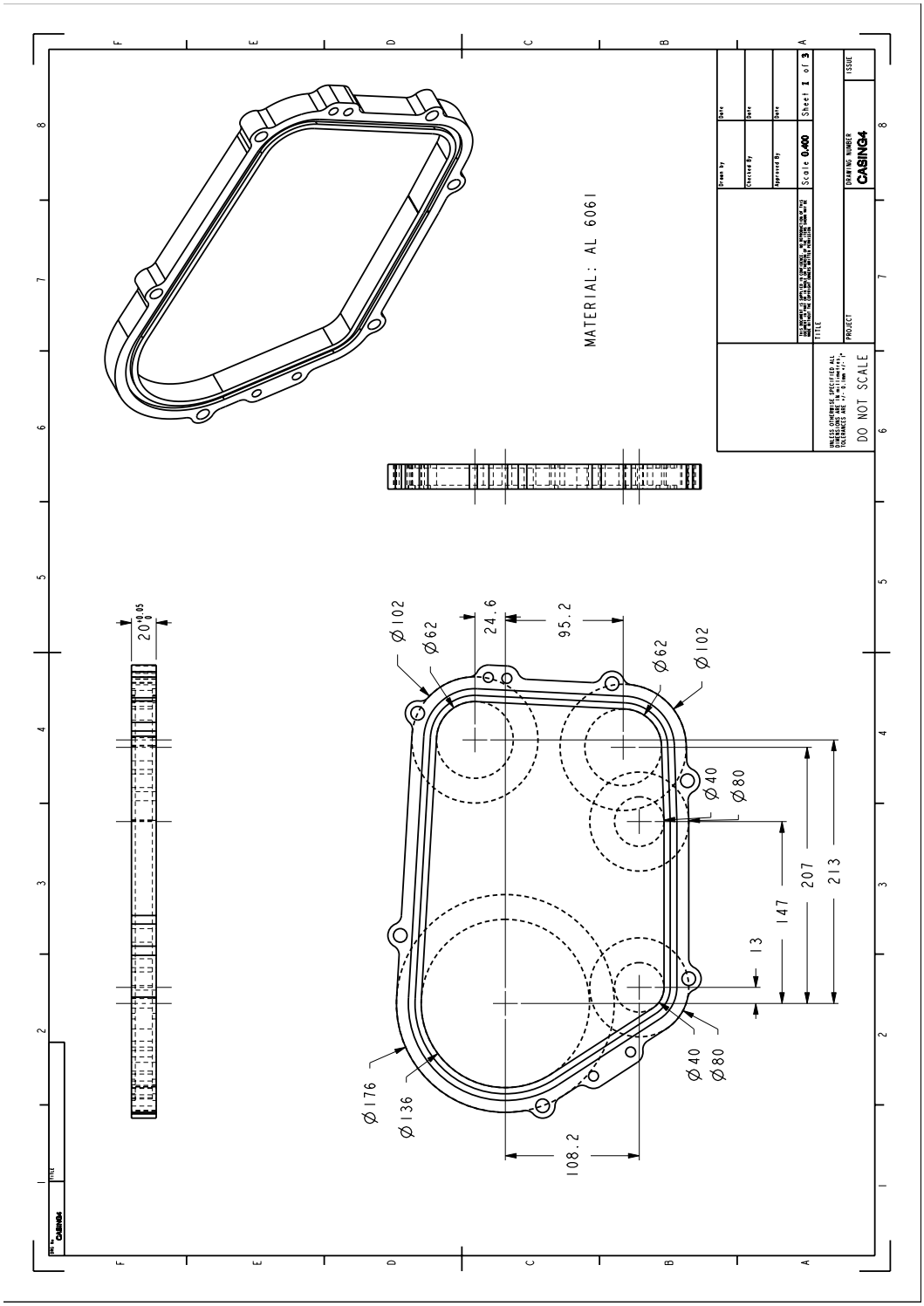
MATERIAL: AL 6061
DO NOT SCALE
CASING4
Scale 0.400
Sheet 1 of 3
Ø102
Ø62
24.6
95.2
Ø62
Ø102
Ø40
Ø80
147
207
213
13
Ø40
Ø80
Ø176
Ø136
108.2
20

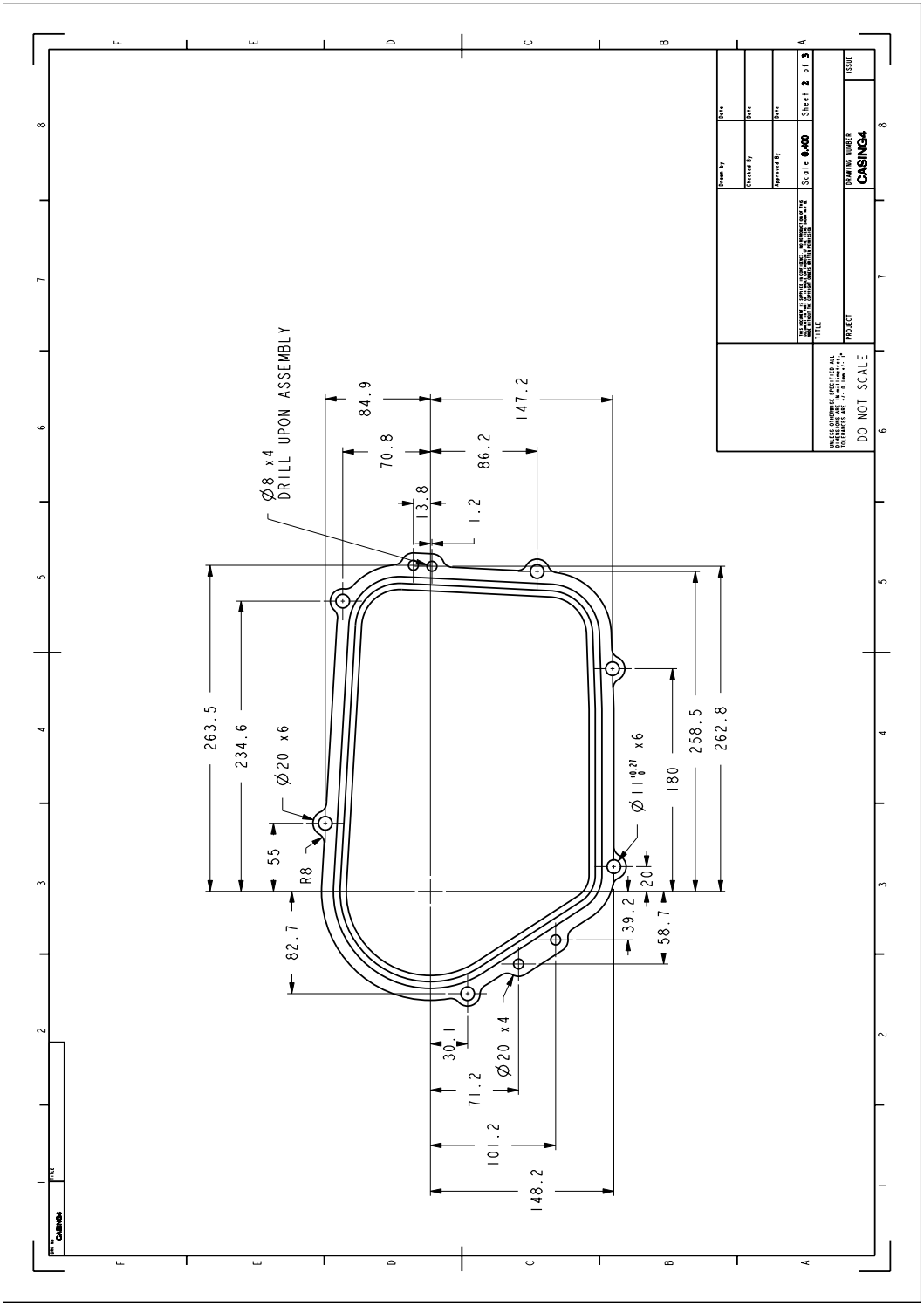
Ø8 x4
DRILL UPON ASSEMBLY
84.9
70.8
13.8
1.2
147.2
86.2
263.5
234.6
Ø20 x6
55
R8
82.7
Ø11 +0.27 0 x6
180
258.5
262.8
20
39.2
58.7
30.1
71.2
Ø20 x4
101.2
148.2
DO NOT SCALE
CASING4
Scale 0.400
Sheet 2 of 3

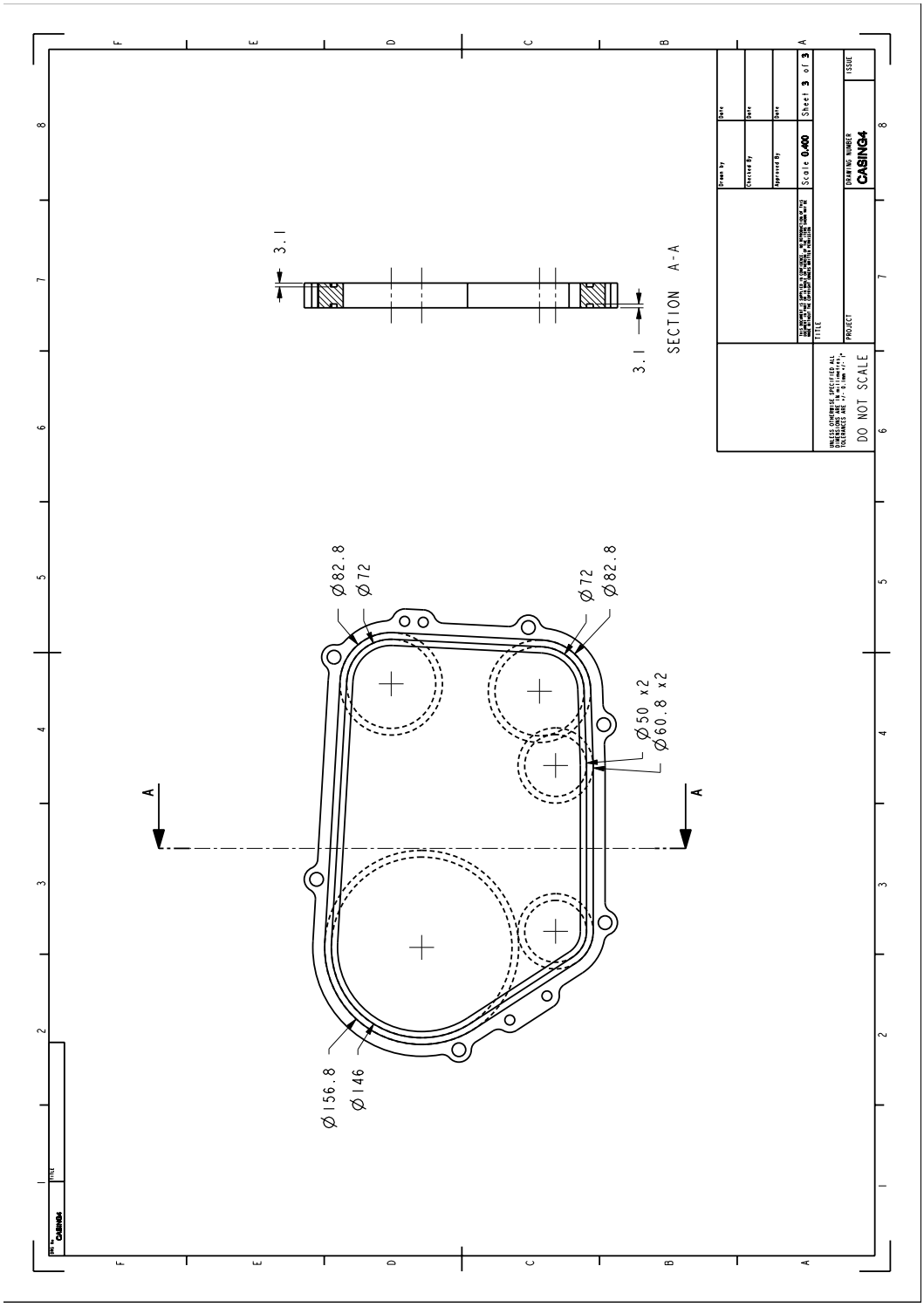
3.1
3.1
SECTION A-A
Ø82.8
Ø72
Ø72
Ø82.8
Ø50 x2
Ø60.8 x2
Ø156.8
Ø146
A
A
DO NOT SCALE
CASING4
Sheet 3 of 3
Scale 0.400

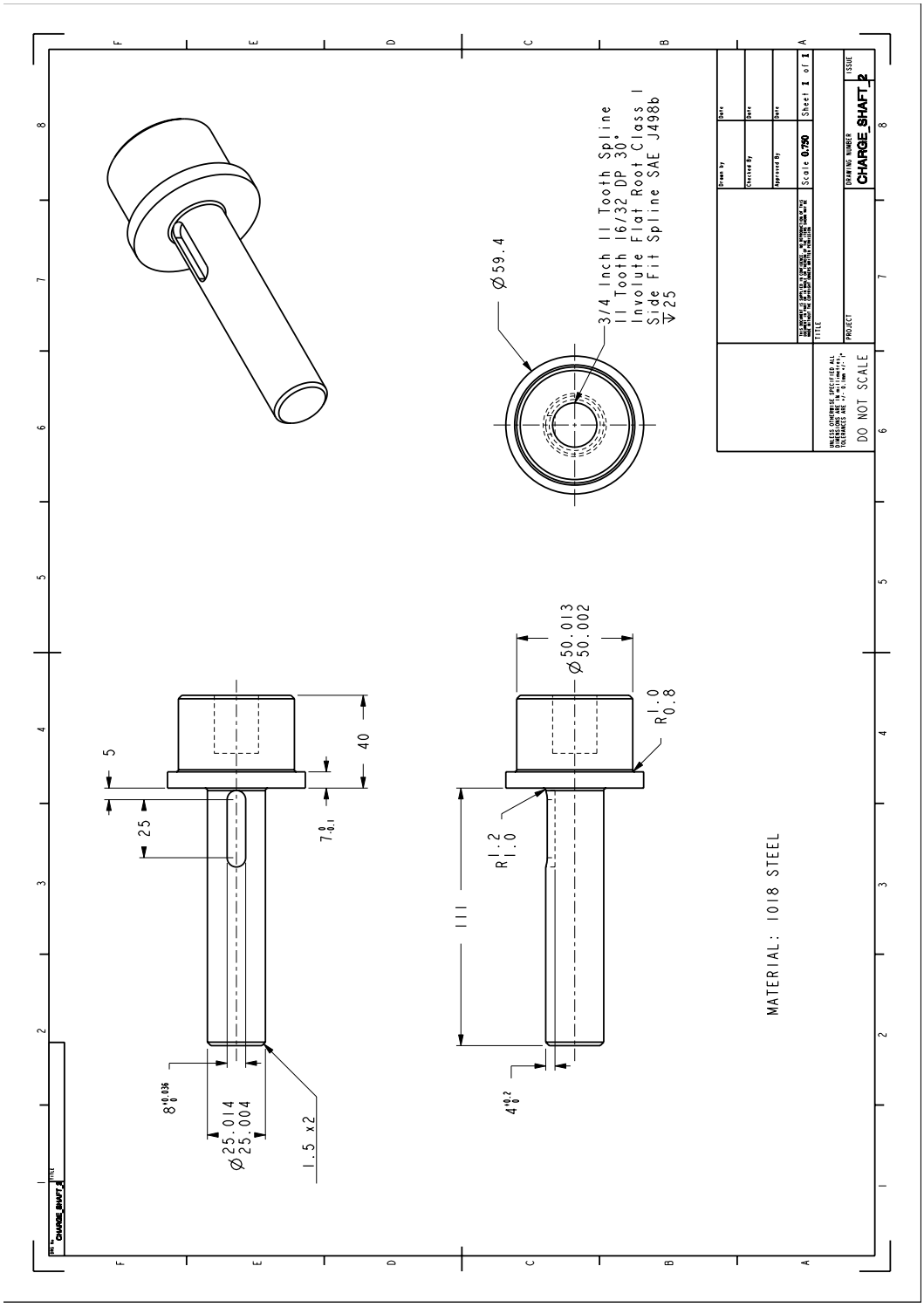
Ø59.4
3/4 Inch 11 Tooth Spline
11 Tooth 16/32 DP 30°
Involute Flat Root Class 1
Side Fit Spline SAE J498b
▽25
Ø50.013
Ø50.002
R1.0
0.8
R1.2
1.0
111
40
5
25
7.0 0.1
8 0.036 0
Ø25.014
Ø25.004
1.5 x2
4 0.2 0
MATERIAL: 1018 STEEL
DO NOT SCALE
PROJECT
DRAWING NUMBER
CHARGE_SHAFT_2
ISSUE
Scale 0.750
Sheet 1 of 1
Drawn by
Checked By
Approved By
Date
TITLE
CHARGE_SHAFT_2

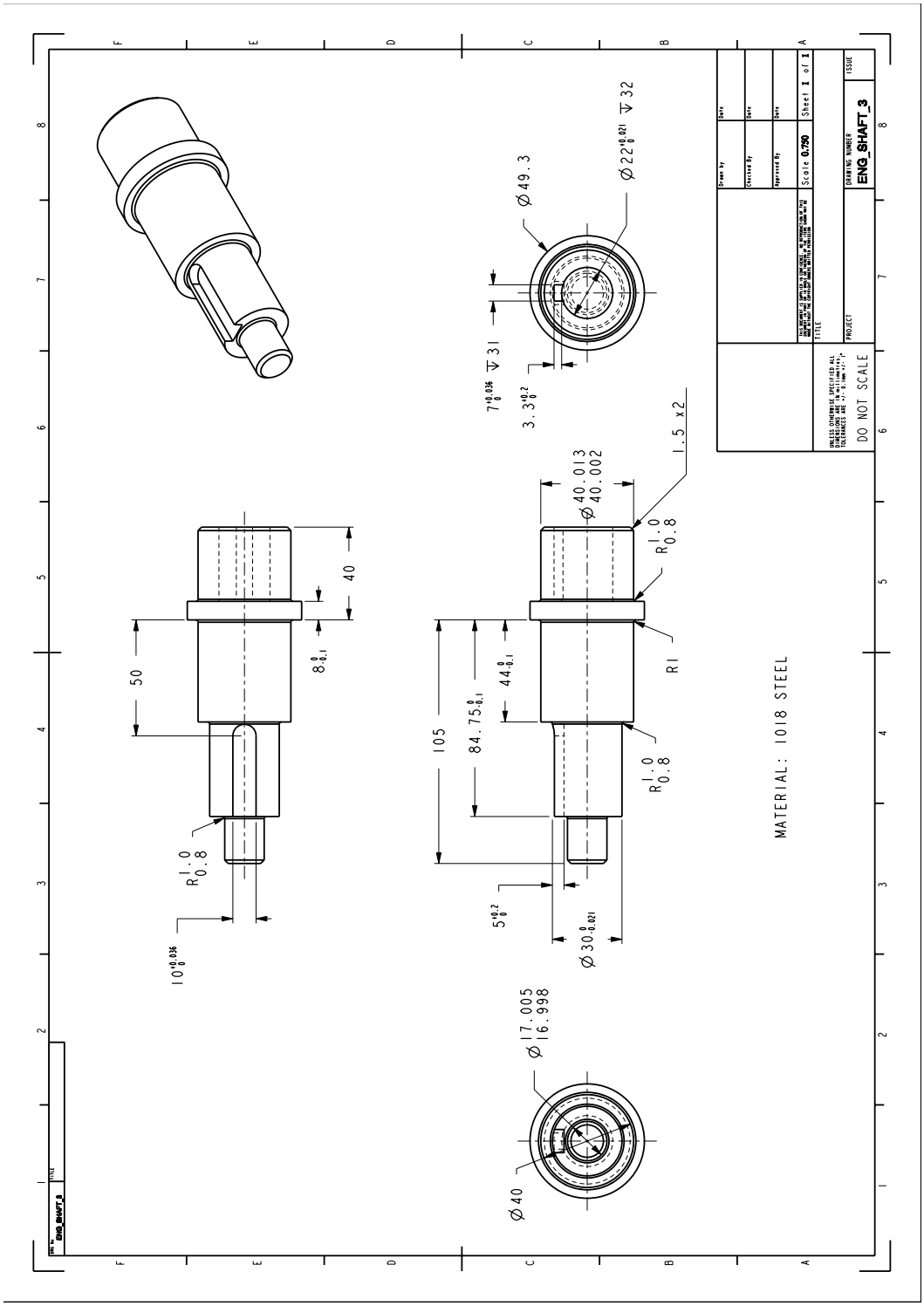
ENG_SHAFT_3
Scale 0.750
Sheet 1 of 1
DRAWING NUMBER
ENG_SHAFT_3
ISSUE
PROJECT
DO NOT SCALE
MATERIAL: 1018 STEEL
105
84.75
50
40
44
8
10
7
3.3
5
1.5 x2
R1
Ø49.3
Ø22
Ø40.013
Ø40.002
Ø30
Ø17.005
Ø16.998
Ø40

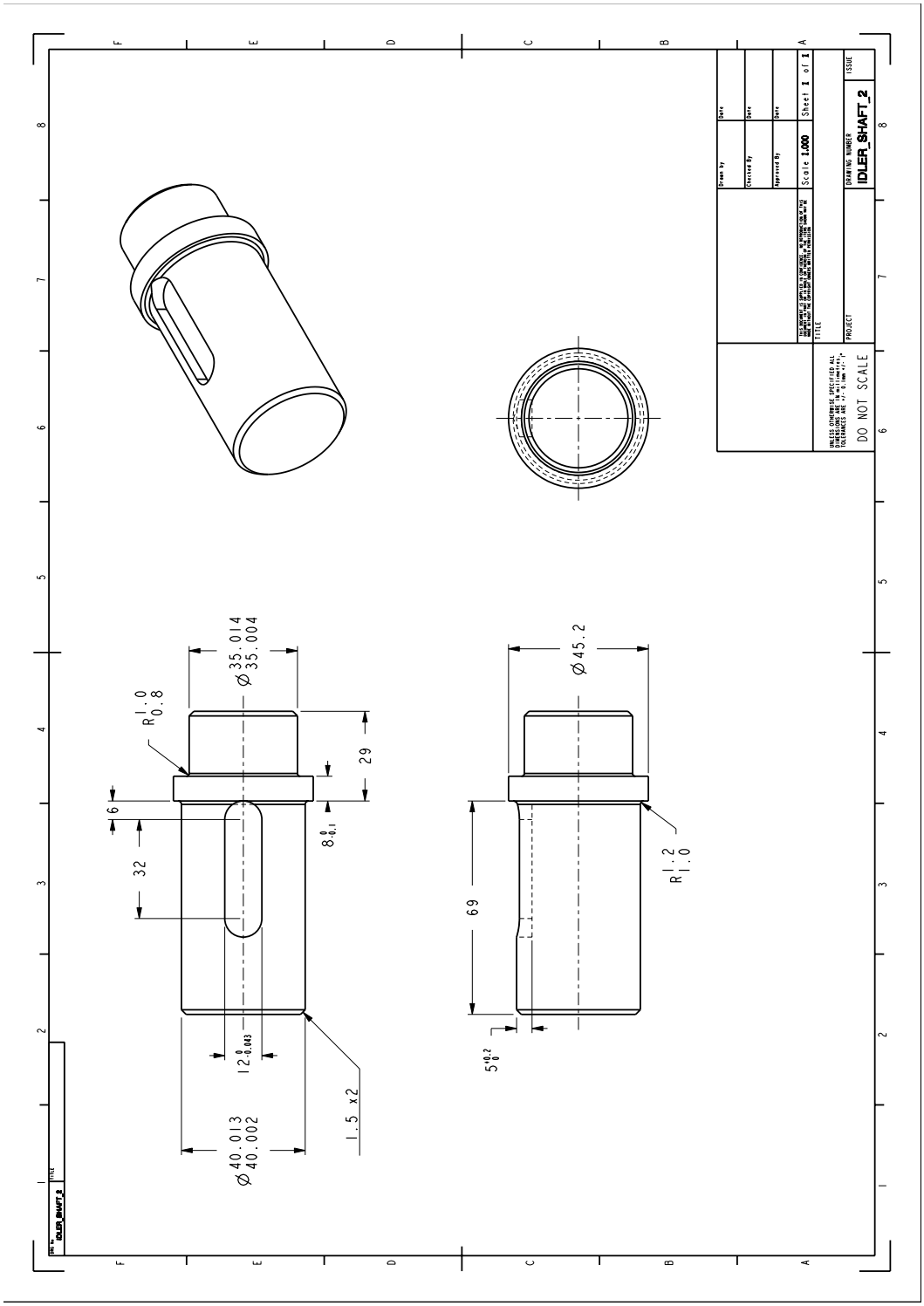
DO NOT SCALE
IDLER_SHAFT_2
Scale 1.000
Sheet 1 of 1
Ø35.014
Ø35.004
R1.0
0.8
29
6
32
8
0.1
12
0.043
Ø40.013
Ø40.002
1.5 x2
Ø45.2
69
R1.2
1.0
5
0.2
0

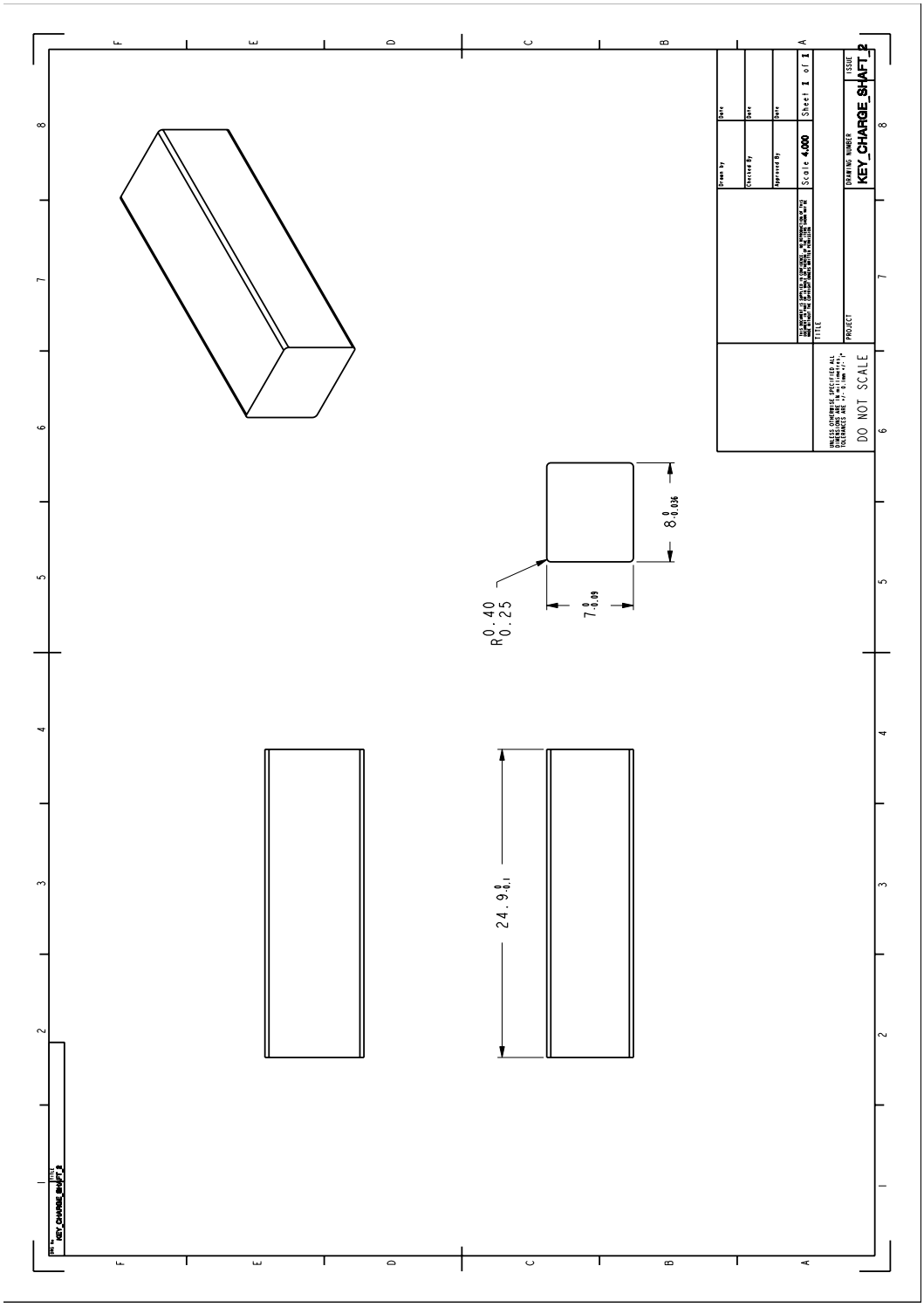
DO NOT SCALE
KEY_CHARGE_SHAFT_2
Scale 4.000
Sheet 1 of 1
24.9
7
8
R0.40
R0.25

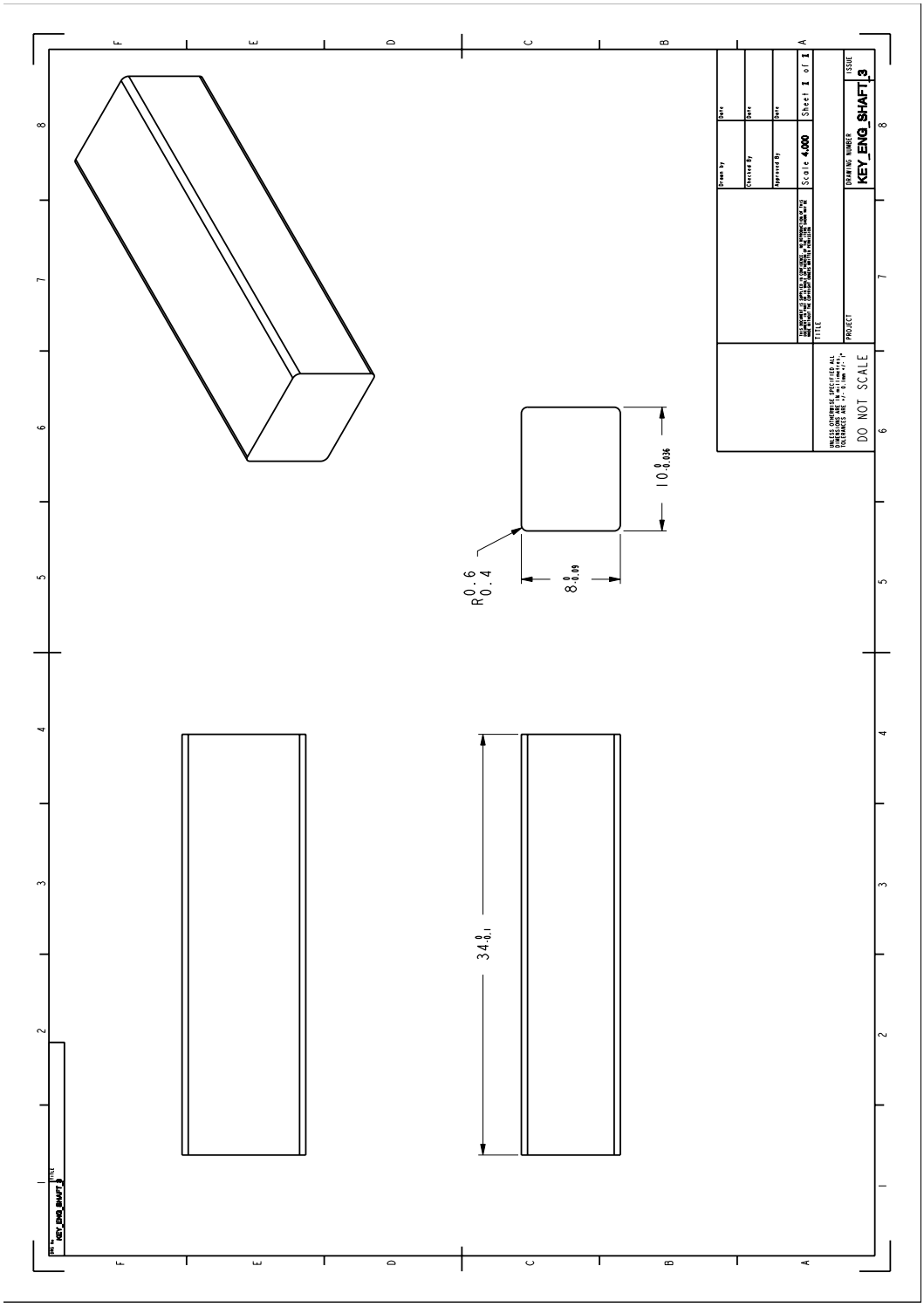
R 0.6 0.4
8 0 -0.09
10 0 -0.036
34 0 -0.1
DO NOT SCALE
KEY_ENG_SHAFT_3
Scale 4.000
Sheet 1 of 1

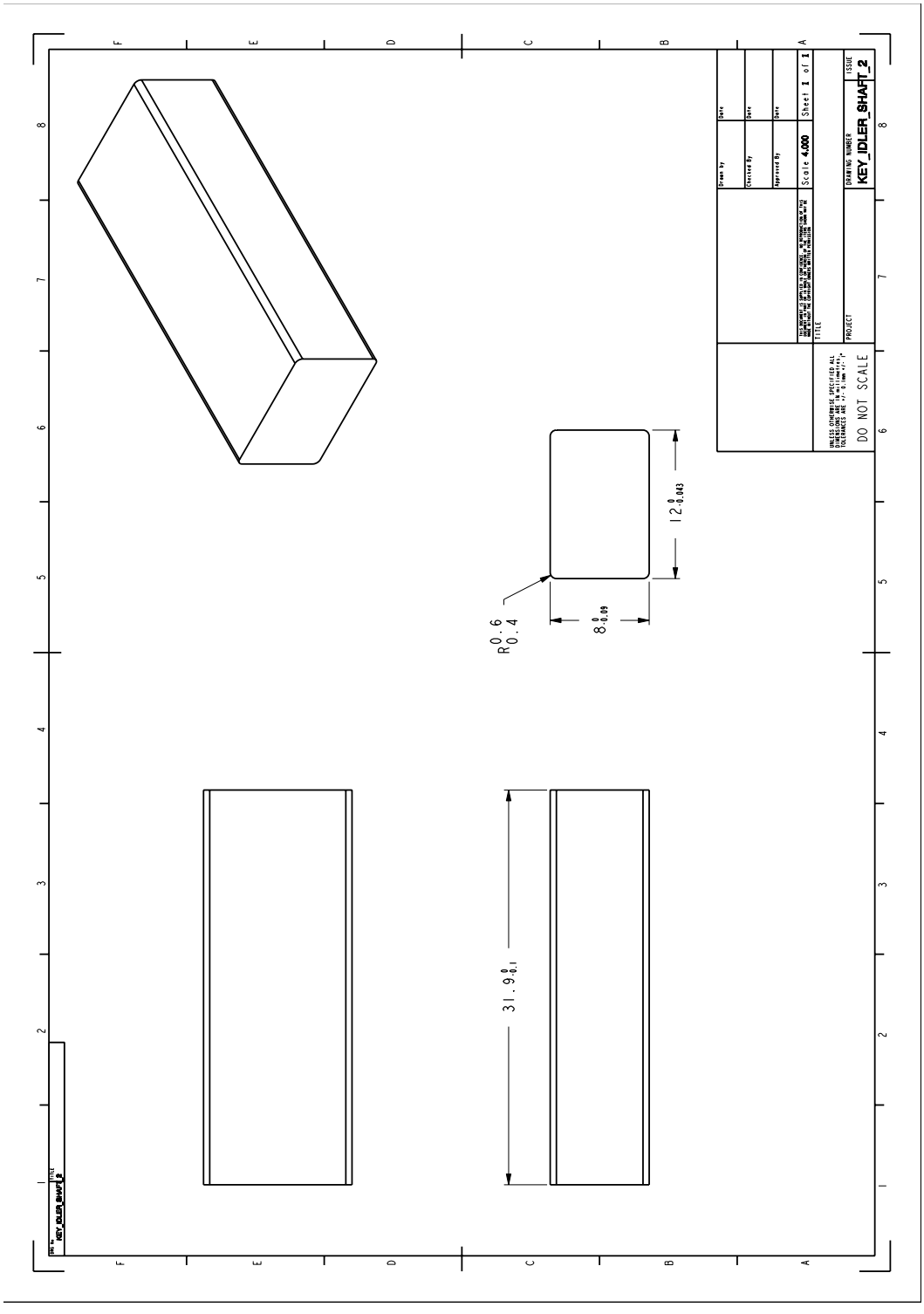
DO NOT SCALE
KEY_IDLER_SHAFT_2
Scale 4.000
Sheet 1 of 1
31.9
12
8
R0.6

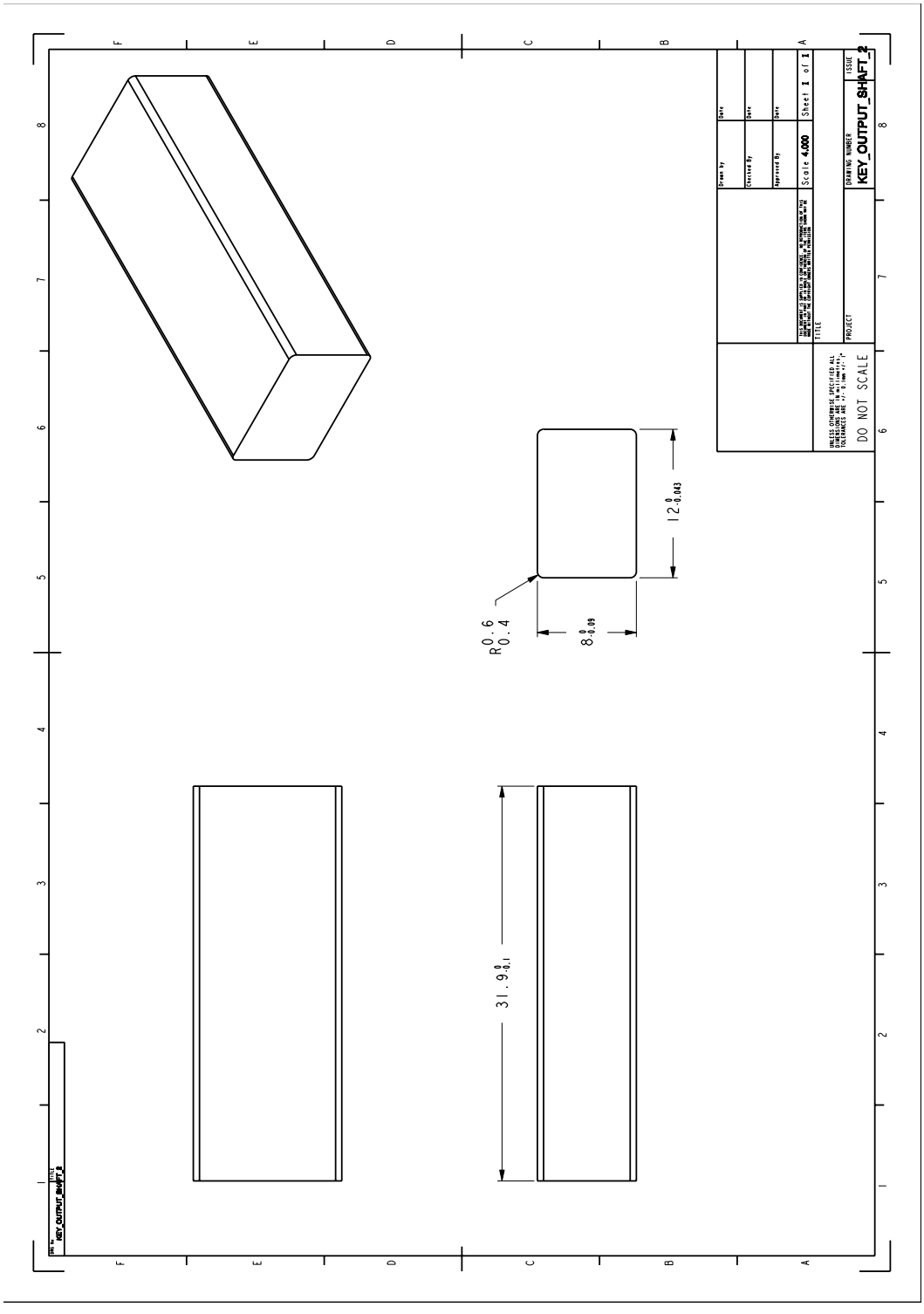
DO NOT SCALE
KEY_OUTPUT_SHAFT_2
Scale 4.000
Sheet 1 of 1
31.9
12
8
R0.6

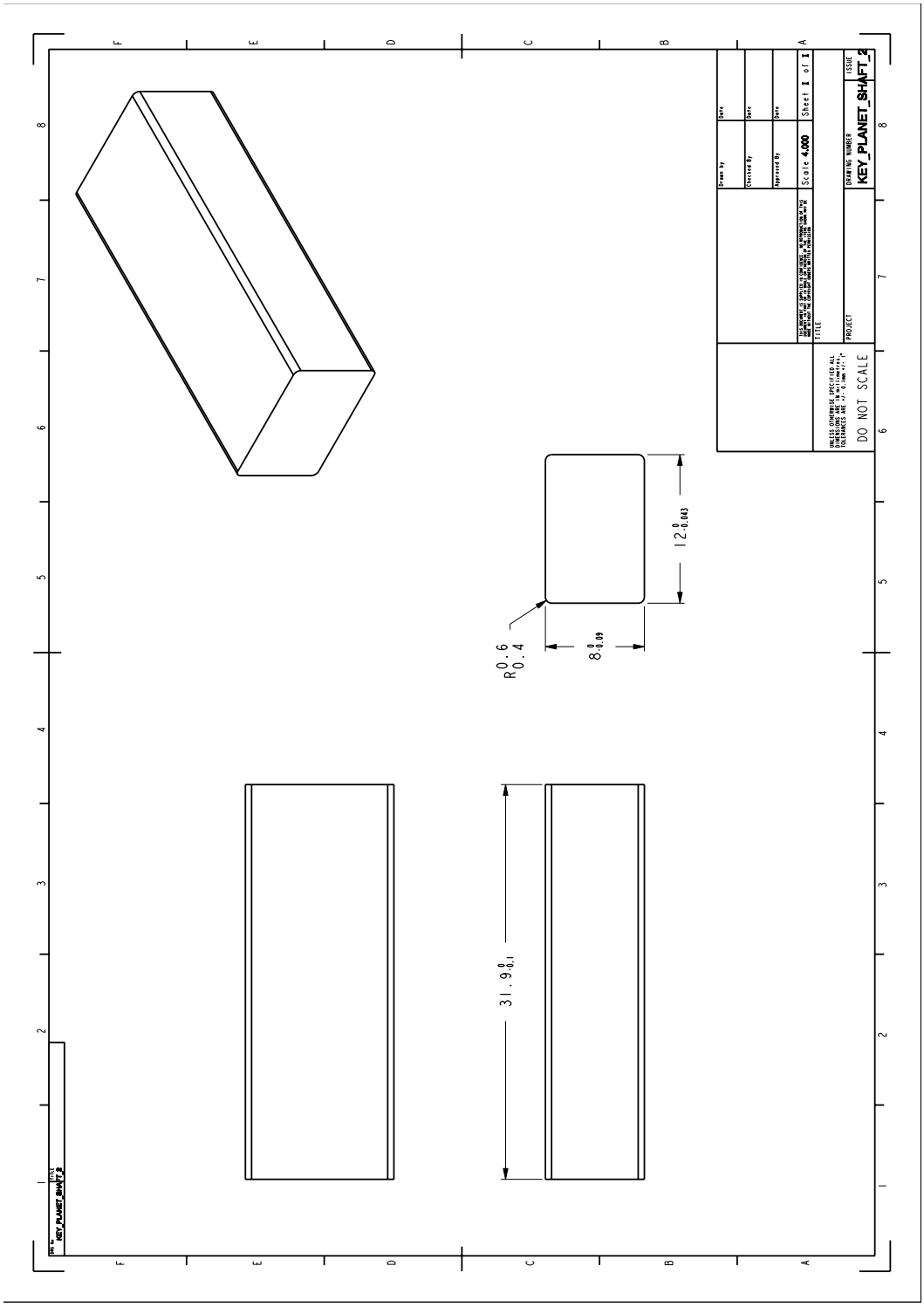
KEY_PLANET_SHAFT_2
Drawn by
Checked By
Approved By
Date
Scale 4.000
Sheet 1 of 1
PROJECT
DRAWING NUMBER
KEY_PLANET_SHAFT_2
ISSUE
DO NOT SCALE
12.0 -0.043
8.0 -0.09
R0.6 0.4
31.9 -0.1

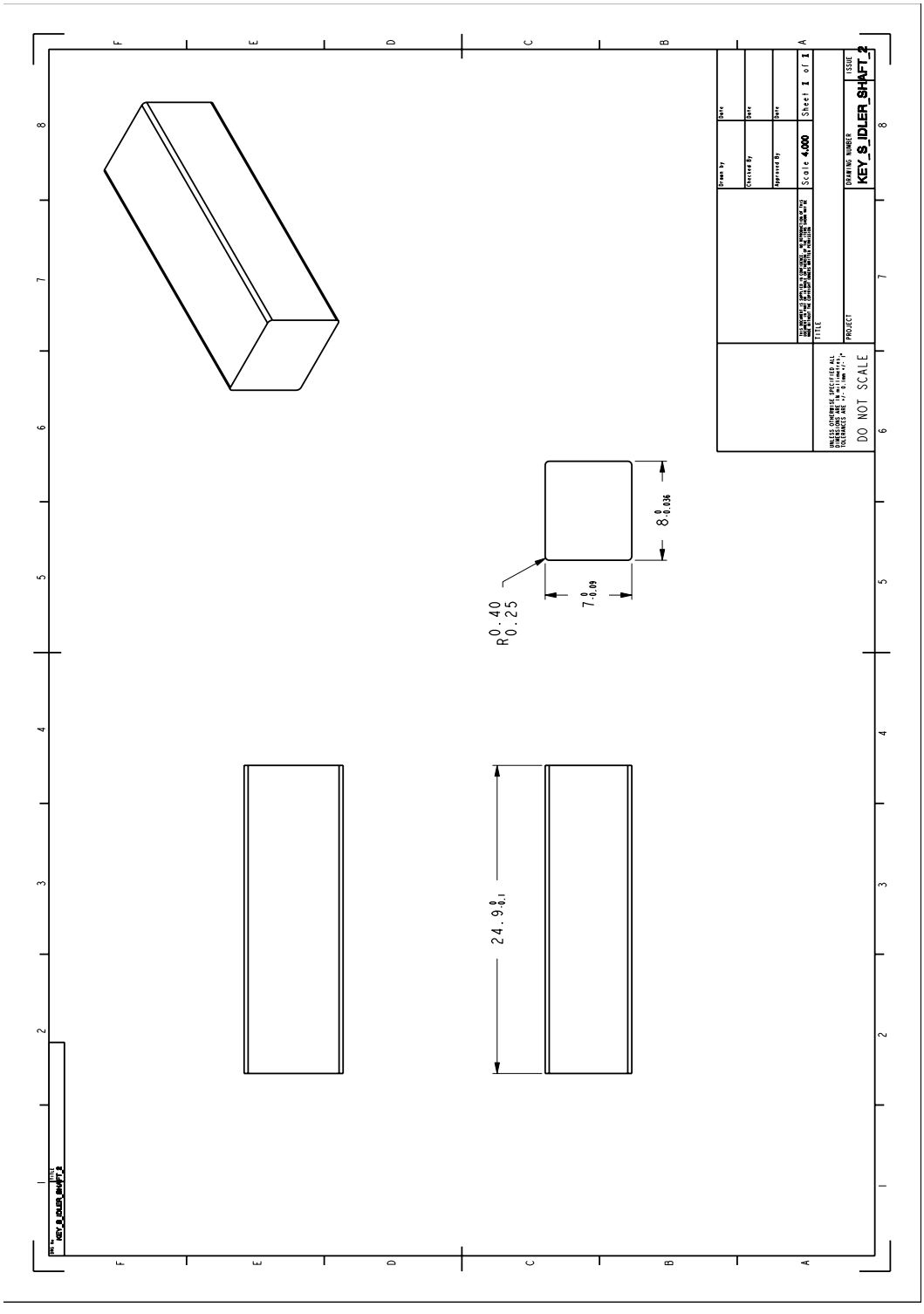
DO NOT SCALE
Scale 4.000
Sheet 1 of 1
KEY_9_IDLER_SHAFT_2
R0.40
0.25
7.0
0.09
8.0
0.036
24.9
0.1

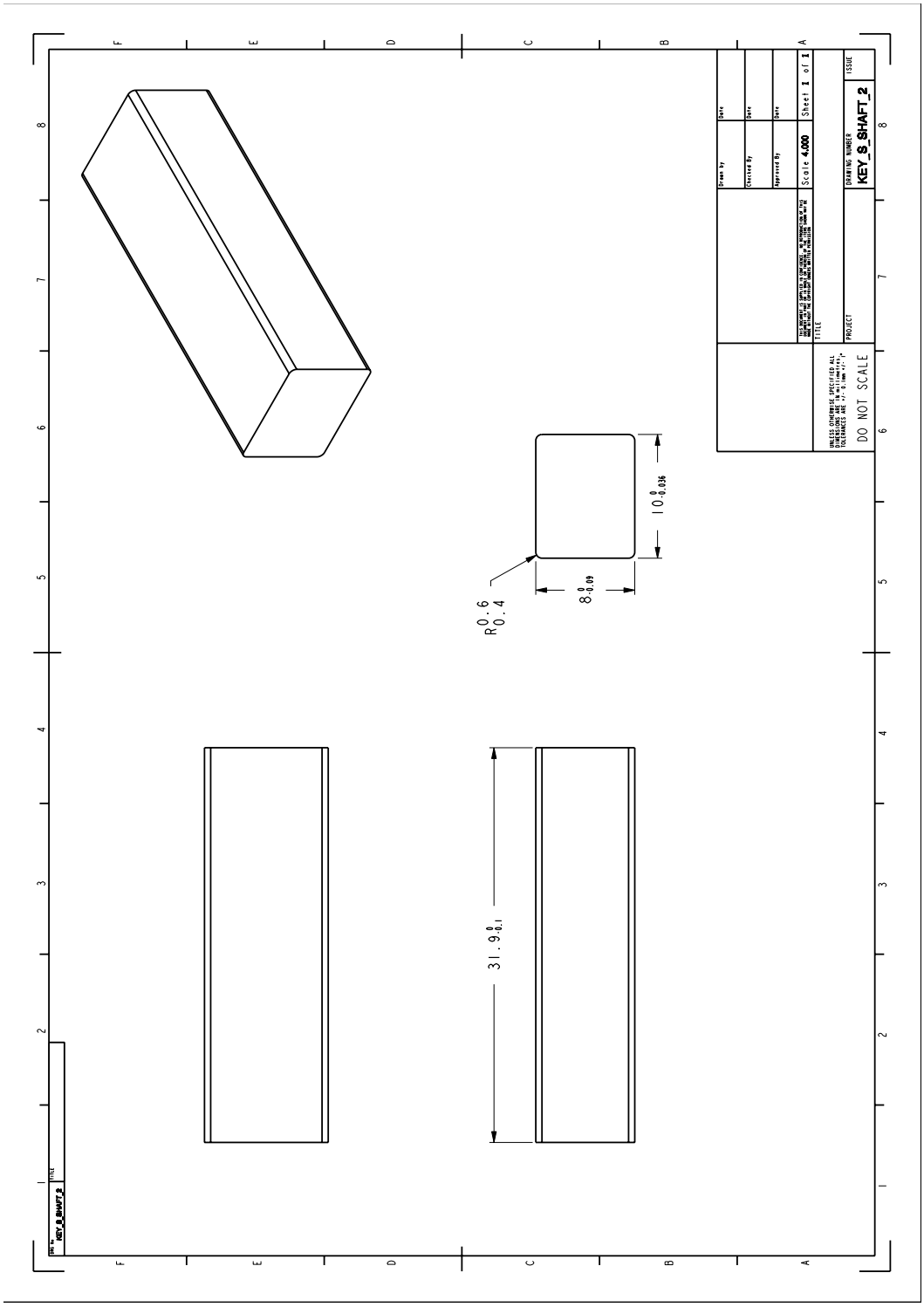
DO NOT SCALE
KEY_S_SHAFT_2
Scale 4.000
Sheet 1 of 1
31.9 0 -0.1
10 0 -0.036
8 0 -0.09
R 0.6 0.4

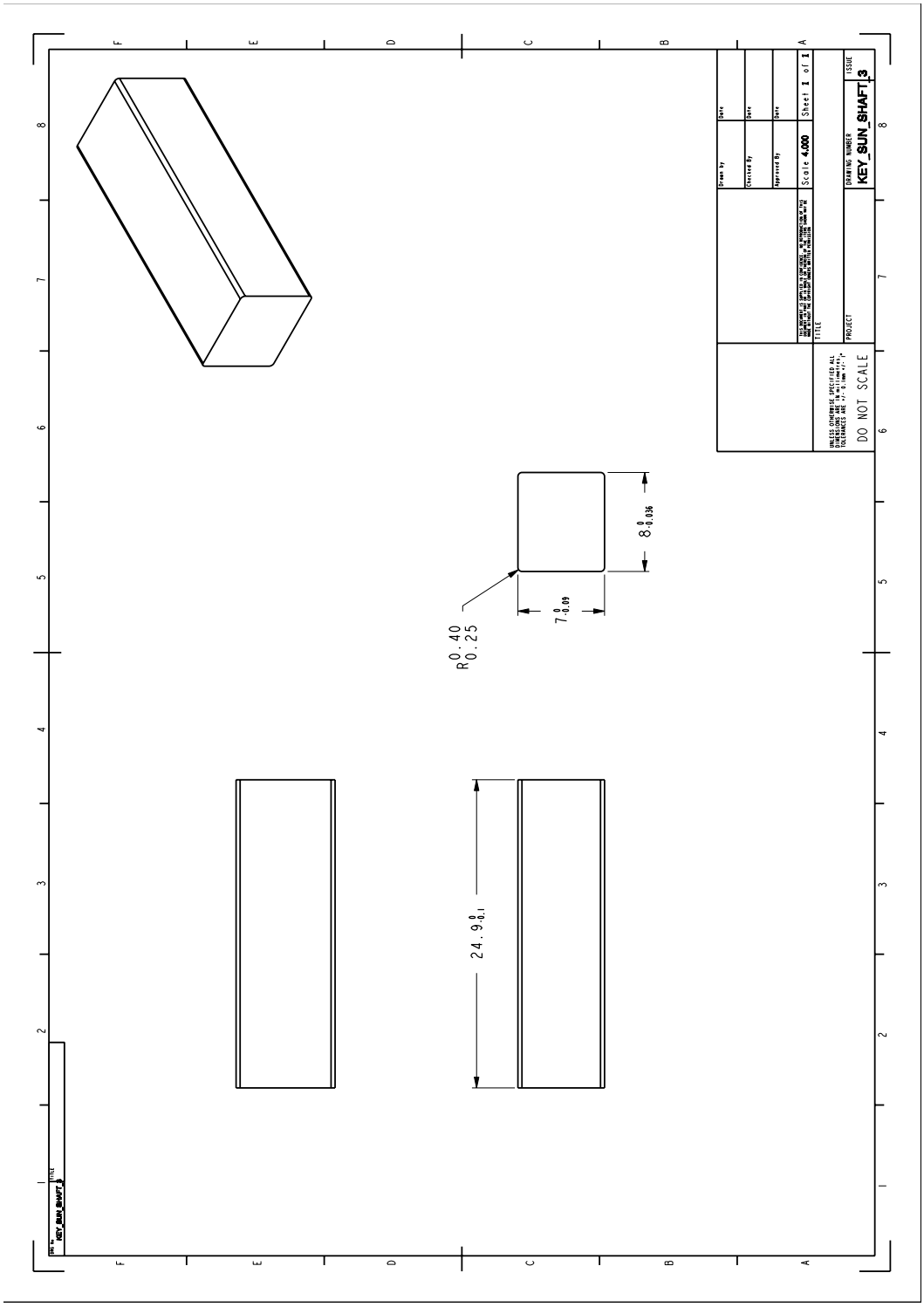
DO NOT SCALE
KEY_SUN_SHAFT_3
Scale 4.000
Sheet 1 of 1
R0.40
R0.25
7.0
8.0
24.9

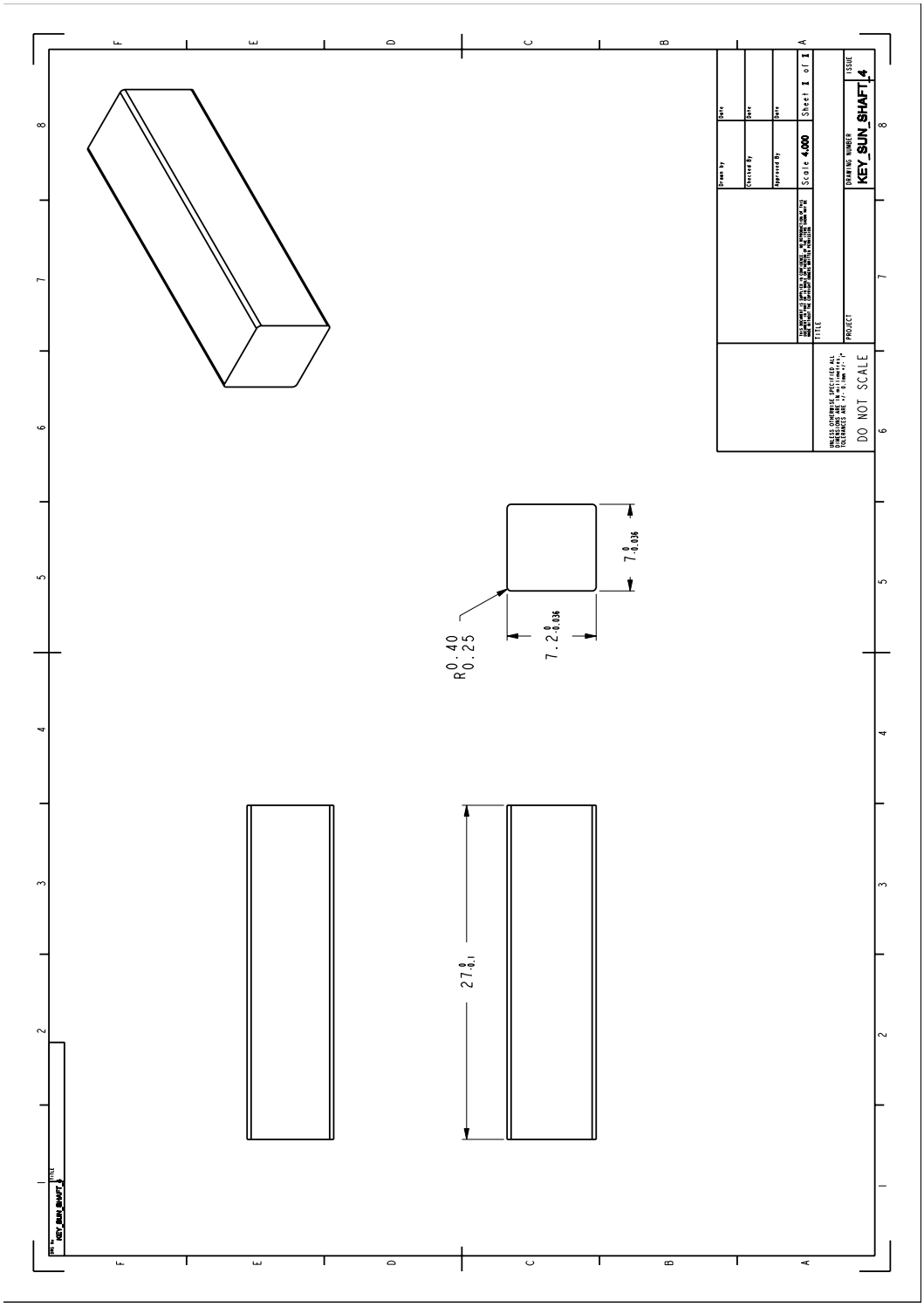
DO NOT SCALE
KEY_SUN_SHAFT_4
Scale 4.000
Sheet 1 of 1
R0.40
R0.25
7.2
7.0
27.8

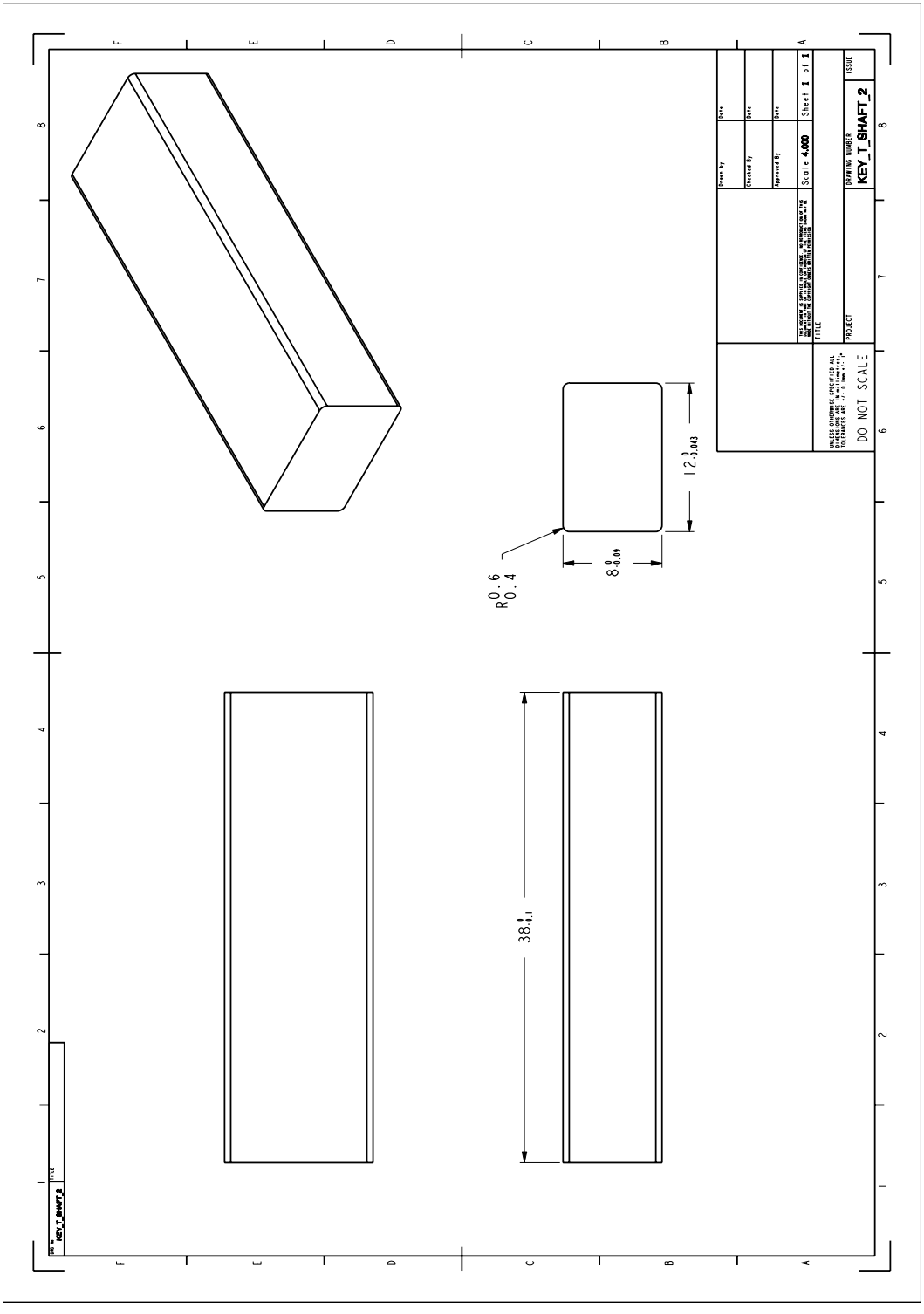
DO NOT SCALE
KEY_T_SHAFT_2
Scale 4.000
Sheet 1 of 1
38
8
12
R0.6
0.4

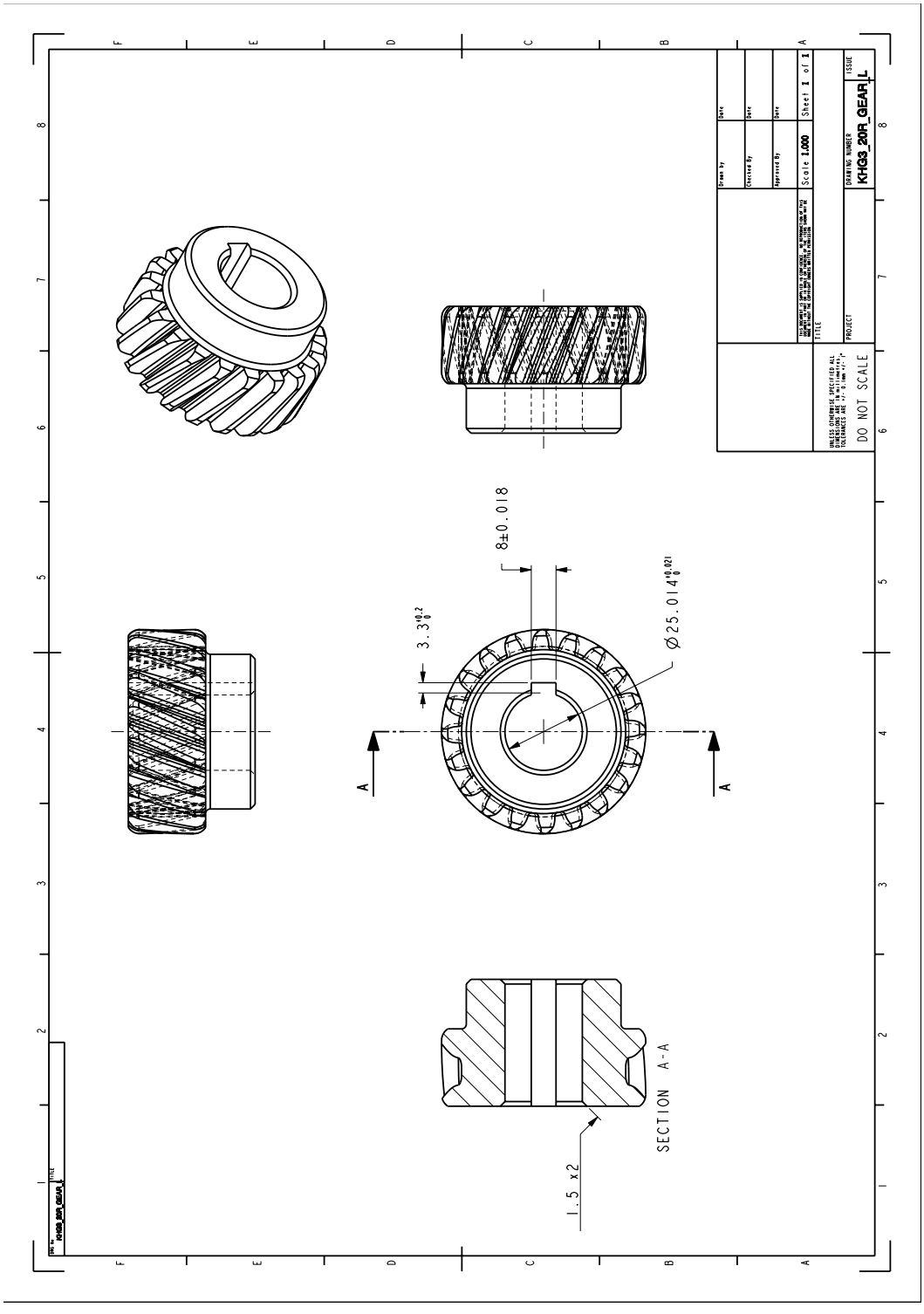
8±0.018
3.3
Ø25.014
A
A
SECTION A-A
1.5 x2
DO NOT SCALE
Scale 1.000
Sheet 1 of 1
KHG3_20R_GEAR_L

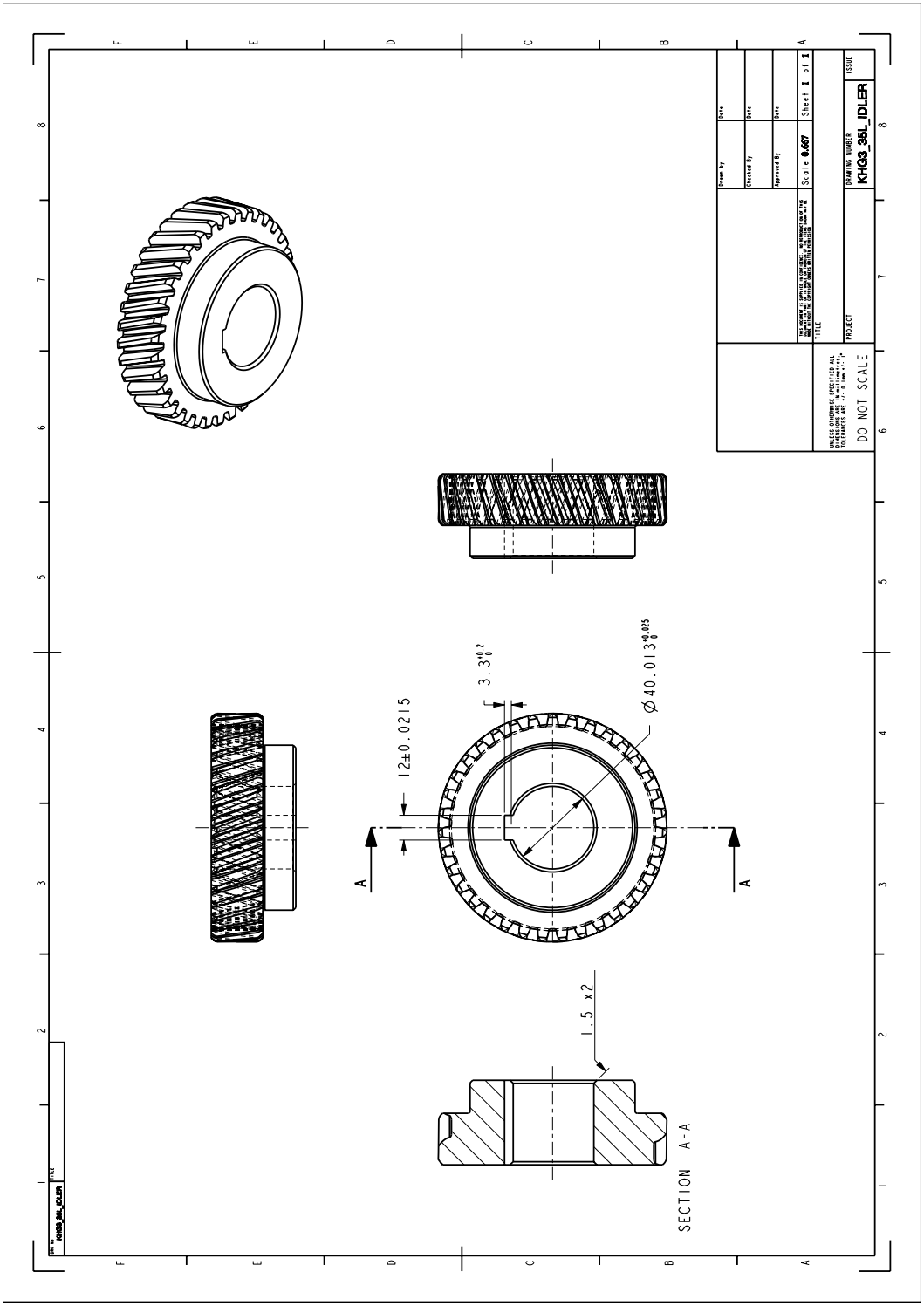
DO NOT SCALE
KHG3_36L_IDLER
Scale 0.667
Sheet 1 of 1
12±0.0215
3.3
Ø40.013
1.5 x2
SECTION A-A
A
A

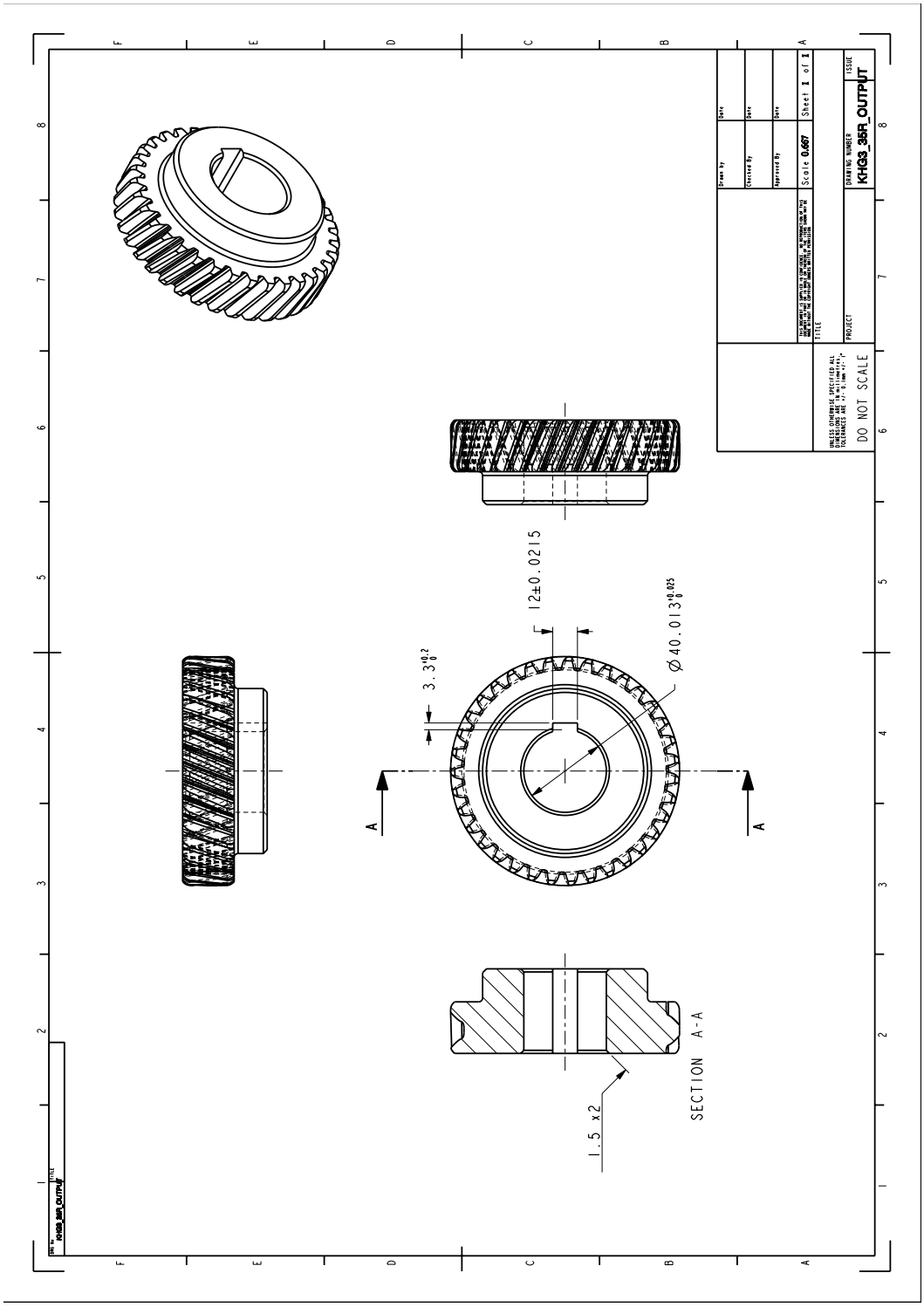
12±0.0215
$\emptyset 40.013^{+0.025}_{0}$
$3.3^{+0.2}_{0}$
A
A
SECTION A-A
1.5 x2
DO NOT SCALE
KHG3_36R_OUTPUT
Sheet 1 of 1
Scale 0.667

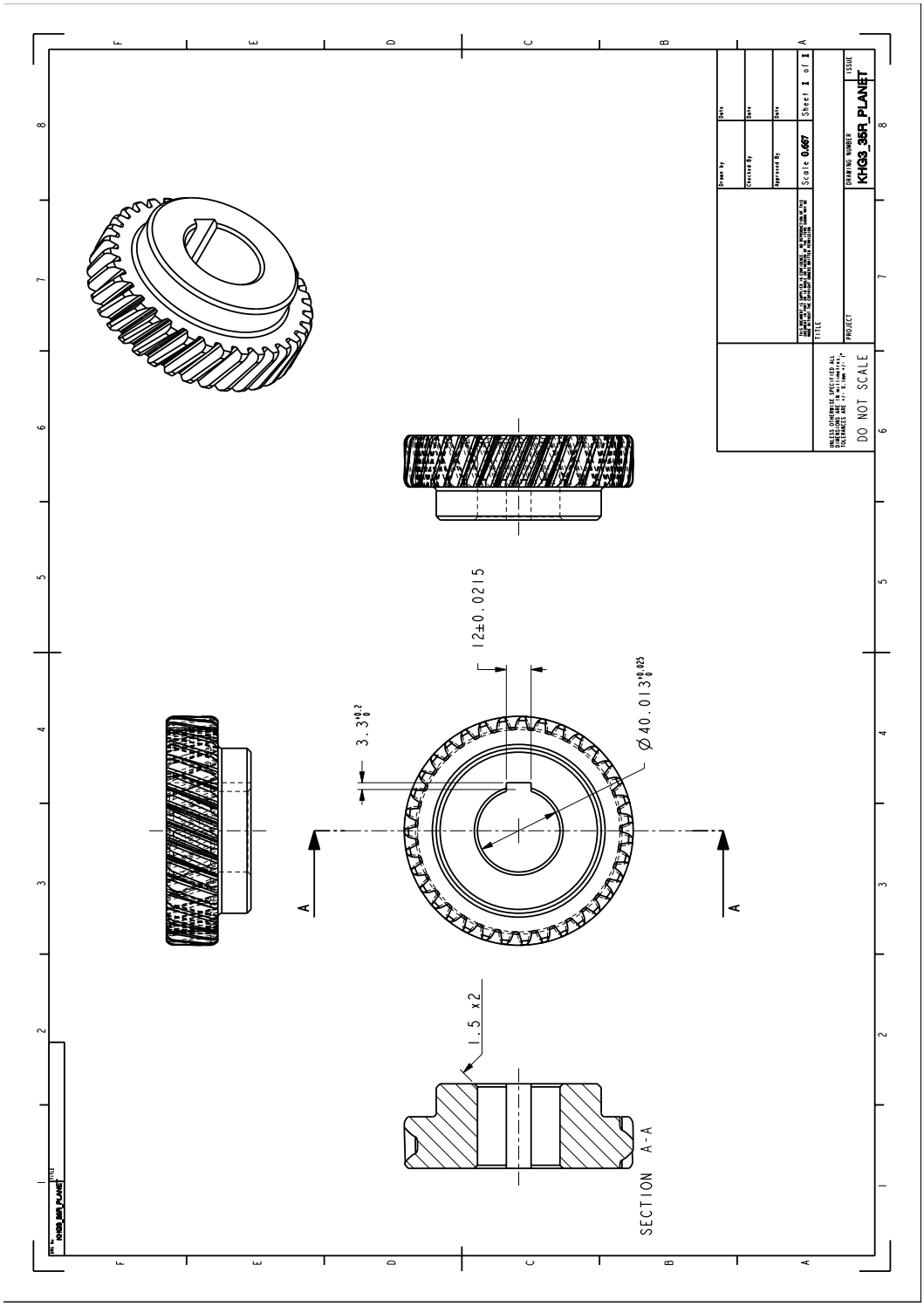
12±0.0215
3.3
Ø40.013
A
A
1.5 x2
SECTION A-A
DO NOT SCALE
KHG3_36R_PLANET
Scale 0.667
Sheet 1 of 1

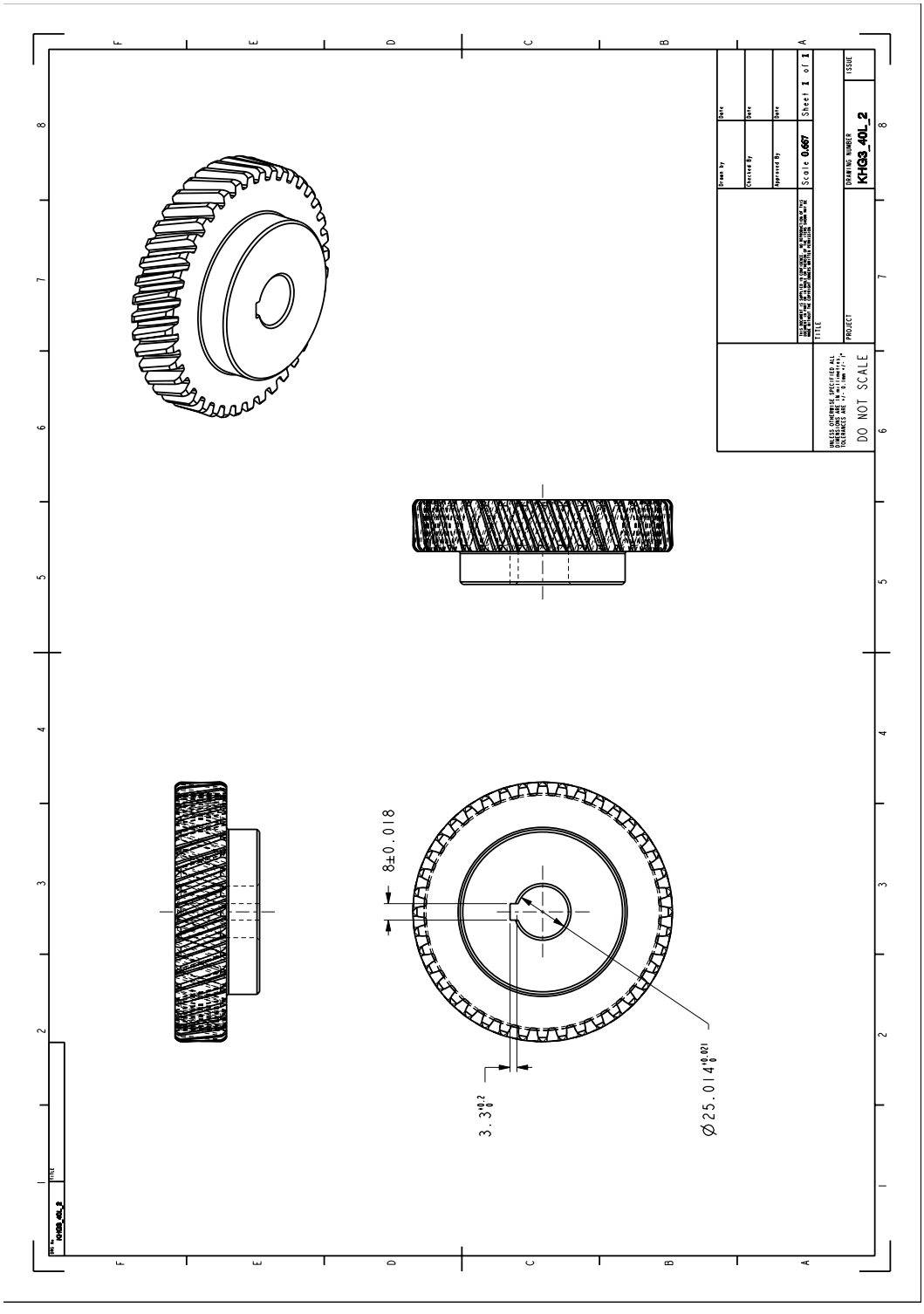
8±0.018
3.3
Ø25.014
DO NOT SCALE
KHG3_40L_2
Scale 0.667
Sheet 1 of 1

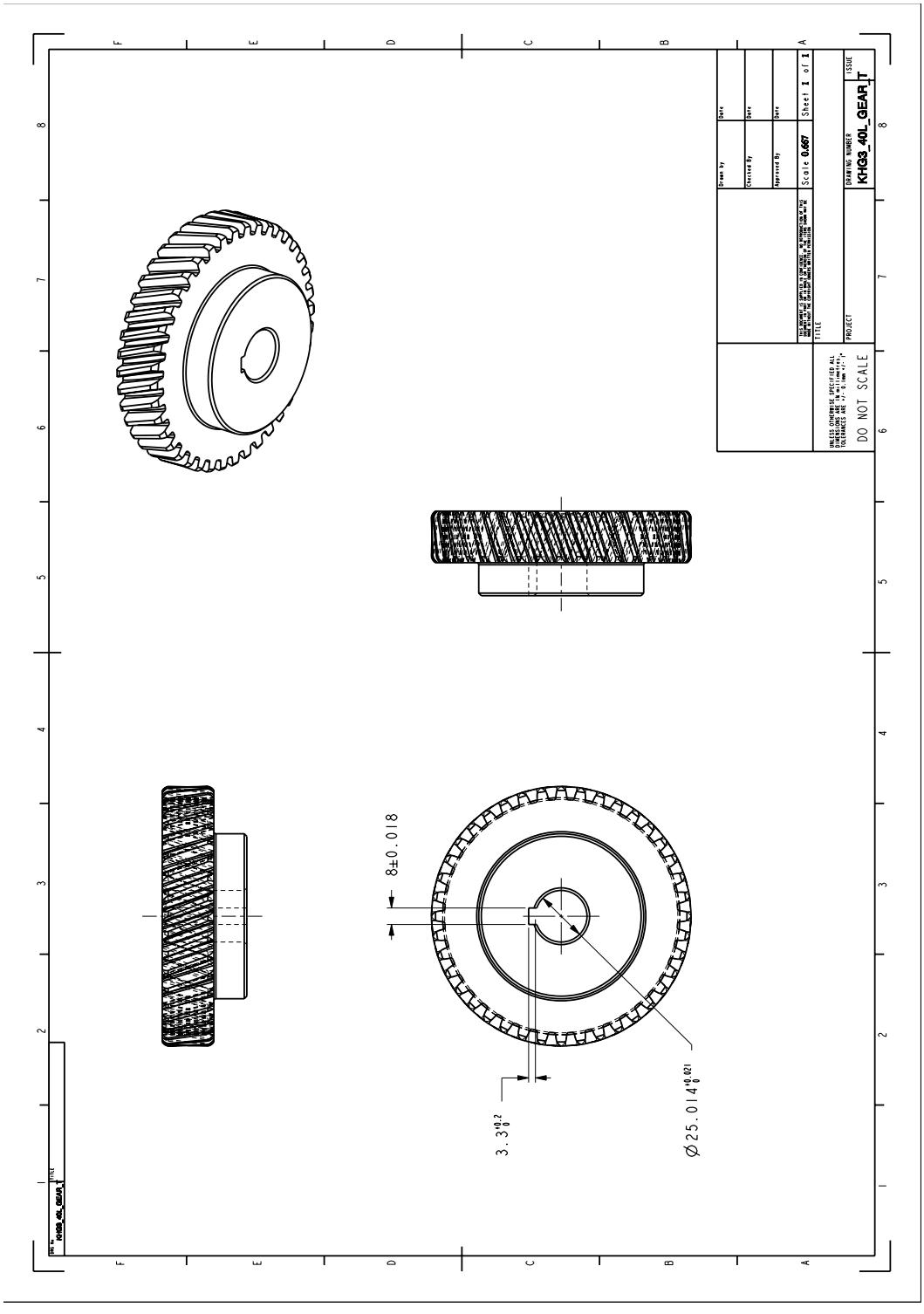
8±0.018
3.3 +0.2 0
Ø25.014 +0.021 0
DO NOT SCALE
KHG3_40L_GEAR_T
Sheet 1 of 1
Scale 0.667

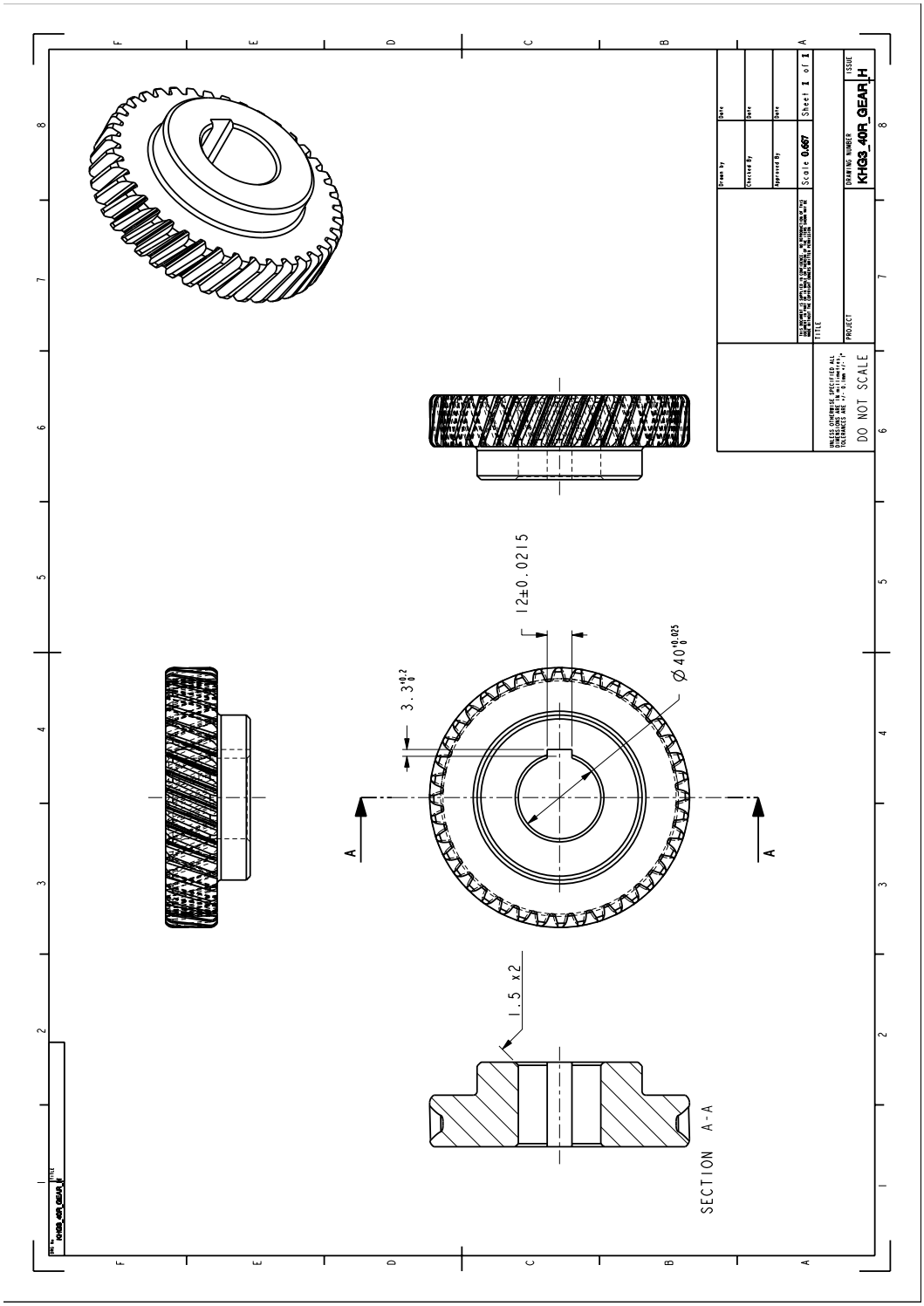
12±0.0215
Ø40 +0.025 0
3.3 +0.2 0
1.5 x2
SECTION A-A
A
A
DO NOT SCALE
KHG3_40R_GEAR_H

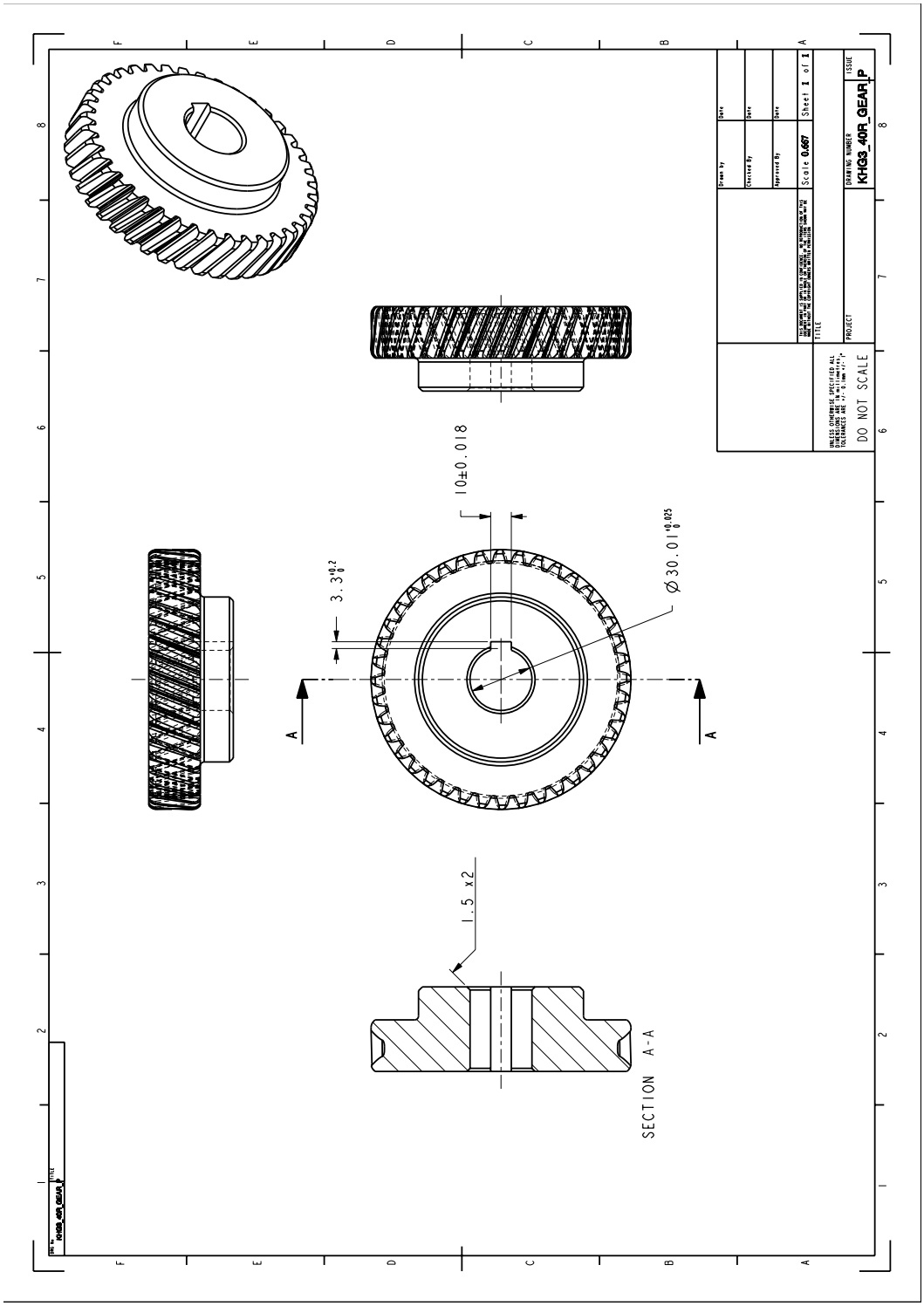
10±0.018
Ø30.01 +0.025 0
3.3 +0.2 0
1.5 x2
A
A
SECTION A-A
DO NOT SCALE
KHG3_40R_GEAR_P
Sheet 1 of 1
Scale 0.667

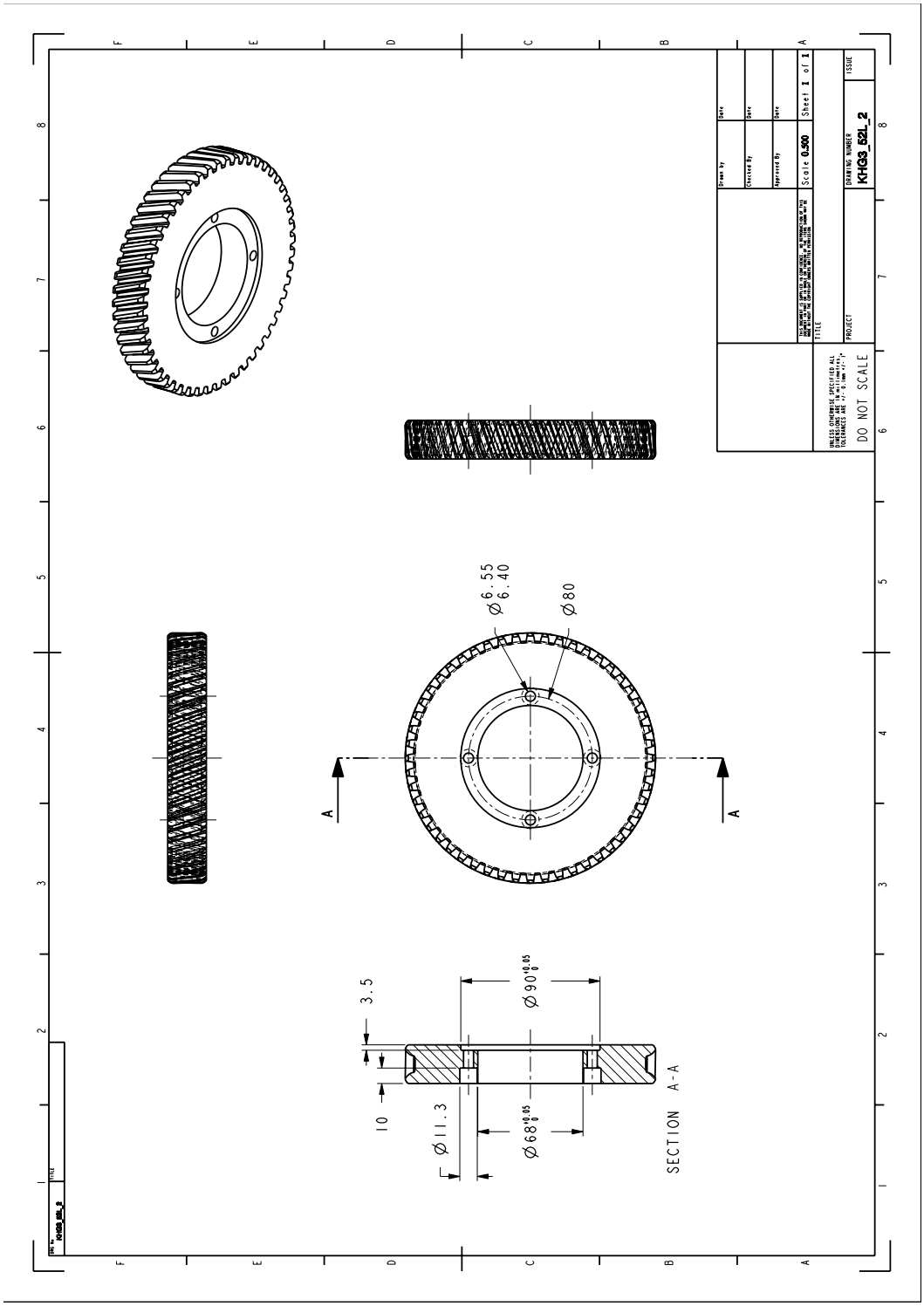
Ø6.55
6.40
Ø80
A
A
3.5
Ø90 +0.05 0
10
Ø11.3
Ø68 +0.05 0
SECTION A-A
DO NOT SCALE
Scale 0.500
Sheet 1 of 1
KHG3_62L_2

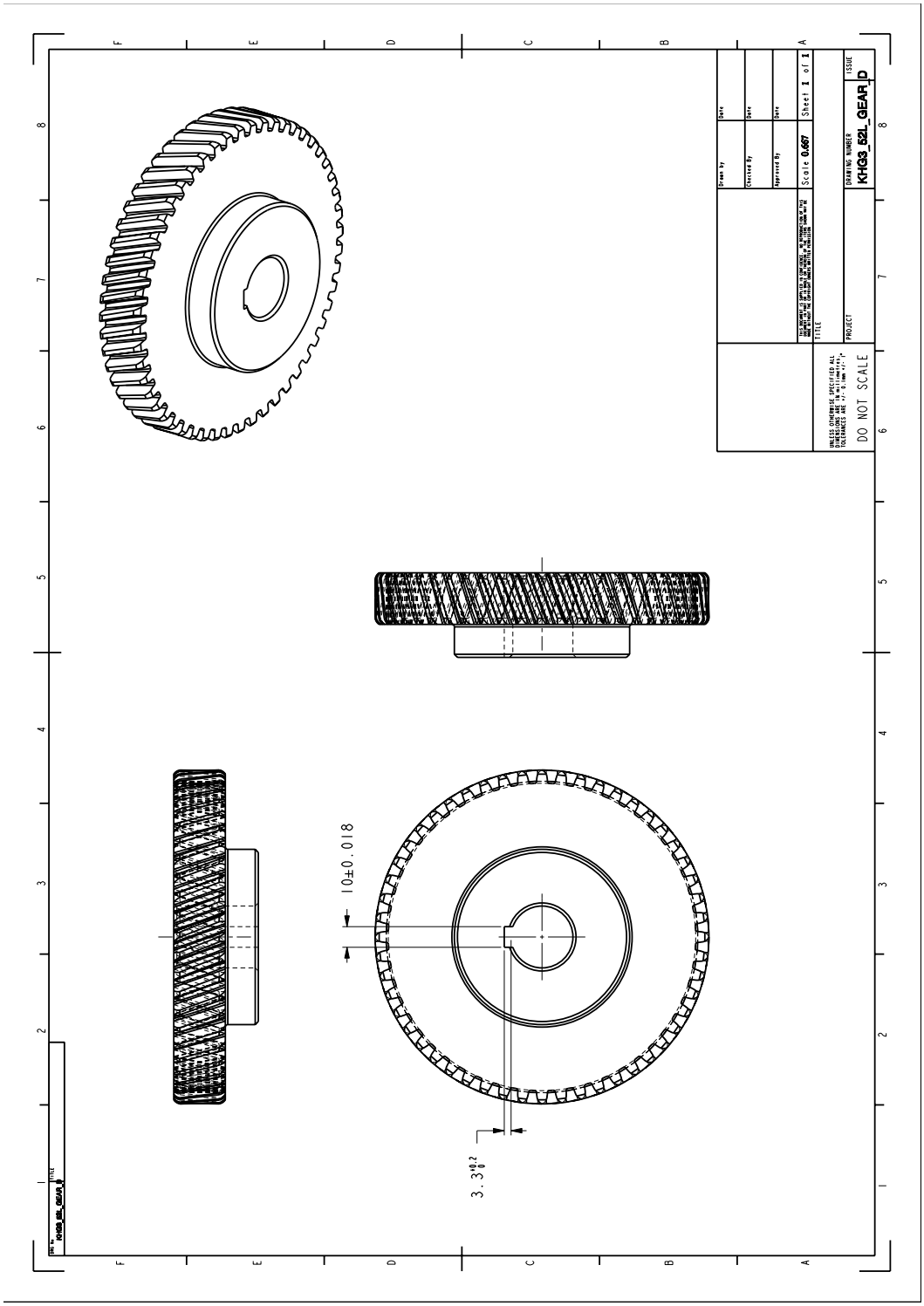
10±0.018
3.3 +0.2 0
DO NOT SCALE
Scale 0.667
Sheet 1 of 1
KHG3_52L_GEAR_D

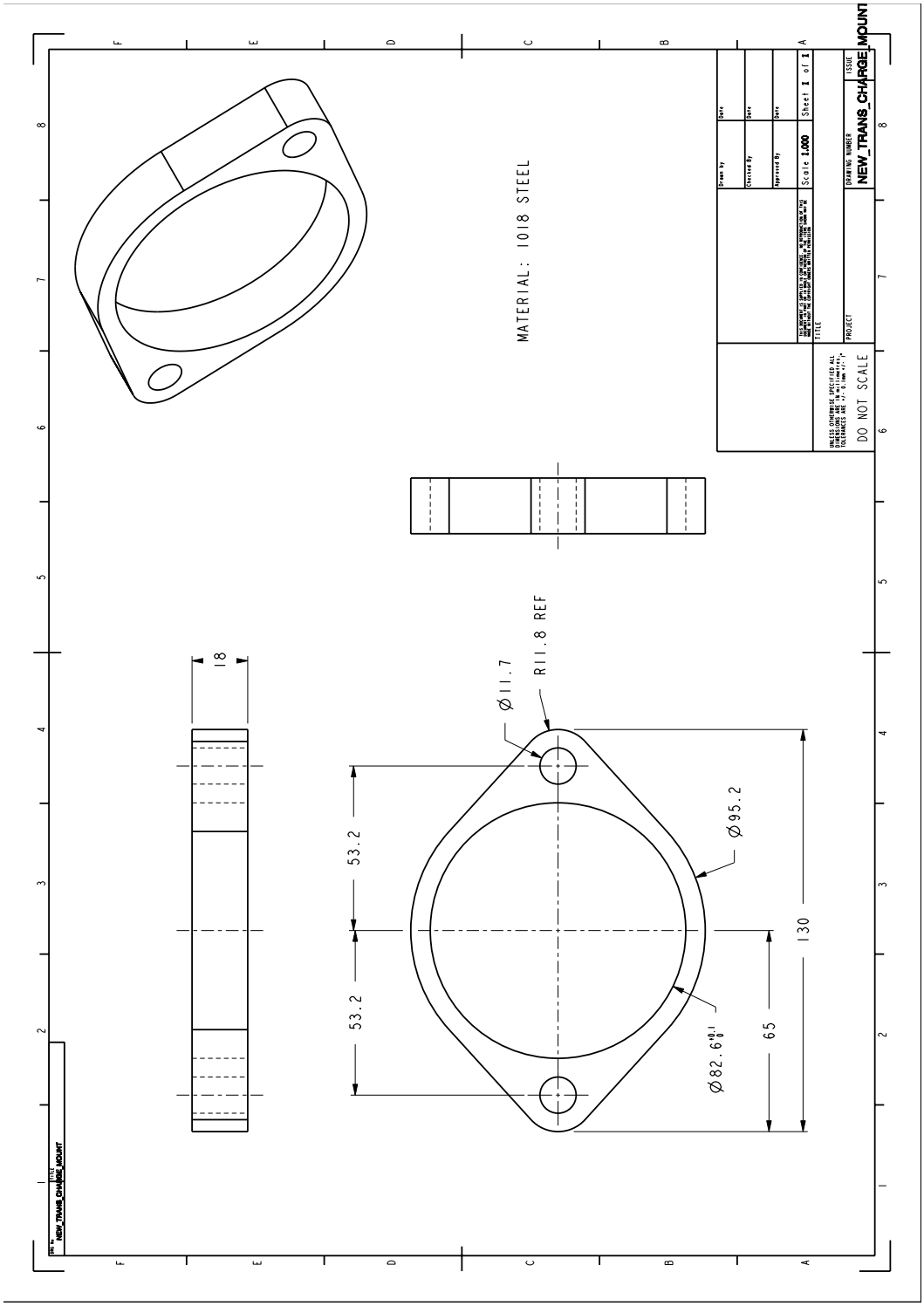
MATERIAL: 1018 STEEL
Ø11.7
R11.8 REF
18
53.2
53.2
Ø95.2
130
65
Ø82.60 +0.1 -0
DO NOT SCALE
NEW_TRANS_CHARGE_MOUNT
Scale 1.000
Sheet 1 of 1

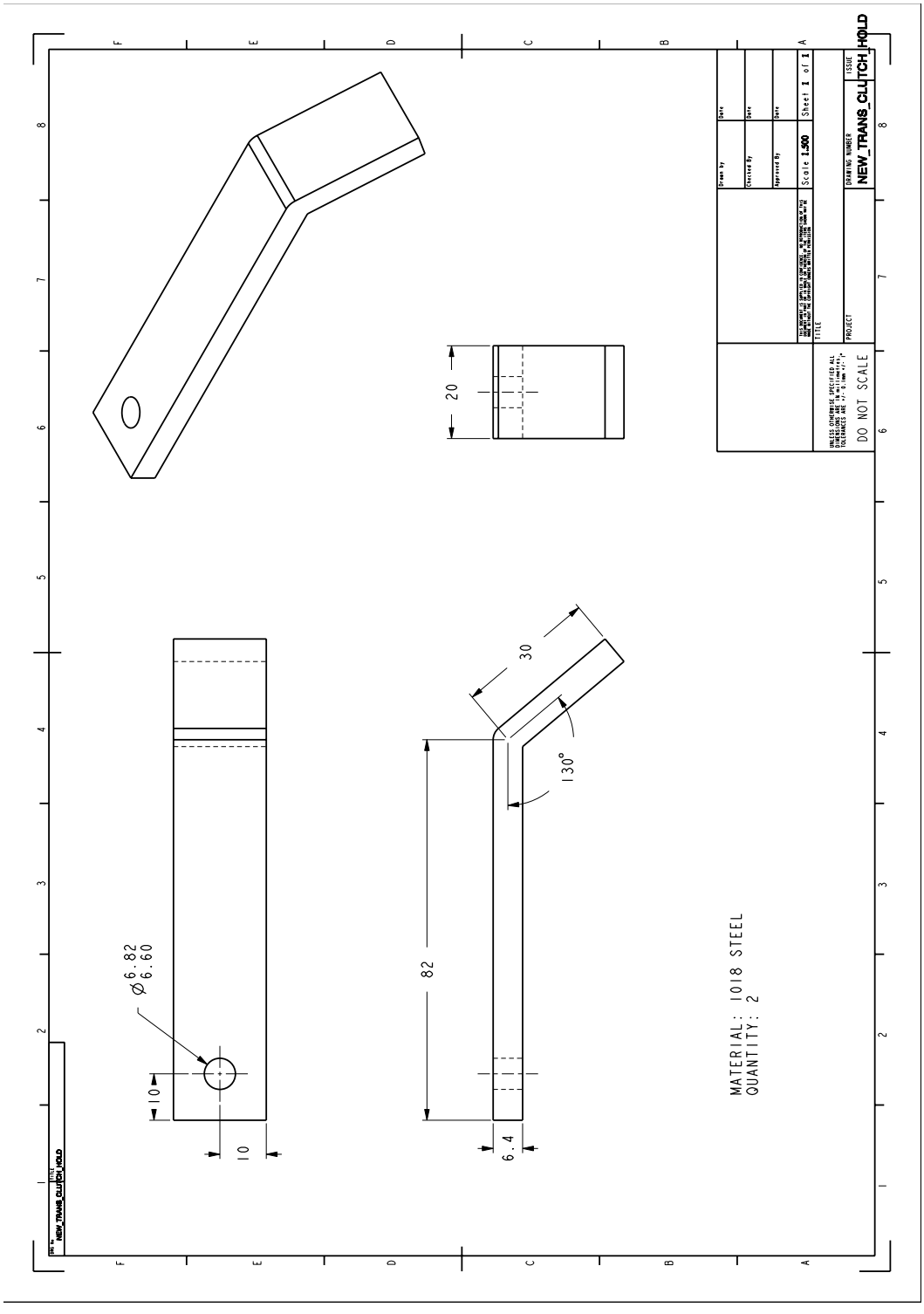
NEW_TRANS_CLUTCH_HOLD
DO NOT SCALE
Scale 1.500
Sheet 1 of 1
NEW_TRANS_CLUTCH_HOLD
MATERIAL: 1018 STEEL
QUANTITY: 2
20
30
130°
82
6.4
10
10
Ø6.82
Ø6.60

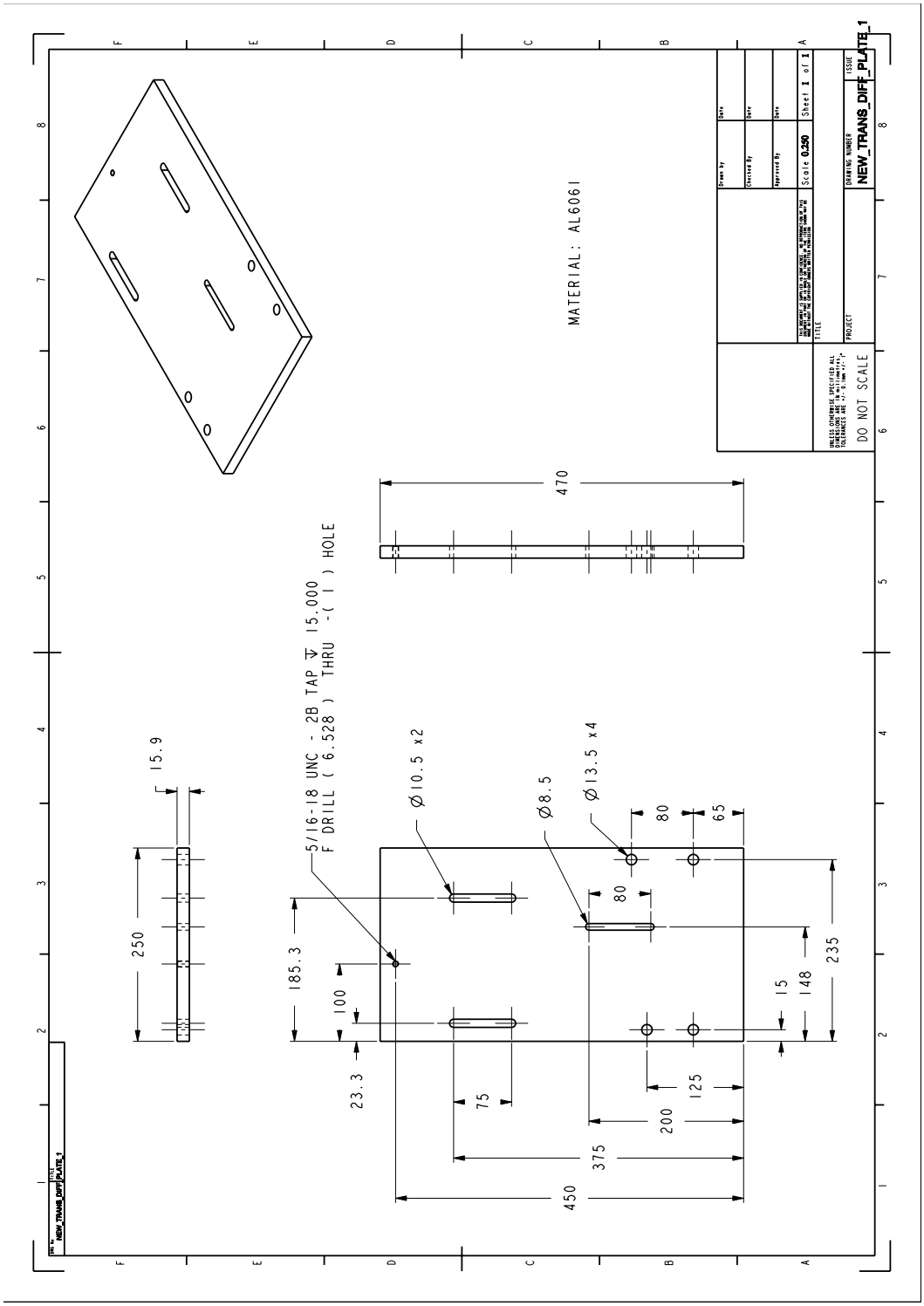
MATERIAL: AL6061
470
5/16-18 UNC - 2B TAP ∓ 15.000
F DRILL (6.528) THRU -(1) HOLE
Ø10.5 x2
Ø8.5
Ø13.5 x4
15.9
250
185.3
100
23.3
80
80
65
15
148
235
75
200
125
375
450
DO NOT SCALE
Scale 0.250
Sheet 1 of 1
NEW_TRANS_DIFF_PLATE_1

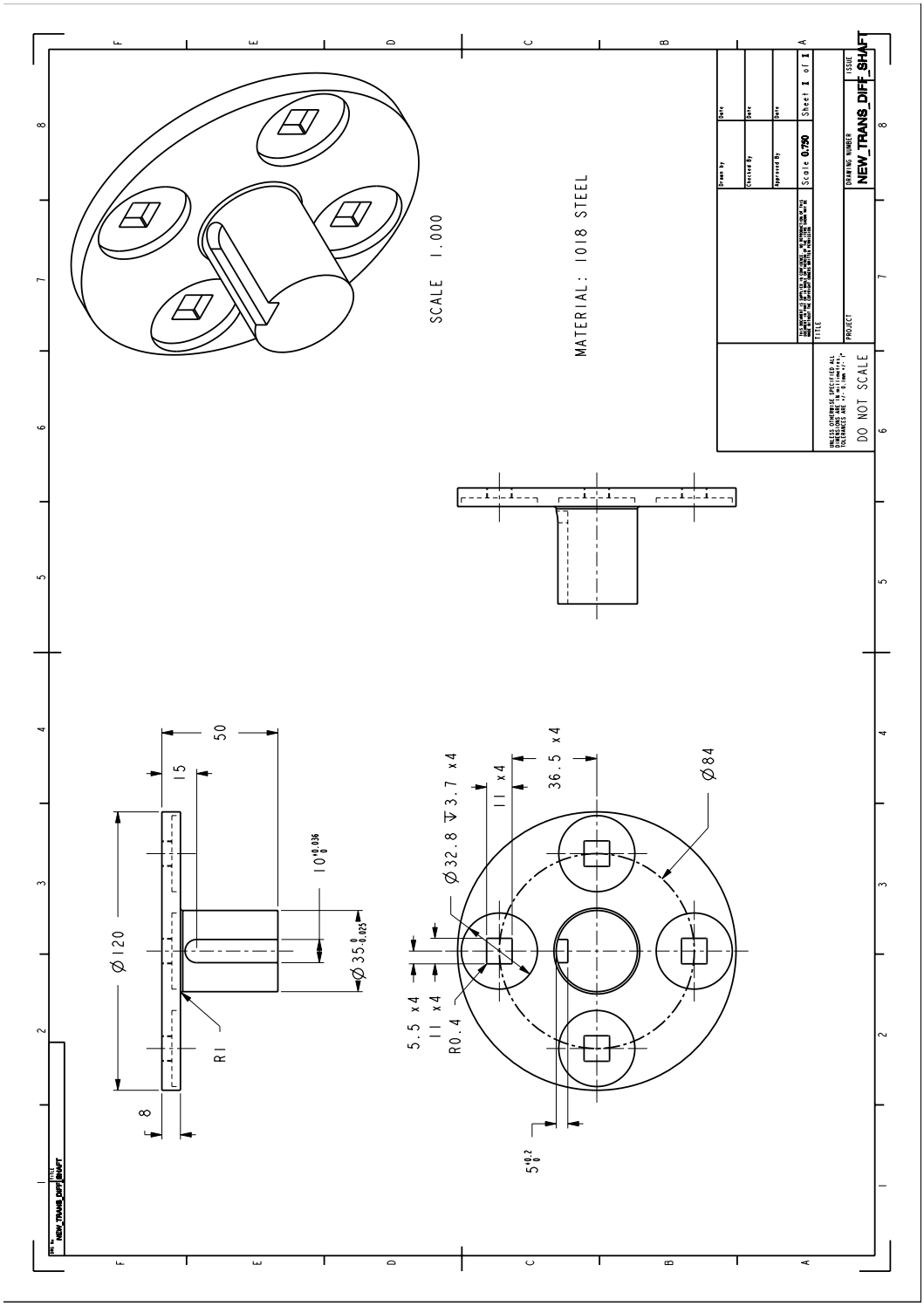
SCALE 1.000
MATERIAL: 1018 STEEL
DO NOT SCALE
NEW_TRANS_DIFF_SHAFT
Ø120
50
15
8
R1
Ø84
Ø32.8 ∓3.7 x4
11 x4
36.5 x4
5.5 x4
11 x4
R0.4

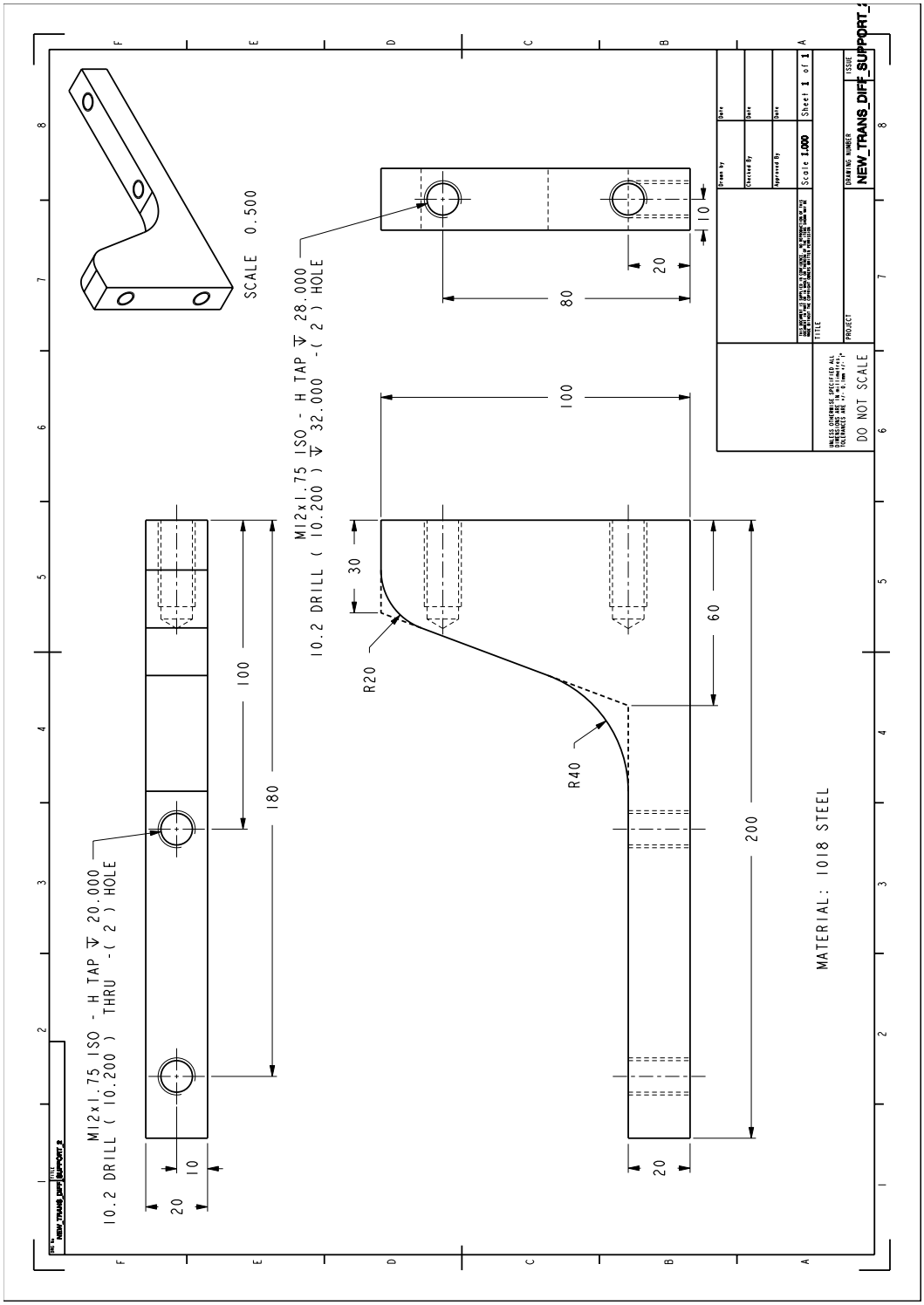
SCALE 0.500
M12x1.75 ISO - H TAP ↧ 28.000
10.2 DRILL (10.200) ↧ 32.000 -(2) HOLE
M12x1.75 ISO - H TAP ↧ 20.000
10.2 DRILL (10.200) THRU -(2) HOLE
R20
R40
MATERIAL: 1018 STEEL
DO NOT SCALE
NEW_TRANS_DIFF_SUPPORT_A

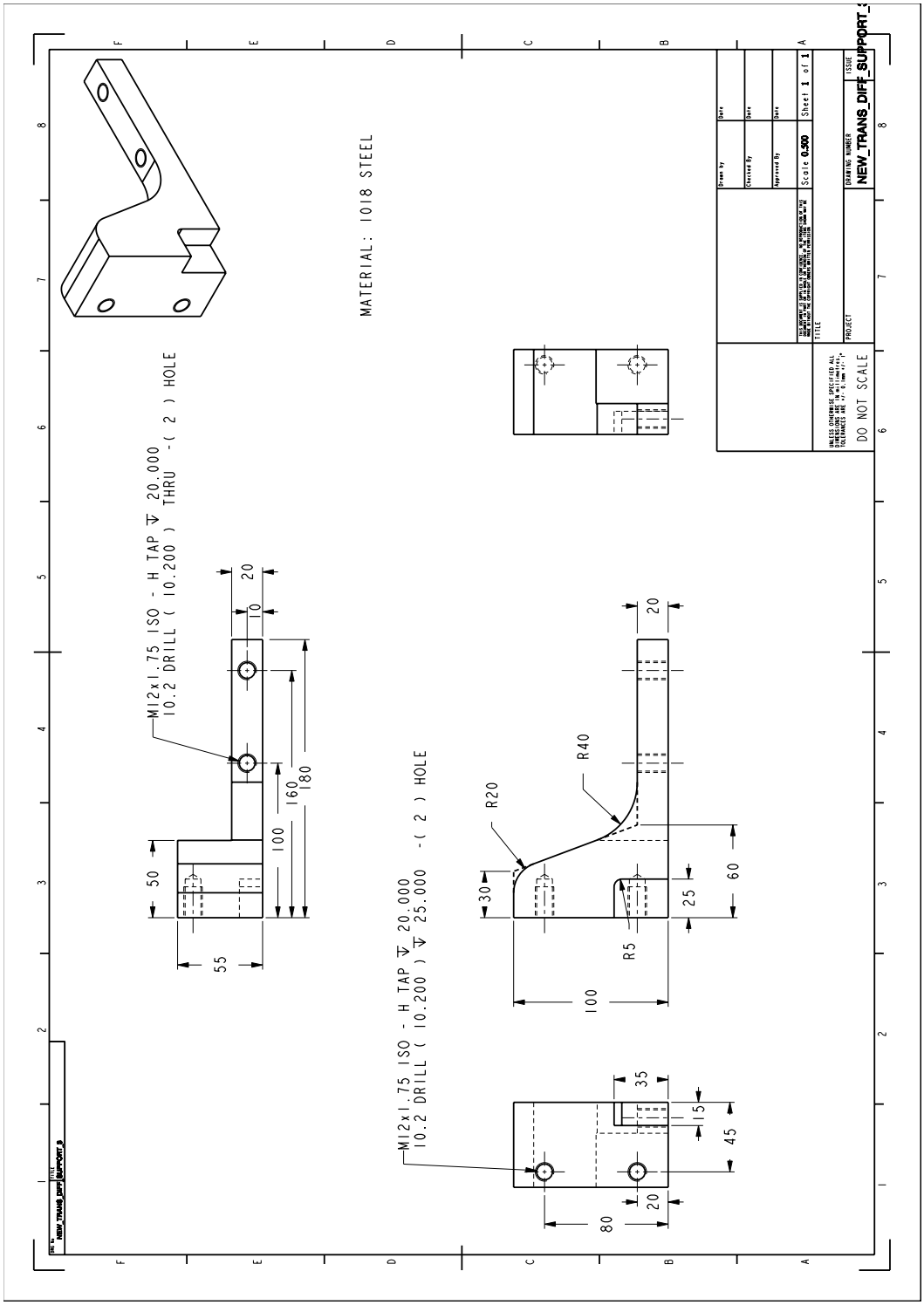
MATERIAL: 1018 STEEL
M12x1.75 ISO - H TAP ↧ 20.000
10.2 DRILL (10.200) THRU -(2) HOLE
M12x1.75 ISO - H TAP ↧ 20.000
10.2 DRILL (10.200) ↧ 25.000 -(2) HOLE
R40
R20
R5
DO NOT SCALE
NEW_TRANS_DIFF_SUPPORT_S

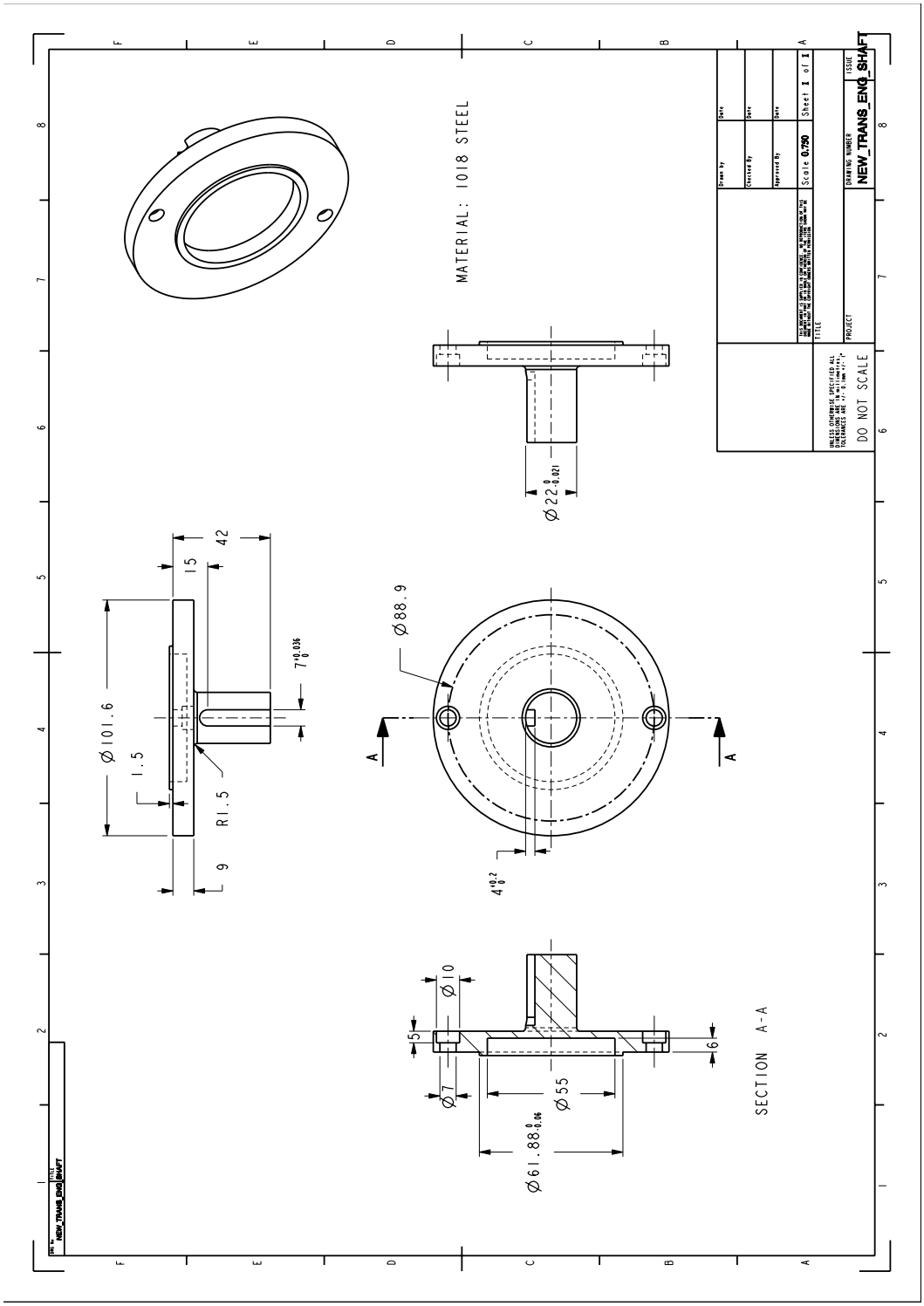
MATERIAL: 1018 STEEL
DO NOT SCALE
NEW_TRANS_ENG_SHAFT
SECTION A-A
Ø101.6
Ø88.9
Ø55
Ø10
Ø7
42
15
1.5
R1.5
9
5
6

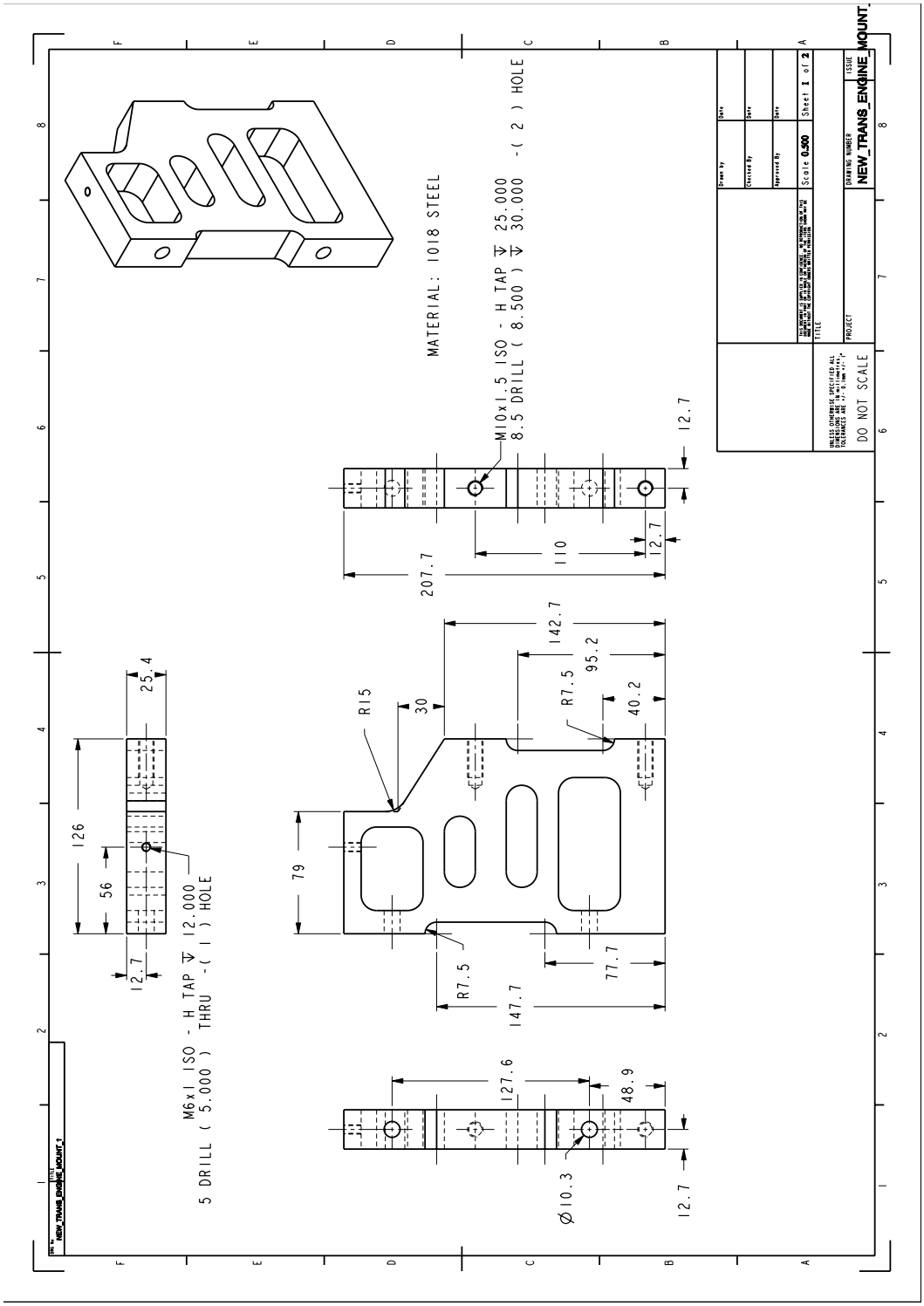
MATERIAL: 1018 STEEL
M10x1.5 ISO - H TAP ↧ 25.000
8.5 DRILL (8.500) ↧ 30.000 -(2) HOLE
M6x1 ISO - H TAP ↧ 12.000
5 DRILL (5.000) THRU -(1) HOLE
DO NOT SCALE
NEW_TRANS_ENGINE_MOUNT
Scale 0.500
Sheet 1 of 2

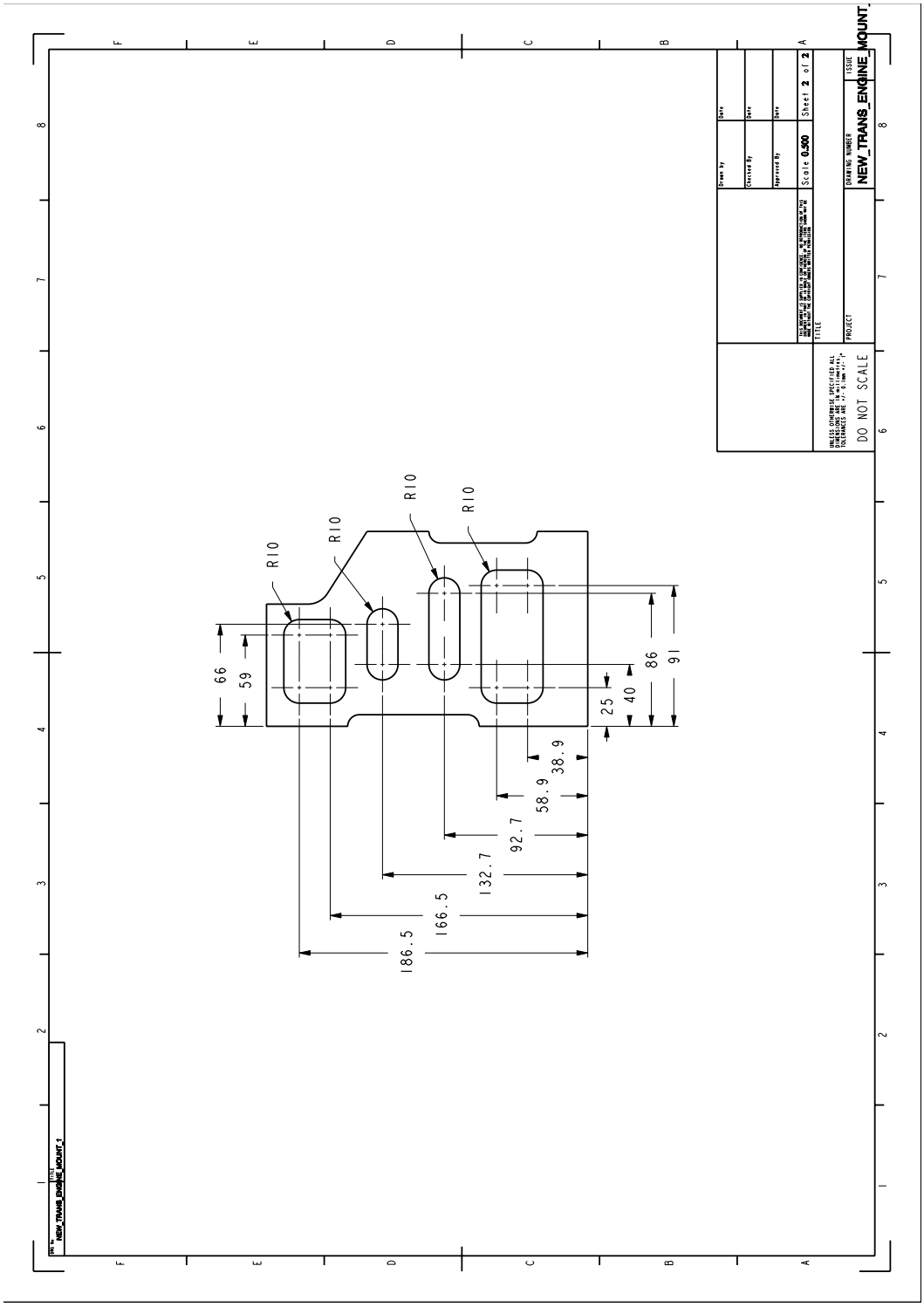
R10
R10
R10
R10
66
59
86
91
25
40
38.9
58.9
92.7
132.7
166.5
186.5
DO NOT SCALE
NEW_TRANS_ENGINE_MOUNT
Scale 0.500
Sheet 2 of 2

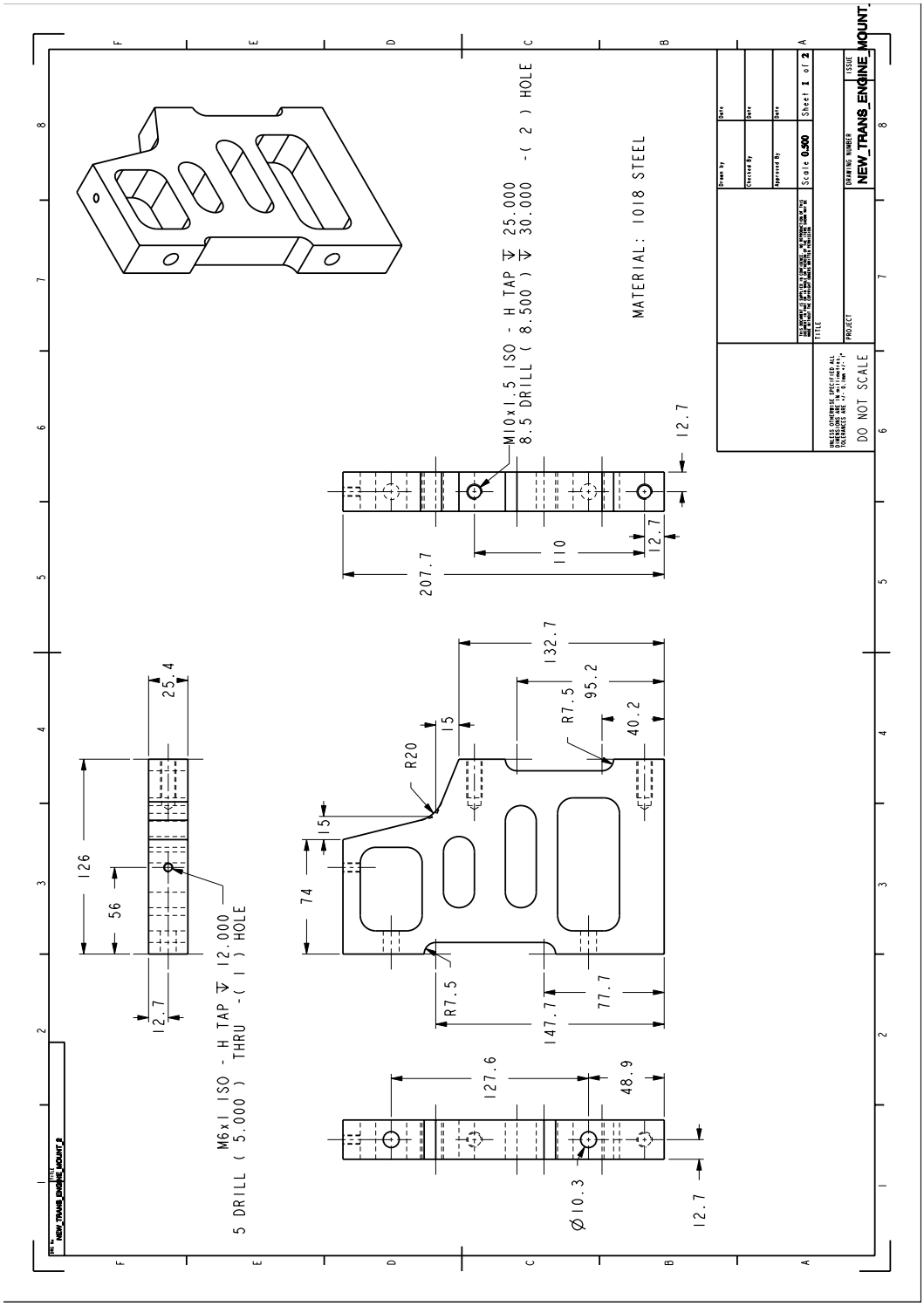
M10x1.5 ISO - H TAP ↧ 25.000
8.5 DRILL (8.500) ↧ 30.000 -(2) HOLE
MATERIAL: 1018 STEEL
12.7
207.7
110
12.7
132.7
95.2
40.2
R7.5
15
R20
15
74
126
56
25.4
12.7
M6x1 ISO - H TAP ↧ 12.000
5 DRILL (5.000) THRU -(1) HOLE
R7.5
147.7
77.7
127.6
48.9
Ø10.3
12.7
DO NOT SCALE
Scale 0.500
Sheet 1 of 2
NEW_TRANS_ENGINE_MOUNT

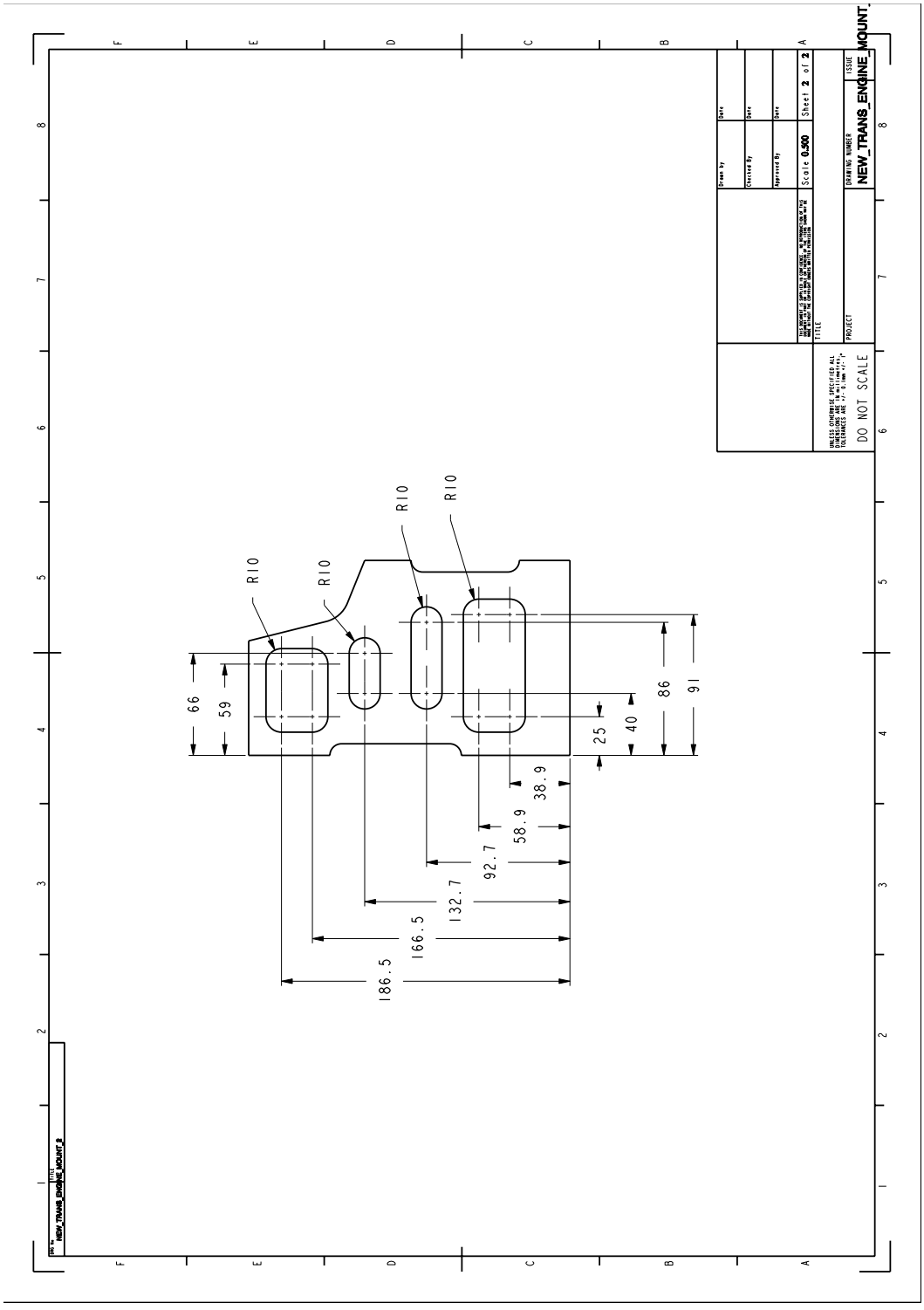
R10
R10
R10
R10
66
59
86
91
25
40
38.9
58.9
92.7
132.7
166.5
186.5
DO NOT SCALE
NEW_TRANS_ENGINE_MOUNT
Scale 0.500
Sheet 2 of 2

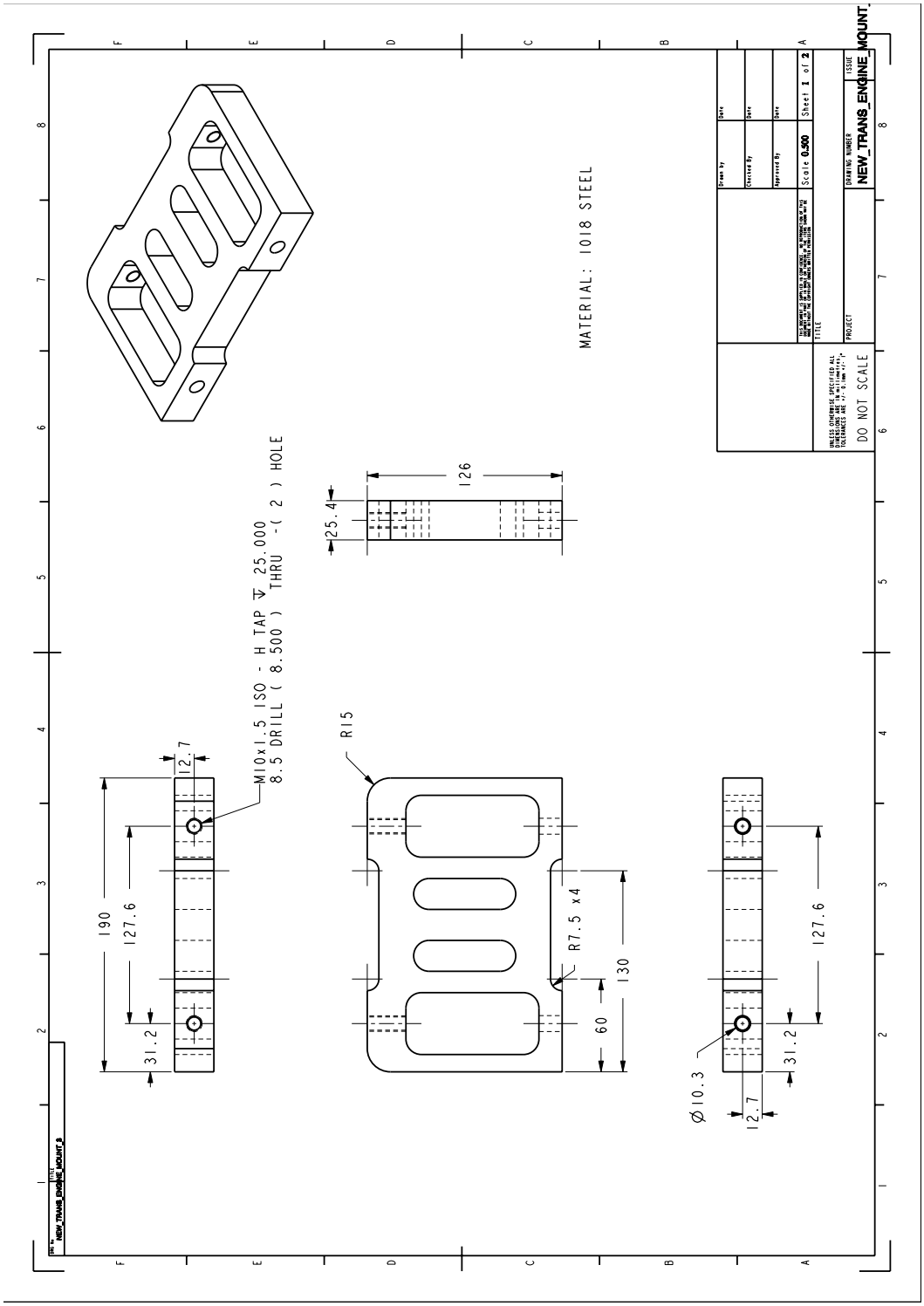
MATERIAL: 1018 STEEL
M10x1.5 ISO - H TAP ∓ 25.000
8.5 DRILL (8.500) THRU -(2) HOLE
R15
R7.5 x4
126
25.4
190
127.6
31.2
12.7
130
60
Ø10.3
DO NOT SCALE
NEW_TRANS_ENGINE_MOUNT
Sheet 1 of 2
Scale 0.500

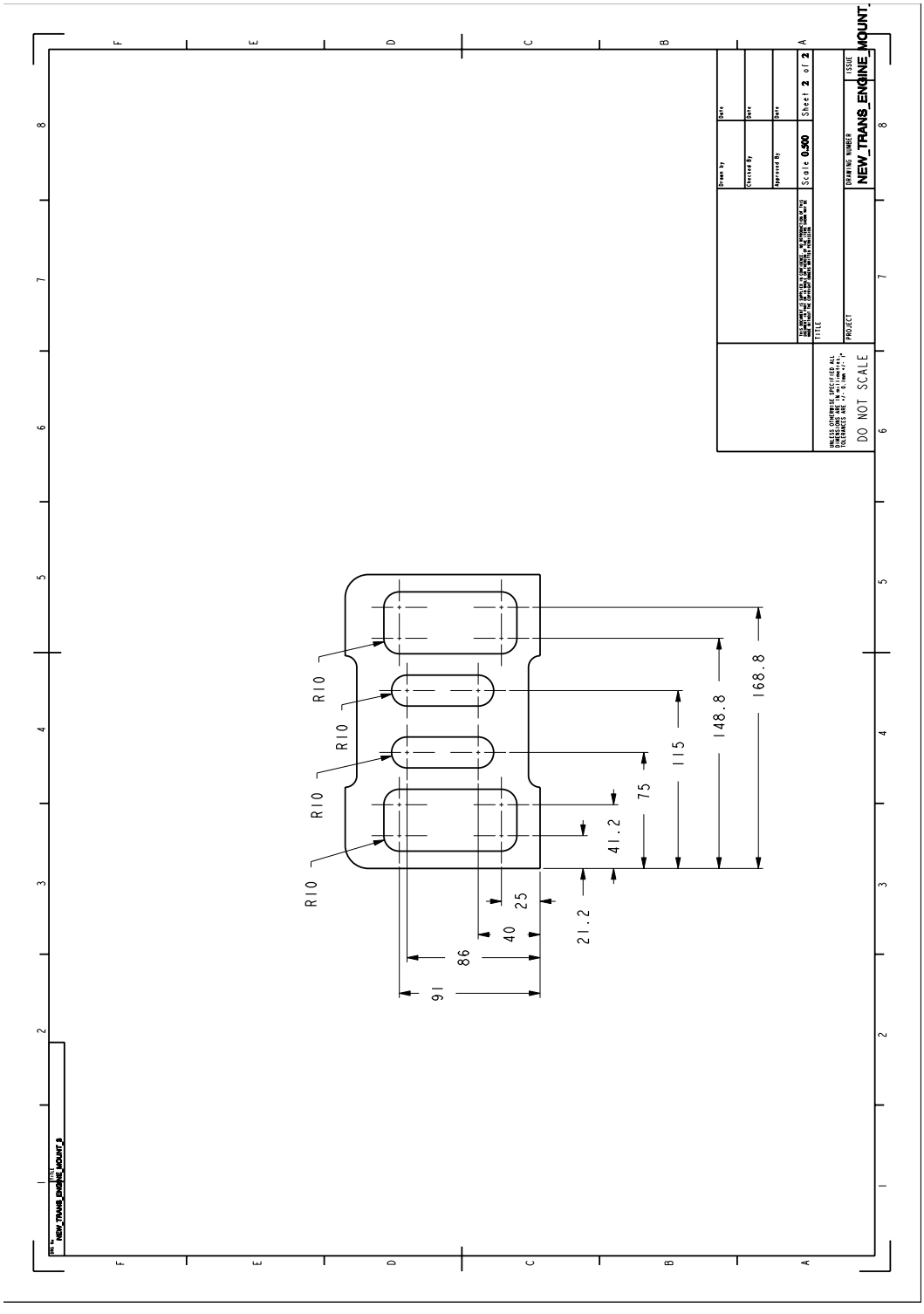
R10
R10
R10
R10
168.8
148.8
115
75
41.2
21.2
25
40
86
91
DO NOT SCALE
NEW_TRANS_ENGINE_MOUNT
Scale 0.500
Sheet 2 of 2

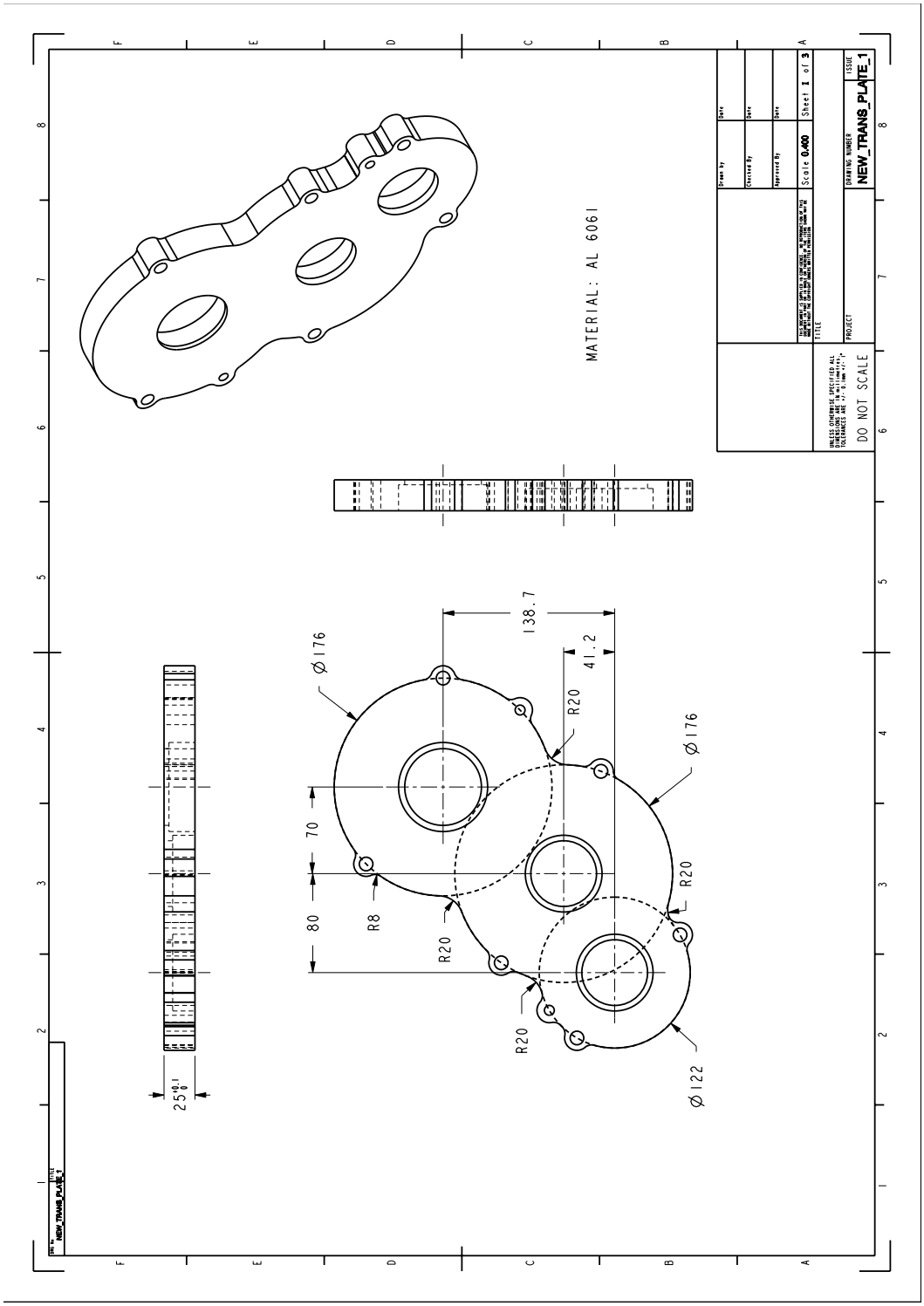
MATERIAL: AL 6061
DO NOT SCALE
NEW_TRANS_PLATE_1
Scale 0.400
Sheet 1 of 3
138.7
41.2
Ø176
R20
70
80
R8
Ø122
25

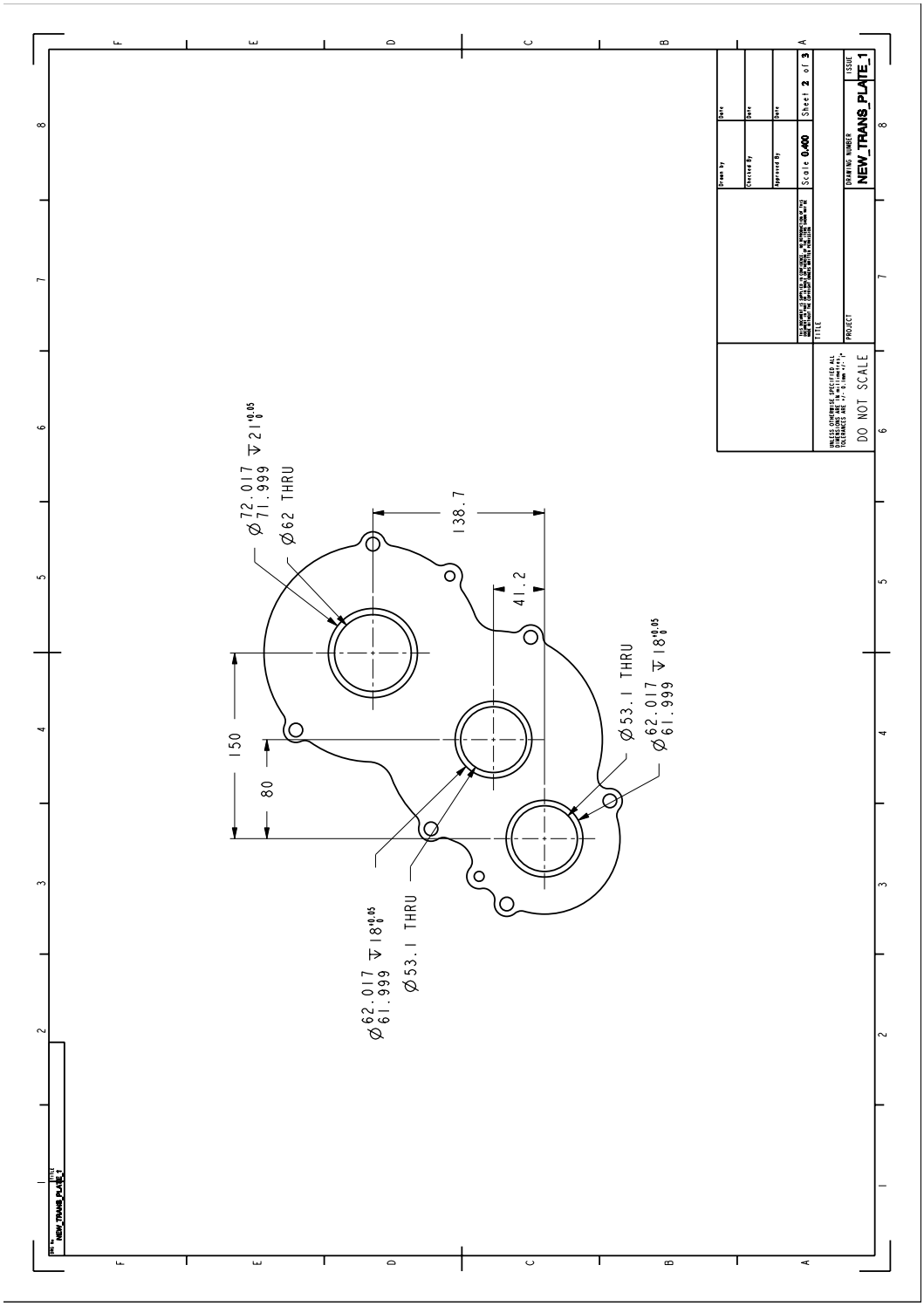
Ø72.017
Ø71.999
Ø62 THRU
138.7
41.2
150
80
Ø53.1 THRU
Ø62.017
Ø61.999
Ø62.017
Ø61.999
Ø53.1 THRU
DO NOT SCALE
Scale 0.400
Sheet 2 of 3
NEW_TRANS_PLATE_1

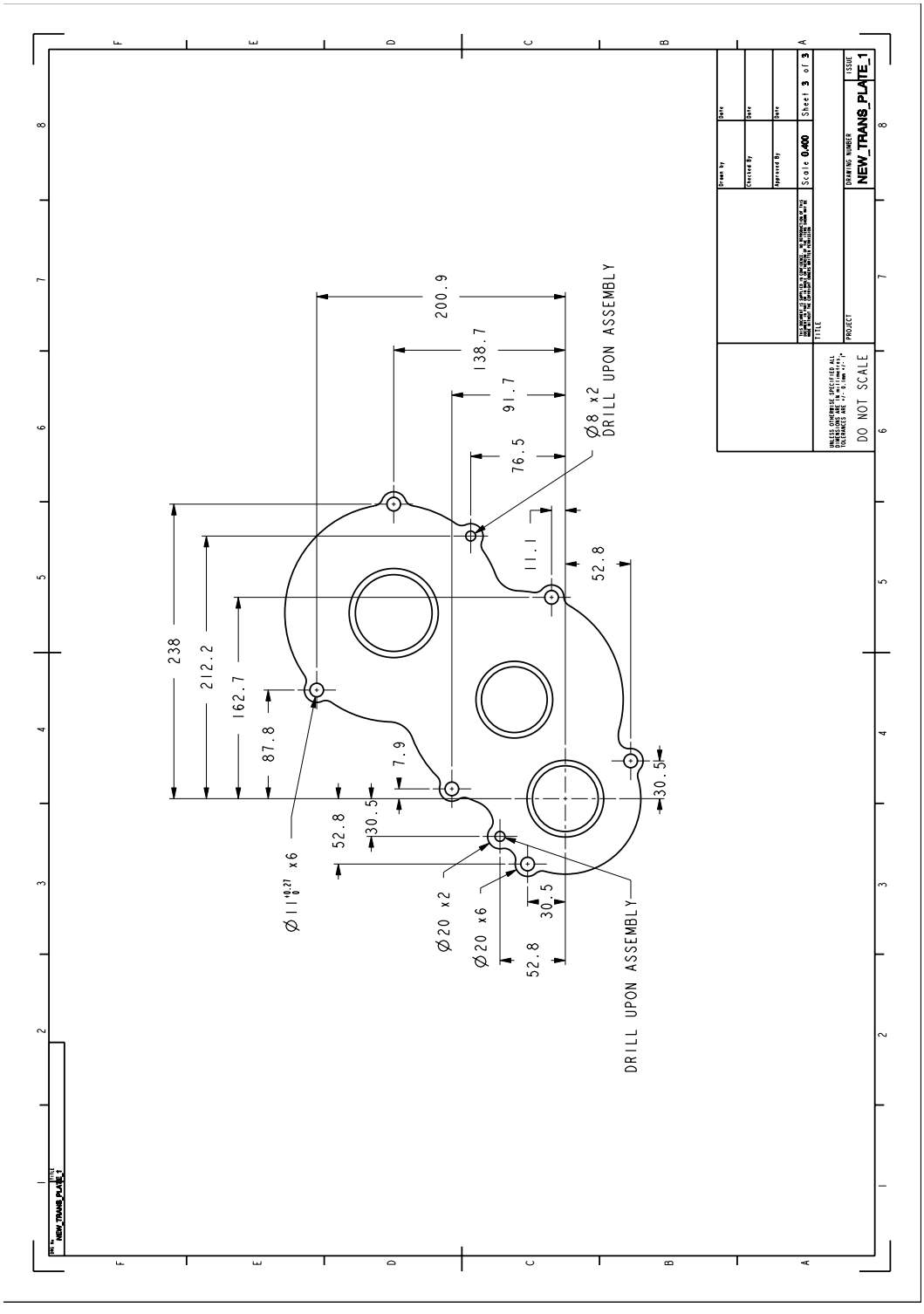
200.9
138.7
91.7
76.5
11.1
52.8
238
212.2
162.7
87.8
7.9
30.5
52.8
30.5
30.5
52.8
Ø8 x2
DRILL UPON ASSEMBLY
Ø11 x6
Ø20 x2
Ø20 x6
DRILL UPON ASSEMBLY
DO NOT SCALE
NEW_TRANS_PLATE_1
Scale 0.400
Sheet 3 of 3

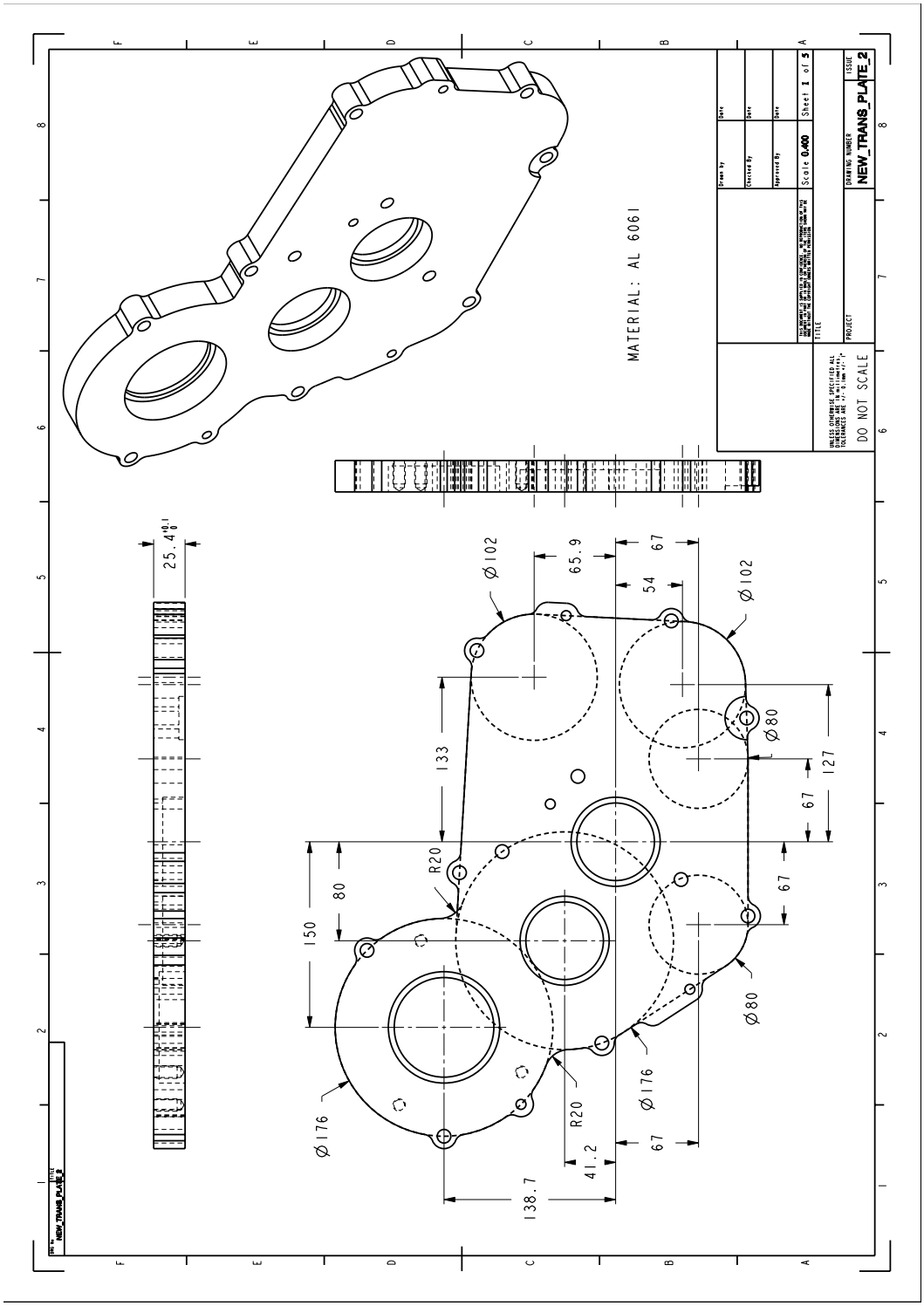
MATERIAL: AL 6061
DO NOT SCALE
NEW_TRANS_PLATE_2
Scale 0.400
Sheet 1 of 5
Ø102
65.9
54
67
Ø80
133
127
R20
80
150
Ø176
41.2
138.7
25.4

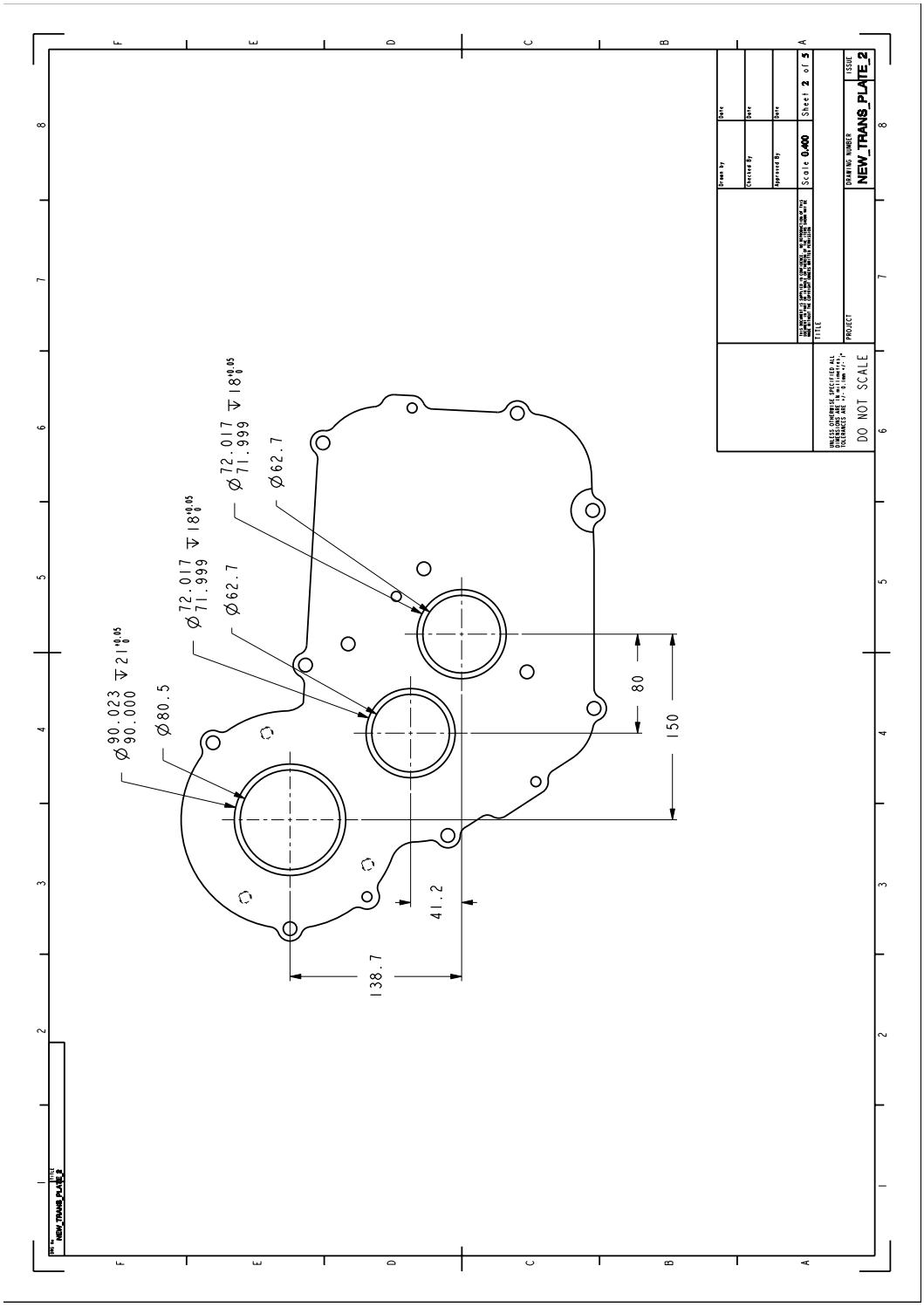
Ø90.023
90.000
Ø80.5
Ø72.017
71.999
Ø62.7
Ø72.017
71.999
Ø62.7
80
150
41.2
138.7
DO NOT SCALE
NEW_TRANS_PLATE_2
Scale 0.400
Sheet 2 of 5

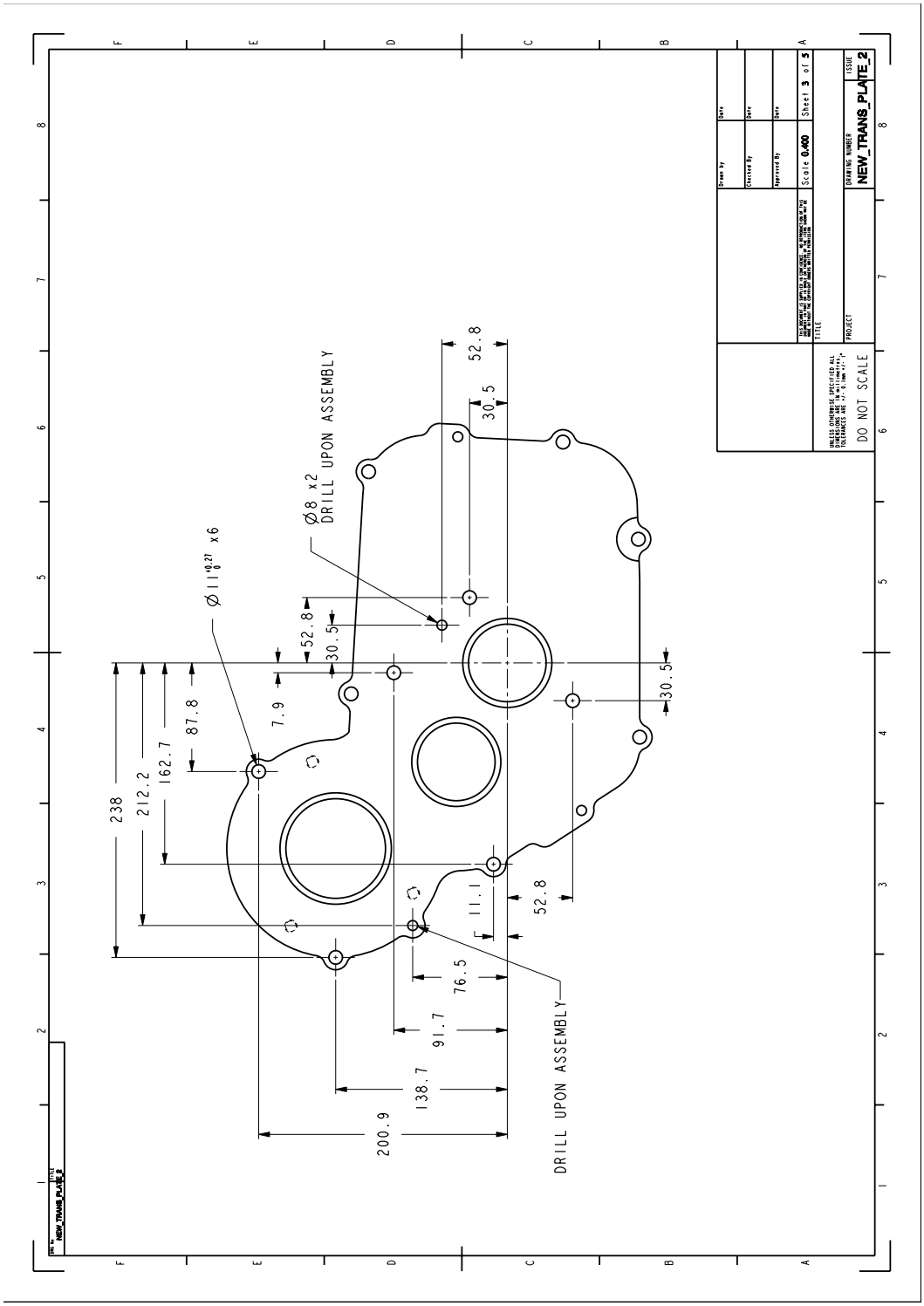
Ø8 x2
DRILL UPON ASSEMBLY
Ø 11 +0.27 0 x6
52.8
30.5
7.9
87.8
162.7
212.2
238
52.8
30.5
30.5
11.1
52.8
76.5
91.7
138.7
200.9
DRILL UPON ASSEMBLY
DO NOT SCALE
Scale 0.400
Sheet 3 of 5
NEW_TRANS_PLATE_2

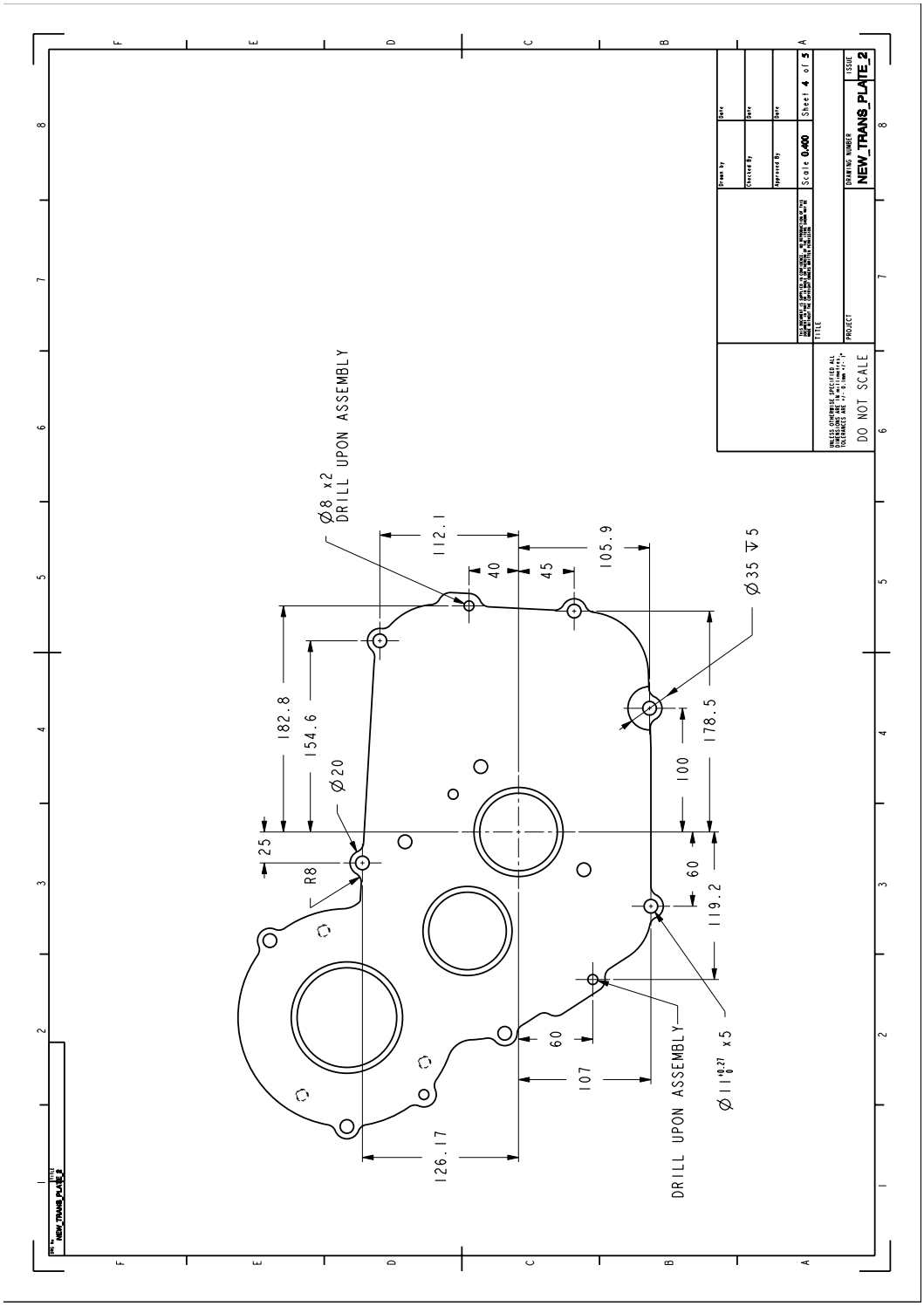
Ø8 x2
DRILL UPON ASSEMBLY
112.1
40
45
105.9
Ø35 ∓5
182.8
154.6
Ø20
178.5
100
25
R8
60
119.2
60
107
126.17
DRILL UPON ASSEMBLY
Ø11 +0.27 0 x5
DO NOT SCALE
Scale 0.400
Sheet 4 of 5
NEW_TRANS_PLATE_2
NEW_TRANS_PLATE_2

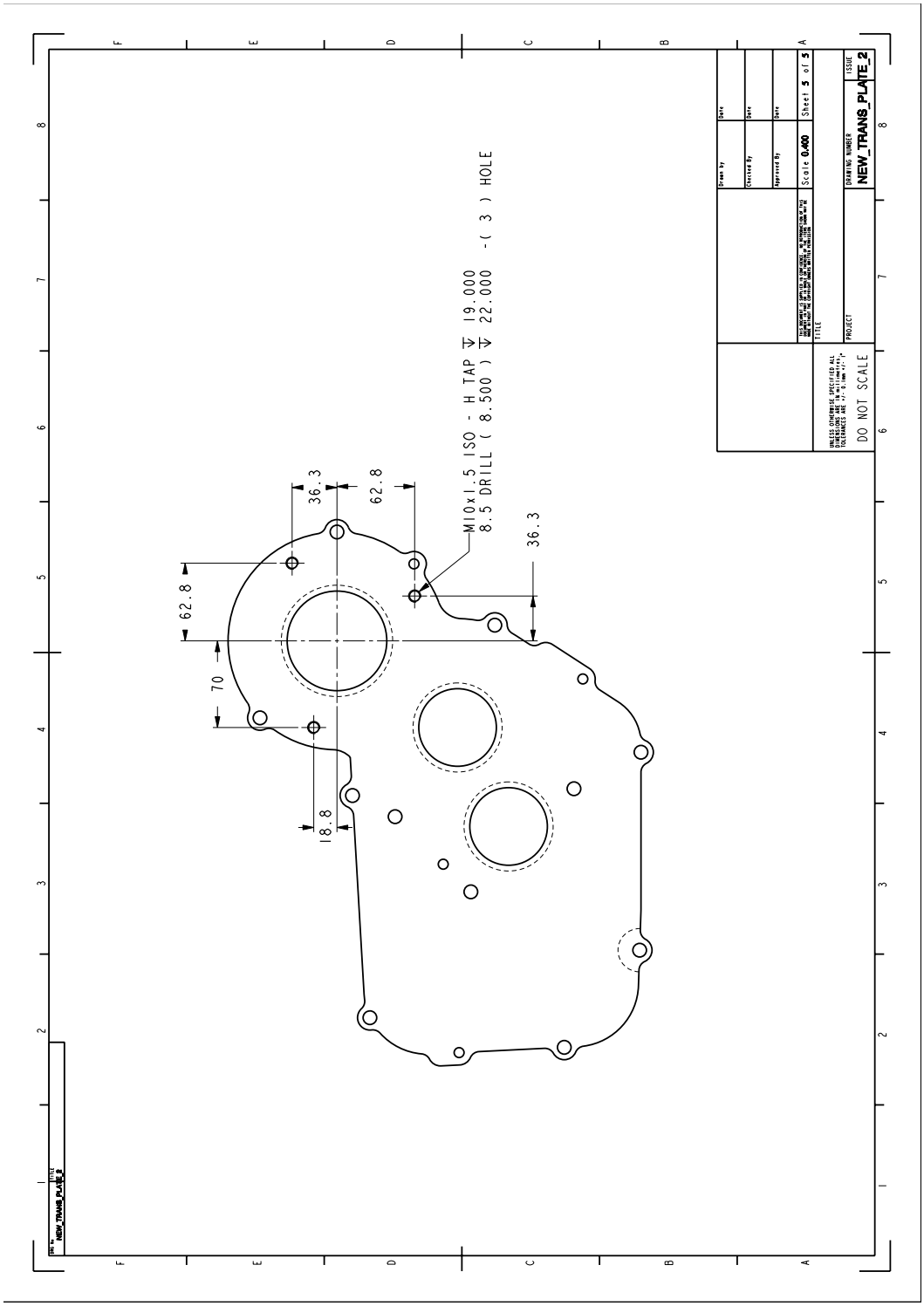
M10x1.5 ISO - H TAP ↧ 19.000
8.5 DRILL (8.500) ↧ 22.000 -(3) HOLE
36.3
62.8
62.8
36.3
70
18.8
DO NOT SCALE
NEW_TRANS_PLATE_2
Scale 0.400
Sheet 5 of 5

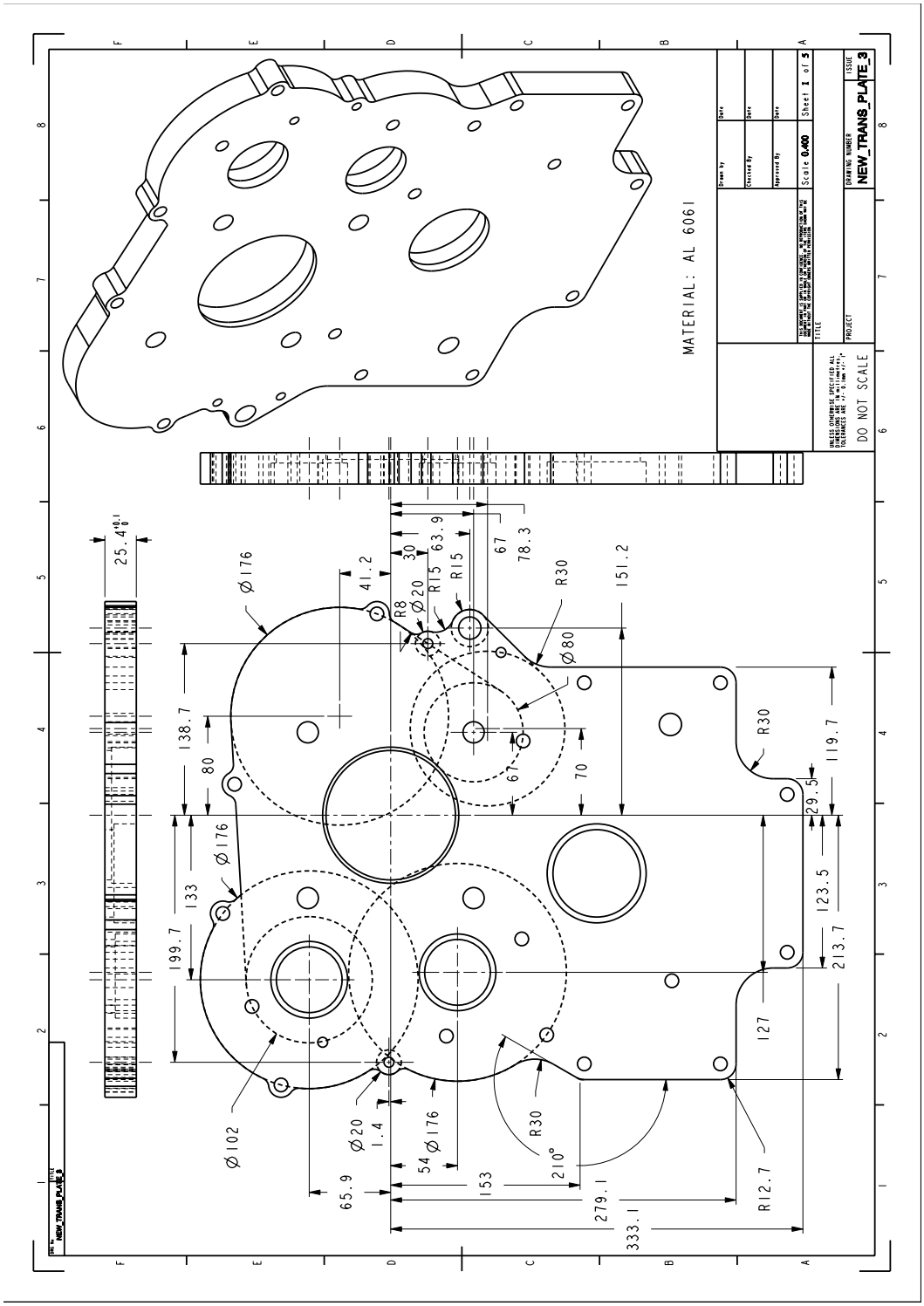
MATERIAL: AL 6061
DO NOT SCALE
NEW_TRANS_PLATE_3
Scale 0.400
Sheet 1 of 5
Ø176
Ø102
Ø20
Ø80
R8
R15
R30
R12.7
25.4
41.2
30
63.9
67
78.3
151.2
138.7
80
133
199.7
70
119.7
29.5
123.5
213.7
127
1.4
54
153
210°
65.9
279.1
333.1

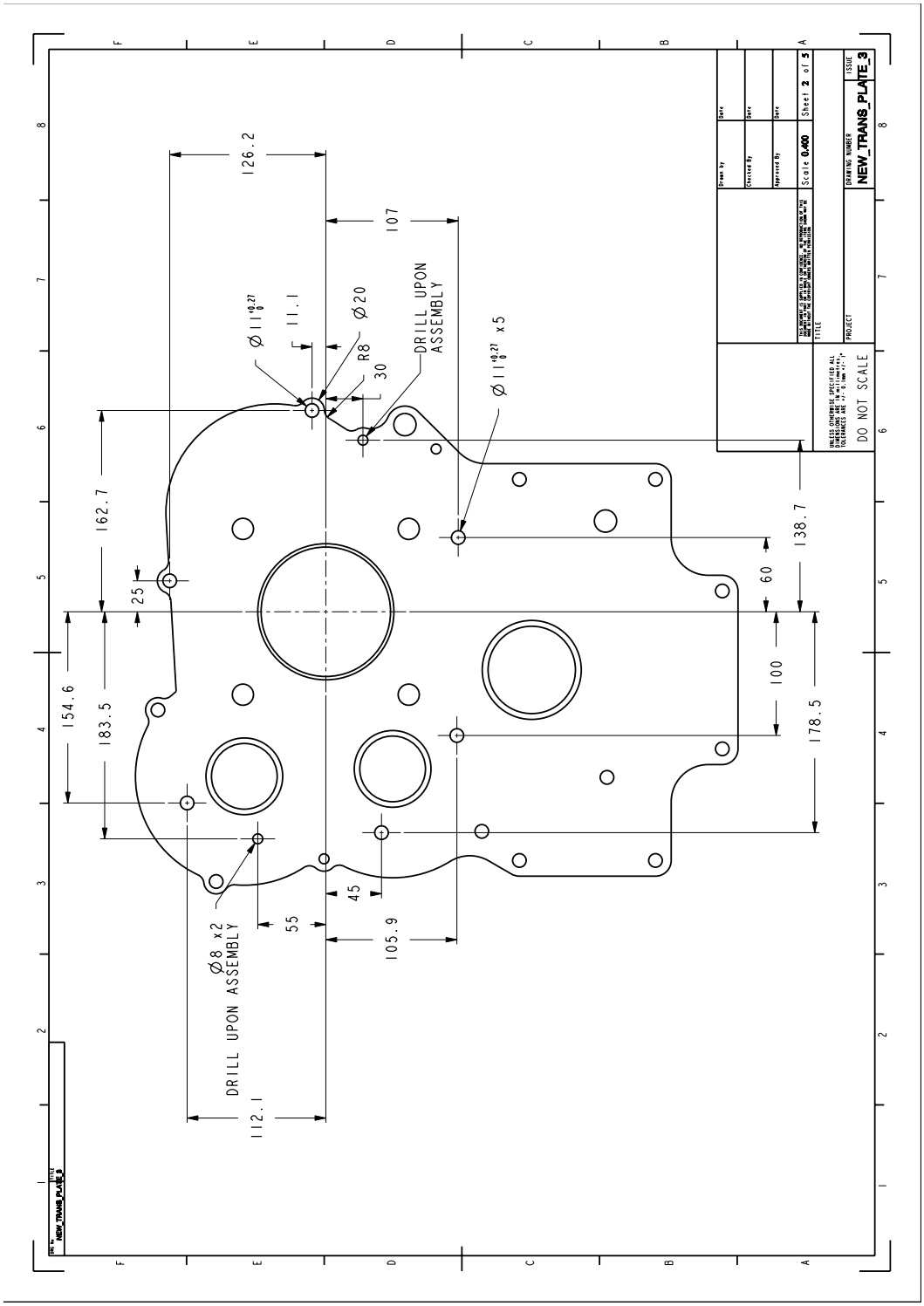
126.2
107
Ø11 +0.27 0
11.1
Ø20
R8
30
DRILL UPON ASSEMBLY
Ø11 +0.27 0 x5
162.7
25
154.6
183.5
138.7
60
100
178.5
45
55
105.9
Ø8 x2
DRILL UPON ASSEMBLY
112.1
DO NOT SCALE
NEW_TRANS_PLATE_3
Sheet 2 of 5
Scale 0.400

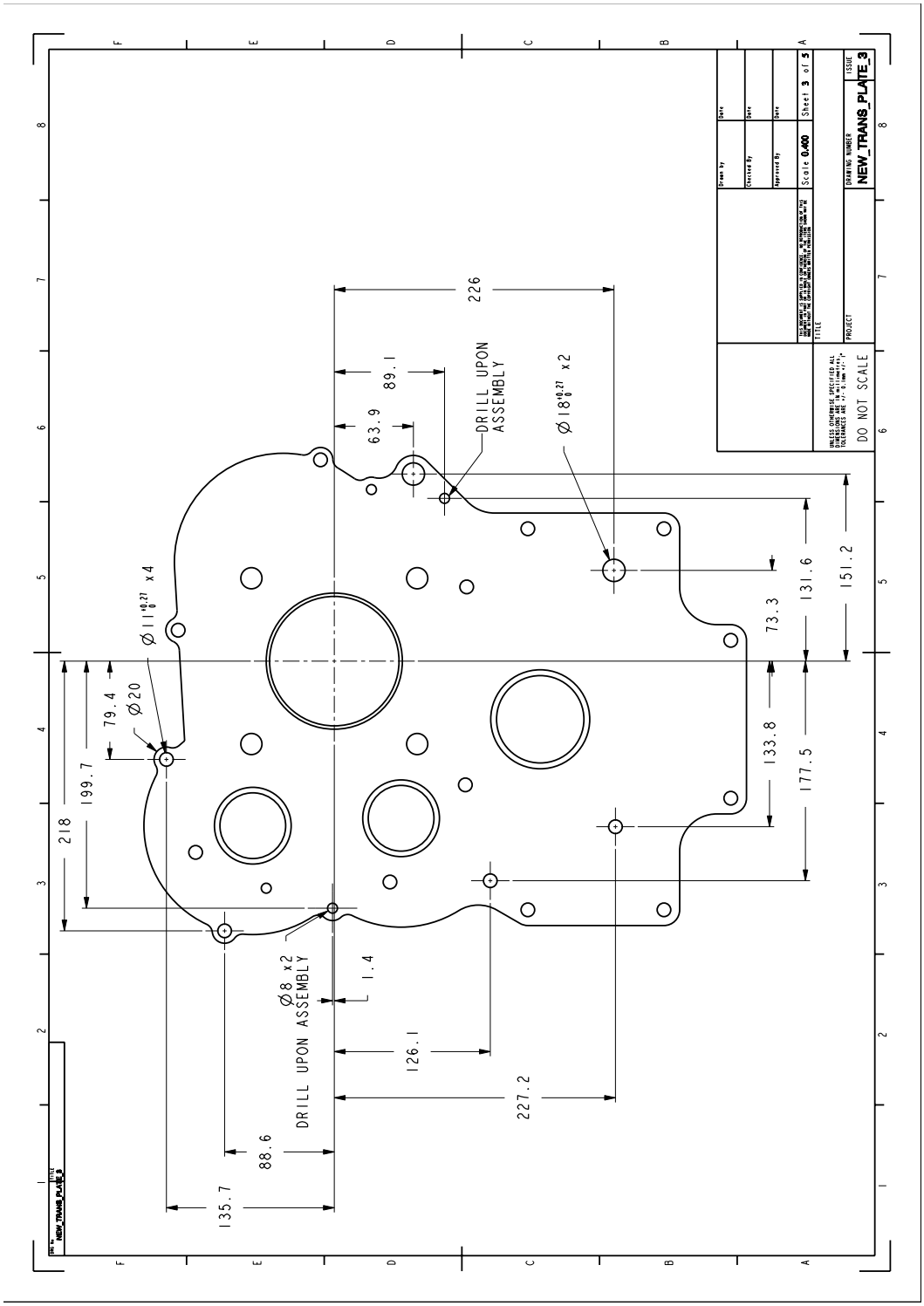
226
89.1
63.9
DRILL UPON ASSEMBLY
Ø18 +0.27 0 x2
Ø11 +0.27 0 x4
Ø20
79.4
199.7
218
73.3
131.6
151.2
133.8
177.5
Ø8 x2
DRILL UPON ASSEMBLY
1.4
126.1
227.2
88.6
135.7
DO NOT SCALE
Scale 0.400
Sheet 3 of 5
NEW_TRANS_PLATE_3
PROJECT

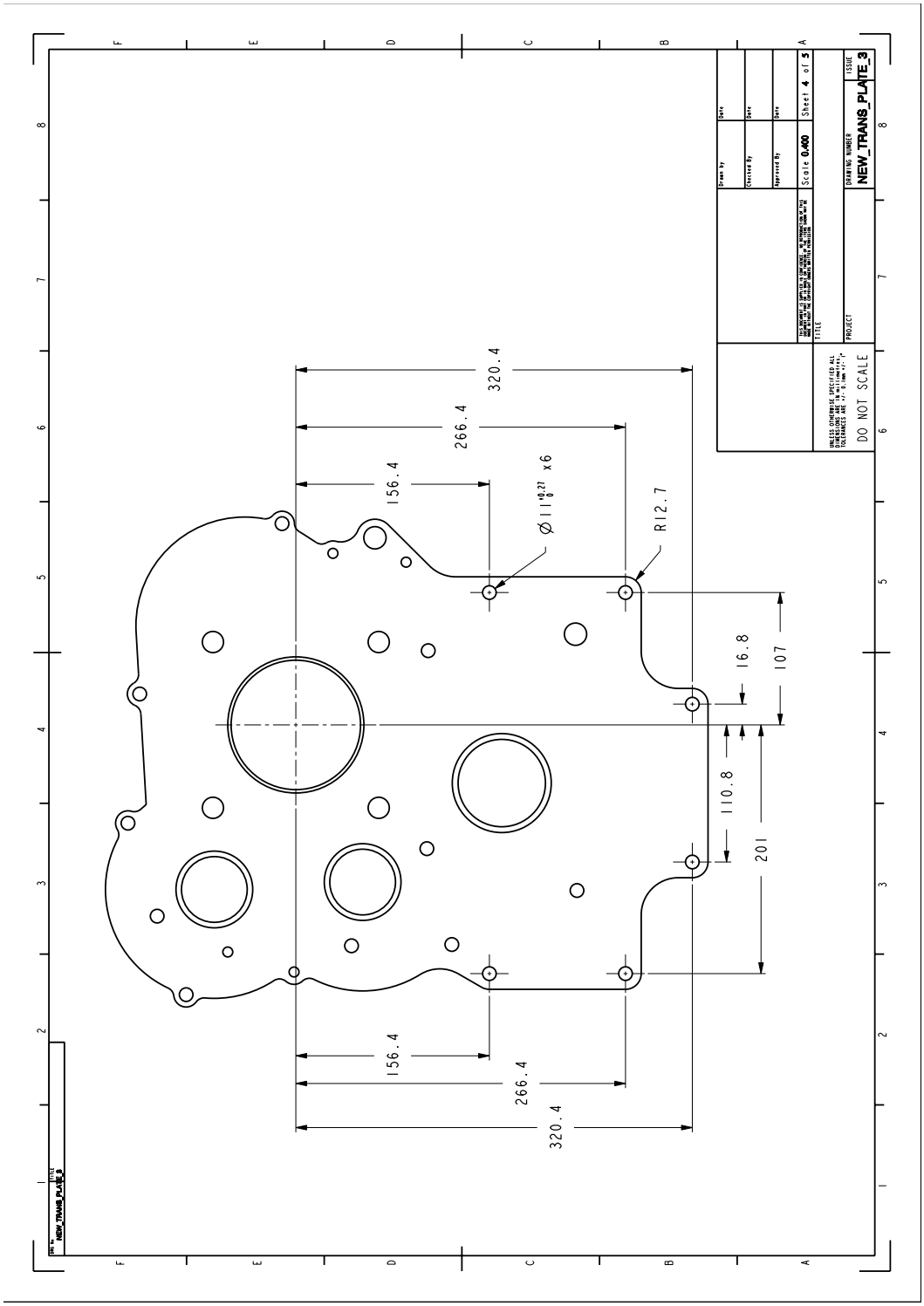
320.4
266.4
156.4
Ø11 +0.27 0 x6
R12.7
16.8
107
110.8
201
156.4
266.4
320.4
DO NOT SCALE
Scale 0.400
Sheet 4 of 5
NEW_TRANS_PLATE_3

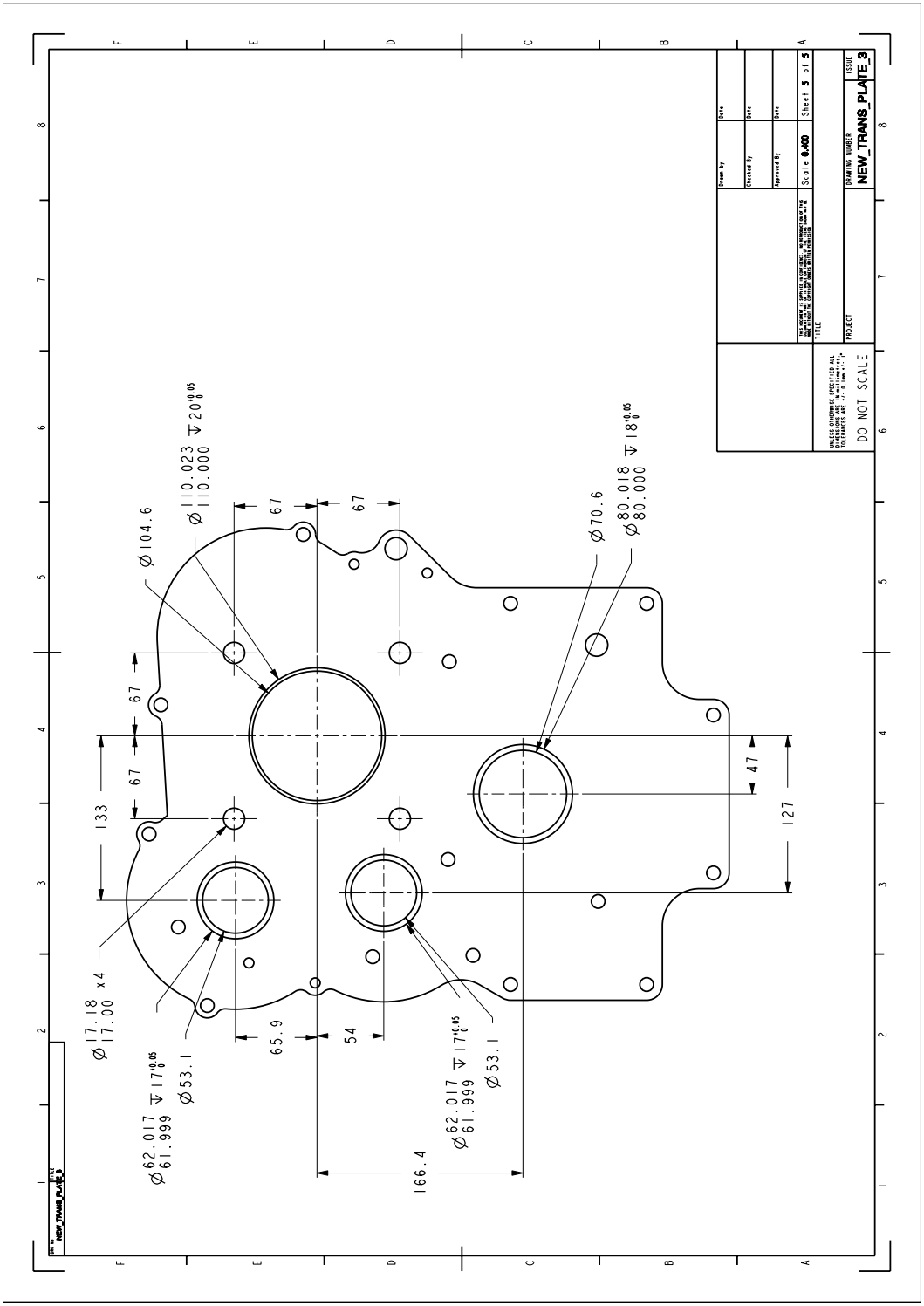
DO NOT SCALE
NEW_TRANS_PLATE_3
Scale 0.400
Sheet 5 of 5
Ø104.6
Ø110.023 / 110.000 ∓ 20 +0.05 0
Ø70.6
Ø80.018 / 80.000 ∓ 18 +0.05 0
Ø17.18 / 17.00 x4
Ø62.017 / 61.999 ∓ 17 +0.05 0
Ø53.1
133
67
67
67
67
47
127
65.9
54
166.4

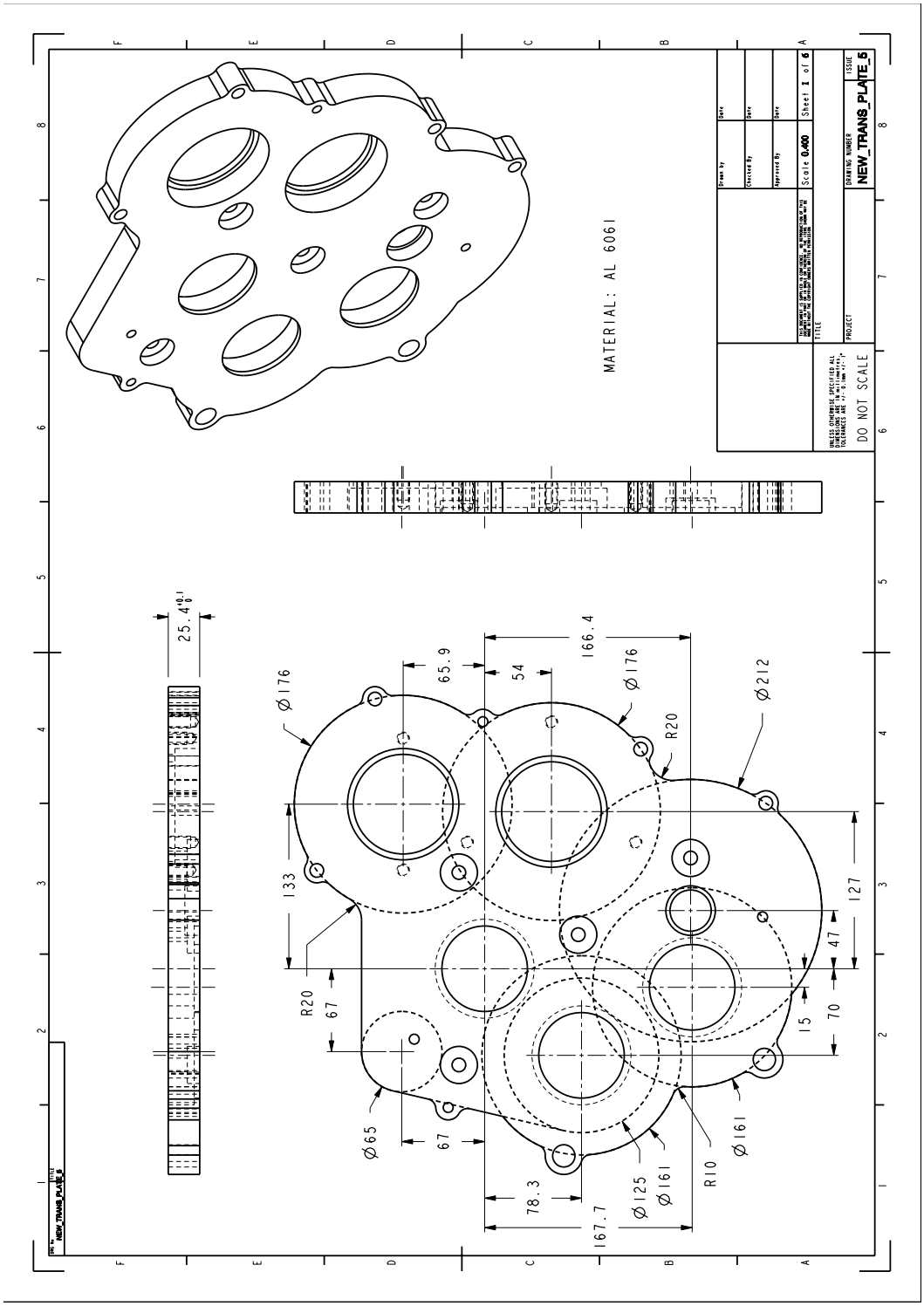
MATERIAL: AL 6061
DO NOT SCALE
NEW_TRANS_PLATE_5
Scale 0.400
Sheet 1 of 6
25.40
166.4
65.9
54
Ø176
Ø176
R20
Ø212
133
R20
67
Ø65
67
78.3
167.7
Ø125
Ø161
R10
Ø161
127
47
15
70

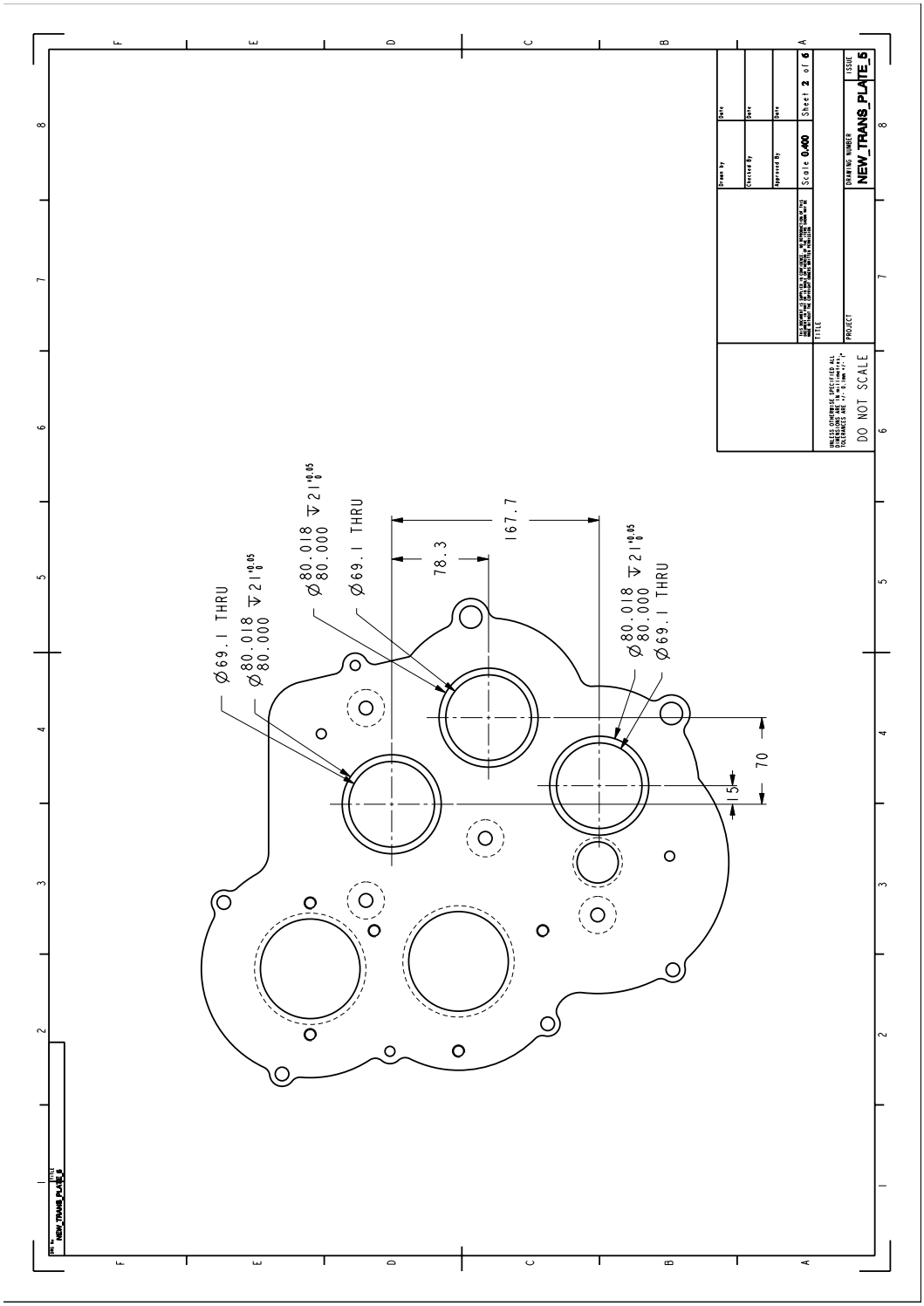
Ø69.1 THRU
Ø80.018 Ø80.000 ∓21 +0.05 0
Ø80.018 Ø80.000 ∓21 +0.05 0
Ø69.1 THRU
78.3
167.7
Ø80.018 Ø80.000 ∓21 +0.05 0
Ø69.1 THRU
15
70
DO NOT SCALE
Scale 0.400
Sheet 2 of 6
NEW_TRANS_PLATE_5

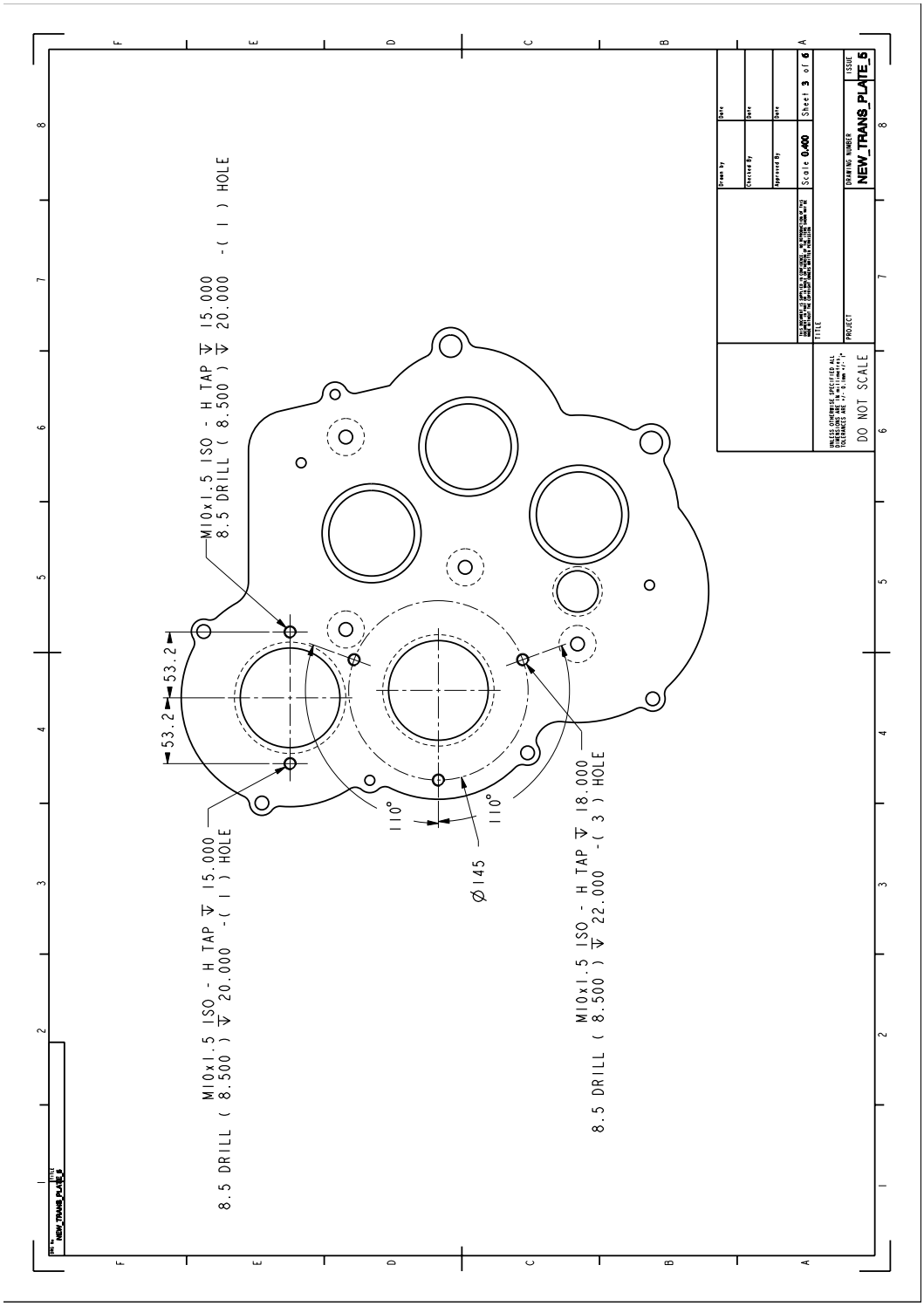
M10x1.5 ISO - H TAP ↧ 15.000
8.5 DRILL (8.500) ↧ 20.000 -(1) HOLE
53.2
53.2
M10x1.5 ISO - H TAP ↧ 15.000
8.5 DRILL (8.500) ↧ 20.000 -(1) HOLE
110°
110°
Ø145
M10x1.5 ISO - H TAP ↧ 18.000
8.5 DRILL (8.500) ↧ 22.000 -(3) HOLE
DO NOT SCALE
Scale 0.400
Sheet 3 of 6
NEW_TRANS_PLATE_5

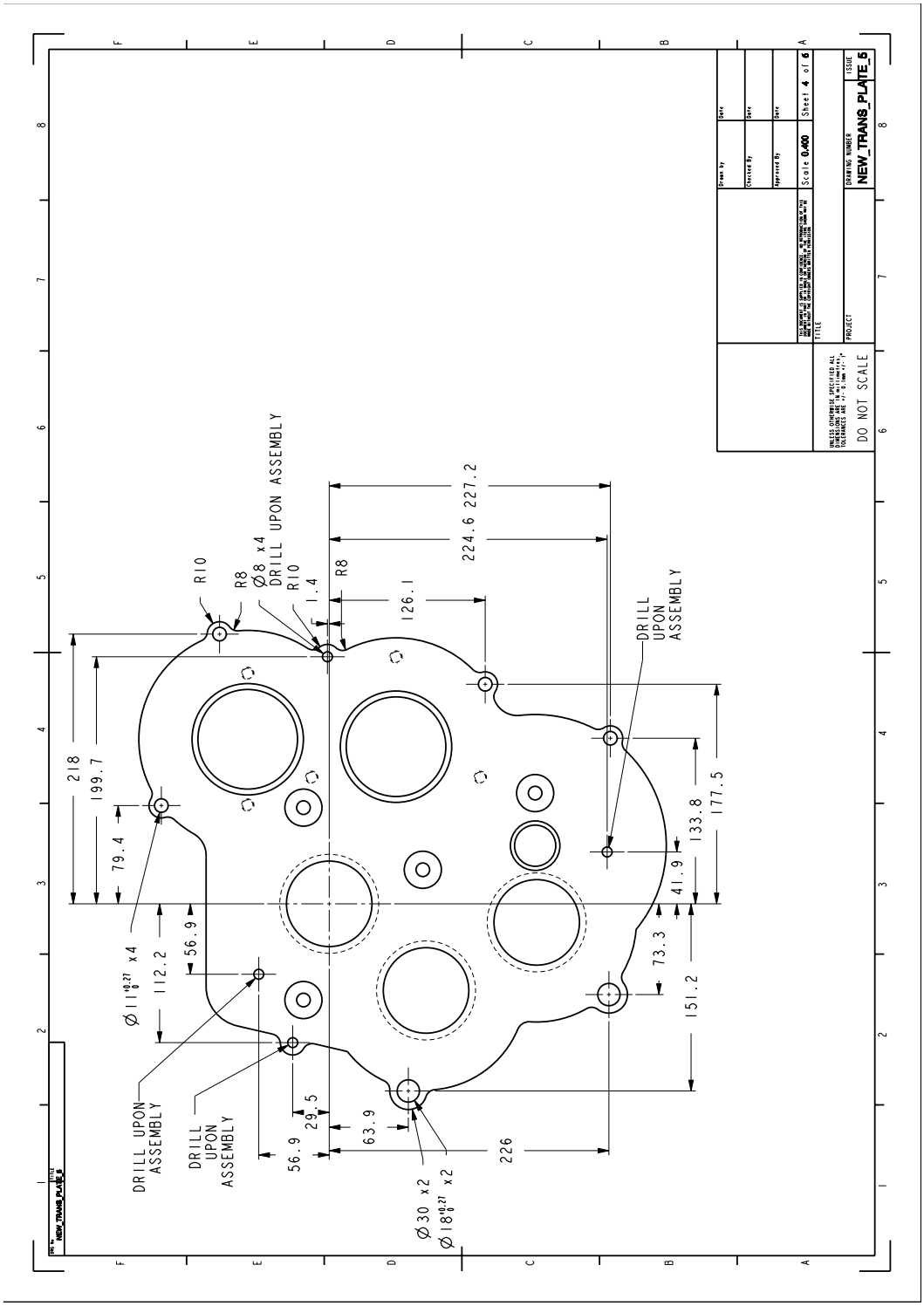
R10
R8
Ø8 x4
DRILL UPON ASSEMBLY
R10
1.4
R8
126.1
224.6 227.2
DRILL
UPON
ASSEMBLY
218
199.7
79.4
Ø11 +0.27 -0 x4
112.2
56.9
DRILL UPON
ASSEMBLY
DRILL
UPON
ASSEMBLY
56.9
29.5
63.9
Ø30 x2
Ø18 +0.27 -0 x2
226
73.3
41.9
133.8
177.5
151.2
DO NOT SCALE
Scale 0.400
Sheet 4 of 6
PROJECT
DRAWING NUMBER
NEW_TRANS_PLATE_5
ISSUE
Drawn by
Checked By
Approved By
Date
TITLE
NEW_TRANS_PLATE_5

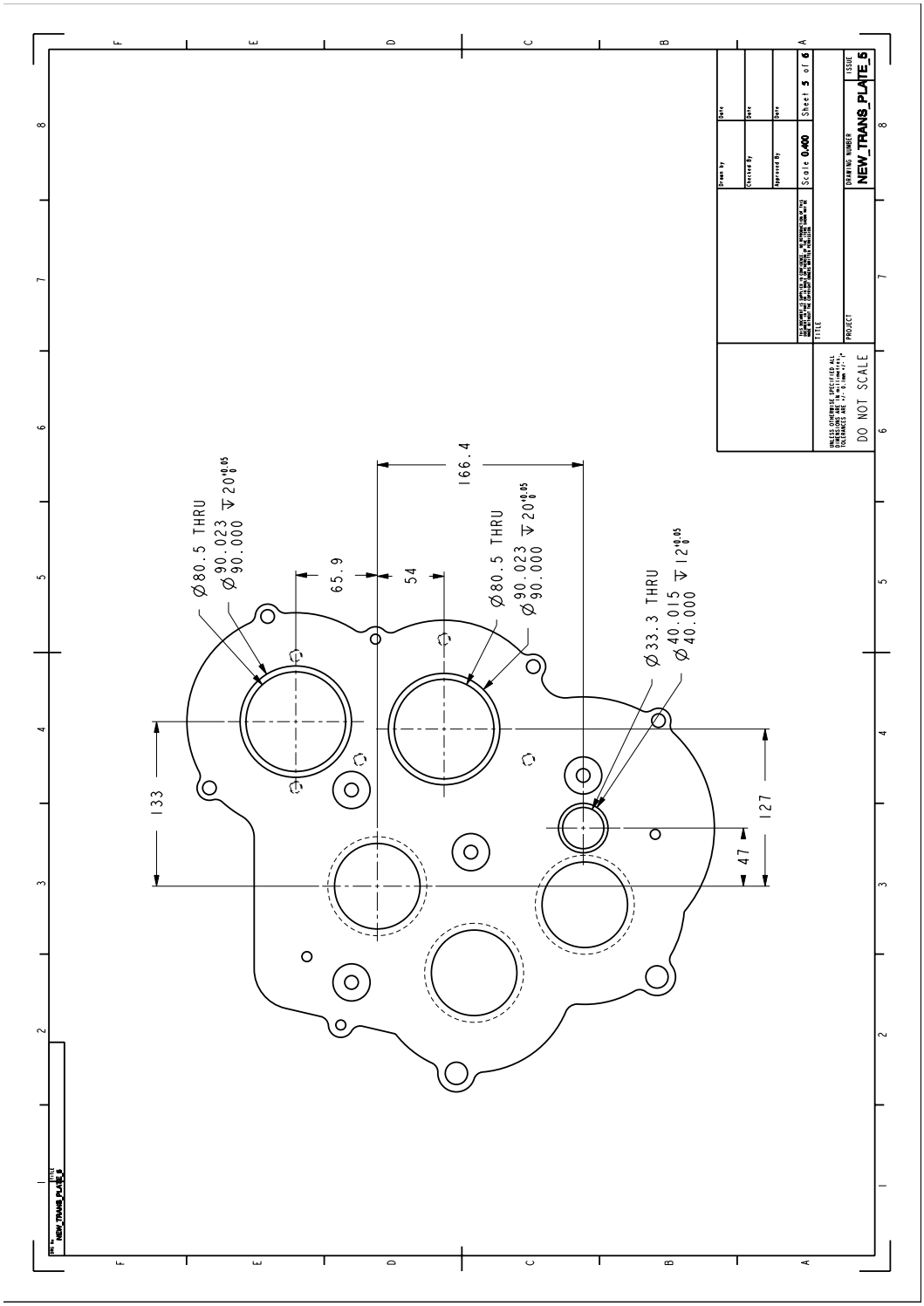
Ø80.5 THRU
Ø90.023 ∓20 +0.05 0
Ø90.000
65.9
54
166.4
Ø80.5 THRU
Ø90.023 ∓20 +0.05 0
Ø90.000
Ø33.3 THRU
Ø40.015 ∓12 +0.05 0
Ø40.000
133
127
47
DO NOT SCALE
Scale 0.400
Sheet 5 of 6
NEW_TRANS_PLATE_5
NEW_TRANS_PLATE_5

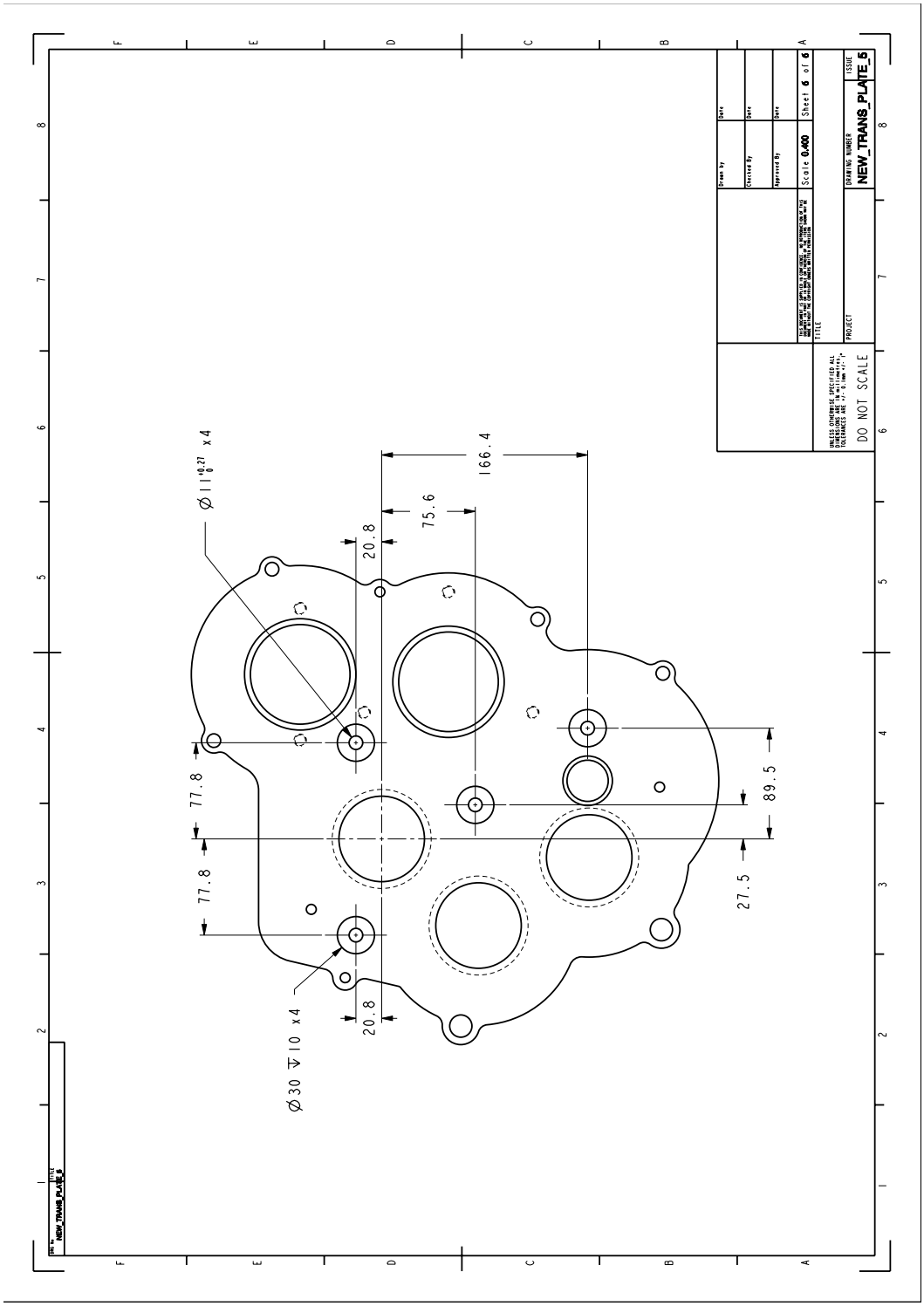
Ø 30 ∓ 10 x4
Ø 11 +0.27 0 x4
166.4
75.6
20.8
20.8
77.8
77.8
89.5
27.5
DO NOT SCALE
NEW_TRANS_PLATE_5
Scale 0.400
Sheet 6 of 6

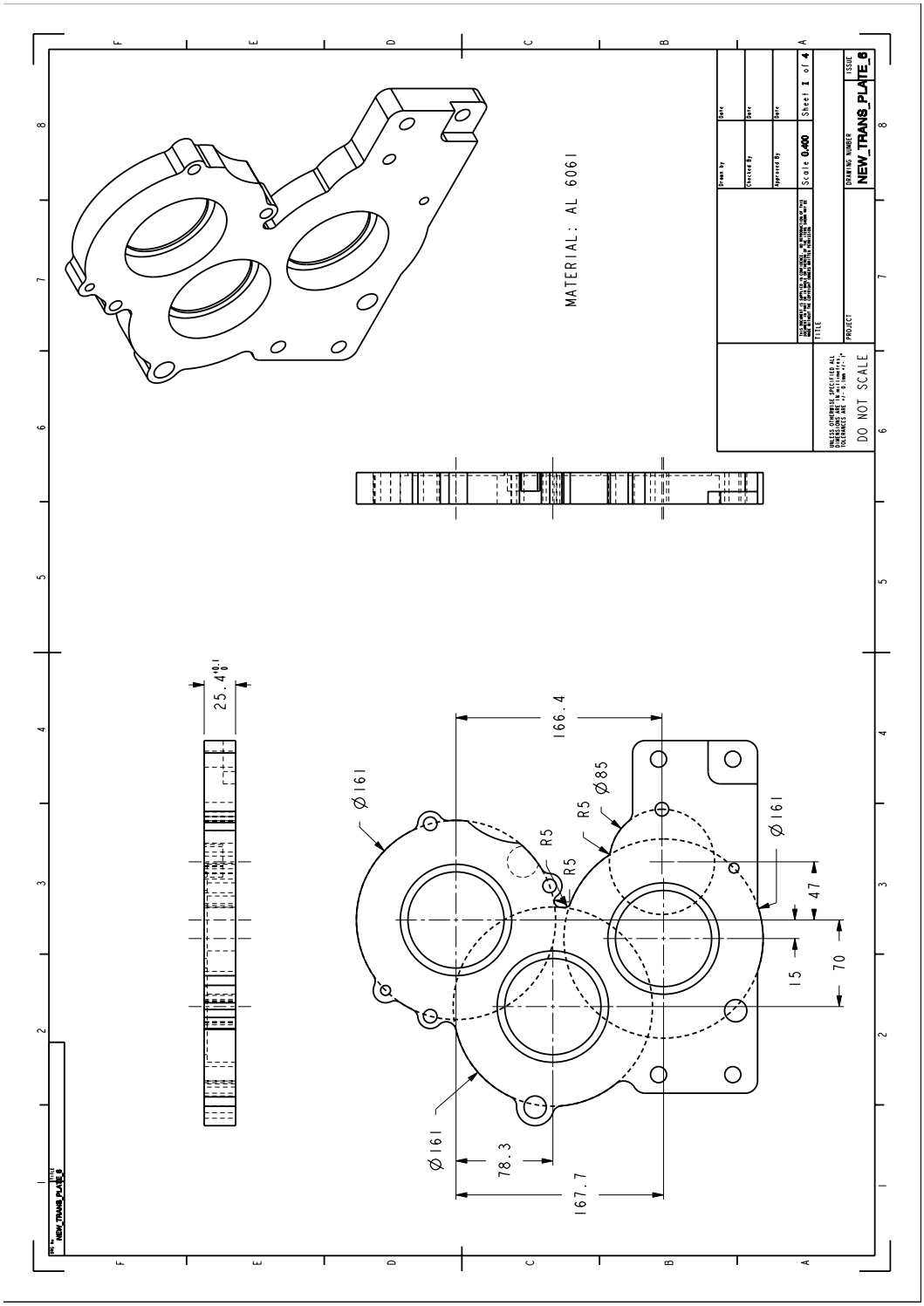
MATERIAL: AL 6061
DO NOT SCALE
NEW_TRANS_PLATE_0
Scale 0.400
Sheet 1 of 4
25.4
166.4
Ø161
Ø85
R5
R5
R5
Ø161
47
15
70
Ø161
78.3
167.7

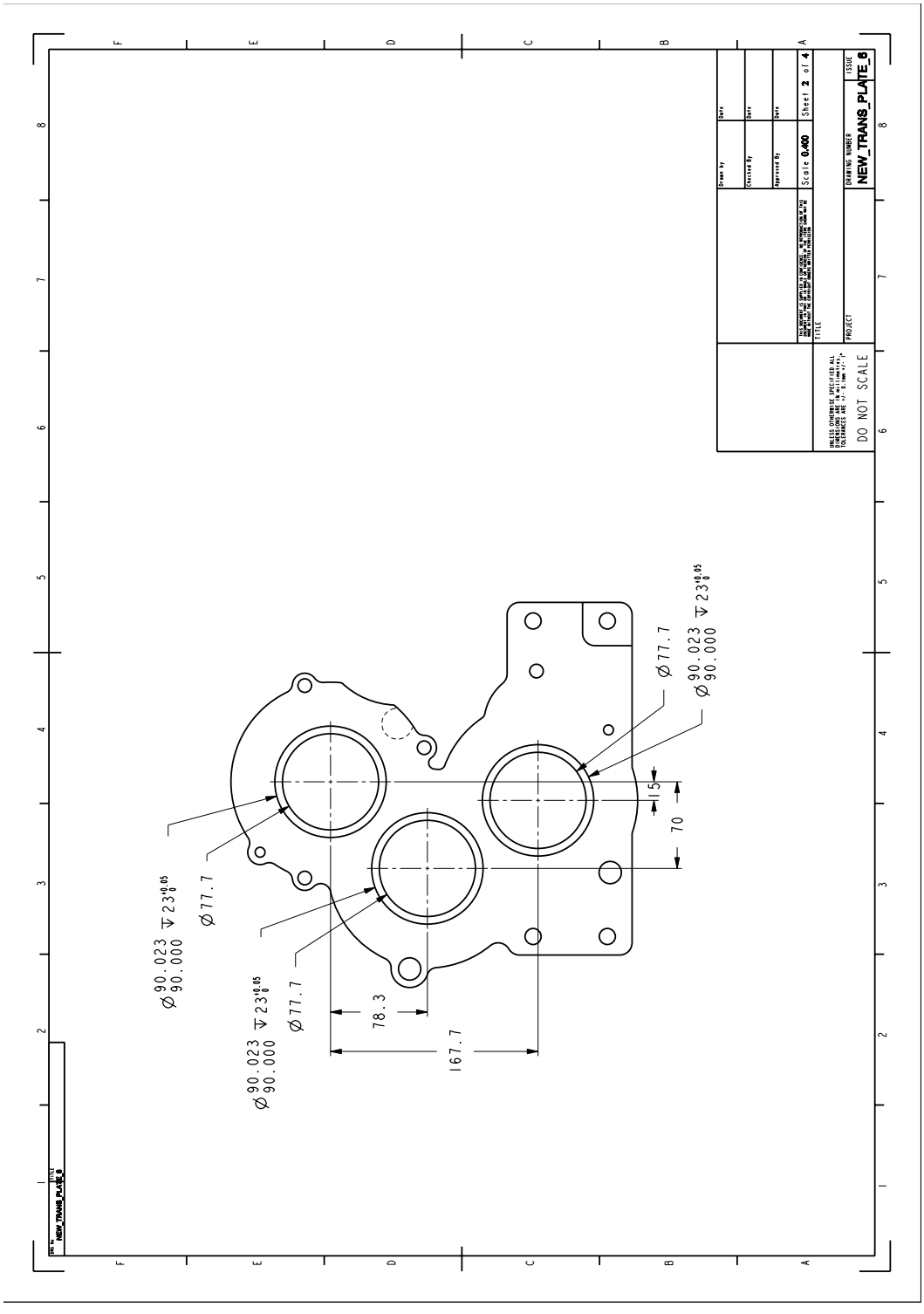
DO NOT SCALE
NEW_TRANS_PLATE_0
Scale 0.400
Sheet 2 of 4
Ø90.023 Ø90.000 ∓23 +0.05 0
Ø77.7
Ø17.7
78.3
167.7
15
70

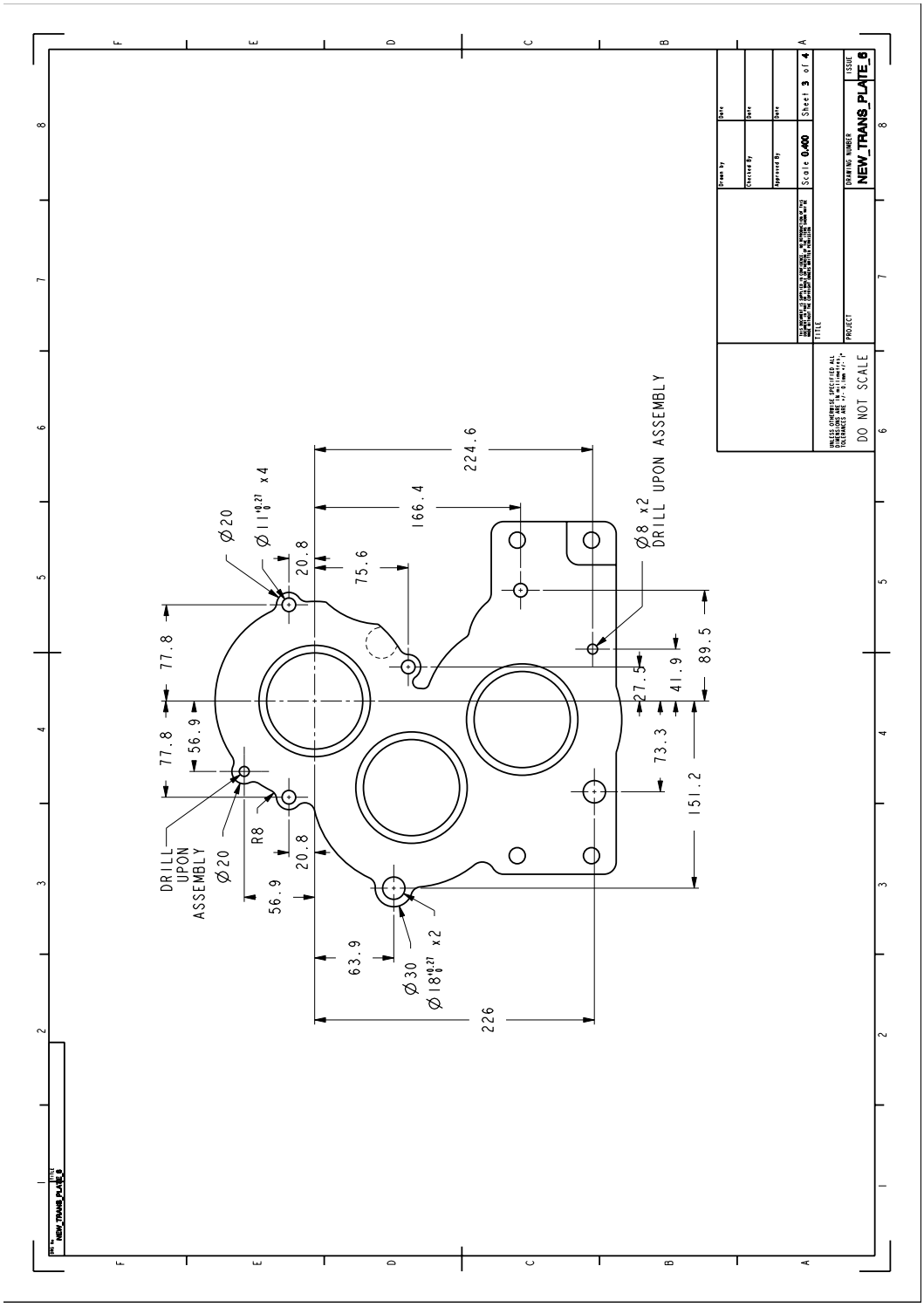
224.6
166.4
Ø20
Ø11 +0.27 0 x4
20.8
75.6
Ø8 x2
DRILL UPON ASSEMBLY
77.8
89.5
77.8
56.9
27.5
41.9
73.3
151.2
DRILL UPON ASSEMBLY
Ø20
R8
20.8
56.9
63.9
Ø30
Ø18 +0.27 0 x2
226
DO NOT SCALE
Scale 0.400
Sheet 3 of 4
NEW_TRANS_PLATE_0

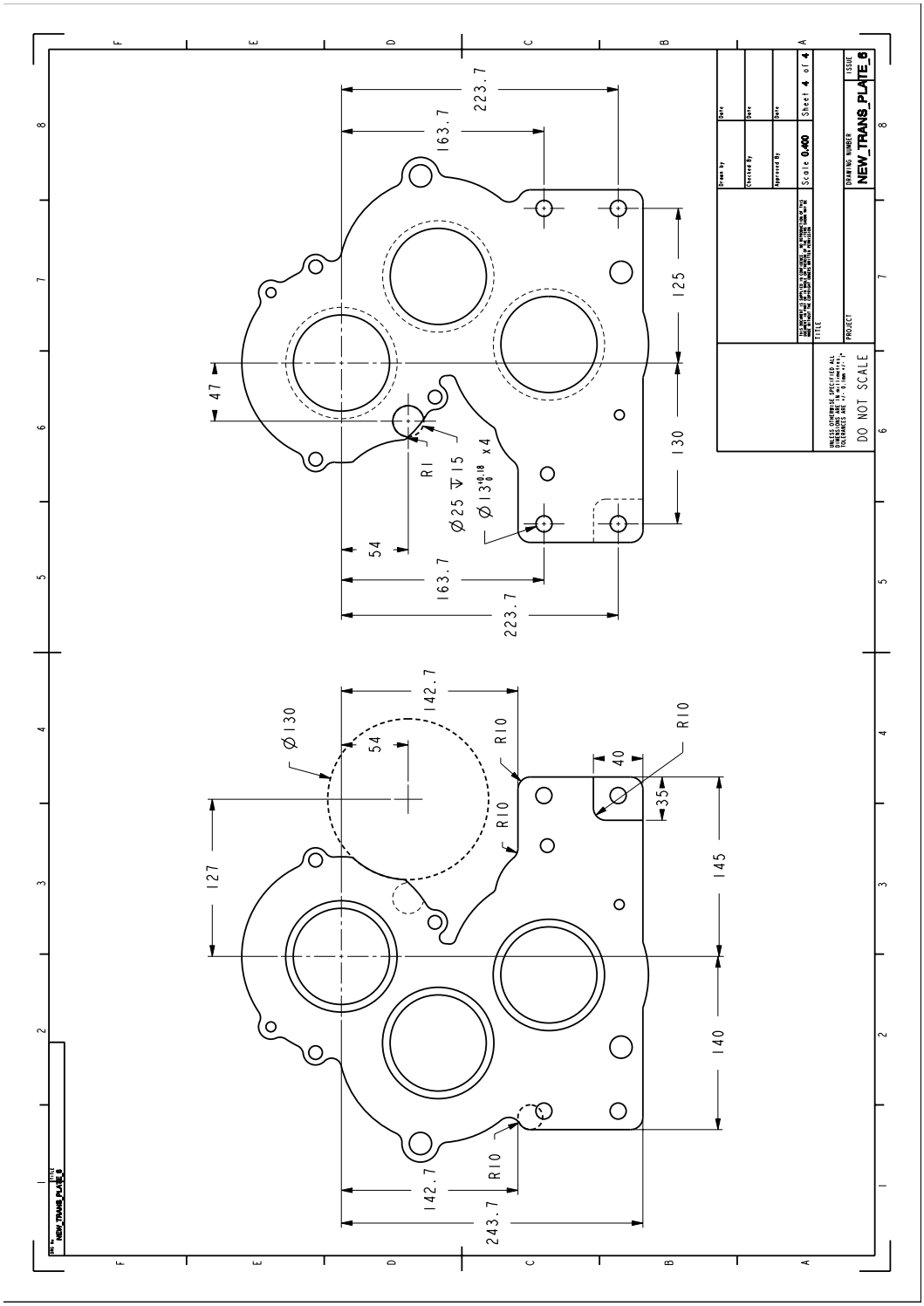
NEW_TRANS_PLATE_8
223.7
163.7
125
130
47
54
R1
Ø25 ∓ 15
Ø13 +0.18 0 x4
142.7
Ø130
R10
40
35
127
145
140
243.7
Scale 0.400
Sheet 4 of 4
DRAWING NUMBER
NEW_TRANS_PLATE_8
ISSUE
PROJECT
DO NOT SCALE

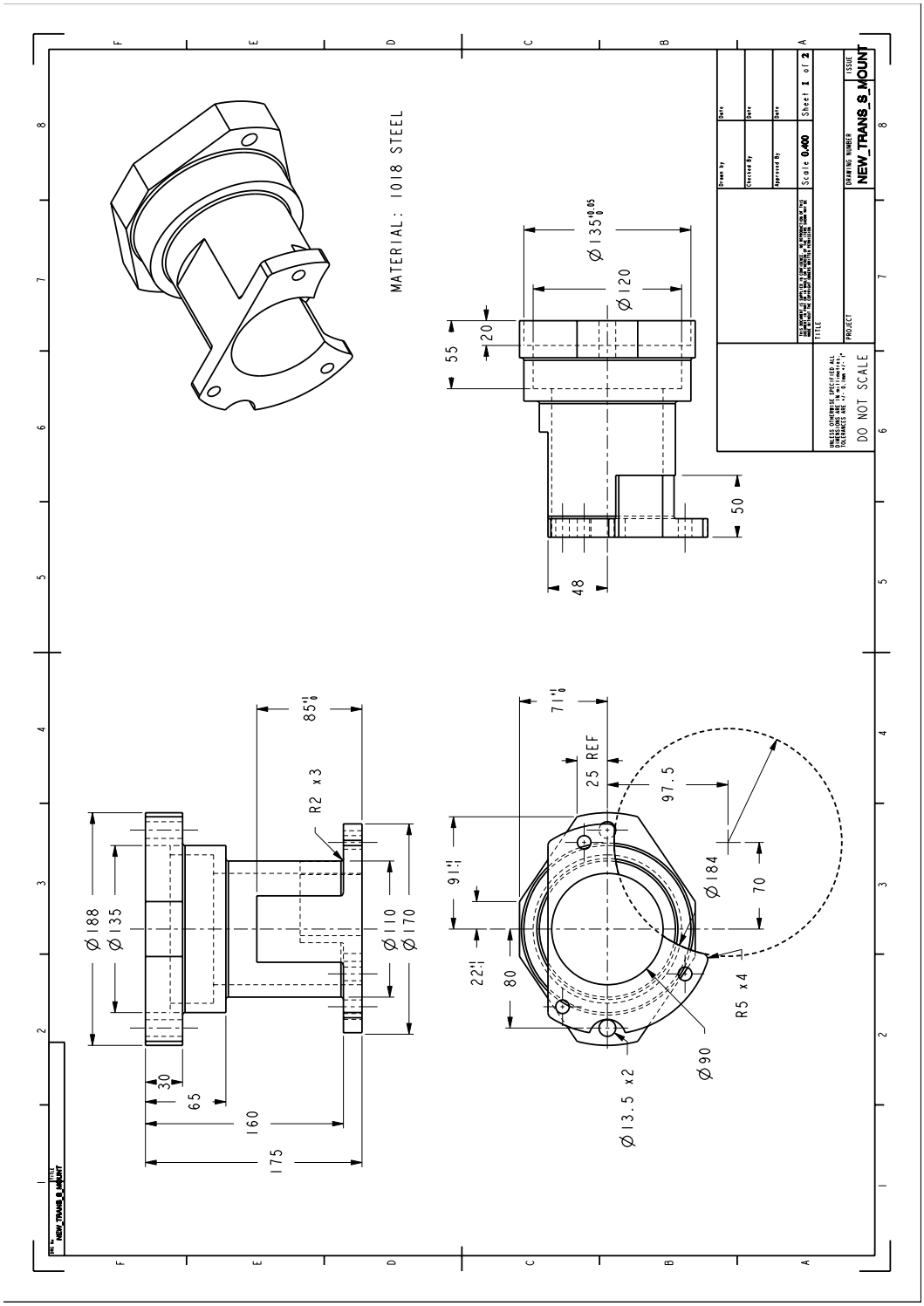
MATERIAL: 1018 STEEL
Ø135 +0.05 -0
Ø120
55
20
50
48
Ø188
Ø135
Ø110
Ø170
R2 x3
85 +1 -0
30
65
160
175
71 +1 -0
25 REF
97.5
91 +1 -1
Ø184
70
22 +1 -1
80
R5 x4
Ø90
Ø13.5 x2
Scale 0.400
Sheet 1 of 2
DRAWING NUMBER
NEW_TRANS_S_MOUNT
ISSUE
PROJECT
DO NOT SCALE
UNLESS OTHERWISE SPECIFIED ALL
DIMENSIONS ARE IN MILLIMETERS
TOLERANCES ARE +/- 0.1mm
Drawn by
Checked By
Approved By
Date
TITLE
NEW_TRANS_S_MOUNT

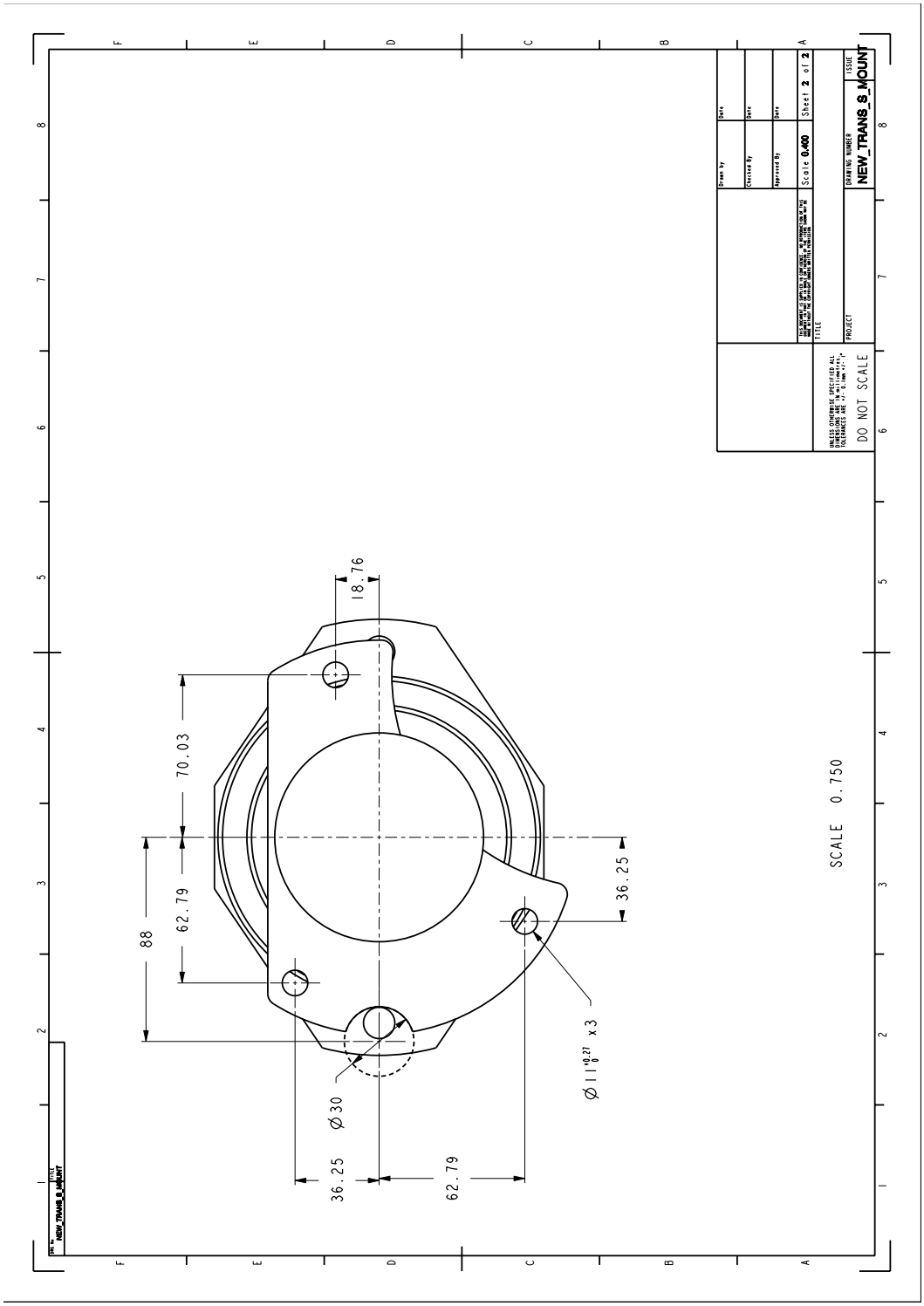
18.76
70.03
62.79
88
36.25
Ø30
36.25
62.79
Ø11 +0.27 0 x3
SCALE 0.750
DO NOT SCALE
NEW_TRANS_S_MOUNT
Sheet 2 of 2
Scale 0.400

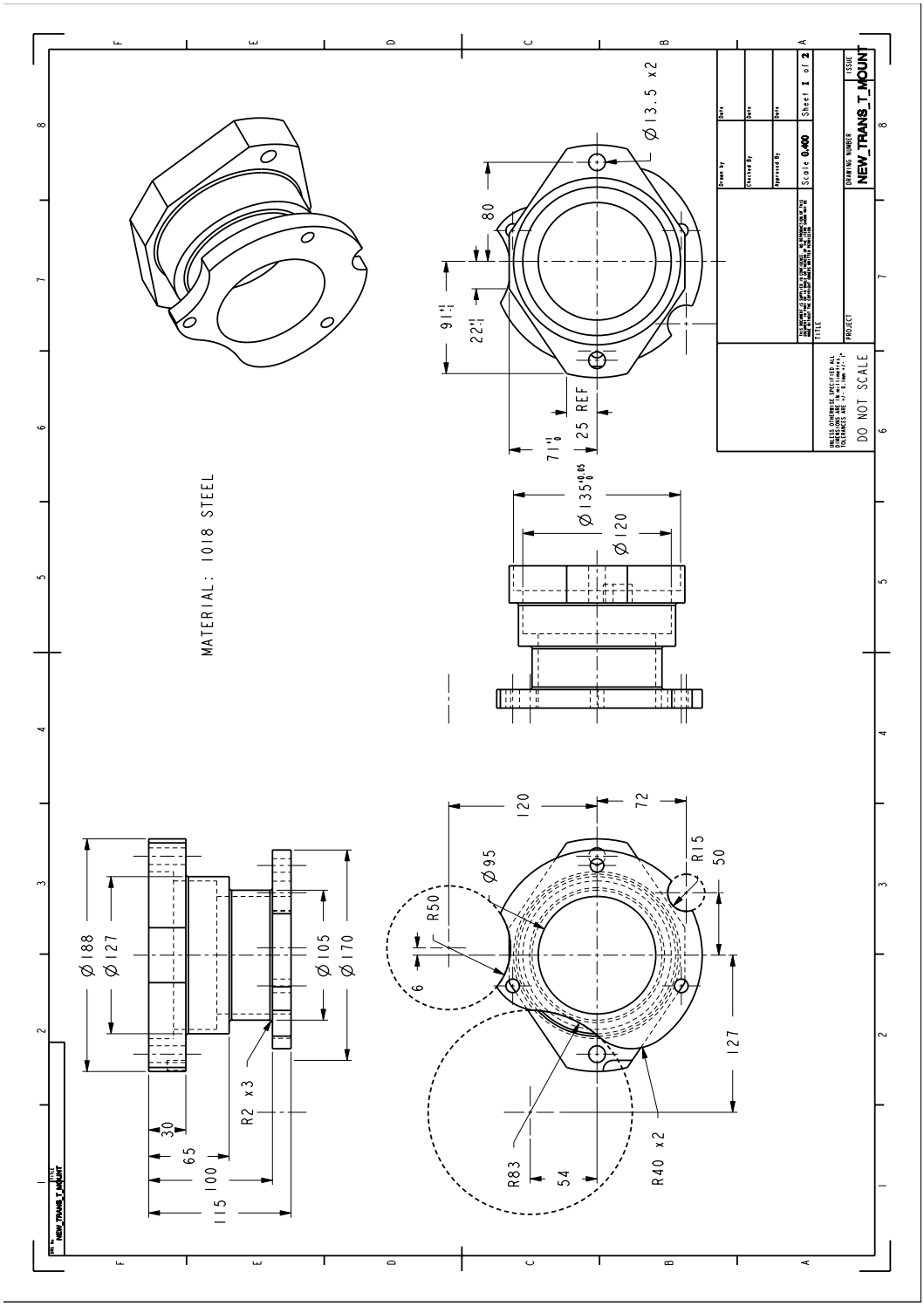
MATERIAL: 1018 STEEL
Ø 13.5 x2
80
91 +1 -1
22 +1 -1
71 +0 -1
25 REF
Ø 135 +0.05 -0.05
Ø 120
120
72
Ø 95
R15
50
R50
6
127
R83
54
R40 x2
Ø 188
Ø 127
Ø 105
Ø 170
R2 x3
30
65
100
115
DO NOT SCALE
NEW_TRANS_T_MOUNT
Sheet 1 of 2
Scale 0.400

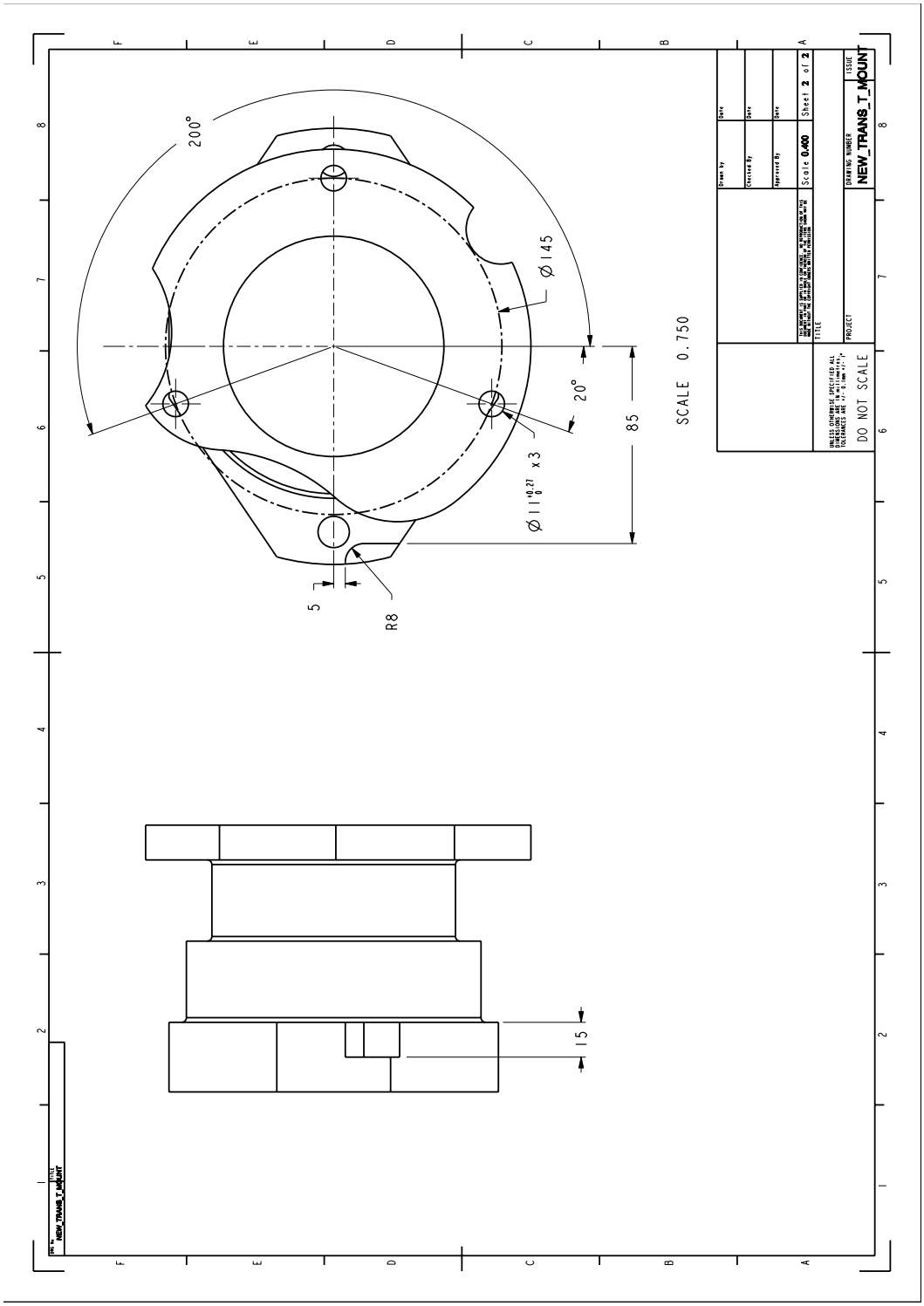
200°
Ø145
20°
85
Ø11 +0.27 0 x3
5
R8
15
SCALE 0.750
Scale 0.400
Sheet 2 of 2
DRAWING NUMBER
NEW_TRANS_T_MOUNT
ISSUE
PROJECT
DO NOT SCALE
TITLE
NEW_TRANS_T_MOUNT

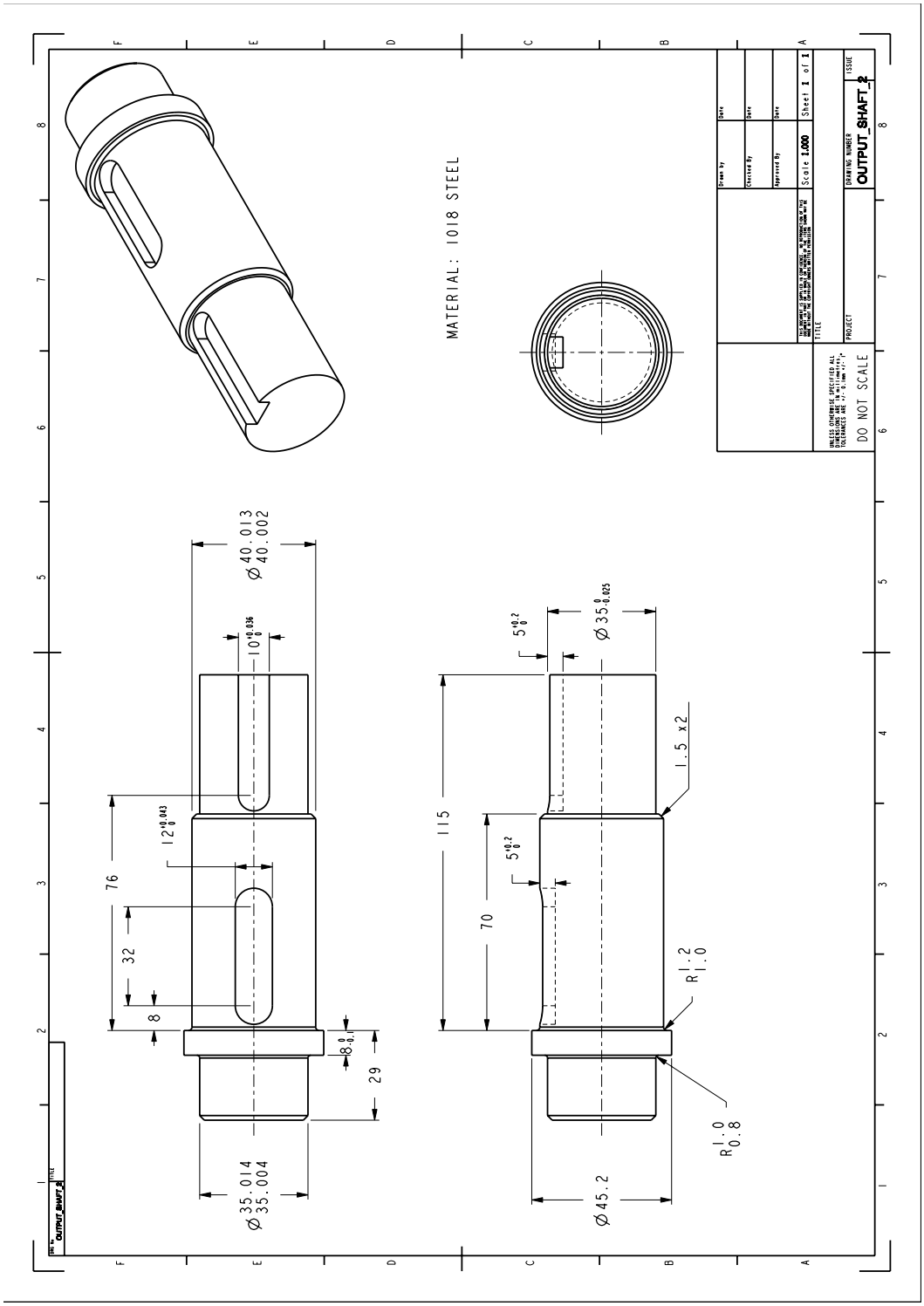
MATERIAL: 1018 STEEL
DO NOT SCALE
OUTPUT_SHAFT_2
Scale 1.000
Sheet 1 of 1
Ø40.013
Ø40.002
Ø35.014
Ø35.004
Ø45.2
Ø35
10
12
76
32
8
29
115
70
5
1.5 x2
R1.2
R1.0
R1.0
R0.8

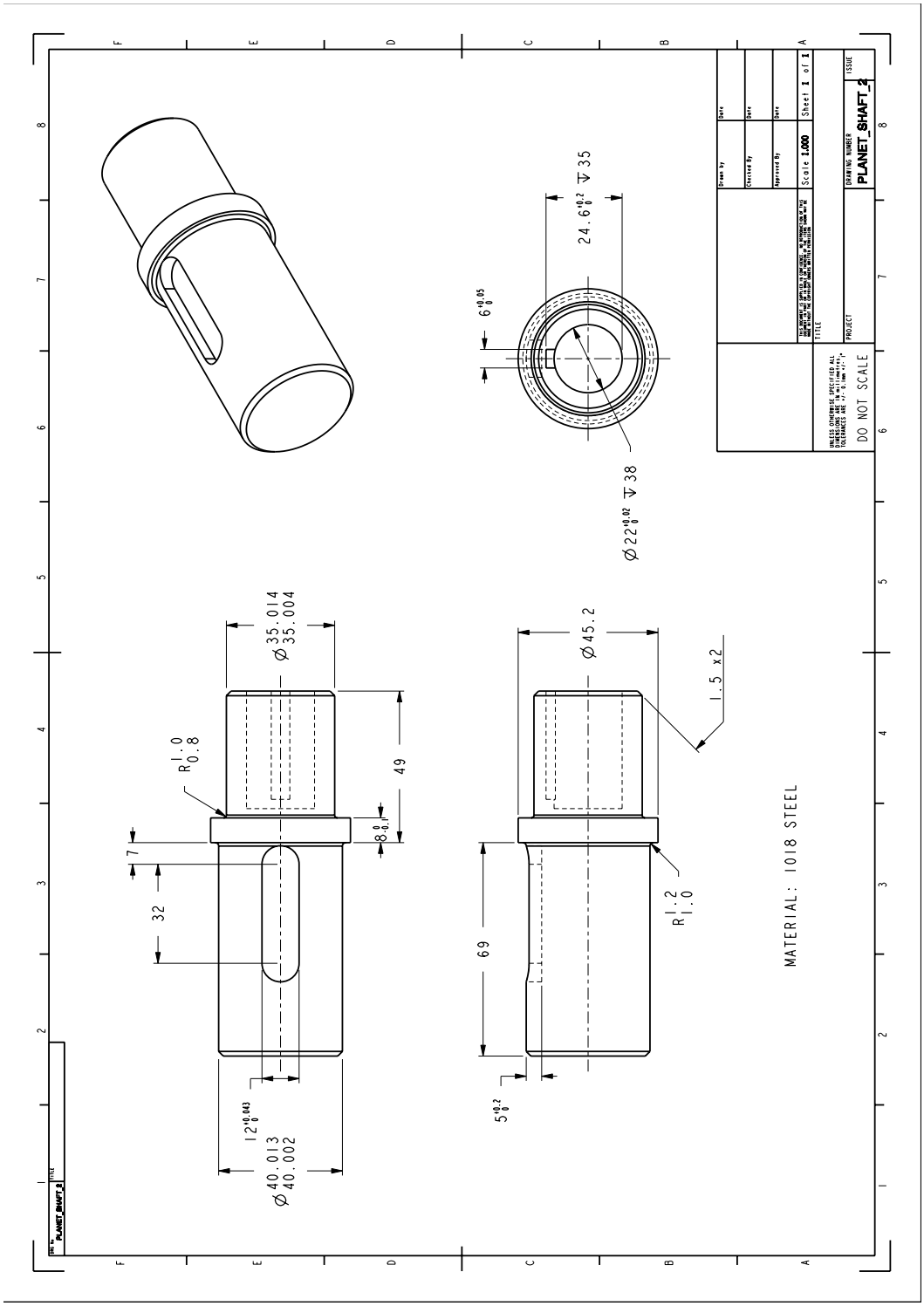
PLANET_SHAFT_#2
DRAWING NUMBER
PLANET_SHAFT_2
ISSUE
Scale 1.000
Sheet 1 of 1
Drawn by
Checked By
Approved By
Date
PROJECT
DO NOT SCALE
MATERIAL: 1018 STEEL
1.5 x2
49
32
7
69
Ø45.2
Ø35.014
Ø35.004
Ø40.013
Ø40.002
24.6
35
6
38
Ø22

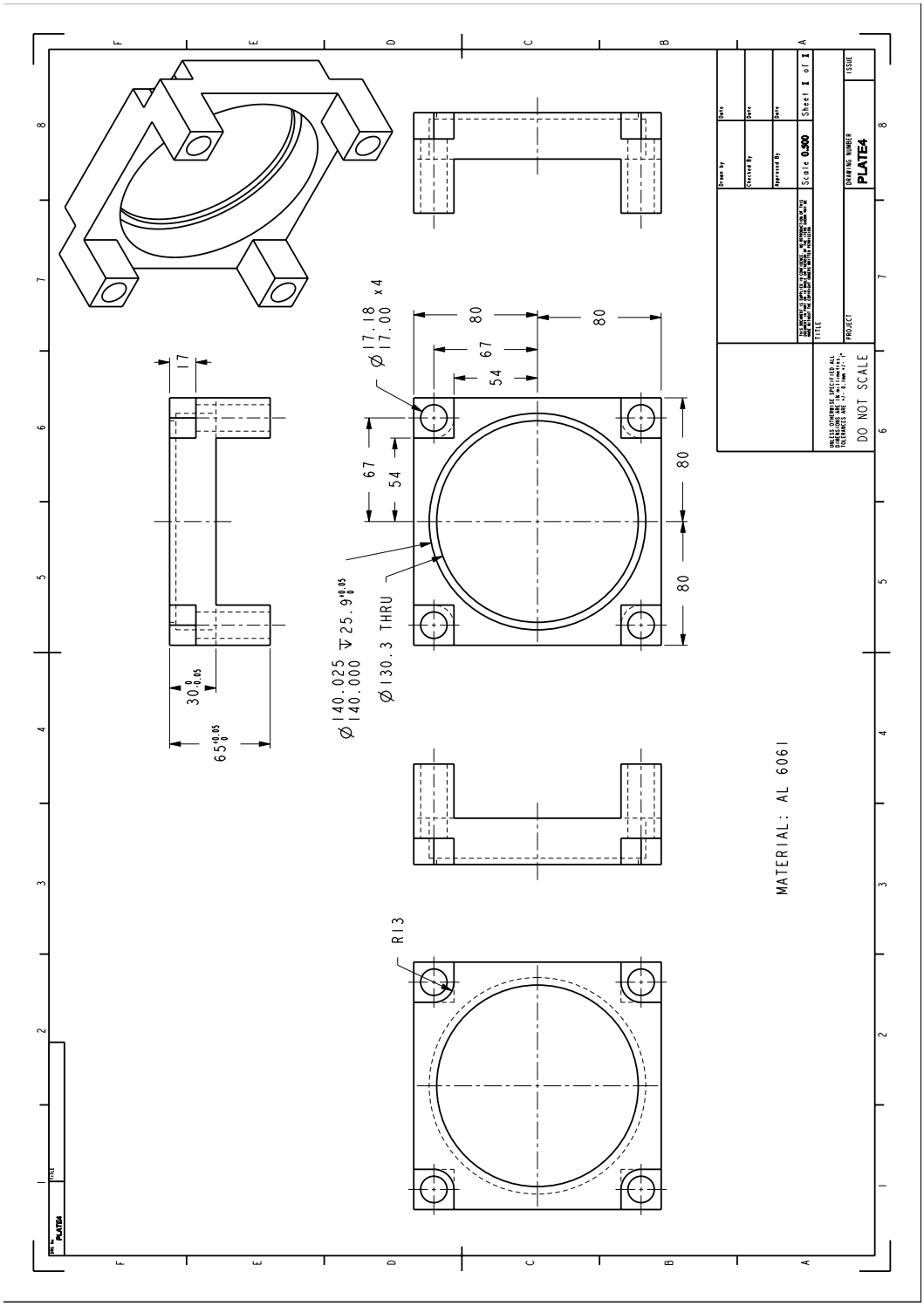
MATERIAL: AL 6061
DO NOT SCALE
PLATE4
Scale 0.500
Sheet 1 of 1
R13
80
67
54
17
Ø130.3 THRU

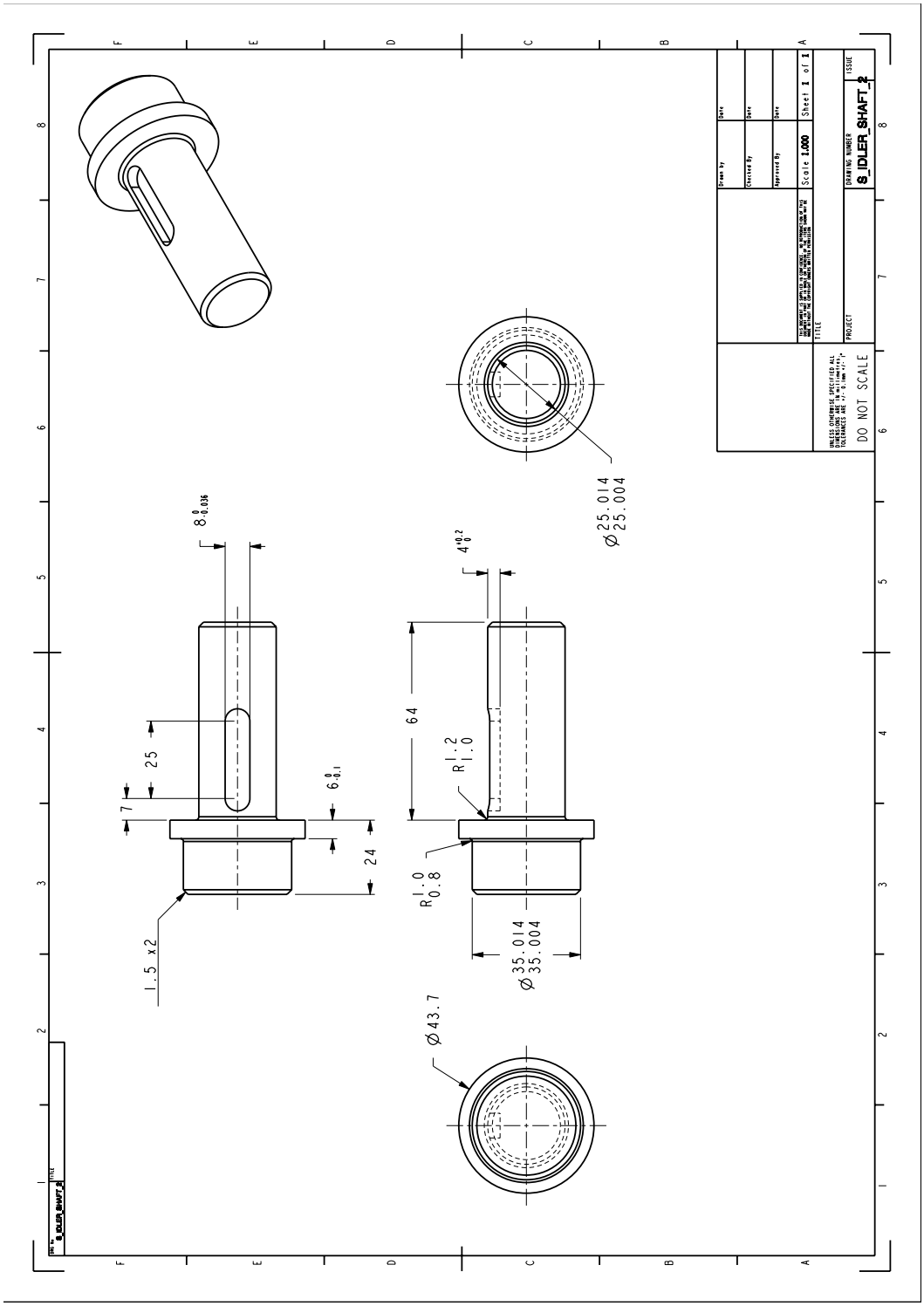
S_IDLER_SHAFT_2
DO NOT SCALE
Scale 1.000
Sheet 1 of 1
DRAWING NUMBER
S_IDLER_SHAFT_2
ISSUE
PROJECT
Drawn by
Checked By
Approved By
Date
TITLE
Ø25.014
25.004
8.0
-0.036
4
+0.2
-0
64
25
7
6.0
-0.1
24
R1.2
1.0
R1.0
0.8
1.5 x2
Ø35.014
35.004
Ø43.7

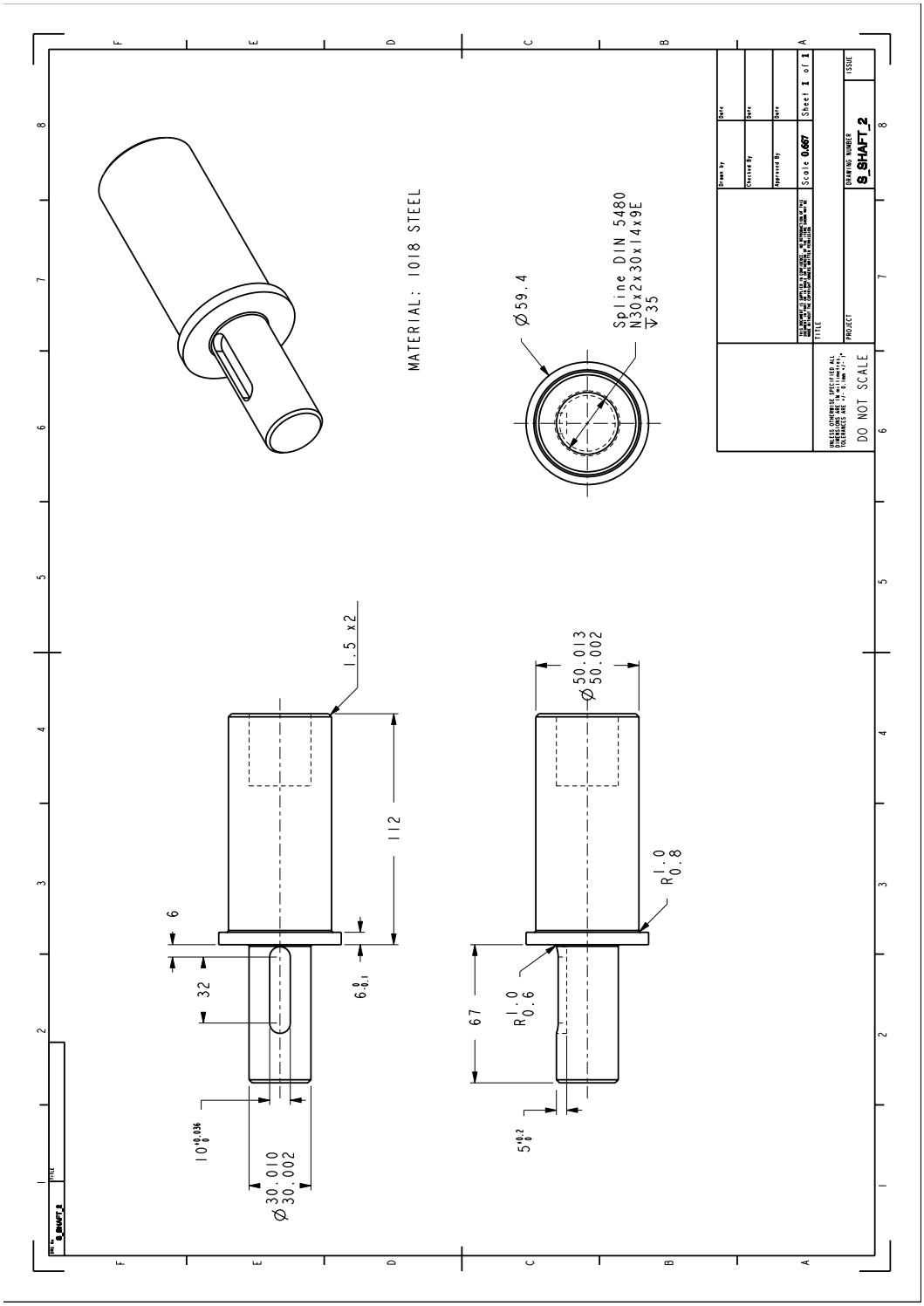
MATERIAL: 1018 STEEL
Ø59.4
Spline DIN 5480
N30x2x30x14x9E
35
1.5 x2
112
6
32
6 0 -0.1
10 +0.036 0
Ø 30.010 30.002
Ø 50.013 50.002
67
R 1.0 0.6
R 1.0 0.8
5 0 -0.2
DO NOT SCALE
PROJECT
DRAWING NUMBER
S_SHAFT_2
ISSUE
Sheet 1 of 1
Scale 0.667
Drawn by
Checked By
Approved By
Date
TITLE
S_SHAFT_2

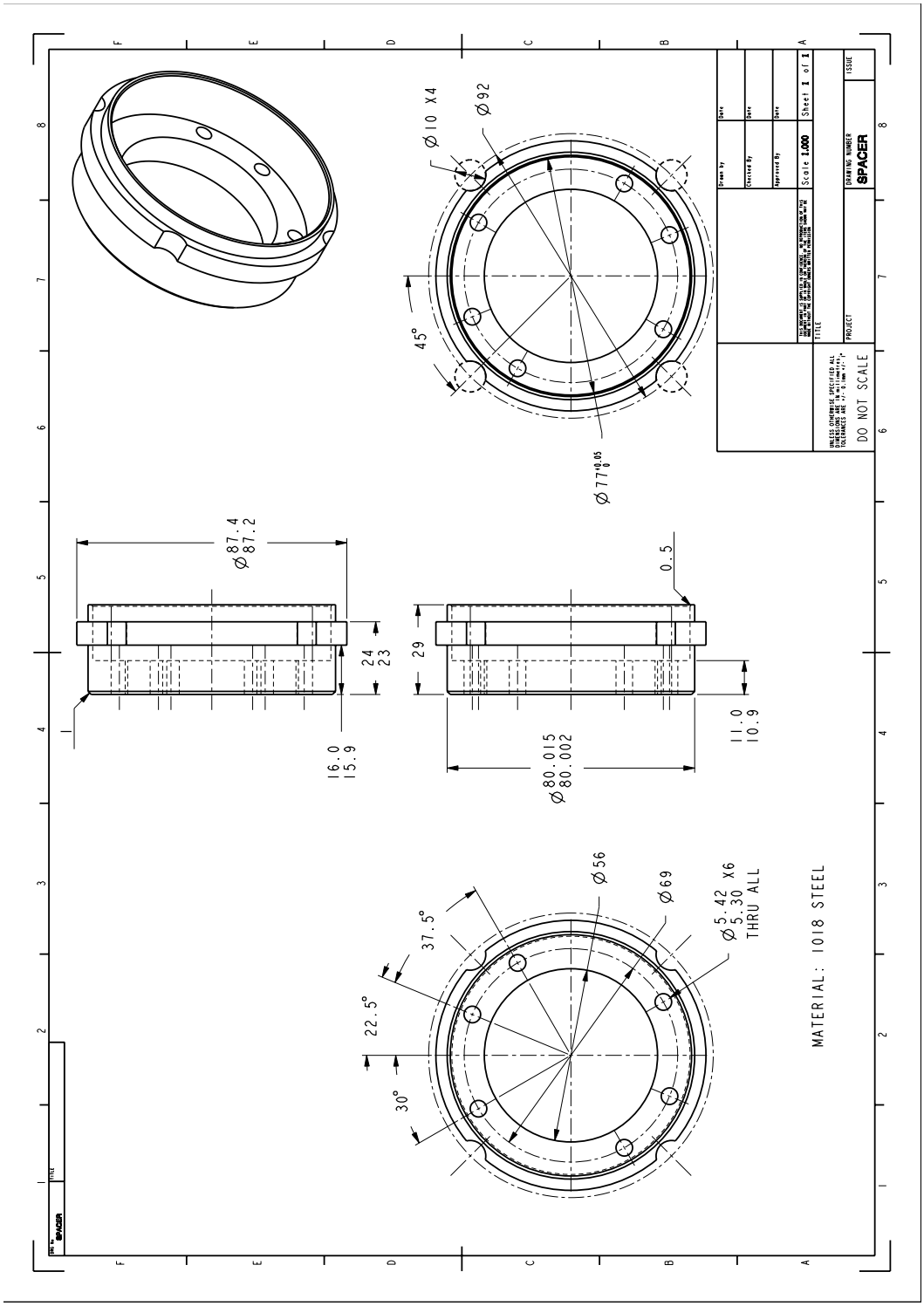
Ø10 X4
Ø92
45°
Ø77 +0.05 0
Ø87.4
Ø87.2
24
23
16.0
15.9
0.5
29
11.0
10.9
Ø80.015
Ø80.002
Ø56
Ø69
Ø5.42 X6
Ø5.30 X6
THRU ALL
37.5°
22.5°
30°
MATERIAL: 1018 STEEL
DO NOT SCALE
SPACER
Scale 1.000
Sheet 1 of 1

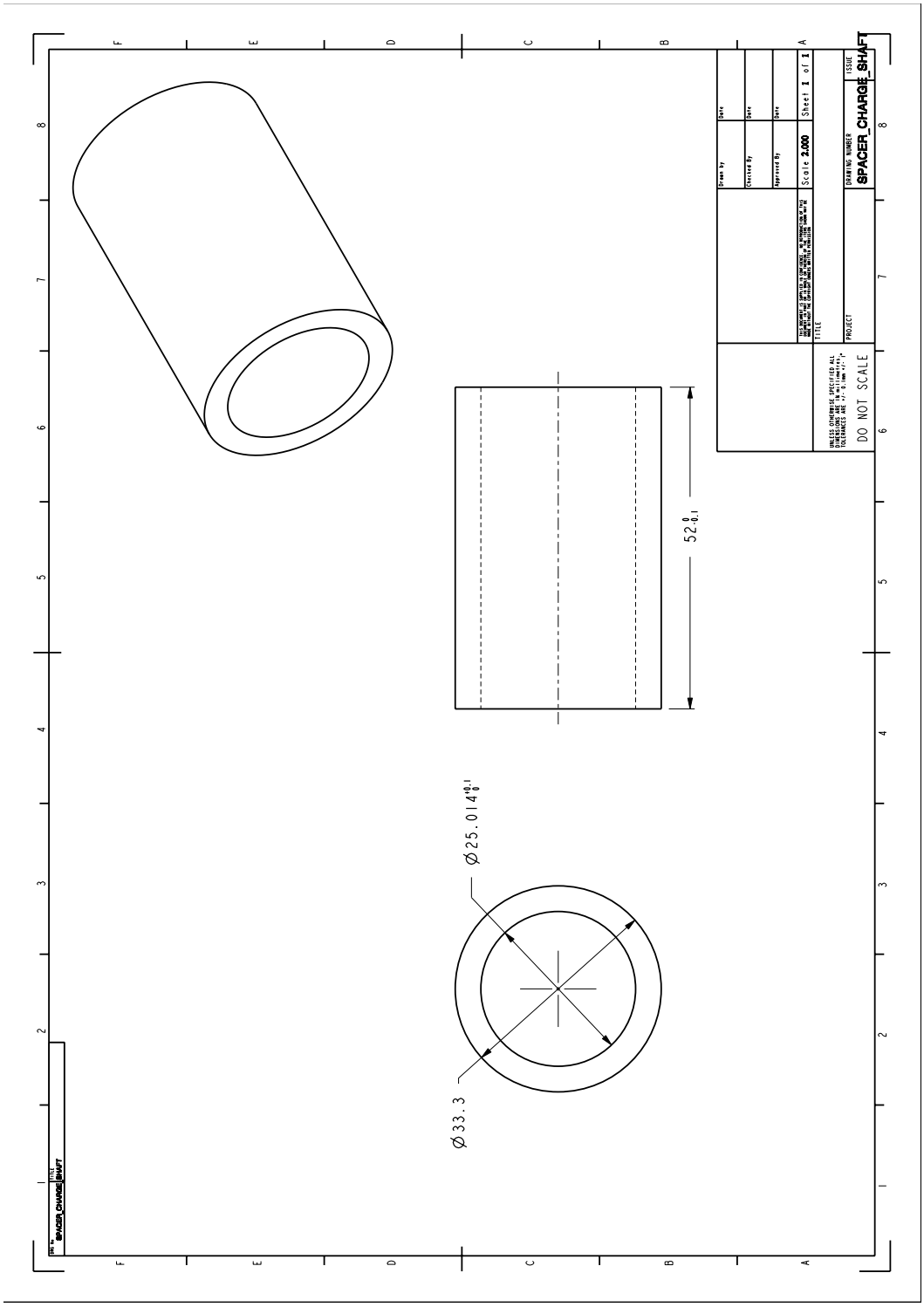
SPACER_CHARGE_SHAFT
Ø25.014
Ø33.3
52
DO NOT SCALE
Scale 2.000
Sheet 1 of 1
SPACER_CHARGE_SHAFT

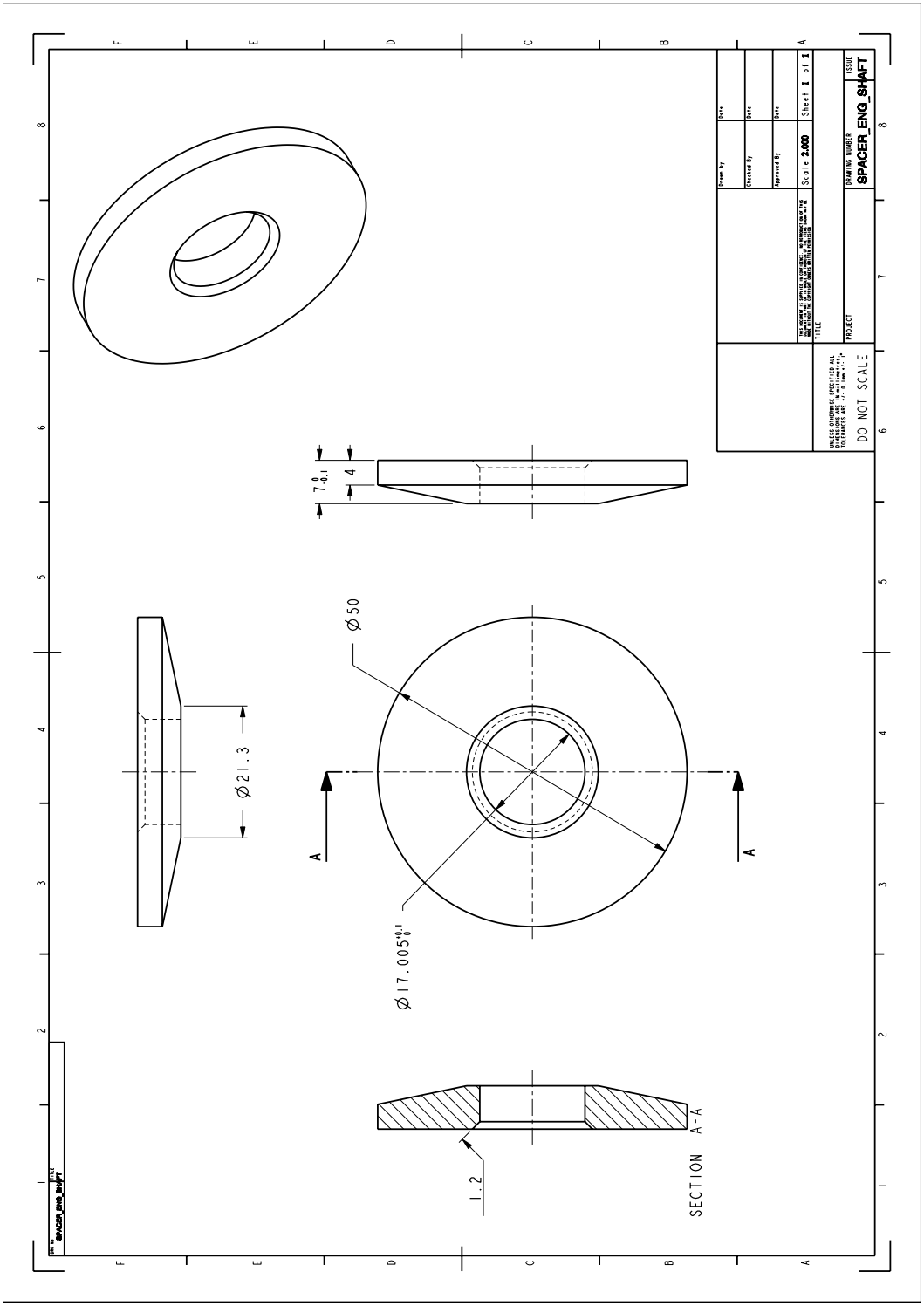
SPACER_ENG_SHAFT
Ø50
Ø21.3
Ø17.005
7
4
1.2
SECTION A-A
A
A
DO NOT SCALE
Scale 2.000
Sheet 1 of 1
SPACER_ENG_SHAFT

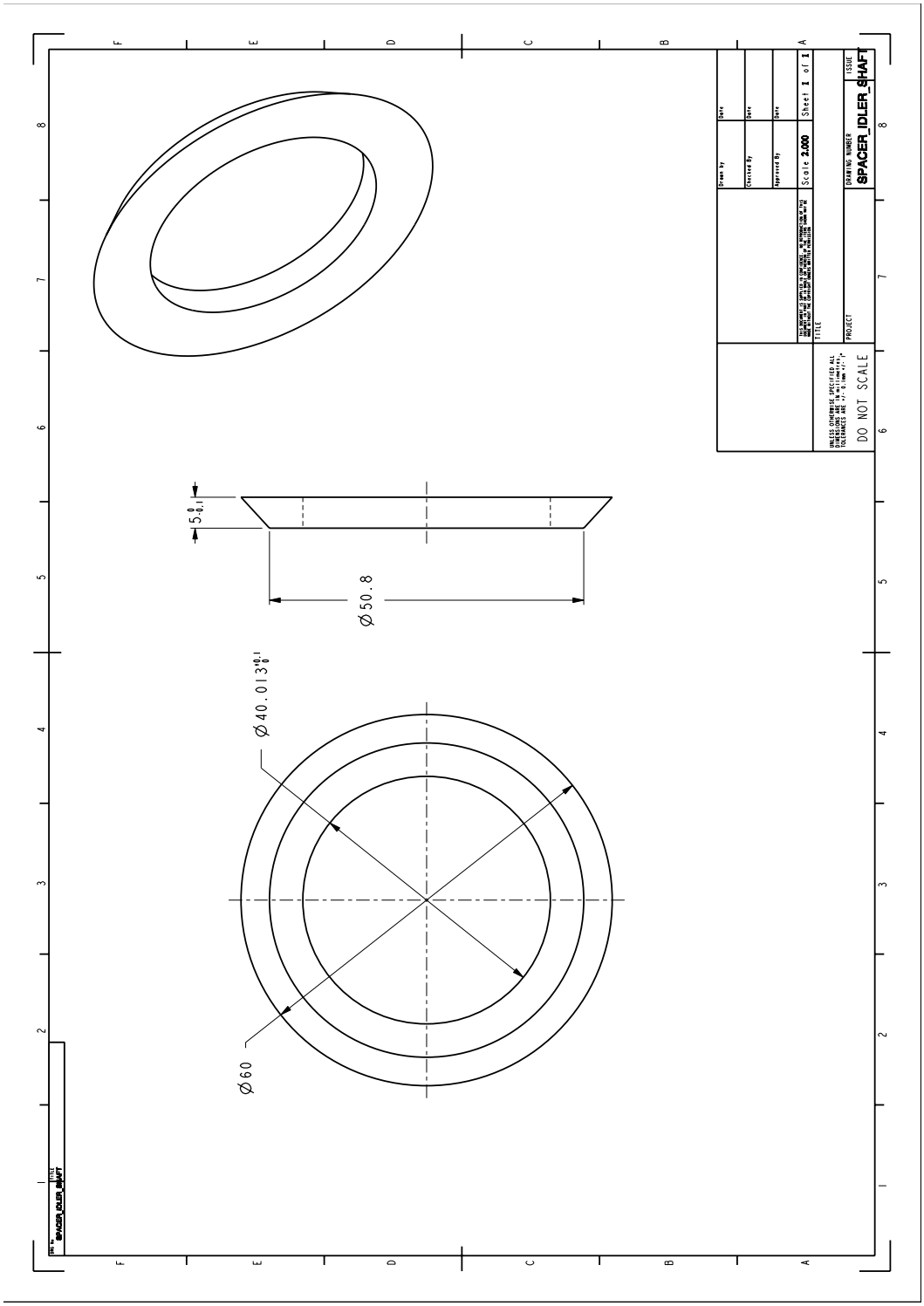
5.0 ±0.1
Ø50.8
Ø40.013 +0.1 0
Ø60
DO NOT SCALE
SPACER_IDLER_SHAFT
Scale 2.000
Sheet 1 of 1

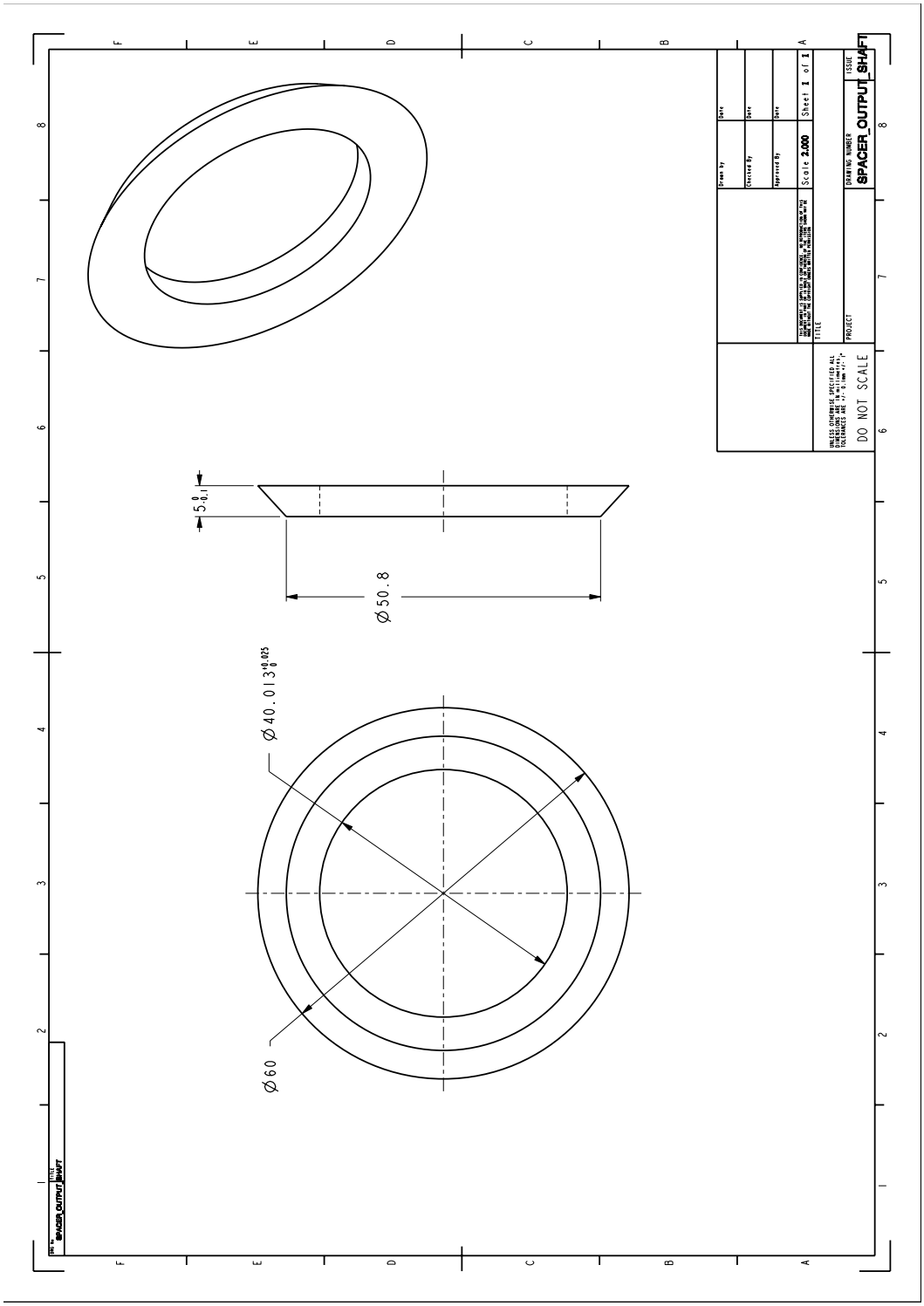
SPACER_OUTPUT_SHAFT
DO NOT SCALE
Scale 2.000
Sheet 1 of 1
Ø50.8
Ø60

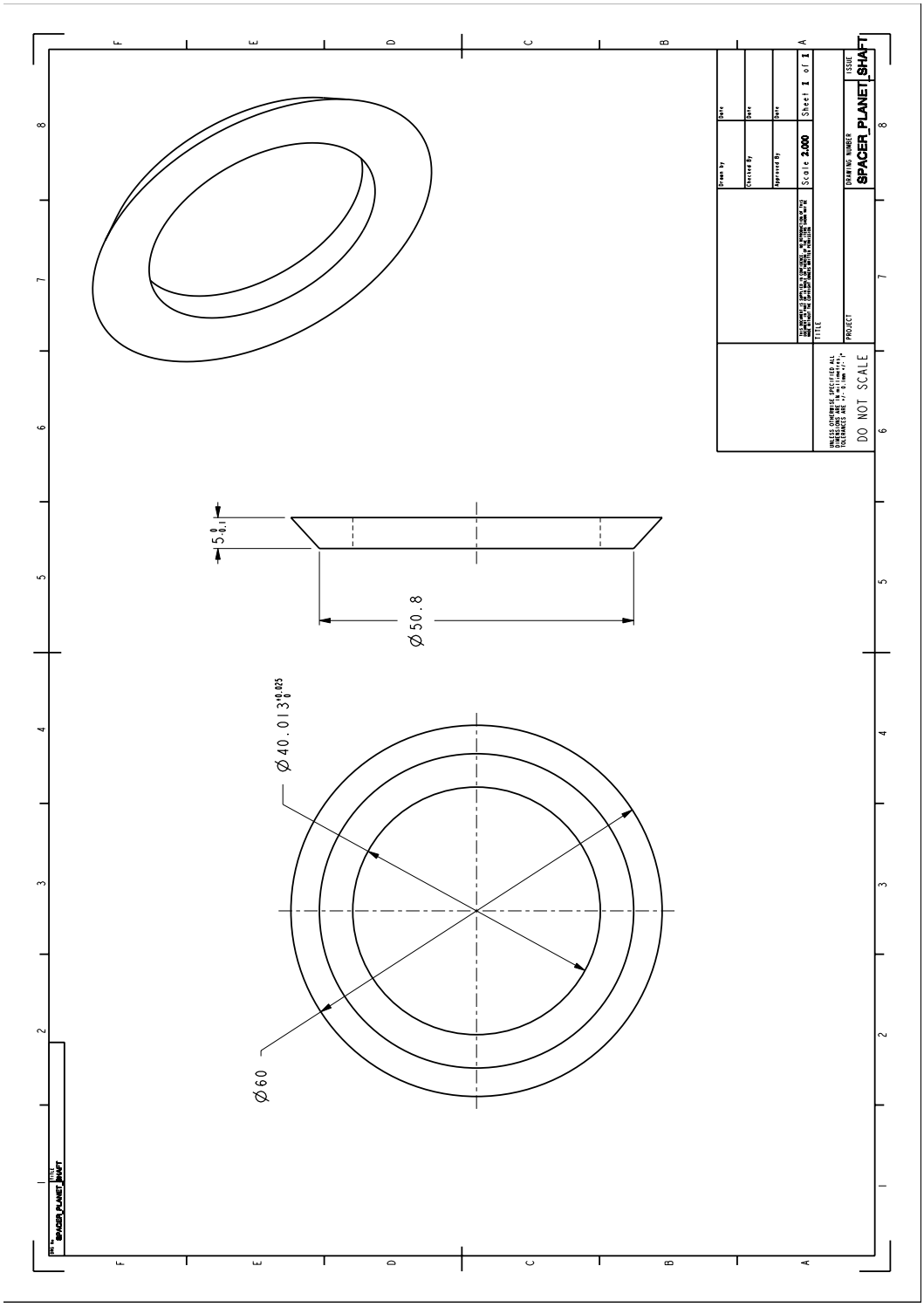
Ø40.013 +0.025 0
Ø60
Ø50.8
5 -0.1 0
DO NOT SCALE
SPACER_PLANET_SHAFT
Scale 2.000
Sheet 1 of 1

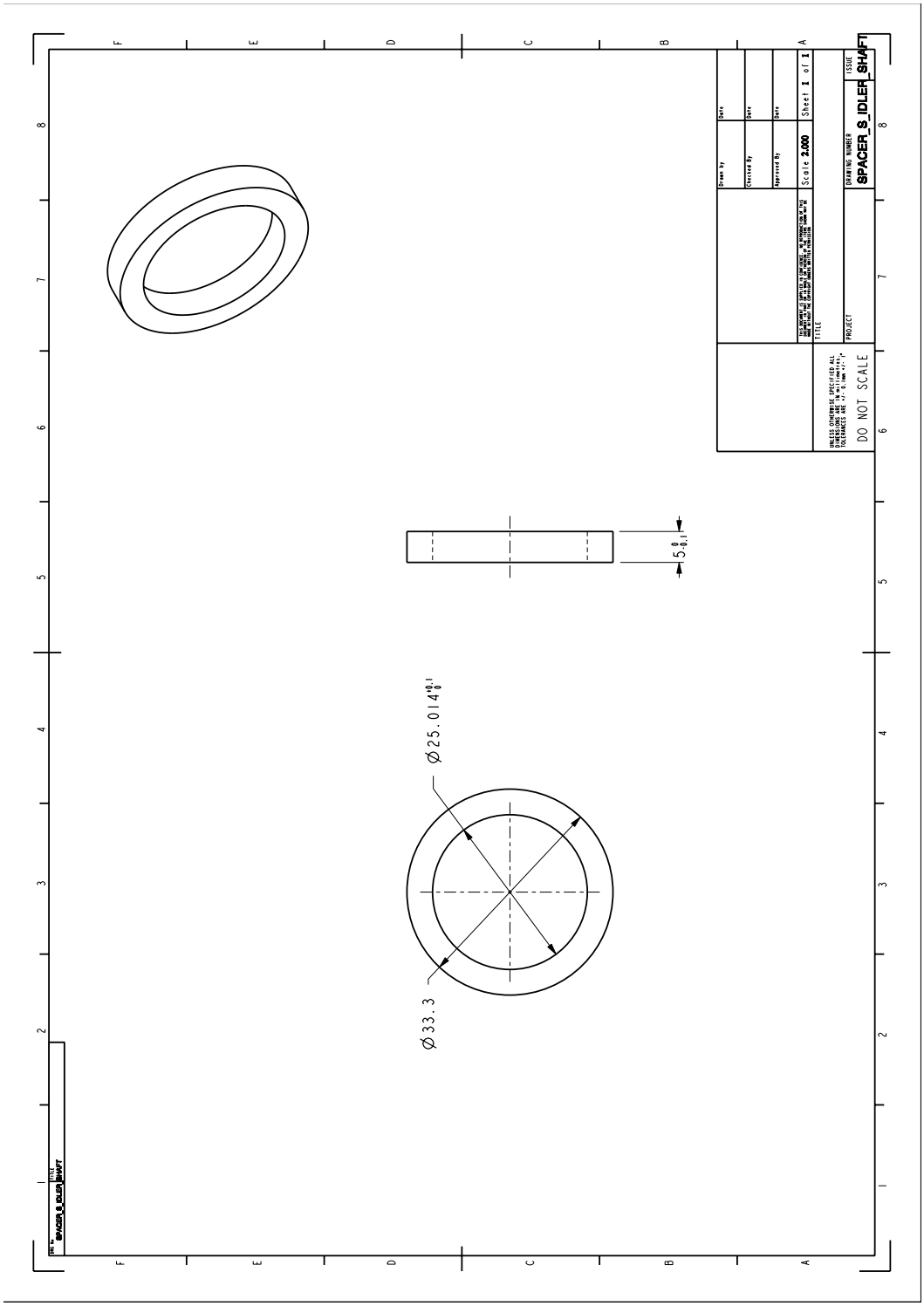
SPACER_S_IDLER_SHAFT
Drawn by
Checked By
Approved By
Date
Scale 2.000
Sheet 1 of 1
PROJECT
DRAWING NUMBER
SPACER_S_IDLER_SHAFT
ISSUE
DO NOT SCALE
5.0 -0.1
Ø25.014 +0.1 0
Ø33.3

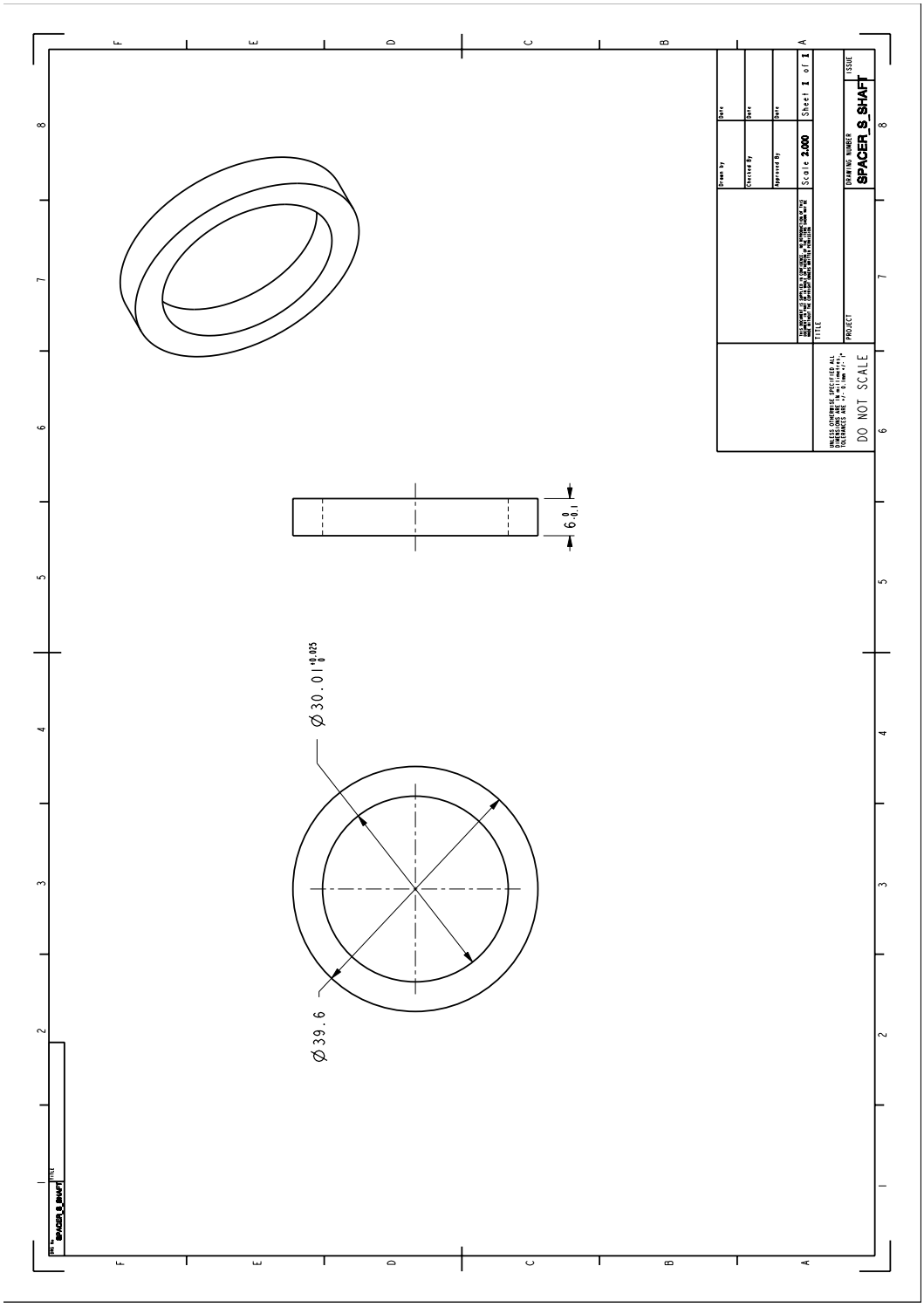
Ø30.01 +0.025 0
Ø39.6
6 0 -0.1
DO NOT SCALE
SPACER_S_SHAFT
Scale 2.000
Sheet 1 of 1

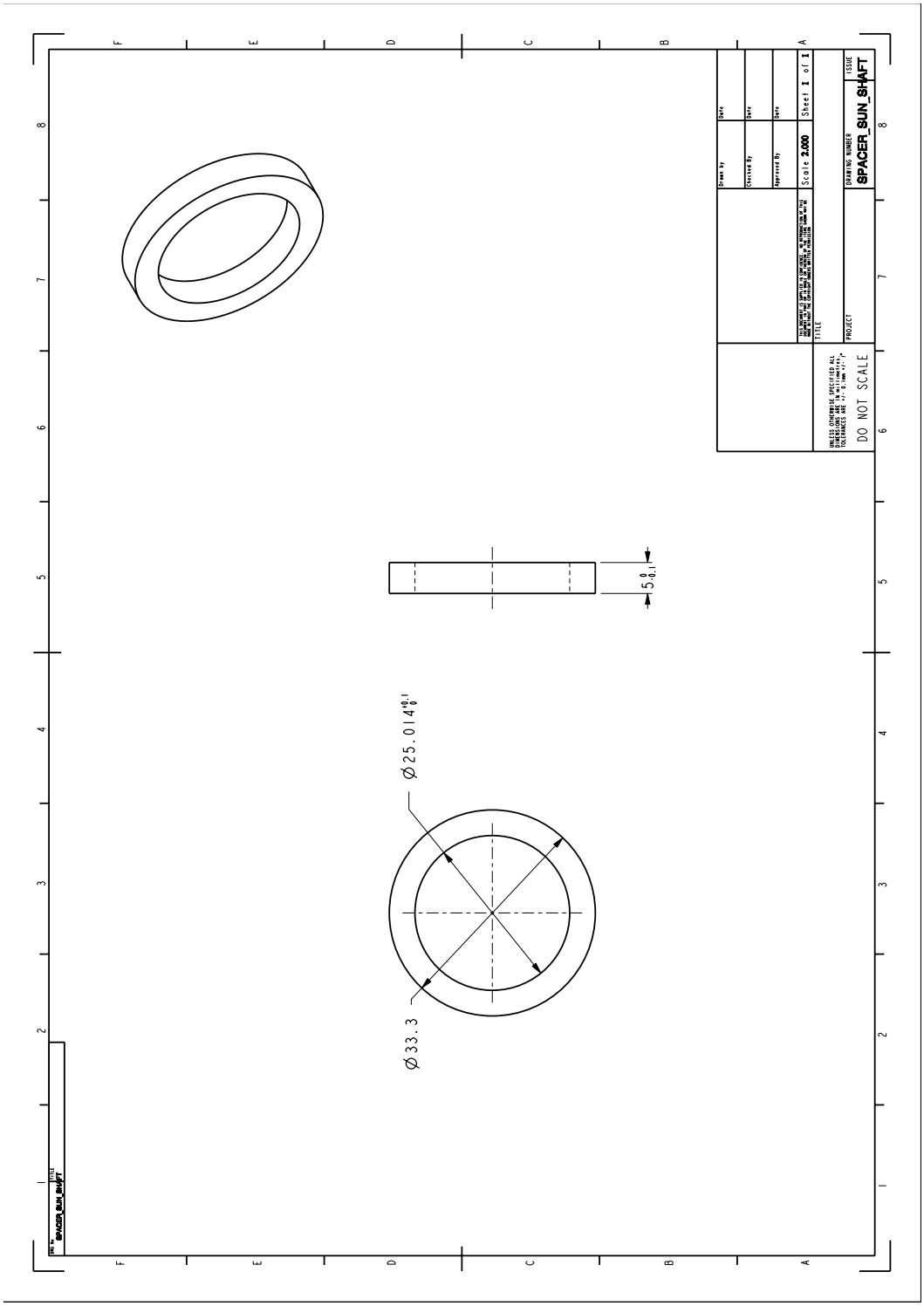
DO NOT SCALE
SPACER_SUN_SHAFT
Scale 2.000
Sheet 1 of 1
Ø25.014
Ø33.3
5.8

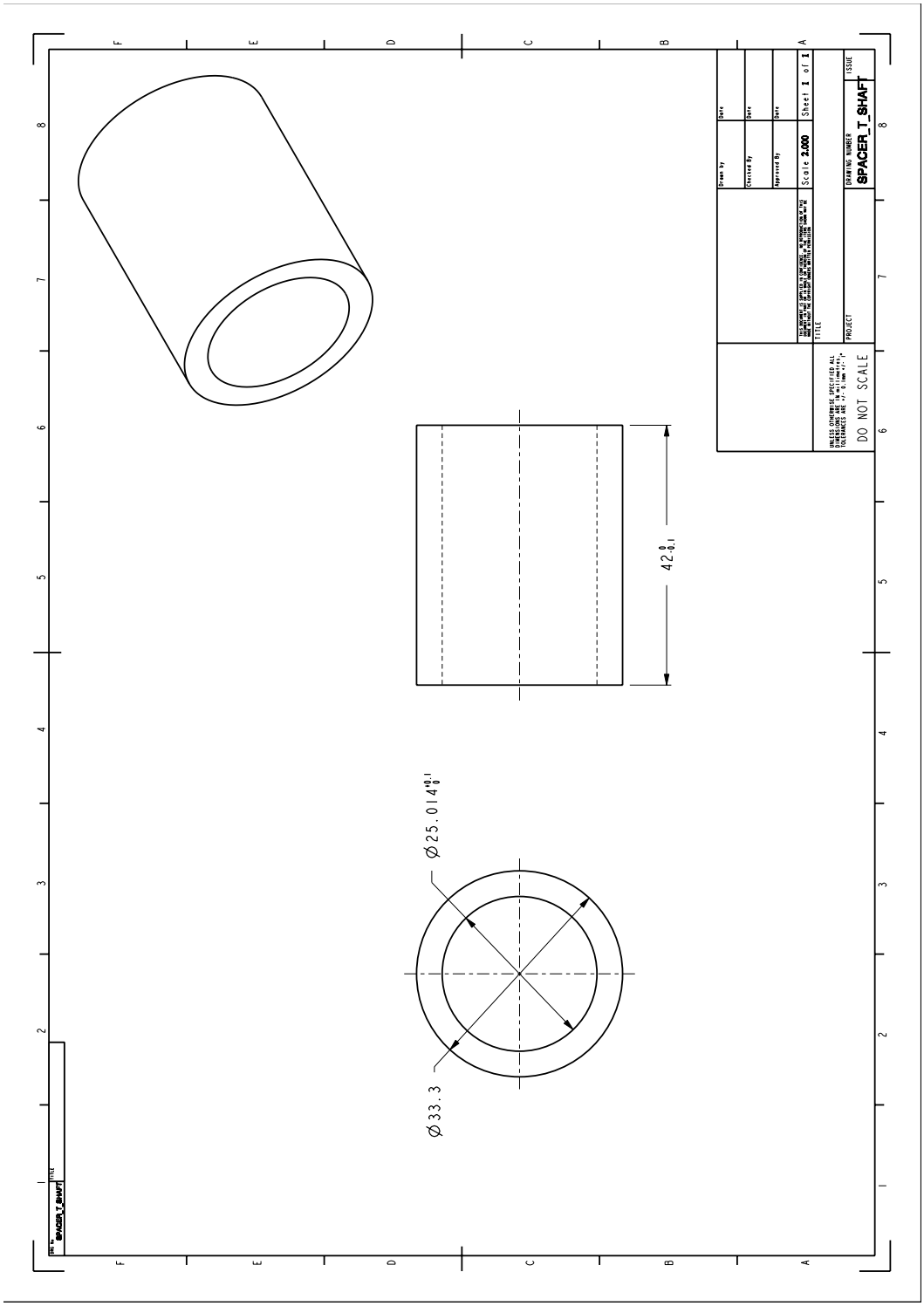
DO NOT SCALE
SPACER_T_SHAFT
Scale 2.000
Sheet 1 of 1
Ø25.014
Ø33.3
42

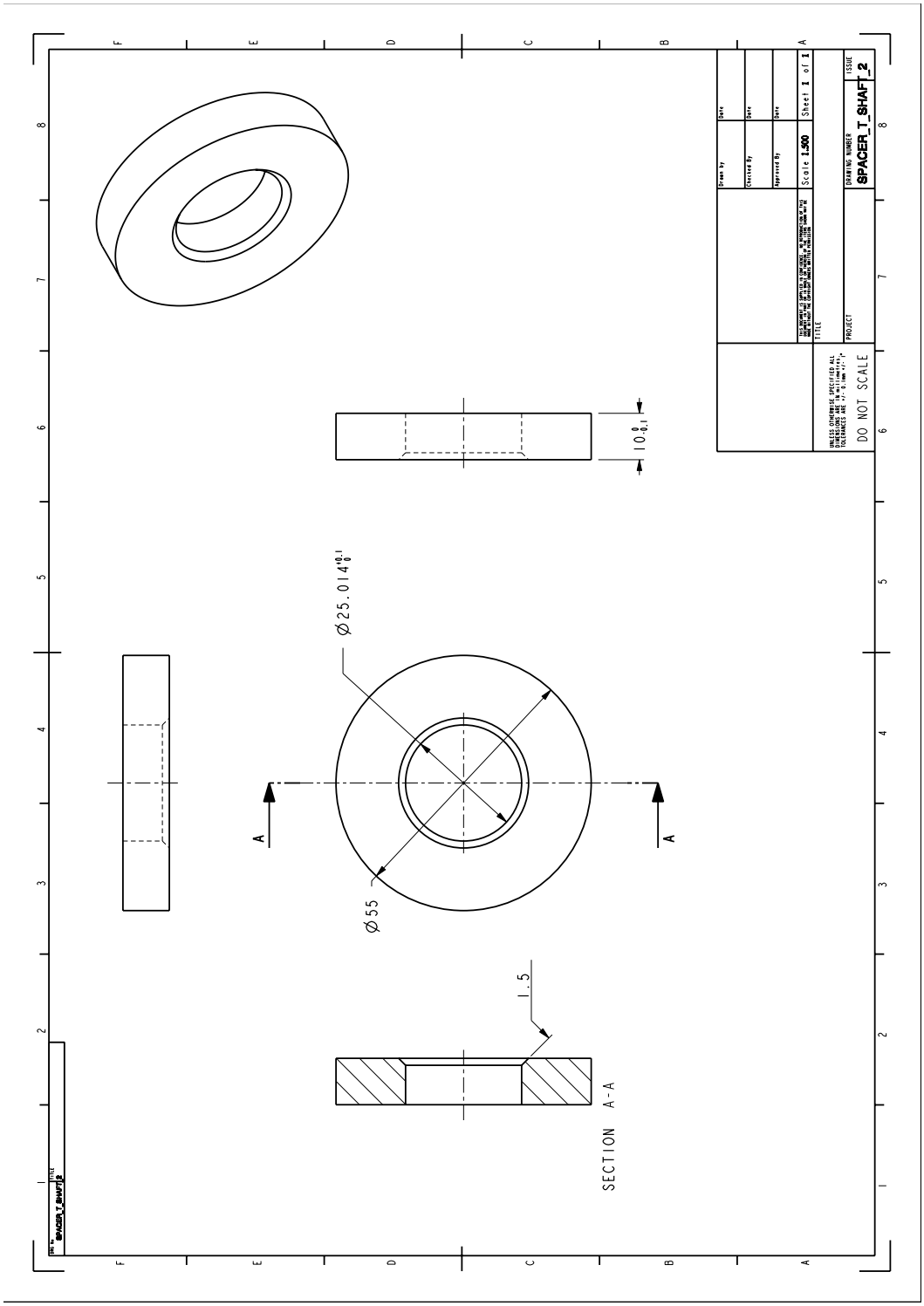
Ø25.014
Ø55
A
A
10
1.5
SECTION A-A
DO NOT SCALE
SPACER_T_SHAFT_2
Sheet 1 of 1
Scale 1.500

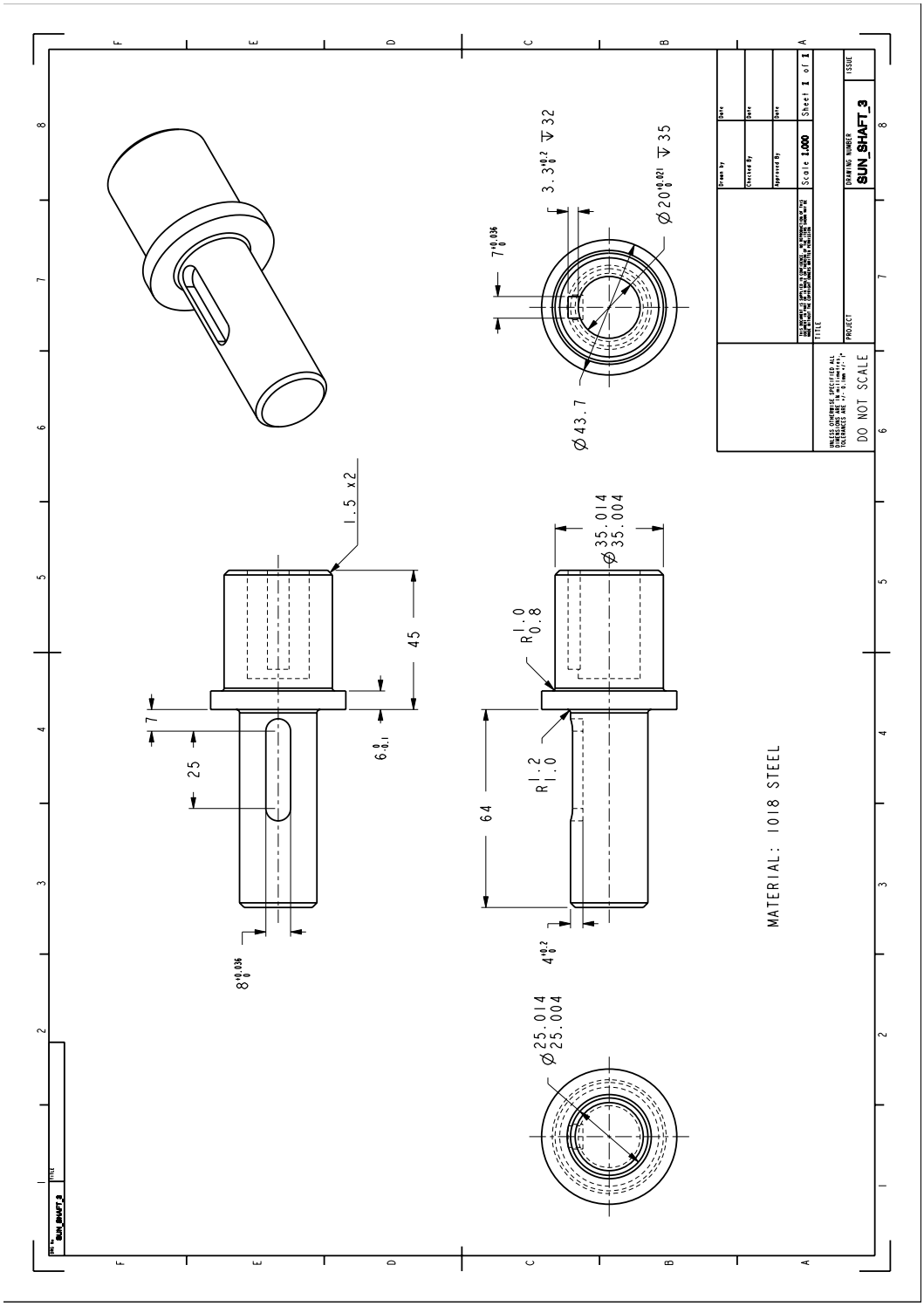
1.5 x2
45
7
25
64
R1.0
0.8
R1.2
1.0
Ø35.014
35.004
Ø25.014
25.004
Ø43.7
Ø20
3.3
32
35
MATERIAL: 1018 STEEL
DO NOT SCALE
SUN_SHAFT_3
Scale 1.000
Sheet 1 of 1

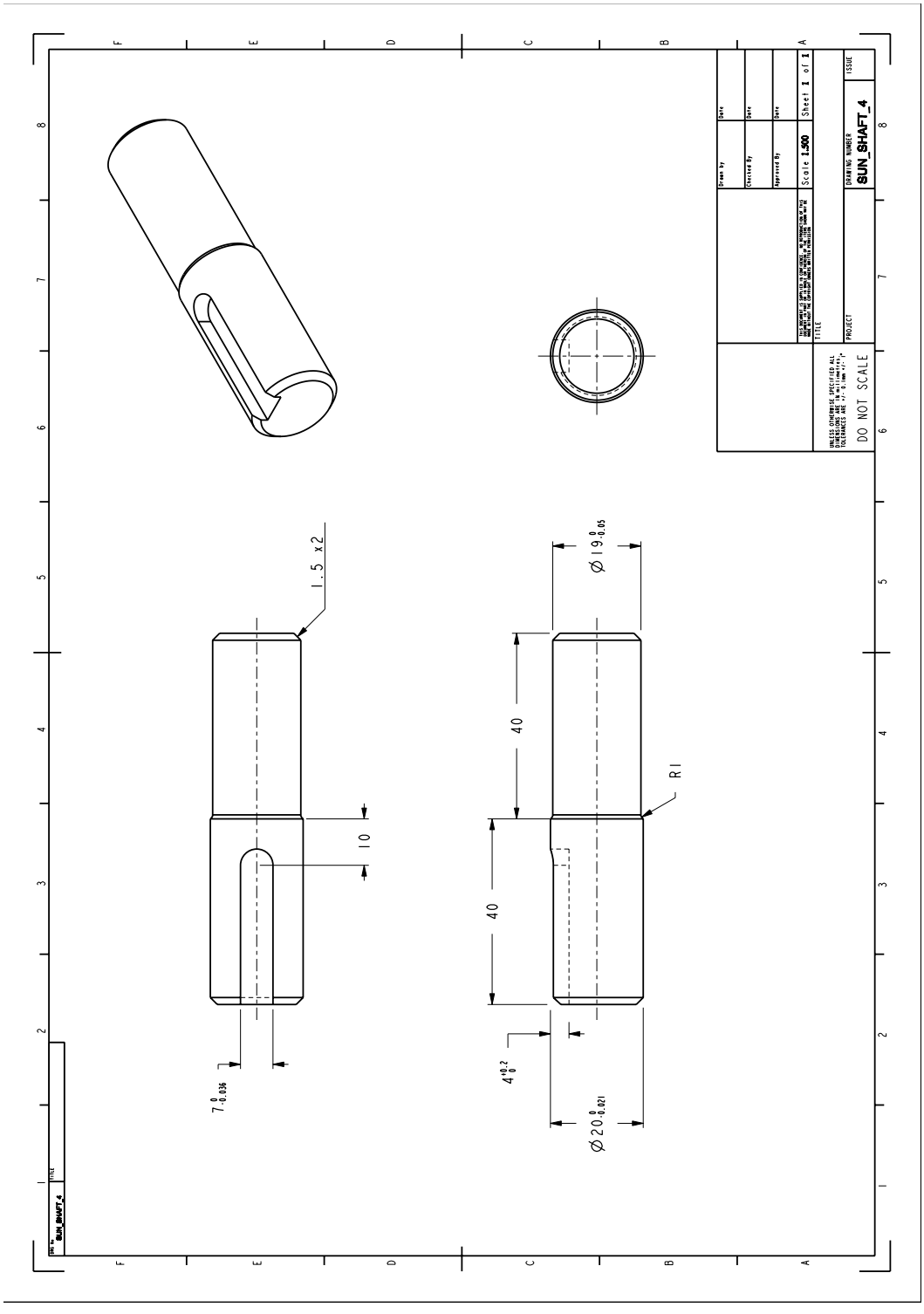
SUN_SHAFT_4
Scale 1.500
Sheet 1 of 1
DRAWING NUMBER
SUN_SHAFT_4
PROJECT
DO NOT SCALE
1.5 x2
10
40
40
R1
Ø19
Ø20
7
4

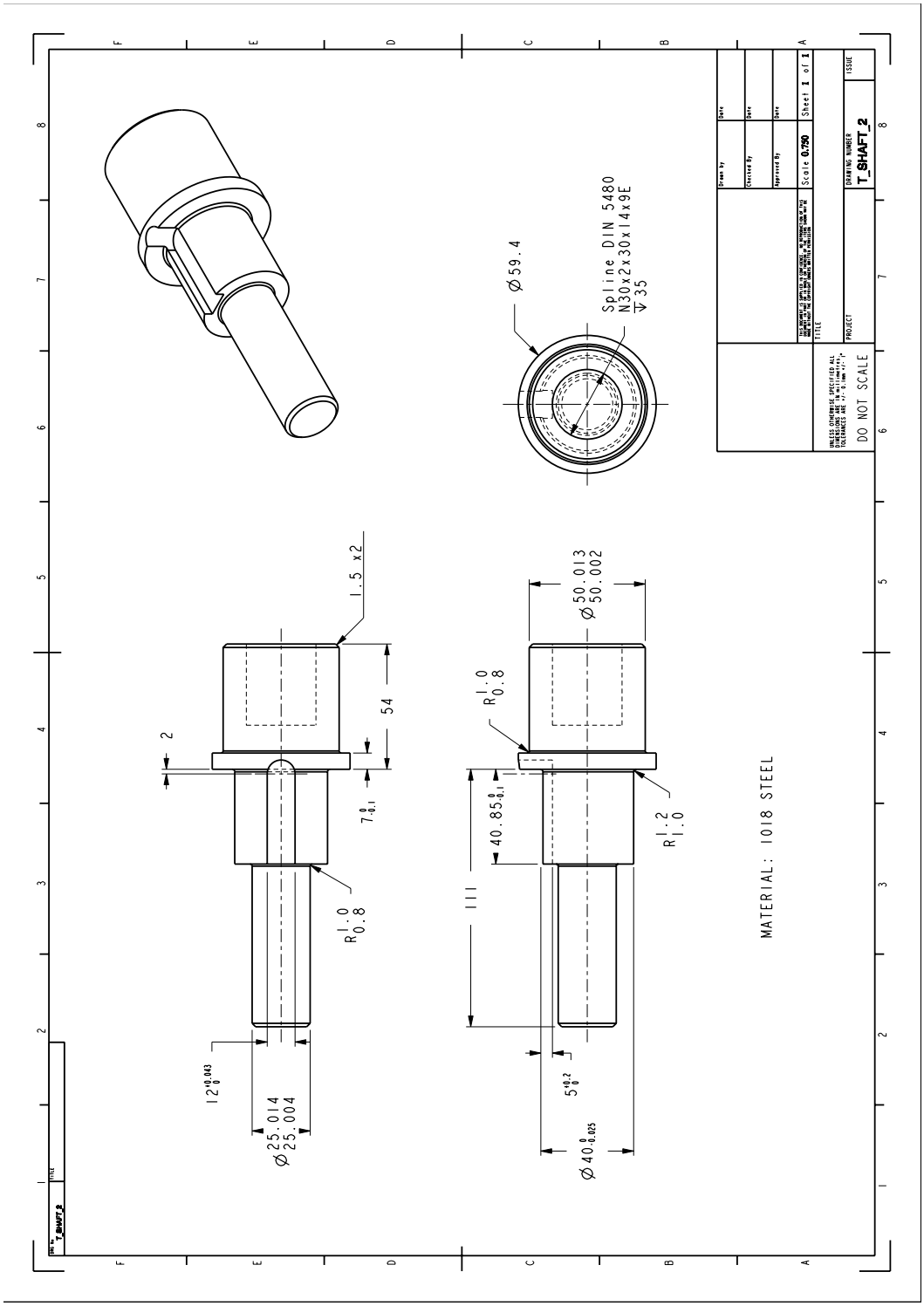
Spline DIN 5480
N30x2x30x14x9E
Ø59.4
1.5 x2
54
2
111
MATERIAL: 1018 STEEL
DO NOT SCALE
T_SHAFT_2
Scale 0.750
Sheet 1 of 1